UNIVERSIDADE FEDERAL DE SÃO CARLOS
CENTRO DE CIÊNCIAS EXATAS E DE TECNOLOGIA
DEPARTAMENTO DE QUÍMICA
PROGRAMA DE PÓS-GRADUAÇÃO EM QUÍMICA

Chemical characterization and proposal for the recovery of noble elements from electronic waste

Dennis Da Silva Ferreira*

Tese apresentada como parte dos requisitos para obtenção do título de DOUTOR EM CIÊNCIAS, área de concentração: QUÍMICA ANALÍTICA

Orientador: Prof. Dr. Edenir Rodrigues Pereira Filho

*** Bolsista CNPq (processo 140867/2021-0)**

São Carlos - SP
2025

UNIVERSIDADE FEDERAL DE SÃO CARLOS

Centro de Ciências Exatas e de Tecnologia
Programa de Pós-Graduação em Química

Folha de Aprovação

Defesa de Tese de Doutorado do candidato Dennis da Silva Ferreira, realizada em 07/08/2025.

Comissão Julgadora:

Prof. Dr. Edenir Rodrigues Pereira Filho (UFSCar)

Profa. Dra. Carla Jovania Gomes Colares (UFT-Gurupi)

Prof. Dr. Diêgo Victor de Babos (UFU)

Prof. Dr. Alexandre Luis Magalhães Levada (UFSCar)

Prof. Dr. Wallace Duarte Fragoso (UFPB)

O Relatório de Defesa assinado pelos membros da Comissão Julgadora encontra-se arquivado junto ao Programa de Pós-Graduação em Química.

“In the end we will conserve only what we love, we will love only what we understand, and we will understand only what we are taught.”

Baba Dioum, 1968

“Dedico este trabalho à minha família, aos amigos e aos professores que me apoiaram e incentivaram ao longo de toda essa jornada.”

AGRADECIMENTOS

Primeiramente, agradeço a Deus pela vida, pelas bênçãos, pelas oportunidades e pelas pessoas que colocou em meu caminho e que me ajudaram a concretizar este sonho.

Agradeço profundamente à minha família, pelo suporte incondicional ao longo desta jornada. Aos meus pais, Aristides e Iraci, e à minha irmã Karita, meu muito obrigado por todo apoio, incentivo e amor durante esse período.

Ao professor Dr. Edenir Rodrigues Pereira Filho, minha sincera gratidão pela orientação, atenção, amizade e carinho. Obrigado pelas oportunidades, pelos valiosos ensinamentos e pelo incentivo constante, que foram fundamentais para meu desenvolvimento acadêmico e pessoal ao longo dos últimos quatro anos.

Agradeço à professora Dra. Fabíola Manhas Verbi Pereira pela atenção, apoio, amizade e pelos conhecimentos compartilhados. Obrigado por abrir as portas da UNESP/Araraquara, pelas oportunidades e incentivo que tanto contribuíram para o desenvolvimento do meu trabalho durante o doutorado.

À Dra. Lucimar Lopes Fialho e aos membros e ex-membros do Grupo de Análise Instrumental Aplicada (Gaia), agradeço pela amizade, pelo aprendizado, pela parceria e pela ajuda nas etapas experimentais realizadas no laboratório. Foi um prazer conviver com vocês e dividir momentos de troca de conhecimento e descontração.

Ao professor Dr. Alejandro Olivieri, minha gratidão pela orientação, confiança e oportunidades durante o estágio de doutorado sanduíche na Argentina. Aos amigos Esteban, Soledad e professor Juan, obrigado pela acolhida, pelos bons momentos e por fazerem parte dessa etapa especial da minha trajetória.

Aos incríveis amigos que fiz durante meu tempo na UFSCar, Vinicius Sousa, João Paulo (Carioca), Heyder, Paula Scarabotto, Rafael Esteves, Chimba (Luiz Felipe) e Felipe De Paula, muito obrigado pela convivência, amizade e momentos de descontração que foram essenciais ao longo do percurso.

Aos meus irmãos de república, Borges, Caloi, Mathew, Maps e Adigol, obrigado pelo apoio nas diferentes fases do doutorado, pelas ideias criativas, pelas conversas e pelas risadas que tornaram essa caminhada mais leve e divertida.

Agradeço à Universidade Federal de São Carlos (UFSCar) e ao Departamento de Química pelo acolhimento, bem como a todos envolvidos na Pós-Graduação em Química, pela disponibilidade e atenção constantes.

Às editoras Elsevier e SBQ, agradeço pela autorização para o uso dos artigos publicados e apresentados nesta tese.

Ao CNPq, agradeço pelo apoio financeiro por meio da bolsa concedida.

O presente trabalho foi realizado com apoio da Coordenação de Aperfeiçoamento de Pessoal de Nível Superior – CAPES, código de financiamento 001.

Muito Obrigado!

This PhD thesis is based on the following publications which are presented in the original format:

"Principal component analysis (PCA) para a avaliação de dados químicos e geração de heat maps: um tutorial"

Dennis da Silva Ferreira, Leticia da Silva Rodrigues, Fabiola Manhas Verbi Pereira, Edenir Rodrigues Pereira-Filho, Quimica Nova (2023) 747-754

"Electronic waste analysis using laser-induced breakdown spectroscopy (LIBS) and X-ray fluorescence (XRF): Critical evaluation of data fusion for the determination of Al, Cu and Fe"

Dennis da Silva Ferreira, Fabiola Manhas Verbi Pereira, Alejandro César Olivieri, Edenir Rodrigues Pereira-Filho, Analytica Chimica Acta (2024) 342522

"A preliminary study of a sequential leaching process to recover Ag, Au, Cu, and Sn from E-waste"

Dennis Silva Ferreira, Edenir Rodrigues Pereira-Filho, Hydrometallurgy (2025) 106476

"LIBS and Hyperspectral Imaging as a Real-Time Process Control Tool for Metal Recovery from E-Waste"

Dennis Silva Ferreira, Edenir Rodrigues Pereira-Filho, Journal of the Brazilian Chemical Society (JBCS) (2025) 20250130

LIST OF ACRONYMS

μ-ED-XRF	Micro-Energy-Dispersive X-ray Fluorescence
AAS	Atomic Absorption Spectrometry
ABS	Acrylonitrile-Butadiene-Styrene
ANATEL	Agência Nacional de Telecomunicações
ANN	Artificial Neural Networks
CCD	Charge-Coupled Device
CFC	Chlorofluorocarbon
CPCB	Central Pollution Control Board
CPS	Cyber-Physical Systems
CRT	Cathode Ray Tube
DVD	Digital Versatile Disc
ECPR	Error Covariance Penalized Regression
ED-XRF	Energy-Dispersive X-ray Fluorescence
EEE	Electrical and Electronic Equipment
EoL	End of Life
FTIR	Fourier Transform Infrared
IBGE	Instituto Brasileiro de Geografia e Estatística
ICCD	Intensified Charge-Coupled Device
ICP OES	Inductively Coupled Plasma Optical Emission Spectrometry
ICP-MS	Inductively Coupled Plasma Mass Spectrometry
IR	Infrared
IT	Information Technology
LCD	Liquid Crystal Display
LED	Light-Emitting Diode
LIBS	Laser-Induced Breakdown Spectroscopy
LoD	Limits of Detection
LoQ	Limits of Quantification
MLE	Maximum Likelihood Estimation
MLPCR	Maximum Likelihood Principal Component Regression
MLR	Multiple Linear Regression
Mt	Megaton (million metric tons)
NIR	Near-Infrared

PAHs	Polycyclic Aromatic Hydrocarbons
PBB	Polybrominated Biphenyls
PBDE	Polybrominated Diphenyl Ethers
PCA	Principal Component Analysis
PCB	Printed Circuit Board
PCR	Principal Component Regression
PDD	Persistent Organic Pollutants from Domestic Devices
PLS	Partial Least Squares
PNAD	Pesquisa Nacional por Amostra de Domicílios
PNRS	Política Nacional de Resíduos Sólidos
PSO	Particle Swarm Optimization
RoHS	Restriction of Hazardous Substances
SVM	Support Vector Machines
UN	United Nations (Nações Unidas)
UNITAR	United Nations Institute for Training and Research
USA	United States of America
WD-XRF	Wavelength-Dispersive X-ray Fluorescence
WEEE	Waste Electrical and Electronic Equipment
XRF	X-ray Fluorescence

LIST OF FIGURES

LIST OF TABLES

RESUMO

CARACTERIZAÇÃO QUÍMICA E PROPOSTA DE RECUPERAÇÃO DE ELEMENTOS NOBRES DE LIXO ELETRÔNICO. Esta tese aborda a problemática dos resíduos de equipamentos eletroeletrônicos (REEE), um desafio ambiental e uma oportunidade de mineração urbana. Globalmente, 62 milhões de toneladas foram geradas em 2022, com apenas 22,3% de reciclagem, apesar de conterem um valor estimado de 91 bilhões de dólares em metais como Au, Ag, Cu e Sn. Diante desse cenário, o objetivo desta tese foi desenvolver e propor uma abordagem sustentável para a caracterização química e a recuperação seletiva desses metais a partir de placas de circuito impresso (PCIs). A metodologia de caracterização priorizou métodos analíticos diretos para minimizar a preparação de amostras e o risco de contaminação. Foram utilizadas as técnicas de espectroscopia de emissão óptica com plasma induzido por laser (LIBS) e fluorescência de raios X por dispersão de energia (ED-XRF), com os dados espectrais complexos sendo tratados por ferramentas quimiométricas e rotinas computacionais desenvolvidas para esse fim. A Análise de Componentes Principais (PCA) foi fundamental para a análise exploratória e para a geração de imagens hiperespectrais, que permitiram visualizar a distribuição espacial dos elementos nas amostras. Adicionalmente, foram exploradas estratégias de fusão de dados de LIBS e ED-XRF com modelos de regressão como MLPCR e ECPR, foram exploradas para aprimorar a quantificação. Para a recuperação dos metais, foi desenvolvida uma rota hidrometalúrgica, uma alternativa mais sustentável aos processos pirometalúrgicos tradicionais por operar em temperaturas abaixo de 100 °C e evitar a formação de subprodutos perigosos como dioxinas e furanos. O método consistiu em um processo de lixiviação sequencial, cuja sequência mais eficiente e de baixo impacto ambiental foi: i) lixiviação de Cu com HNO_3; ii) extração de Sn com HCl; e iii) coextração de Ag e Au com uma solução de I_2/KI. A principal inovação foi a aplicação da LIBS combinada com imagens hiperespectrais como ferramenta de controle de processo em tempo real. Esta abordagem permitiu monitorar a eficiência de cada etapa de lixiviação de forma rápida, econômica e com resolução espacial. A análise espacial confirmou a uniformidade da extração, superando a limitação de métodos convencionais que fornecem apenas concentrações médias. Os resultados, validados pela técnica de referência ICP OES, confirmaram a eficácia do processo, com taxas de recuperação de 100% para Cu e Ag, 97% para Sn e 86% para Au. Esta tese, portanto, válida uma rota tecnológica viável para a mineração urbana, promovendo a economia circular e oferecendo uma solução sustentável para a valorização do lixo eletrônico, com potencial aplicação em escala industrial.

ABSTRACT

CHEMICAL CHARACTERIZATION AND PROPOSED RECOVERY OF NOBLE ELEMENTS FROM ELECTRONIC WASTE. This thesis addresses the issue of waste electrical and electronic equipment (WEEE), an environmental challenge and an opportunity for urban mining. Globally, 62 million tons were generated in 2022, with only 22.3% recycled, despite containing an estimated value of US$91 billion in metals such as Au, Ag, Cu, and Sn. Given this scenario, the objective of this thesis was to develop and propose a sustainable approach for the chemical characterization and selective recovery of these metals from printed circuit boards (PCBs). The characterization methodology prioritized direct analytical methods to minimize sample preparation and the risk of contamination. Laser-induced breakdown spectroscopy (LIBS) and energy-dispersive X-ray fluorescence (ED-XRF) techniques were used, with complex spectral data being processed by chemometric tools and computational routines developed for this purpose. Principal Component Analysis (PCA) was fundamental for exploratory analysis and for generating hyperspectral images, which allowed the spatial distribution of elements in the samples to be visualized. In addition, strategies for merging LIBS and ED-XRF data with regression models such as MLPCR and ECPR were explored to improve quantification. For metal recovery, a hydrometallurgical route was developed, a more sustainable alternative to traditional pyrometallurgical processes because it operates at temperatures below 100 °C and avoids the formation of hazardous by-products such as dioxins and furans. The method consisted of a sequential leaching process, whose most efficient and environmentally friendly sequence was: i) Cu leaching with HNO_3; ii) Sn extraction with HCl; and iii) co-extraction of Ag and Au with an I_2/KI solution. The main innovation was the application of LIBS combined with hyperspectral imaging as a real-time process control tool. This approach allowed the efficiency of each leaching step to be monitored quickly, economically, and with spatial resolution. Spatial analysis confirmed the uniformity of extraction, overcoming the limitation of conventional methods that only provide average concentrations. The results, validated by the ICP OES reference technique, confirmed the effectiveness of the process, with recovery rates of 100% for Cu and Ag, 97% for Sn, and 86% for Au. This thesis, therefore, validates a viable technological route for urban mining, promoting the circular economy and offering a sustainable solution for the recovery of electronic waste, with potential application on an industrial scale.

SUMMARY

Chapter 1 - Introduction

Motivation

This thesis is organized into five chapters, which were structured based on experimental studies and analyses applied to the characterization and reuse of metals present in waste electrical and electronic equipment (WEEE). The growing volume of WEEE and the environmental impacts associated with its poor management have motivated the search for fast, sustainable and effective analytical solutions. Given this scenario, this study proposes integrated approaches that involve chemical and spectroscopic characterization of materials to the development of recovery methods based on sequential leaching and optical monitoring techniques.

Chapter 1 presents a comprehensive review of the topic of electrical and electronic waste, covering its classification, the main recycling processes and the legislative aspects applicable in Brazil and other countries. This chapter aims to contextualize the importance of the topic in the scientific, environmental and economic scenario, laying the foundations for subsequent discussions.

Chapter 2 details the procedures for the chemical characterization of electronic waste, with emphasis on the application of principal component analysis (PCA) as a chemometric tool for the treatment of large volumes of spectral data. This chapter is based on the article:

"Principal component analysis (PCA) for the evaluation of chemical data and the generation of heat maps: A tutorial" (Química Nova, 2023).

Chapter 3 presents an analytical method for the non-destructive analysis and quantification of metals in WEEE, based on the fusion of data from the Laser-Induced Breakdown Spectroscopy (LIBS) and Energy Dispersive X-ray Fluorescence (ED-XRF) techniques. The fusion of data at different levels, associated with multivariate calibration, is discussed as a strategy to increase the sensitivity and robustness of the models. This chapter corresponds to the article:

"Electronic waste analysis using laser-induced breakdown spectroscopy (LIBS) and X-ray fluorescence (XRF): Critical evaluation of data fusion for the determination of Al, Cu and Fe" (Analytica Chimica Acta, 2024).

Chapter 4 proposes optimized sequential leaching protocols for the selective recovery of valuable metals present in printed circuit boards (PCBs), using reagents with a lower environmental impact. In addition, real-time monitoring data with LIBS and hyperspectral images are presented, demonstrating the feasibility of direct analytical control during the extraction process. This chapter brings together the results of two published articles:

"A preliminary study of a sequential leaching process to recover Ag, Au, Cu, and Sn from E-waste" (Hydrometallurgy, 2025)

And

"LIBS and Hyperspectral Imaging as a Real-Time Process Control Tool for Metal Recovery from E-Waste " (Journal of the Brazilian Chemical Society, 2025).

Finally, Chapter 5 presents the general conclusions of the study, highlighting the contributions of the thesis to the advancement of analytical method applied to the recovery of electronic waste, as well as pointing out prospects for future research aimed at sustainability, circular economy and technological innovation in the treatment of WEEE.

1. Introduction

1.1. What is electronic waste (e-waste)?

Electrical and electronic equipment (EEE) has been evolving at an increasingly fast pace over the last few decades. The fast development of these electronics is related to the constant evolution of technology, the short life cycle, and technological innovations of many electronic devices. As new models and features are introduced to the market, consumers are encouraged to upgrade their devices, making old ones obsolete in a short interval of time. In addition, the demand for faster, more efficient and multifunctional electronic devices stimulates the frequent replacement of old products, which consequently generate a large increase in the accumulation of these instruments [1–3].

This WEEE is known as electronic waste or e-waste and is defined as any equipment at the end of its life (EoL). It covers a wide range of electronic equipment such as household appliances, information technology (IT) equipment, medical devices and consumer electronics such as computers and cell phones [4].

The accumulation of e-waste is directly linked to the consumption of accelerated EEE. In general, 2.5 million metric tons (Mt) are produced per year globally. The amount of e-waste generated has increased significantly over the years. According to data from the E-waste Global monitor, the global generation of WEEE in 2019 was 53.6 Mt, equivalent to filling 120 Empire States buildings with an average of 6.9 kg per person. The main WEEE generating countries are the United States of America (USA) and China. In China it is estimated that 10.1 Mt are generated per year at an average of 7.2 kg per person and in the United States 6.9 Mt at an average of 21 kg per person [5].

The flow of this type of waste is the fastest growing in the world, growing by 3% to 5% a year. It is estimated that this waste represents 8% of urban waste. According to the United Nations (UN), 20 to 50 Mt of e-waste is generated every year worldwide and only 20-25% of this volume is formally recycled. During the COVID-19 pandemic period there was a reduction of 4.9 Mt in the first quarters of 2020 [5,6]. In 2022, the United Nations Institute for Training and Research (UNITAR) estimated that 62.0 million tons of electronic waste were generated, of which only 22.3% was properly recycled [7]. WEEE is expected to exceed 74 Mt in 2030 and reach 110 Mt in 2050 [8].

1.2. Classification and disposal of EEE

In general, EEE can be divided into: TVs, computers, notebooks, smartphones, Digital Versatile Disc (DVD) players, washing machines, refrigerators, monitors and so on. Figure 1 classifies e-waste into two types: electronic (50%) from electronic products and electrical (50%) from household appliances [9].

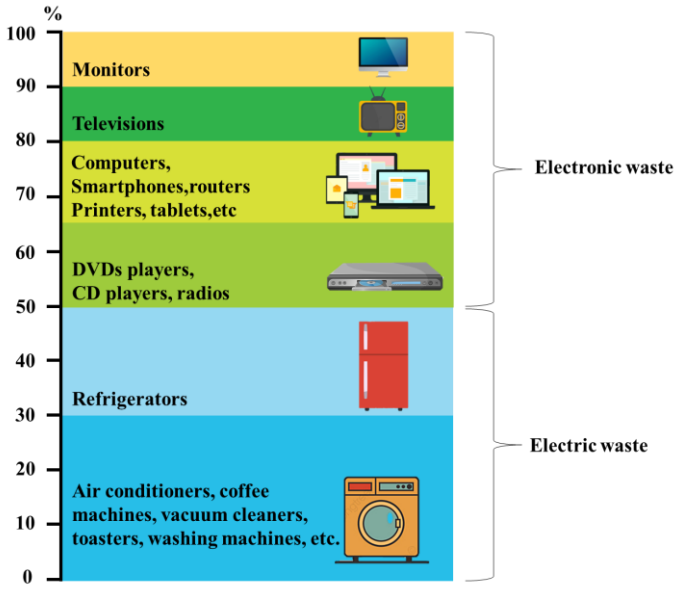

FIGURE 1 - Classification of electronic waste.

Electronic waste can be divided into three categories: large household appliances (refrigerators and washing machines), information and communication technologies (computers, notebooks, monitors) and consumer equipment (TVs, DVDs, recreation equipment). Electronic components such as batteries, lead capacitors and circuit boards fall into the category of e-waste [10].

Most e-waste is still disposed inaccurately, remaining in households, or being donated inappropriately, or even exported illegally from developed to developing countries. These attitudes can have a serious impact on the environment and human life, affecting the efficiency of recycling companies, which are only able to treat 25% of this material. In addition, there is the increased risk to life of the people who live near the or are exposed to the hazardous compounds [11].

Most of this WEEE is exported to emerging countries such as China, India, Nigeria, Ghana, Pakistan and Kenya, which are considered hot spots for e-waste disposal. These illegal exports do not take into account the safety of recycling workers or environmental impacts, apart from the primitive handling and recycling techniques that need to be improved in these countries [12].

This large volume of WEEE generated is a worrying problem due to its rapid increase and complex global flow. Making it one of the world's main sources of waste, according to a UN report it is estimated that the amount of WEEE produced is increasing exponentially due to various factors such as high consumer demand and a high obsolescence rate leading to the frequent and unnecessary purchase of EEE [13].

1.3. The composition and processing of WEEE

Electronic waste is made up of a variety of materials, such as plastics, metals and glass, most of which can be systematically recovered. Turning these resources back into raw materials for other products. Figure 2 shows the generic material composition of e-waste [14,15].

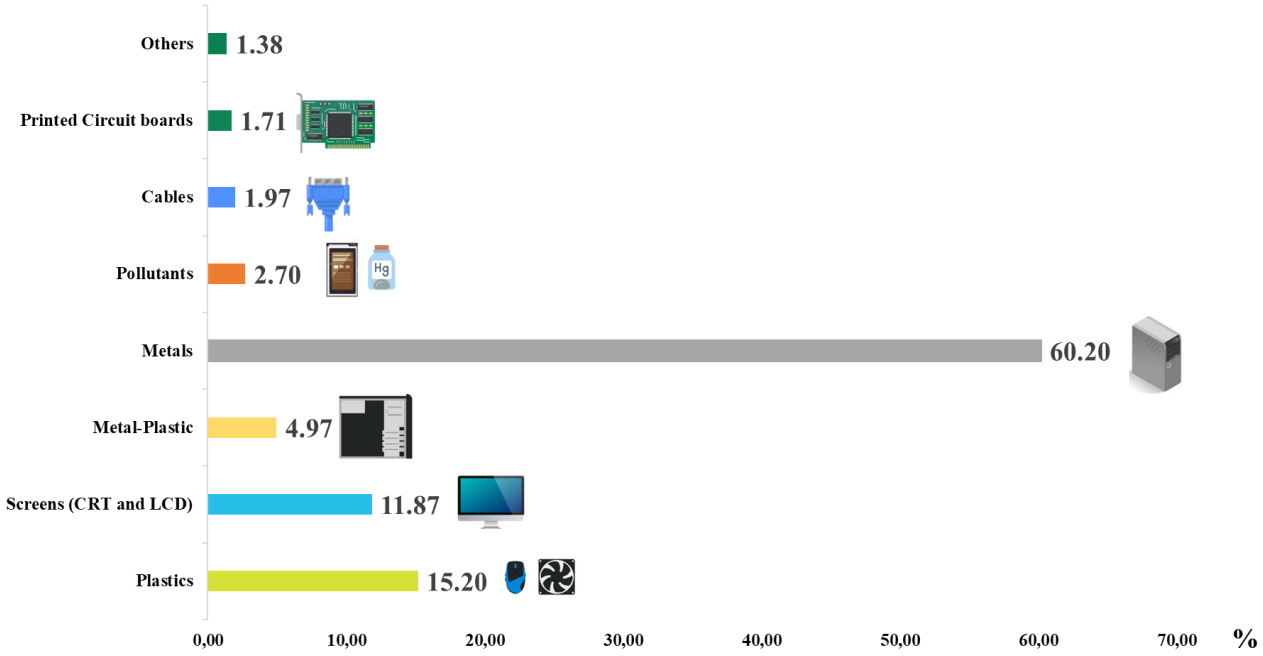

FIGURE 2 - General composition of e-waste.

Valuable metals are found in greater concentration in printed circuit board (PCB), which can reach approximately 30%, and the rest are non-metals (plastics, ceramics and resins). The copper (Cu) content is around 20% and is considered the main metallic constituent. The gold (Au) content varies between 80-250 g/ton, which is much higher than the average extracted in mining companies [16].

However, the exact chemical composition of electronic waste changes significantly with type, age, origin and manufacturer, as can be seen in Table 1, the variability of precious metal concentrations for different types of computers and cell phones from different years and manufacturers [14].

Elements content [% w w^{-1}]					References
Au	Ag	Cu	Pd	Pt	
0.01	0.09	12.20	-	-	Andrade *et al.*, 2019 [17]
0.02	0.09	14.08	-	-	Andrade *et al.*, 2019 [18]
0.05	0.19	14.60	0.02	-	Hubau *et al.*, 2019 [19]
0.14	0.36	33.50	0.01	0.01	Sahan *et al.*, 2019 [20]
0.08	0.44	85.20	0.08	-	Liu *et al.*, 2019 [21]
0.02	0.01	13.79	0.66	0.81	Buechler *et al.*, 2020 [22]
0.22	0.21	49.39	0.01	0.01	Tunali *et al.*, 2021 [23]
0.02	-	14.8	-	-	Andrade *et al.*, 2021 [24]

"- "not reported in the specific work.

TABLE 1- Chemical composition of computers and mobiles.

The content of precious metals is fundamental to the economics of recycling processes, 90% of which is related to the Au, Pd and Pt contained in this electronic waste. For example, recycling 1 million cell phones would generate 24 kg of Au, 250 kg of Ag, 9 kg of Pd, and 9 tons of Cu, the sum of the values of these metals at the current price (2022) would be around $2.26 million dollars [4].

Extracting the value of the metals contained in this waste can be done by formal (regulated, industrial) and informal (unregulated, artisanal) means. The process typically begins with collection, classification, size reduction and processing. The size reduction technique is used to concentrate or release the metals in order to facilitate subsequent metal recovery. In the formal sector, these can be pyrometallurgical and hydrometallurgical processes, in which electronic waste is both a source of metals and energy, but these strategies are only applied in developed countries [25].

In developing countries, e-waste extraction is largely dominated by semi-formal and informal sectors. These operations typically process electronic materials to obtain concentrates of PCBs, which are then sold to formal industries abroad through intermediary collection points. However, this informal recycling results in cross-border flows of materials that are often undocumented or based on unreliable data [12].

While these practices have traditionally focused on the recovery of valuable metals from PCBs, growing attention is now being directed toward the plastic fraction of e-waste. Previously overlooked, these plastics are increasingly recognized as a significant component in e-waste management. They are now being sorted into specific categories such as Acrylonitrile-Butadiene-Styrene (ABS), Polystyrene, Polycarbonate, and Polypropylene for individual recycling processes [26].

In response to this shift, many researchers have begun developing strategies to recycle these distinct plastic types, seeking to offer economically viable and environmentally

sustainable alternatives that transform e-waste plastics into valuable, high-performance materials [12].

1.4. Potentially toxic substances contained in e-waste and their impact on the environment

Electronic waste not only contains precious metals, but also potentially dangerous substances such as Hg, Cd, Pb, hazardous products such as brominated flame retardants, polycyclic aromatic hydrocarbons (PAHs) and plastics. Due to the high demand for new EEE, the inflow of electronic waste is gradually increasing and with it the composition of electronic scrap and these toxic chemicals [14,27].

For example, cell phones usually contain between 500 and 1000 components, which are potentially toxic metals. An old Cathode Ray Tube (CRT) screen contains between 2 to 3 kg of Pb and even when replaced with flat screens, this concentration drops to less than 1 kg of Pb. Liquid Crystal Display (LCD) monitors, light bulbs and alkaline batteries contain Hg, which can be extremely toxic [28,29].

Table 2 shows some hazardous substances contained in WEEE and possible adverse effects on human health.

Substance	WEEE	Adverse Effects	References
Pb	CRT screens, batteries, PCBs, TVs	Vomiting, diarrhea, seizures, insomnia, headaches, coma, death	[30–32]
Hg	Fluorescent lamps, batteries	Brain and liver damage	
Cr	Data tapes, floppy disks	Eye, skin, and mucous membrane irritation	
Cd	NiCd batteries, toners, CRT	Lung cancer, kidney damage, poisoning	
As	Light Emitting Diode (LEDs)	Skin diseases, lung cancer	
Chlorofluorocarbon (CFC)	Refrigerators, insulation foams	Ozone layer impact, increased skin cancer incidence	
Polychlorinated Biphenyls	Capacitors, transformers	Cancer, immune system, reproductive, nervous, and endocrine system effects	
PBDE and Polybrominated Biphenyls (PBB)	Flame retardants in plastics	Hormonal effects; under thermal treatment, forms dioxins and furans	

TABLE 2- Potentially toxic substances in WEEEs.

Due to these potentially toxic elements, proper management of electronic waste is necessary. This waste pollutes groundwater, acidifies the soil, generates smoke and toxic gases after burning, accumulates fast in municipal disposal areas and releases carcinogenic substances into the air. Environmental contamination can be caused by improper recycling and lead to indirect exposure through soil, air and water contamination around recycling areas [13,33].

An example of water contamination was documented in Guiyu in China, a city of reference in informal recycling of electronic waste. Metal-contaminated sediments and high levels of dissolved metals have been reported in rivers around the city. The release of these hazardous chemicals into nature can lead to bioaccumulation, widespread food contamination and ecological exposure [34].

Long-term exposure to these electronic waste products (Persistent Organic Pollutants from Domestic Devices (PDD), Polybrominated Diphenyl Ethers (PBDE) and PAHs) damages physiological systems such as the nervous, reproductive and endocrine systems. They are also carcinogenic and neurotoxic, such as polychlorinated biphenyl's. Evidence of these substances has been identified in the blood, hair and urine of individuals working in conventional e-waste recycling areas [35,36].

An additional source of indirect exposure is individuals who work informally recycling electronic waste and carry these harmful substances on their clothes, materials or other contaminated objects. This is a great risk to the families of these individuals, as they are exposing themselves at low levels, chronically and over the long term. Studies about exposure have indicated high levels of Pb and Cd in children's blood, and they are linked to their parents' involvement in informal e-waste recycling activities. Another point is that children who work collecting recyclable materials suffer the most significant adverse impacts from this type of recycling [37,38].

Environmental contamination and the resulting ecological exposure need intensive research not only because these hazardous materials have the ability to spread over long distances, but also because they have a high capacity for environmental persistence. They have long half-lives and are substances capable of remaining in the environment for long periods. This ecological exposure can have widespread and long-term health risks [35,39].

1.5. Generation, Recycling, Management, and Legislation of E-Waste Around the World

The China and United States are the largest contributors, with the China producing 10.1 Mt (7.2 kg per capita) and USA generating 6.9 Mt (21 kg per capita). Between 2010 and 2019,

global e-waste grew by 58.6%, driven by a 14.7% increase in population and a 46% rise in per capita e-waste generation. This trend highlights the direct correlation between population growth and e-waste production [40]. E-waste accounts for 8% of total urban waste and contains valuable resources, such as precious metals, as well as hazardous substances like Pb and Hg. The rapid disposal of electronic devices highlights the urgent need for recycling to recover materials and mitigate environmental contamination [32].

In China, e-waste management has become a critical issue due to the country's rapid technological advancement. In 2019, China generated 10.12 Mt of e-waste, a figure projected to reach 51.6 Mt by 2050. The majority of e-waste consists of five categories: washing machines, air conditioners, refrigerators, televisions, and computers, with mobile phones representing 46.5% of the remaining waste. Informal recycling dominates in China, particularly in areas like Guiyu, where primitive methods such as open burning and acid washing have led to severe environmental and health hazards [41]. To address these challenges, the Chinese government implemented a four-stage plan, including certification of formal recycling facilities and stricter regulations like the Restriction of Hazardous Substances (RoHS) 2 policy, which restricts hazardous materials in electronics. Despite these efforts, informal recycling persists due to economic factors, highlighting the need for better enforcement and worker protections [42].

India faces similar challenges, ranking as the third-largest e-waste generator with 3.23 Mt in 2019. Projections indicate a fivefold increase in computer waste and an 18-fold rise in mobile phone waste by 2020. Approximately 95% of e-waste in India is processed informally, often by low-income workers using unsafe methods, posing significant health and environmental risks [43]. The government introduced e-waste rules in 2011, mandating producer responsibility and requiring recyclers to register with the Central Pollution Control Board (CPCB). While these measures increased registered recycling units from 23 to 148, only 30% of e-waste is formally recycled. Weak enforcement and lack of monitoring remain major obstacles to effective e-waste management [44].

The United States is the second-largest e-waste producer, generating 6.9 Mt in 2019. Unlike the European Union, which has uniform e-waste policies, the USA lacks a national framework, relying instead on state-level regulations. These policies primarily target TVs and computers due to their high concentrations of hazardous materials like Pb and Hg [45]. Residential e-waste has declined by 10% since 2015, partly due to the replacement of heavy CRT screens with lighter LCD and LED alternatives. However, CRT screens still account for a third of e-waste mass, presenting recycling challenges. About 25 states have implemented e-

waste recycling laws, but inconsistent policies and economic barriers hinder progress. Strategies such as increasing collection sites and promoting consumer participation are essential for improving e-waste management [46].

1.6. Generation, recycling, management and legislation of E-waste in Brazil

Brazil is considered the largest generator of waste in South America, generating 2.4 Mt of electronic waste in 2022, followed by Argentina 0.5 Mt and Colombia 0.4 Mt. Regulatory policies in Latin America have been established at a slow pace, with only Peru and Colombia being the region's main forces in the environmentally correct management of electronic waste. According to the UN, Brazil is also the country that discards the most electronic waste in nature [7,47].

There is no official data on the generation of WEEE in Brazil. However, some studies have indicated that the average potential generated per capita is 2.6 to 3.8 kg/hab/year. The first estimates were based on secondary sales data collected from different sources, leading only to an indicative exploratory analysis [48].

Another estimate was made based on data from the *Pesquisa Nacional por Amostra de Domicílios* – National Household Sample Survey) (PNAD) and the *Instituto Brasileiro de Geografia e Estatística* – Brazilian Institute of Geography and Statistics (IBGE) in 2011. The former surveyed the presence of only 8 EEEs in households, without considering the quantity by type, while a more recent national estimate, based on the volume placed on the market for the base year 2018 (Decree nº 10.240/2020), pointed out that Brazil generates 2.1 million tons of e-waste annually, equivalent to 10.2 kg per inhabitant [49,50].

Studies carried out by Rodrigues and colleagues (2015) estimate that the municipality of São Paulo-SP has 71.9 million EEEs in households, with around 8.8 million EEEs out of use. From 2006 to 2010, 270 tons of WEEE were discarded, and the most discarded EEEs were cell phones, steam irons, fridges, washing machines, and refrigerators [51].

On a national scale, it's no different. According to *Agência Nacional de Telecomunicações* – Brazilian National Telecommunications Agency (ANATEL), there are 202.7 million cell phones in circulation, which allows us to project the possibility of recovering 26 tons of Cu and 68.9 kg of Au. On average in Brazil, a cell phone is discarded every 1.5 years (18 months) due to programmed obsolescence, marketing strategies, and the business strategies of manufacturers and operators that force consumers to look for new devices [52].

Environmental justice also bears responsibility for electronic waste, since 80% of this e-waste is transported from developed countries to developing countries (Africa, India, and

Asia) for inadequate repair and recycling. This issue of illegal imports is no different in Brazil, where governments are aware of the environmental issues surrounding electronic waste [52].

While public participation can be improved, the implementation of policies associated with electronic waste has advanced significantly. In Brazil, the *Política Nacional de Resíduos Sólidos* (PNRS), implemented in 2010, obliges the structuring of reverse logistics systems. This system is now formally operational, managed by entities like Abree and Green Eletron, with progressive recovery goals based on the volume of products placed on the market in the base year of 2018. For 2023, the goal was to recover 6% of this 2018 volume. Demonstrating the system's progress, the entity Green Eletron recovered 4,280 tons, exceeding the target by reaching 6.4% of the baseline. Although 2023 data for the Abree entity was not available, its recovery in 2022 amounted to 15,350 tons. The system is designed for growth, with the recovery goal for 2024 set to increase to 12% of the 2018 market volume [53,54].

1.7. Goal and scope of this PhD thesis

The main goal of this thesis was to propose environmentally friendly sequential recovery methods for precious metals (such as Au and Ag,) in PCB samples, using spectroanalytical techniques such as LIBS and ED-XRF as operational screening between the leaching steps.

To test the central hypothesis that the integration of rapid, non-destructive spectroanalytical techniques (LIBS and ED-XRF) as a screening tool can increase the efficiency and reduce the costs of the sequential leaching process compared to traditional methods, the following specific objectives were established:

- Literature review on the characterization and leaching of electronic waste;
- Develop an analytical method for the characterization and direct determination of precious and base metals (Al, Cu, Fe) in electronic waste;
- Fusion data from LIBS and ED-XRF analyses;
- Developing an analytical method for selective leaching of Ag, Au, Cu and Sn, and designing a sequential procedure for these leaching's;
- To develop an alternative non-destructive method using the LIBS technique as a screening in the sequencing of leaching's;
- Use of chemometrics to design or select optimal measurement procedures and experiments and provide maximum relevant chemical information through the analysis of chemical data.

Chapter 2 - Characterization and direct analysis of e-waste samples

2. Characterization and direct analysis of e-waste samples

2.1. Direct solid sample analysis

Most traditional analytical techniques are applied to samples in the liquid state, due to their ease of handling and analysis. However, a large proportion of samples are naturally available in the solid state, which makes prior preparation necessary, consisting of conversion from the solid to the liquid state. These additional steps can represent disadvantages in the analytical process since they depend on the characteristics of the sample, the analytes present, and their concentrations [55]. This preparation step can introduce a series of systematic errors, such as contamination or loss of analytes through volatilization, directly affecting the precision and accuracy of the results obtained [56].

Direct sampling of solids has emerged as an efficient alternative to conventional sample preparation, allowing information on elemental composition to be obtained without the need for extensive chemical treatments or complex preparation [57]. This method has several advantages over the traditional wet procedure, such as the reduction or elimination of pre-treatment, minimizing the risk of contamination and loss of analytes. In addition, there is a significant reduction in the use of chemical reagents and the generation of waste, making the process more sustainable. This direct analysis approach also requires a reduced amount of sample, offering rapid analysis and results with high analytical yields [58,59].

Despite these advantages, direct analysis of solids presents intrinsic challenges and disadvantages that cannot be ignored. One of the main limitations is sample heterogeneity. Unlike homogeneous liquid solutions, solids often have an uneven distribution of their components, which can lead to results that are not representative of the whole [60]. Another critical obstacle is matrix effects, where the overall composition of the sample (the matrix) can suppress or intensify the analyte signal, complicating accurate quantification [61]. In addition, calibration for quantitative analysis is notably more complex, as it requires solid calibration standards with a matrix similar to that of the sample (matrix-matched), which are difficult to obtain or prepare [62].

In this context, some analytical elemental analysis techniques, such as Energy Dispersive X-ray Fluorescence (ED-XRF), Wavelength Dispersive X-ray Fluorescence (WD-XRF), and Laser-Induced Breakdown Spectroscopy (LIBS), can be used for direct analysis of solid samples. These techniques can also be complemented by wet analysis methods, such as Inductively Coupled Plasma Optical Emission Spectrometry (ICP OES).

This chapter will discuss X-ray fluorescence and plasma techniques based on LIBS applied to the direct analysis of PCB samples. The following sections will present a discussion of the main fundamentals and aspects of these techniques, considering their qualitative and quantitative applications in the direct analysis of solid samples.

2.1.1. LIBS as an alternative technique

LIBS is an analytical technique that stands out for its versatility, speed and ability to carry out multi-element analysis in a practically non-destructive way and with minimal sample preparation [63]. The principle of the technique is based on focusing a high-energy laser pulse - usually from Nd:YAG systems operating at 1064 nm - on the surface of the sample, ablating a small fraction of the material, which is vaporized, atomized and ionized, forming a plasma with temperatures of over 10,000 K [64]. During the relaxation of the atoms, ions, and transient diatomic molecules present in this plasma, radiation, composed of both sharp atomic/ionic lines and broad molecular bands, is emitted at characteristic wavelengths, which are collected by an optical system and directed to a spectrometer coupled to detectors, such as Charge-Coupled Device (CCD) or Intensified Charge-Coupled Device (ICCD), making it possible to identify and quantify the elements present [65].

The typical instrumentation of a LIBS system consists of a laser source, optical elements for focusing, a sample holder, a system for collecting the radiation emitted via optical fiber, a spectrometer and a detector, all integrated with a computer system for control and data acquisition, see the components of the LIBS system in Fig. 3 [66]. This arrangement gives the technique one of its main advantages: the possibility of carrying out direct analysis on solid, liquid or gaseous samples, often without the need for complex preparation steps such as chemical digestions or prior separations [67]. In fact, the possibility of direct analysis represents a distinctive and strategic feature of LIBS, contributing to its wide application in contexts where speed, portability and minimizing the use of reagents are essential, such as in environmental, metallurgical, forensic and electronic waste monitoring analyses [68].

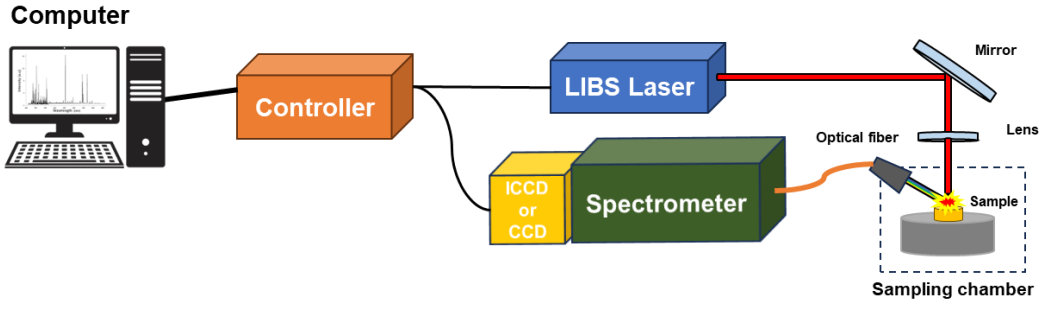

FIGURE 3 - A schematic of a typical LIBS system.

In addition, LIBS stands out for enabling simultaneous multielement analysis, since the formation of the plasma induces the emission of multiple spectral lines associated with the various elements present in the sample, providing a complete spectral profile in a few seconds [69]. The high analytical frequency, the practically non-destructive nature - given that only a tiny fraction of the sample is consumed during ablation - and the possibility of carrying out in situ and remote analyses are attributes that give LIBS a high degree of applicability and flexibility, particularly in situations that require fast and reliable analytical responses [70].

These characteristics, together with the simplicity and robustness of the instruments, explain the exponential growth in scientific and technological interest in LIBS in recent decades. The technique has thus established itself as one of the most promising in the field of analytical chemistry and is continually being improved in terms of instrumentation and methodological approaches [71,72].

2.1.2. XRF non-destructive technique

The XRF analytical technique is well-established and widely used for the qualitative and quantitative analysis of materials in various matrices, and is particularly valued for its multielement capacity, speed, non-destructiveness and the possibility of direct analysis of solid, liquid or gaseous samples [73]. Based on the interaction between ionizing radiation and matter, the technique consists of the excitation of the atoms present in the sample through the incidence of primary radiation (usually from X-ray tubes or radioactive sources), causing the ejection of electrons from the inner layers and the subsequent emission of characteristic radiation, which is detected and analyzed spectrometrically [74].

The principle of XRF is therefore based on the detection of these characteristic emissions, which allow the elements present in the sample to be identified and quantified. There are two main configurations of XRF spectrometers: ED-XRF (Fig. 4a) and WD-XRF (Fig. 4b). WD-XRF, traditionally used in industrial and laboratory applications, offers high spectral resolution by using single crystals to discriminate the energies emitted; ED-XRF, on the other hand, uses semiconductor detectors, providing simultaneous multi-element analysis, with more compact and often portable equipment [75]. Recent advances in miniaturized sources, ultra-thin window detectors and high-efficiency optical systems have significantly expanded the analytical reach of XRF, especially for low atomic number elements and for two- and three-dimensional imaging applications with micrometric resolution [76].

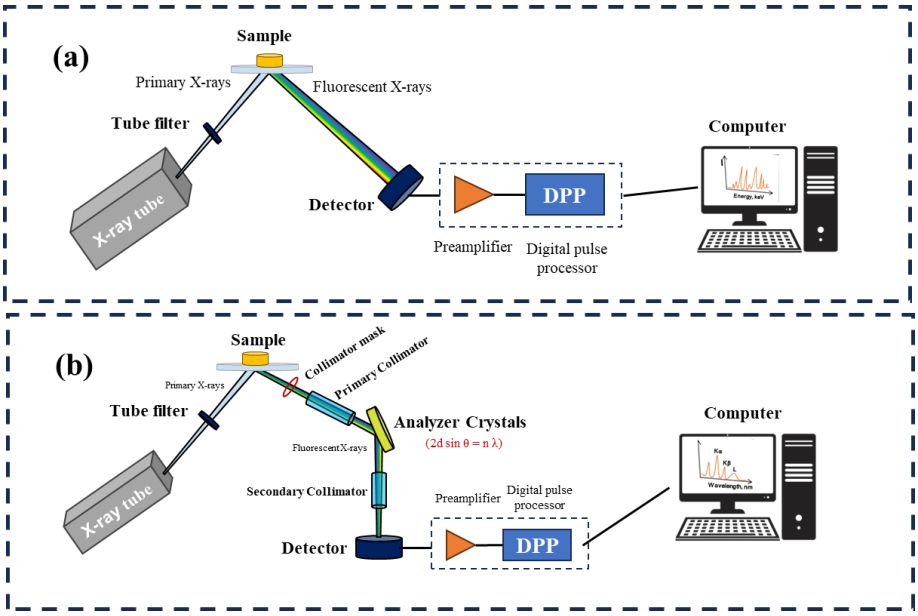

FIGURE 4- Schematic of a typical ED-XRF (a) and WD-XRF (b) systems.

Among the main advantages of XRF is the possibility of carrying out direct analysis of samples, often without the need for complex preparation steps, such as acid digestions, which are common in conventional atomic spectrometry techniques [77]. This feature not only reduces the time and cost of analysis, but also minimizes the generation of chemical waste, in line with the principles of Green Analytical Chemistry. The portability of various ED-XRF systems also enables in situ and real-time analysis, which is particularly useful for environmental, archaeological and industrial assessments [78].

Moreover, XRF has adequate sensitivity to detect absolute mass as low as 10^{-8} g (µ-ED-XRF), depending on the element and the instrumental configuration used [79]. The non-destructive nature and simultaneous multi-element analysis capabilities make the technique extremely attractive for applications involving valuable or unrecoverable samples, such as archaeological artifacts and works of art [80,81]. The development of portable and micro-XRF (µ-ED-XRF) systems with capillary focusing optics and pixelated detectors has boosted new applications, such as obtaining elemental images on a micro-scale, expanding the technique's potential in environmental, forensic, biological and cultural heritage investigations [82–84].

2.1.3. Quantitative and qualitative analysis

In recent decades, the association of spectroanalytical techniques, such as XRF and LIBS, with chemometric methods has significantly boosted advances in materials analysis, especially in the direct evaluation of solid samples [85]. The large volume of spectral data generated by these techniques, often characterized by high dimensionality and complexity,

requires robust mathematical-statistical approaches for the efficient extraction of relevant chemical information [86].

Chemometrics, in this context, has emerged as an indispensable field for the treatment and interpretation of analytical data from XRF and LIBS. Techniques such as PCA and Partial Least Squares (PLS) regression have become standard tools, not only for multivariate calibration, but above all for exploratory data analysis, sample classification and the detection of hidden patterns [87,88].

In the context of exploratory analysis, PCA plays a central role by reducing the dimensionality of the data, preserving as much variance as possible, which facilitates the visualization and interpretation of trends and natural groupings between samples. In the case of LIBS, whose spectral acquisition involves multiple emission lines simultaneously, PCA is widely applied to discriminate classes of materials, identify spectral interferences and understand the sources of variability associated with sample heterogeneity or experimental conditions [89].

Recent studies show that the application of PCA associated with LIBS is particularly effective in distinguishing different types of e-waste, allowing not only the identification of materials of interest, such as Cu and Al, but also the spatial visualization of their distribution through the construction of hyperspectral maps [90,91]. This type of approach makes it easier, for example, to target recycling processes, minimizing costs and environmental impacts.

With regard to XRF, the use of PCA also stands out in the exploratory evaluation of data, especially in archaeometric and environmental studies, where the identification of groups or patterns related to the origin or degree of contamination of samples is fundamental [92,93]. The ease of XRF in generating multielement spectra quickly and without destructive preparation, coupled with PCA's ability to reveal latent structures in the data, makes this combination highly efficient in contexts that require analytical screening of large sets of samples [94].

In summary, the incorporation of chemometric methods into the analysis of XRF and LIBS data represents a significant advance, enabling not only more precise calibration of quantitative models, but above all, promoting a deeper and more integrated understanding of the systems analyzed. Among these approaches, PCA stands out, whose application in the exploratory analysis of spectral data is essential for identifying patterns, groupings and anomalies, playing a strategic role in the development of more efficient and sustainable analytical methods [95–97].

2.2. Elemental determination by ICP OES

The ICP OES analytical technique has established itself in recent decades as one of the most powerful and versatile techniques for multi-element determination in various areas, such as environmental, industrial, food, pharmaceutical and geological analysis [98,99]. Its popularity stems mainly from its ability to carry out simultaneous analysis of multiple elements with high sensitivity, wide linear dynamic range, high tolerance to matrix effects and low limits of detection, reaching levels in the order of μg L^{-1} [100].

The fundamental principle of ICP OES is based on introducing the sample - typically in liquid form - into a radiofrequency-induced argon plasma, where it is rapidly desolvated, vaporized, atomized and excited [101]. The excitation of the atoms and ions present results in the emission of electromagnetic radiation at characteristic wavelengths, proportional to the concentration of the elements analyzed. The emitted radiation is spectrally separated using optical systems such as monochromators or Echelle spectrometers, and detected by semiconductor devices such as CCDs, which convert the light intensity into electrical signals processed by specialized software, see a brief schematic of the technique in Fig. 5 [102].

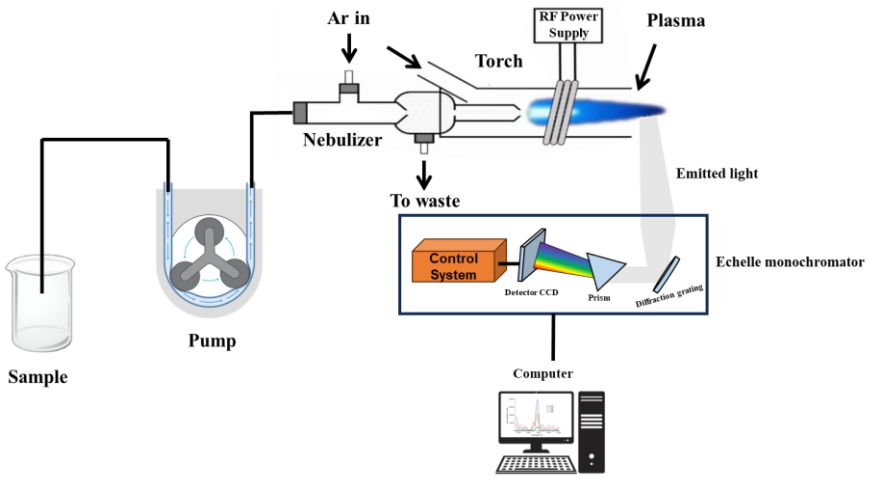

FIGURE 5- Schematic of an ICP OES operating system.

Among the instrumental configurations available are sequential systems, which read each element successively, and simultaneous systems, which allow multiple elements to be analyzed in real time. The introduction of advances such as ultrasonic nebulizers and detection systems with Echelle spectrometers has provided substantial improvements in the sensitivity, precision and robustness of the technique [103,104]. In addition, the versatility of ICP OES allows for the analysis of different types of samples, including aqueous solutions, organic matrices and, with appropriate preparation procedures, solid and gaseous samples [105,106].

The advantages of ICP OES are widely recognized: in addition to multielementarity and high sensitivity, the short analysis time, robustness to chemical and spectral interferences, and the ability to operate with high analytical yield, reaching up to 70 elements simultaneously [99,107]. Compared to other spectroanalytical techniques, such as atomic absorption spectrometry (AAS) and inductively coupled plasma mass spectrometry (ICP-MS), ICP OES offers a balance between cost, performance and operational ease, and is particularly advantageous in applications that require routine analysis of large volumes of samples with adequate precision and accuracy [108,109].

This chapter presents a study of the characterization of e-waste by ICP OES, ED-XRF and LIBS, complemented by exploratory analyses by PCA and heatmap.

2.3. Principal Component Analysis (PCA) for chemical data evaluation and heat maps preparation: A tutorial

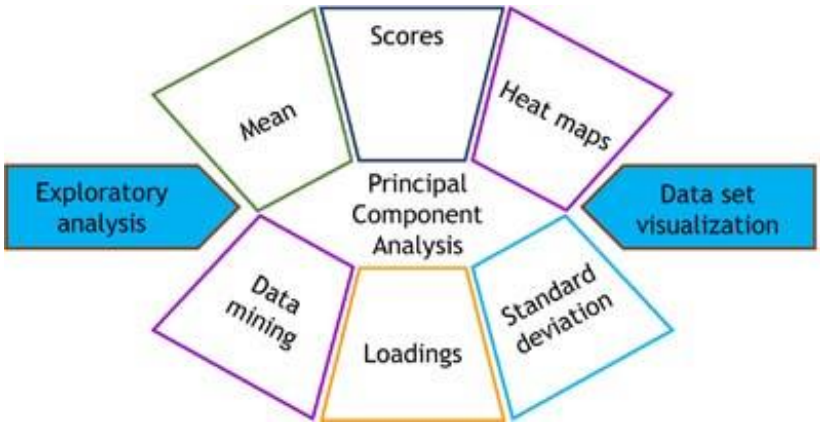

Nota Técnica

PRINCIPAL COMPONENT ANALYSIS (PCA) PARA A AVALIAÇÃO DE DADOS QUÍMICOS E GERAÇÃO DE *HEAT MAPS*: UM TUTORIAL

Dennis da Silva Ferreira[a], Leticia da Silva Rodrigues[b], Fabiola Manhas Verbi Pereira[b] e Edenir Rodrigues Pereira-Filho[a,*]

[a]Departamento de Química, Universidade Federal de São Carlos, 13565-905 São Carlos – SP, Brasil
[b]Instituto de Química, Universidade Estadual Paulista, 14800-060 Araraquara – SP, Brasil

Recebido em 17/10/2022; aceito em 11/01/2023; publicado na web 08/03/2023

PRINCIPAL COMPONENT ANALYSIS (PCA) FOR CHEMICAL DATA EVALUATION AND HEAT MAPS PREPARATION: A TUTORIAL. This tutorial shows a step-by-step guide on handling big datasets using principal component analysis (PCA). A dataset of chemical elements' concentration, emission spectrum, and energy-dispersive X-ray fluorescence (EDXRF) of e-waste were used as examples. Five routines were proposed to apply data processing and PCA calculation focusing data from laser-induced breakdown spectroscopy (LIBS), EDXRF, and heat maps preparation. These routines can be used in various softwares such as MatLab, Octave, R, and Python. PCA was applied in three examples; the first was for concentrations, and the other two were for spectra. An example of heat maps assembling a hyperspectral image of a printed circuit was also described. In addition, a playlist was created on YouTube using the available examples. Therefore, with this tutorial, it may be possible to learn how to deal with a large volume of data by applying PCA. The authors hope to contribute to those researching in the area.

Keywords: exploratory analysis; data mining; data visualization; direct solid sample analysis; laser; X-ray fluorescence.

INTRODUÇÃO

A tecnologia na geração de dados está presente em diversos segmentos da sociedade contemporânea e impacta significativamente o cotidiano das pessoas.[1] De forma geral, uma única pessoa pode gerar e/ou transmitir cerca de 3 Mbytes de dados por segundo. A geração de dados atingiu cifras elevadas, onde cerca de 64 Zettabytes (10^{21}) foram gerados no ano de 2020 e estima-se que essa marca possa atingir mais de 180 até 2025.[2] A área de química não fica em desvantagem neste aspecto, pois a instrumentação analítica moderna aliada ao rápido desenvolvimento tecnológico tem permitido a obtenção de sinais de diversas regiões do espectro eletromagnético e de outras fontes, tais como fluorescência de raios-X (*X-ray fluorescence*, XRF), ultravioleta (*ultraviolet*, UV), visível (Vis), infravermelho (*infrared*, IR), de massas, entre outros. Todos esses dados podem ser obtidos em um curto intervalo de tempo e com uma facilidade jamais vista.[3,4]

A correta organização, transformação e interpretação dos dados em informações é uma tarefa crucial para qualquer tipo de análise. A Quimiometria[5] e a análise exploratória de dados[6] têm papel fundamental nesse aspecto com a apresentação de uma gama diversificada de ferramentas, como exemplo, a *principal component analysis* (PCA)[7,8] que possibilita a projeção dos dados multidimensionais em um número reduzido de variáveis denominadas *principal component* (PC), como mostra a equação 1:[8,9]

$$X = TL^T \quad (1)$$

onde a matriz X contém os dados de interesse, que são decompostos em duas matrizes: a de *scores* T e a matriz ortonormal de pesos ou *loadings* L. *Scores* e *loadings* trazem informações das amostras e das variáveis, respectivamente. Com a análise exploratória e mineração de dados (*data mining*) é possível também ter uma melhor compreensão das informações, identificando a correlação entre as variáveis e informações subjacentes. Assim, é possível a identificação das principais características dos dados, possibilitando a tomada de decisões. A PCA[10] ocupa um papel importante neste tipo de tratamento de dados sendo a ferramenta mais comumente empregada na química.

Assim, neste terceiro tutorial de uma série que teve início em 2018,[11] e uma continuidade em 2021,[12] o objetivo é mostrar a aplicação da PCA em três exemplos: (i) dados de concentrações de elementos químicos; (ii) espectros de emissão obtidos por *laser-induced breakdown spectroscopy* (LIBS) e de ED-XRF (*energy-dispersive* XRF) e (iii) obtenção de *heat maps* por meio de imagens hiperspectrais.[13] Os tópicos que serão abordados visam também, complementar as publicações sobre a PCA e anteriormente apresentadas pelos grupos dos professores Poppi,[14] Ferreira,[15] Fragoso[16] e Valderrama.[17]

PARTE EXPERIMENTAL

Variáveis provenientes de concentrações de elementos químicos

Nesta parte do tutorial foram utilizados resíduos eletrônicos (*e-waste*) compostos por computadores (*desktops* e *laptops*), celulares e *tablets*. O resíduo obtido foi desmontado e segregado em diferentes partes: polímeros, cabos e circuitos eletrônicos (*printed circuit board*, PCB). O objetivo foi a determinação de analitos, tais como elementos nobres (Ag, Au, Pt e Pd), convencionais ou metais base (Al, Cu e Fe) e potencialmente tóxicos (As, Cr e Pb) nos PCB's. Ao todo foram obtidos dois *desktops*, quatro *laptops*, sete celulares e três *tablets*. As PCB's foram moídas em moinho de facas (Tecnal TE-650, Piracicaba, Brasil), peneiradas e segregadas em quatro diferentes tamanhos de partícula: (i) < 106 µm; (ii) 106-212 µm; (iii) 212-600 µm e (iv) > 600 µm. Ao final do processo de peneiramento foram obtidas 57 amostras.

O material foi mineralizado em bloco digestor (Marconi MA4025, Piracicaba, Brasil) com o emprego de água régia diluída 1:1 com água desionizada Milli-Q e frascos fechados de tetrafluoroethylene-perfluoro (alkoxy vinyl ether) (PFA). A temperatura de aquecimento

*e-mail: erpf@ufscar.br

dos tubos foi de 95 °C e o tempo de preparo foi da ordem de 2 horas. O extrato ácido resultante foi diluído para 50 mL com água desionizada e as determinações foram executadas em ICP OES (Thermo Fisher, iCap 7000 series, EUA). A Tabela 1 mostra as condições instrumentais empregadas nas determinações por ICP OES. A acurácia dos dados foi verificada por meio da utilização de uma amostra de referência de *e-waste* preparada por Andrade *et al.*[18,19] Ao final do processo foi possível obter uma matriz X com 57 amostras (n) e 10 variáveis (m) que representam as concentrações dos 10 analitos determinados. Assim, a matriz X terá a dimensão n:m (57:10).

Tabela 1. Condições instrumentais do ICP OES empregado nas determinações dos elementos de interesse e os LoD para cada analito

Parâmetros do instrumento	Condições operacionais	
Tempo de integração (s)	15 a 5	
Potência aplicada (kW)	1,15	
Vazão gás refrigerante (L min^{-1})	12,0	
Vazão do gás auxiliar (L min^{-1})	0,5	
Vazão do gás no nebulizador (L min^{-1})	0,7	
Vazão da amostra (L min^{-1})	2,10	
Nebulizador	Mira Mist	
Câmara de estabilização	Ciclônico	
Analito e comprimento de onda	Ag I 328.068,[a] Al I 308.215,[a] As I 189.042,[b] Au I 267.595,[a] Cr I 283.563,[b] Cu I 327.396,[a] Fe II 259.940,[a] Pb I 220.353,[b] Pd I 340.458,[a] Pt I 265.945[a]	
LoD (mg kg^{-1})	Ag - 0,001	Cu - 0,006
	Al - 0,02	Fe - 0,004
	As - 0,01	Pb - 0,01
	Au - 0,004	Pd - 0,002
	Cr - 0,001	Pt - 0,01

[a]Modo de visualização axial; [b]modo de visualização radial.

Variáveis provenientes das técnicas LIBS e EDXRF

Os espectros estudados neste tutorial foram compostos por dados espectrais das técnicas analíticas LIBS[20] e EDXRF. Para as medidas LIBS das 57 amostras de *e-waste* descritas na seção anterior, foi necessário obter pastilhas por meio de uma prensa (Shimadzu, SSP-10). O diâmetro e a espessura das pastilhas obtidas tiveram cerca de 10 e 2 mm, respectivamente. O instrumento LIBS utilizado foi o modelo J200 (Applied Spectra, Fremont, EUA). As condições operacionais foram: laser de Nd:YAG com comprimento de onda de 1064 nm; *spot size* de 100 µm; *delay time* de 1 µs e energia de 80 mJ. Com os parâmetros descritos foi possível obter uma fluência teórica de cerca de 1000 J cm^{-2}. Ao todo foram adquiridos 130 espectros por amostra utilizando o modo varredura de análise (*raster*). Para este instrumento, os espectros de emissão abrangem a faixa entre 186 e 1042 nm. O sistema de detecção é constituído por 6 espectrômetros: (i) 186 até 311 nm (resolução de 0,059 nm); (ii) 311 até 465 nm (resolução de 0,073 nm); (iii) 465 até 591 nm (resolução de 0,062 nm); (iv) 591 até 693 nm (resolução de 0,050 nm); (v) 693 até 884 nm (resolução de 0,094 nm) e (vi) 884 até 1042 nm (resolução de 0,079 nm). A quantidade de variáveis registradas é de 12288.

Os resultados empregados nos cálculos subsequentes foram as médias aritméticas de cada conjunto de espectros obtidos por amostra. Assim, foi estudada uma matriz X de 57 amostras por 12288 variáveis (matriz 57:12288).

No caso da EDXRF foi utilizado um espectrômetro NEX QC+, (Rigaku, Austin, Texas, EUA). As 57 amostras foram analisadas em ar e atmosfera de gás hélio (He) em 3 condições instrumentais distintas: (i) número atômico alto (faixa do Ru até o Pr e K até o Br), tensão de 50 kV, corrente 10 µA e filtro tipo B; (ii) número atômico intermediário (faixa do K até o Mo e Sn até o U), tensão 30 kV, corrente 10 µA e filtro tipo A e (iii) número atômico baixo (faixa do Sn até o U e Na até o Cl), tensão 6,5 kV, corrente 50 µA e sem filtro. Os espectros gerados cobriram a faixa de 0 até 49,94 keV (0,024 keV de resolução) e foi possível obter 2048 canais de energia (keV) para cada uma das condições instrumentais descritas anteriormente. Ao final foram organizadas seis matrizes de dados com 57 amostras e 2048 variáveis (matrizes 57:2048). Nos cálculos exemplificados nas próximas seções foram utilizados os dados obtidos em atmosfera de He, pois apresentaram maior sensibilidade.

Imagens hiperespectrais

Imagens hiperespectrais podem gerar informações tanto espaciais quanto espectrais. No caso específico do exemplo deste tutorial cada pixel da imagem foi composto por um espectro de emissão obtido pela LIBS. Desta forma, as imagens hiperespectrais[21] são bastante úteis para investigar a composição química de uma amostra e a distribuição de determinados compostos ou elementos ao longo da sua superfície.[22,23] Neste tutorial foi utilizada uma amostra de PCB de placa de som de um dos *laptops* desmontados e, juntamente com a LIBS, a proposta é mostrar e ilustrar o tratamento de dados deste tipo de problema. As condições do laser foram as mesmas descritas anteriormente, mas a aquisição dos espectros foi realizada ponto a ponto, cobrindo uma área de 100 mm^2. O arranjo de dados obtidos foi 10 por 10 e 12288 variáveis. A Figura 1 mostra a superfície da amostra antes (Figura 1(a)) e após (Figura 1(b)) a obtenção dos espectros. Em cada ponto de incidência do laser (ver marcações na Figura 1(b)) foram dados 10 pulsos e a quantidade final de espectros obtidos foi 10 × 10 × 10 = 1000. Ao incidir diversos pulsos de laser no mesmo ponto da amostra é possível fazer inferências sobre a composição da amostra em diferentes profundidades. Esse tipo de informação é importante para amostras de WEEE que são formadas por várias camadas com propriedades distintas: polímeros, metais, materiais isolantes, entre outros. A matriz X de dados foi de 1000:12288.

Rotinas computacionais utilizadas

Para o desenvolvimento desse terceiro tutorial e cálculos dos dados gerados, foram preparadas cinco rotinas computacionais para os programas Matlab (R2019b, The Mathworks, EUA) e Octave (programa livre). Além disso, foi utilizado o Microsoft Excel® para a organização dos dados. Além do Octave, podem ser empregados também os programas livres R e Python. Todas as rotinas estão descritas no Material Suplementar e podem ser implementadas, livremente, nos programas computacionais descritos.

A primeira rotina foi denominada LIBS_inverse e tem como objetivo organizar de forma adequada o arranjo de dados das imagens hiperespectrais. Durante a aquisição dos dados para a formação do arranjo, o instrumento LIBS emprega como padrão uma configuração em zigue-zague que não é adequada para o tratamento matemático das rotinas subsequentes. Assim, a LIBS_inverse regulariza as linhas de obtenção dos dados fazendo com que cada uma inicie da esquerda para a direita. A linha de comando da LIBS_inverse é:

[MATRIZ] = LIBS_inverse (X,NP,NL,NC)

As informações entre parênteses representam os dados de entrada (*input*), onde o parâmetro X representa a matriz com os dados e,

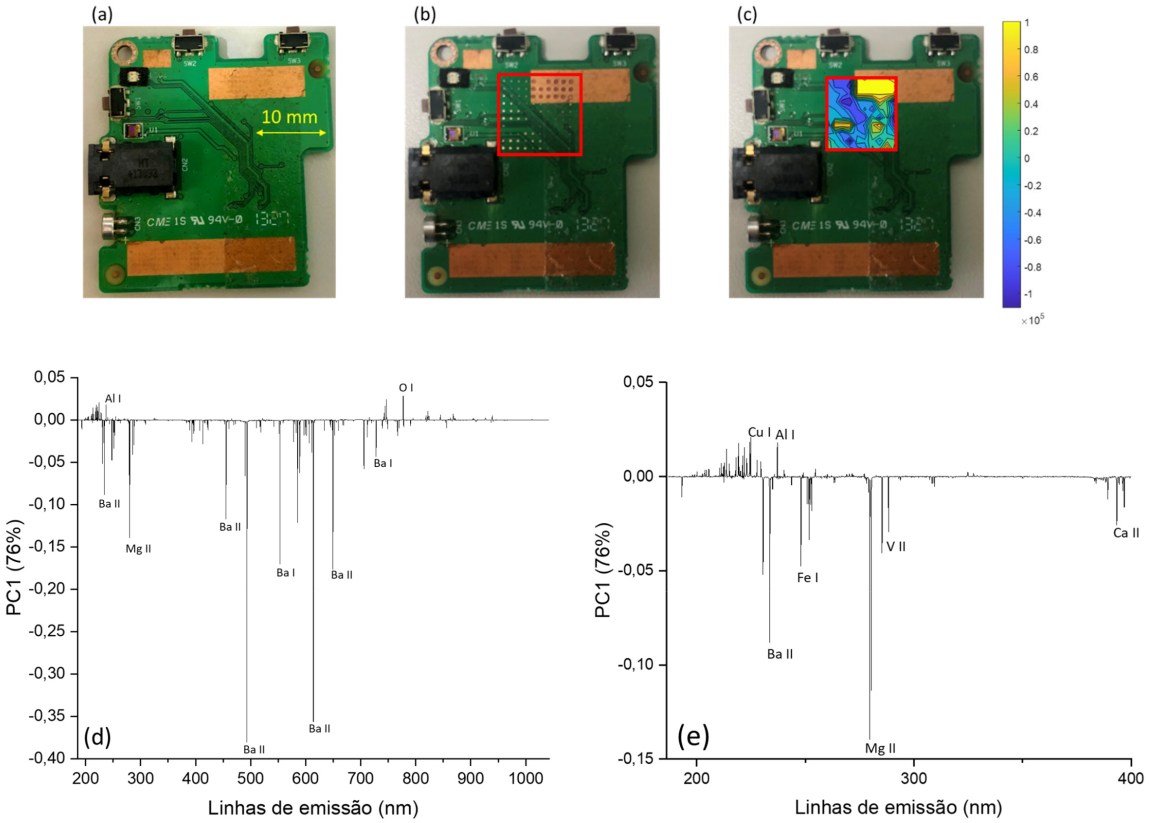

Figura 1. *PCB antes do mapeamento elementar no LIBS (a), após o mapeamento (b), o heat map dos scores (c) da PC1 e para o pulso 5, os loadings da PC1 (d) e pulso 5 e uma ampliação dos valores de loadings para as linhas emissão de 200 a 400 nm (e)*

neste exemplo em específico, as dimensões são 1000:12288. Já os parâmetros NP, NL e NC representam o número de pulsos por ponto, número de linhas e o número de colunas, respectivamente. No exemplo da Figura 1(b) temos que NP, NL e NC são 10, 10, e 10, respectivamente. Como dado de saída (*output*) temos o parâmetro MATRIZ que representa a matriz X inicial com a direção correta da obtenção dos dados.

A segunda rotina é denominada data_pre e tem como objetivo calcular a média aritmética, desvio padrão e realizar o pré-processamento dos dados: centrar na média e autoescalar. A linha de comando da data_pre é:

[Xauto,Xcm,xm,xstd] = data_pre(X)

De forma análoga à rotina LIBS_inverse, a matriz de dados X (entrada dos dados) será pré-processada. Como resultado teremos duas matrizes: Xauto e Xcm que representam a matriz X autoescalada e centrada na média, respectivamente. Além disso, são apresentados dois objetos (xm e xstd) que mostram a média e o desvio padrão das variáveis da matriz X. A escolha da matriz Xauto ou Xcm para os cálculos subsequentes dependerá da natureza dos dados que estão sendo estudados.

Os dados gerados são então utilizados na terceira rotina, denominada pca_dis que efetua os cálculos da PCA, gerando gráficos de variância explicada, *scores* e *loadings*. No caso específico dos *scores* e *loadings*, são mostrados os gráficos para as duas primeiras PC's. As informações das demais PC's podem ser acessadas nas matrizes de saída da função (*scores* e *loads*). A linha de comando da pca_dis é:

[scores,loads,var_exp] = pca_dis (X)

A matriz X representa os dados de entrada e as matrizes *scores* e *loads* mostram os valores de *scores* (n:n) e *loadings* (m:n) calculados. O vetor var_exp mostra a variância explicada para as n PC's (o vetor é n:1). Na análise dos resultados obtidos pela PCA devem ser utilizadas as informações das PC's que apresentam mais informações. Na decisão sobre quantas PC's serão avaliadas, é importante verificar, a partir de qual, a porcentagem de variância explicada apresenta uma queda monotônica.

A quarta rotina denominada libs efetua cálculos que geram mapas de *scores* ou *heat maps* em tensor 4D na forma: número de pulsos (NP) *versus* PC's *versus* número de linhas (NL) *versus* número de colunas (NC). A linha de comando da libs é:

[MAPS,T,P,Var_exp] = libs (MATRIZ,NP,NC,NL,PCS)

Na rotina libs é calculada uma PCA para cada matriz de pulso obtida. No exemplo específico da Figura 1(b) foram calculadas 10 PCAs (uma para cada pulso de laser). Assim, é possível verificar também as diferenças na composição química da amostra, ao passo que são obtidas informações sobre a superfície (pulso 1) e o seu interior (pulso 10). Os dados necessitam ser pré-processados antes da utilização da rotina libs.

A quinta rotina denominada libs_plot é responsável por gerar gráficos *heat maps* provenientes da rotina anterior. MAPS é o tensor gerado na rotina anterior, PULSO e PCS são referentes ao pulso e a quantidade de PC's que serão visualizadas. A linha de comando da libs_plot é:

libs_plot(MAPS,PULSO,PCS)

Para verificar o mapa de *scores* do pulso 2 e das três primeiras PCs, por exemplo deve ser utilizado: libs_plot(MAPS,2,3).

RESULTADOS E DISCUSSÃO

Variáveis provenientes de concentrações de elementos químicos

A Tabela 1 mostra as condições instrumentais do instrumento ICP OES e os limites de detecção (*limits of detection*, LoD) para os 10 analitos determinados. A Tabela 1S, no Material Suplementar, mostra todos os valores de concentrações obtidos. Assim, o leitor poderá reproduzir os cálculos. Além disso, foram preparados vídeos (ver próximas seções) para auxiliar na utilização dos programas computacionais e das rotinas preparadas.

As faixas de concentração variaram de 0,01 mg kg^{-1} para o Au e Pd e até 40% (m/m) para o Cu. As concentrações possuíam magnitudes em faixas diferentes e, assim, os dados foram autoescalados, como mostra a Equação 2:

$$x_{auto} = \frac{x_{ij} - \overline{x_j}}{s_j} \quad (2)$$

onde $\overline{x_j} = \frac{1}{n}\sum_{i=1}^{n} x_{ij}$ e $s_j = \sqrt{\frac{\sum_{i=1}^{n}(x_{ij} - \overline{x_j})^2}{n-1}}$ são a média e o desvio padrão da coluna dos dados (variáveis), respectivamente.

A Figura 1S, no Material Suplementar, mostra os dados originais (Figura 1S(a)) e autoescalados (Figura 1S(b)) para os 10 analitos determinados. Os elementos Ag, As, Au, Pd e Pt apresentaram as menores concentrações e estão representados na unidade de concentração de mg kg^{-1}. Já o Al, Cr, Cu, Fe e Pb estão em faixas superiores e, assim, foram representados em % m/m.

Na Figura 1S(a) a distribuição estatística das amostras possui características assimétricas[24] para quase todos analitos, com exceção da Ag, Al e Cu, este parâmetro informa quão semelhantes são os valores de média, mediana (valor localizado no centro do conjunto de dados) e moda (valor que mais se repete) de cada uma das variáveis. Outro parâmetro importante que pode ser discutido é a curtose.[24] A curtose descreve se os dados apresentam uma distribuição achatada (valores baixos de curtose) ou em cume (valores altos de curtose). Para os dados apresentados na Figura 1S temos que as distribuições mais em cume são as do Cr e Pt e a mais achatada é a do Cu. A Figura 1S(b) mostra uma representação dos dados autoescalados e nota-se que a média (quadrado no interior do *box-plot*) e o desvio padrão são iguais a 0 e 1, respectivamente. Assim, todas as variáveis possuem a mesma escala e podem contribuir de maneira semelhante para os cálculos dos *scores* e *loadings*. Dados de concentração como os apresentados nesta seção devem ser, preferencialmente, autoescalados.[9] Outros exemplos de dados autoescalados são propriedades físico-químicas.[25-27]

Com os dados autoescalados obtidos foi calculada uma PCA e a Figura 2 mostra os resultados obtidos. As Figuras 2(a) e 2(b) mostram os valores de *scores* onde as classes investigadas foram o tipo de *e-waste* e tamanho de partícula, respectivamente. Na Figura 2(c) temos os *loadings*. Com os *scores* e *loadings* é possível fazer inferências sobre o comportamento das amostras. No caso da Figura 2(a), por exemplo, temos um certo agrupamento das amostras de telefones celulares (triângulos azuis) e *tablets* (triângulos invertidos verdes). Para a Figura 2(b), temos que as amostras com tamanho de partícula > 600 µm (triângulos invertidos verdes) apresentam um comportamento distinto das demais. Com o gráfico de *loadings* (Figura 2(c)) podemos verificar as correlações entre as variáveis. As variáveis Cr, Fe e Pt, por exemplo, apresentam valores de coeficiente de correlação (r)[24] variando de 0,6599 (Fe *versus* Pt) até 0,9283 (Cr *versus* Pt), ou seja, os valores de r são positivos

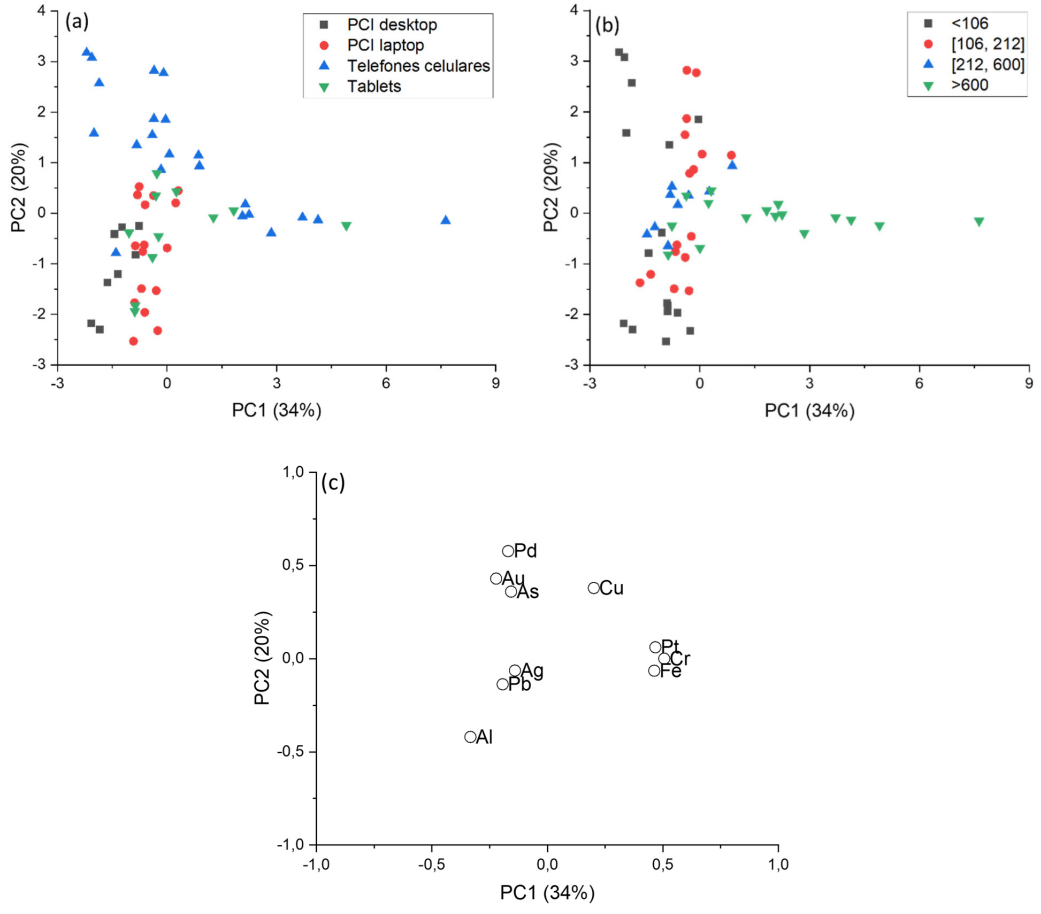

Figura 2. *Scores das concentrações determinadas em função do tipo de amostra (a), tamanho de partícula (b) e seus respectivos valores de loadings (c)*

e isso pode denotar fontes semelhantes dos 3 elementos. Já os elementos Al e Cu apresentaram um r negativo, igual a -0,7025, correspondendo ao fato de amostras que apresentaram concentrações altas de Al, tiveram concentrações baixas de Cu e vice-versa. Além de correlações entre os elementos, é possível também observar quais amostras possuem concentrações mais elevadas de alguns elementos. As amostras situadas no quadrante negativo da PC1 e PC2 da Figura 2(a), por exemplo, apresentam concentrações mais altas de Al (também presente no quadrante negativo da PC1 e PC2 para o gráfico de *loadings*, Figura 2(b)). De fato, tais amostras apresentam concentrações de Al três vezes maiores que as demais (ver Tabela 1S do Material Suplementar).

Variáveis provenientes das técnicas LIBS e EDXRF

Os dados de espectros obtidos por LIBS e EDXRF foram centrados na média. As Figuras 3 e 4 mostram espectros típicos da LIBS e de EDXRF, respectivamente, para uma amostra de PCB de telefone celular.

Na Figura 3 é verificado que os espectros de emissão da LIBS apresentam maiores intensidade para os elementos Ba, Ca, Cu, Mg e Na. A Figura 4 apresenta os três espectros de EDXRF: (i) alto número atômico (Figura 4(a)), apresentou maiores intensidades para os elementos Br, Cu e Sn; (ii) número atômico intermediário (Figura 4(b)), apresentou maiores intensidades para os elementos Br, Cu e Pb e (iii) baixo número atômico (Figura 4(c)), apresentou maiores intensidades para os elementos Ag, Al, Ca e Si. Os espectros mostrados na Figura 4 foram obtidos em atmosfera de He.

Os elementos Ag e Cu fazem parte dos circuitos eletrônicos das amostras de PCB.[28] Já os elementos Pb e Sn são encontrados nas soldas.[26] O Al e o Ba estão presentes em dispositivos da PCB e em capacitores, respectivamente. Já os elementos Ca, Mg e Si fazem parte do isolamento das PCBs. Compostos de Br são constituintes de retardantes de chama.[26,28-30]

Os espectros LIBS foram organizados, e uma PCA foi calculada, como mostra os *scores* na Figura 5(a) e os *loadings* na Figura 5(b). O instrumento LIBS possui uma maior sensibilidade para diferenciar os tamanhos de partícula das amostras quando comparado ao EDXRF. Isto fica evidente na Figura 5(a), com o resultado obtido na PCA é possível identificar diferenças nos padrões de espectro de emissão para os diferentes tamanhos de partículas. As amostras com tamanho de partícula > 600 μm se agruparam a esquerda (triângulos verdes invertidos), as com tamanho < 106 μm (quadrados pretos) e [106, 212] μm (círculos vermelhos) possuem padrões espectrais semelhantes e se agruparam mais à direita, enquanto as com tamanho [212, 600] μm (triângulos azuis) se agruparam mais ao centro da Figura 5(a). Nos *loadings* (Figura 5(b)) foi observado que os elementos presentes com maior sinal foram o Ba e o Mg e que ambos estão positivamente correlacionados.

Os espectros de EDXRF foram organizados da mesma forma e foi escolhida a condição (i) alto número atômico e atmosfera de He, como exemplo, para calcular a PCA. O resultado obtido é apresentado na Figura 6, com os *scores* (Figura 6(a)) e os *loadings* (Figura 6(b)). Nos *scores* (Figura 6(a)) houve um leve agrupamento por diferença de tamanho de partícula e foi notado uma anormalidade quanto aos espectros das PCBs de celulares, que se agruparam independente do seu tamanho de partícula. Esse comportamento é devido aos sinais dessas amostras serem muito semelhantes e se destacarem das demais. Nos *loadings* (Figura 6(b)) os elementos com maiores contribuições foram o Br, Cu, Fe e Sn. O Cu apresentou correlação negativa com os demais elementos, principalmente o Br, como mostra a PC1. Portanto as amostras que estão do lado positivo da PC1 na Figura 6(a) possuem maiores concentração Cu e menores de Br.

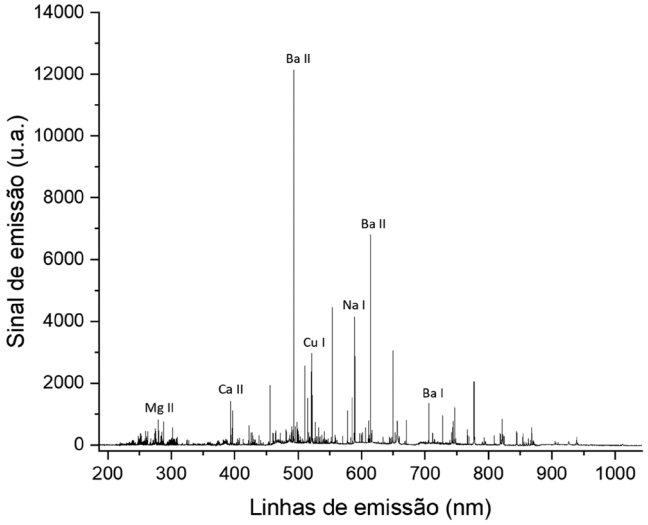

Figura 3. *Espectro de emissão LIBS de uma amostra de celular moída e prensada*

Imagens hiperespectrais

A Figura 1(c) mostra o mapa de *scores* da PC1 para o pulso 5. A PC1 para o pulso 5 apresentou uma variância explicada de 76% e foi a que melhor representou espacialmente a amostra real (Figuras 1(a) e 1(b)). As demais PC's mostraram valores de variância explicada muito baixos (da ordem de 23%). A Figura 2S mostra os valores de variância explicada (%) para as 10 primeiras componentes principais e nota-se que a partir da PC2 há uma queda monotônica na porcentagem de variância.

Na Figura 1(c) temos uma escala de cores que representa a magnitude dos valores de *scores*. Os dados foram centrados na média e os valores positivos e negativos de *scores* são representados pelas cores amarela e azul, respectivamente. Assim, valores positivos de *loadings* (Figura 1(d)) representam elementos químicos identificados na parte em amarelo da Figura 1(c). Já os valores negativos de *loadings*, representam elementos identificados na parte azul da amostra. A Figura 1(e) mostra uma ampliação da região de 200 a 400 nm sendo possível notar que os elementos Al e Cu estão presentes na parte alaranjada da PCB (ver Figuras 1(a) e 1(b)). Já os demais elementos, Ba, Ca, Fe, Mg e V, estão presentes na parte polimérica da PCB. Tais informações são úteis para efetuar uma análise qualitativa da composição química da amostra e, no caso específico do resíduo eletrônico, propor rotas diferentes de segregação e reciclagem, viabilizando a recuperação de elementos, podendo ser aplicadas em escala industrial. A estratégia ilustrada permite a análise e reconhecimento de padrões no processamento de resíduos eletrônicos, facilitando a avaliação e o controle industrial.

O uso de imagens hiperespectrais e LIBS associadas com a geração de mapas de *scores* constituem ferramenta importante para a obtenção de informações sobre a composição da amostra, sendo utilizada em diversas aplicações, tais como a classificação de alimentos[31] e análise de minerais.[32]

CONCLUSÕES

Com este tutorial é possível aprender de maneira didática como utilizar a ferramenta PCA para análises de variáveis provenientes de concentrações e de espectros (de emissão e de fluorescência de raios-X). Além disso, foram também elaboradas as rotinas para outras linguagens e programas computacionais, tais como Python e R (mais detalhes são apresentados no Material Suplementar). Os

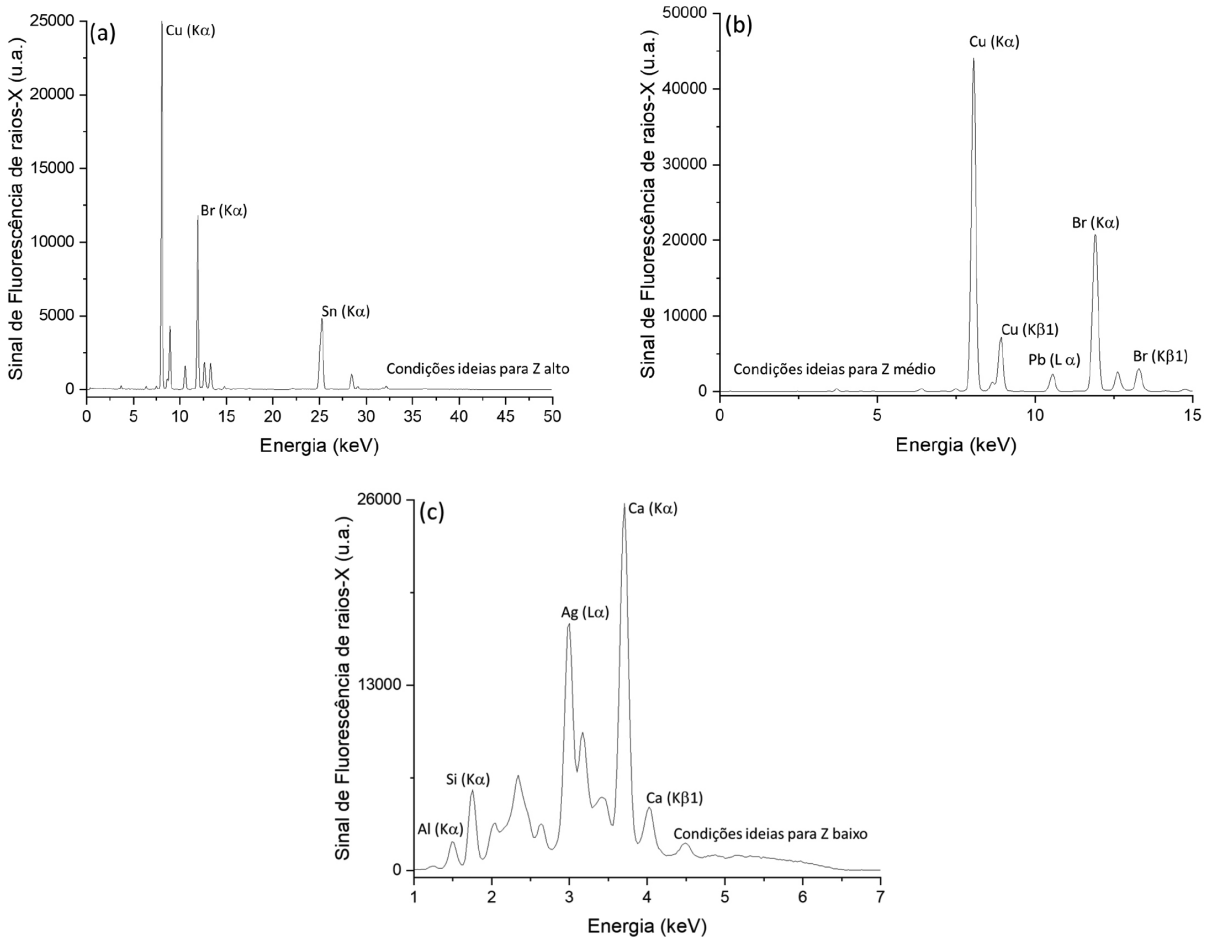

Figura 4. *Espectros de fluorescências de raios-X de uma amostra de celular em atmosfera de He, nas condições (i) número atômico alto (a), (ii) número atômico intermediário (b) e (iii) número atômico baixo (c)*

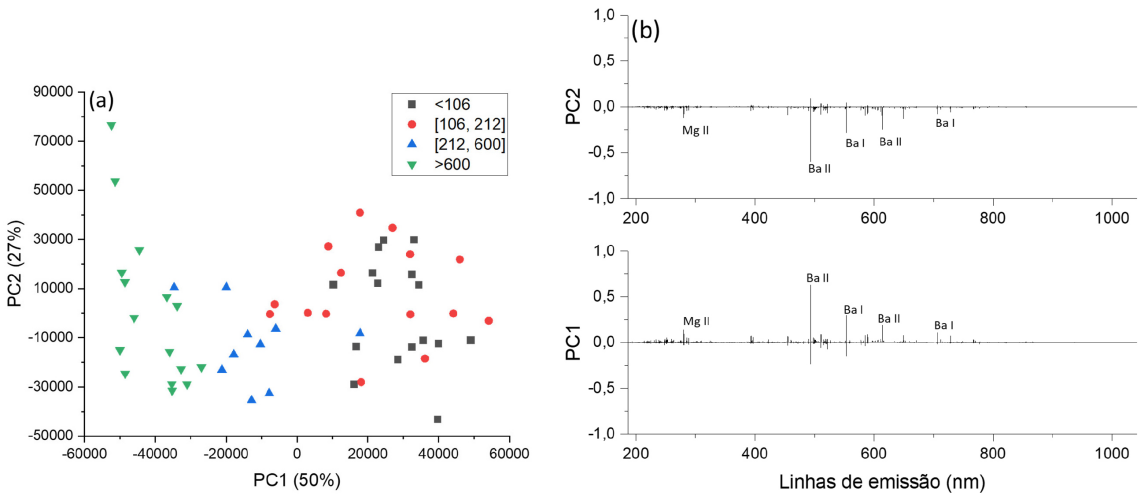

Figura 5. *Scores (a) e loadings (b) dos espectros de emissão LIBS das 57 amostras em função do tamanho de partícula*

exemplos mostrados neste terceiro tutorial podem ser visualizados de forma detalhada na playlist 28 do canal no YouTube do Prof. Edenir R. Pereira Filho (https://www.youtube.com/c/EdenirPereiraFilho). Nesta playlist são disponibilizadas também rotinas computacionais em R e Python e o leitor pode reproduzir os cálculos. Além disso, é mostrada também a utilização do Octave online, que não requer a instalação do programa no computador do analista. A playlist 28 visa complementar as informações já divulgadas nas playlists de 22 até 25 e a lista a seguir mostra uma descrição das mesmas:

Playlist 22 apresenta o programa livre Octave e os detalhes de como utilizá-lo: https://youtube.com/playlist?list=PL4CuftF4l_fAzIX7O373iO-Sf_BHRl_Zd.

Playlists 23 e 24 mostram o programa R e a linguagem Python, respectivamente, e as suas utilizações em planejamento fatorial: https://youtube.com/playlist?list=PL4CuftF4l_fCL_NicWd5Ax5xWlEUn7Zd3 (R) e https://youtube.com/playlist?list=PL4CuftF4l_

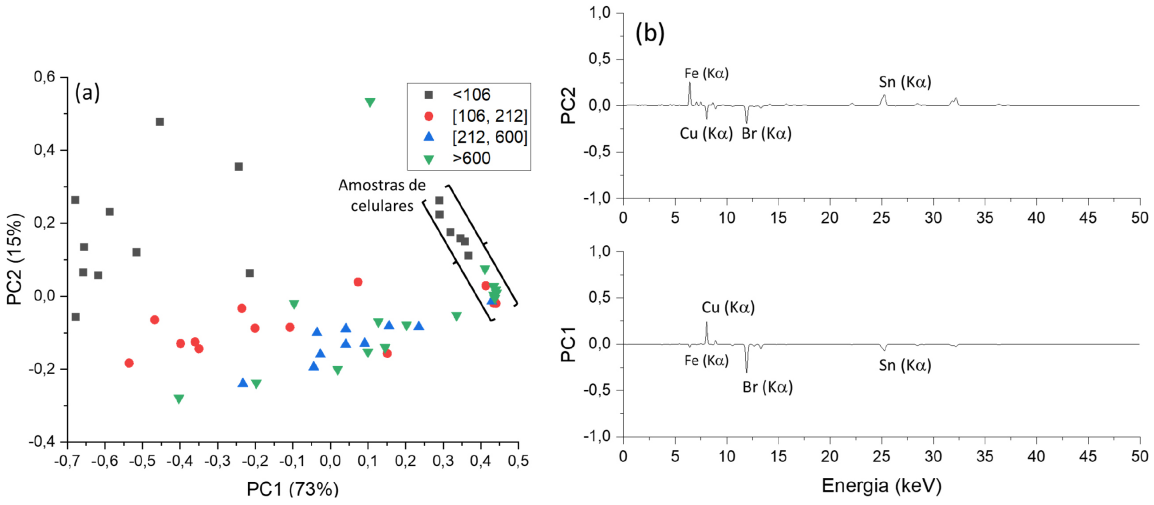

Figura 6. *Scores (a) e loadings (b) dos espectros de fluorescência de raios-X das 57 amostras em função do tamanho de partícula*

fCsdCBY4eaLcTDFhhMaH6VN (Python).

Playlist 25 apresenta diversos detalhes sobre os cálculos efetuados com a PCA empregando o Octave: https://youtube.com/playlist?list=PL4CuftF4l_fAoYAae3a6sucVbfS2f0GiS.

Playlist 28 apresenta os exemplos deste tutorial: https://youtube.com/playlist?list=PL4CuftF4l_fAsDkW2SEIgBtQ9QqV5fPmB.

MATERIAL SUPLEMENTAR

O Material Suplementar apresenta os seguintes itens:

- Figura 1S. *Box-plot* das concentrações dos 10 analitos determinados: dados originais (a) e autoescalados (b).
- Figura 2S. Porcentagem de variância explicada em função do número de componentes principais para o pulso 5.
- Rotinas computacionais: (i) LIBS_inverse; (ii) data_pre; (iii) pca_dis; (iv) libs e (v) libs_plot.
- Tabela 1S. Tabela das concentrações das amostras de *e-waste* determinados em ICP OES.

Todo conteúdo está disponível em http://quimicanova. sbq.org.br, na forma de arquivo PDF, com acesso livre.

AGRADECIMENTOS

Os autores são gratos à Fundação de Amparo à Pesquisa do Estado de São Paulo (FAPESP, processos 2016/17221-8, 2019/24223-5, 2021/10882-7 e 2022/02232-5) e ao Conselho Nacional de Desenvolvimento Científico e Tecnológico (CNPq, processos 140867/2021-0, 302719/2020-2 e 307328/2019–8). O presente trabalho foi realizado com apoio da Coordenação de Aperfeiçoamento de Pessoal de Nível Superior - Brasil (CAPES) - Código de Financiamento 001.

REFERÊNCIAS

1. Berisha, B.; Mëziu, E.; Shabani, I.; *Journal of Cloud Computing* **2022**, *11*, 24. [Crossref]
2. Hastie, T.; Tibshirani, R.; Friedman, J.; *The Elements of Statistical Learning Data Mining, Inference, and Prediction*, 2nd ed.; Springer: New York, 2009.
3. Artavia, G.; Cortés-Herrera, C.; Granados-Chinchilla, F.; *Foods* **2021**, *10*, 1081. [Crossref]
4. Tavares, T. R.; Molin, J. P.; Nunes, L. C.; Alves, E. E. N.; Krug, F. J.; de Carvalho, H. W. P.; *Data Brief* **2022**, *41*, 108004. [Crossref]
5. Neto, B. D. B.; Scarminio, I. S.; Bruns, R. E.; *Quim. Nova* **2006**, *29*, 1401. [Crossref]
6. Brandt, S.; *Data Analysis: Statistical and Computational Methods for Scientists and Engineers*, 3rd ed.; Springer: New York, 1998.
7. Beebe, K. R.; Pell, R. J.; Seasholtz, M. B.; *Chemometrics: A Practical Guide*, 1st ed.; John Wiley & Sons: New Jersey, 1998.
8. Wold, S.; Esbensen, K.; Geladi, P.; *Chemom. Intell. Lab. Syst.* **1987**, *2*, 37. [Crossref]
9. Ferreira, M. M. C.; *Quimiometria: Conceitos, Métodos e Aplicações*, 1ª ed.; Editora da Unicamp: Campinas, 2015.
10. Bro, R.; Smilde, A. K.; *Analitycal Methods* **2014**, *6*, 2812. [Crossref]
11. Manhas, F. M. V.; Pereira-Filho, E. R.; *Quim. Nova* **2018**, *41*, 1061. [Crossref]
12. Hilário, F. F.; Castro, J. P.; Barros, T. E.; Pereira-Filho, E. R.; *Quim. Nova* **2021**, *44*, 874. [Crossref]
13. Amigo, J. M.; Babamoradi, H.; Elcoroaristizabal, S.; *Anal. Chim. Acta* **2015**, *896*, 34. [Crossref]
14. de Souza, A. M.; Poppi, R. J.; *Quim. Nova* **2012**, *35*, 223. [Crossref]
15. Ferreira, M. C. F.; *Quim. Nova* **2022**, *45*, 1251. [Crossref]
16. Lyra, W. S.; Silva, E. C.; Araújo, M. C. U.; Fragoso, W. D.; Veras, G.; *Quim. Nova* **2010**, *33*, 1594. [Link] acessado em fevereiro 2023
17. Valderrama, L.; Paiva, V. B.; Março, P. H.; Valderrama, P.; *Quim. Nova* **2016**, *39*, 245. [Crossref]
18. Andrade, D. F.; Machado, R. C.; Pereira-Filho, E. R.; *J. Anal. At. Spectrom.* **2019**, *34*, 2402. [Crossref]
19. Andrade, D. F.; Machado, R. C.; Bacchi, M. A.; Pereira-Filho, E. R.; *J. Anal. At. Spectrom.* **2019**, *34*, 2394. [Crossref]
20. Pereira-Filho, E. R. Em *Laser-Induced Breakdown Spectroscopy (LIBS): Applications and Calibration Strategies*; Cruz, J. A. S., ed.; Editora Ibero-Americana de Educação: Bauru, 2021.
21. Carneiro, R. L.; Poppi, R. J.; *Spectrochim. Acta, Part A* **2014**, *118*, 215. [Crossref]
22. Chang, C. I.; Song, M.; Zhang, J.; Wu, C. C.; *Remote Sens.* **2019**, *11*, 2012. [Crossref]
23. Tang, S.; Chen, Z.; Zhang, M.; *11th Workshop on Hyperspectral Image and Signal Processing: Evolution in Remote Sensing*, Amsterdam, 2021. [Crossref]
24. Hash-Vaughn, D. L.; Lomax, R. G.; *An Introduction to Statistical Concepts*, 4th ed.; Routledge: United Kingdom, 2020.
25. Andrade, D. F.; de Almeida, E.; de Carvalho, H. W. P.; Pereira-Filho, E. R.; Amarasiriwardena, D.; *Talanta* **2021**, *225*, 122025. [Crossref]
26. Castro, J. P.; Pereira-Filho, E. R.; *Detritus* **2020**, *13*, 131. [Crossref]

27. Ciulu, M.; Serra, R.; Caredda, M.; Salis, S.; Floris, I.; Pilo, M. I.; Spano, N.; Panzanelli, A.; Sanna, G.; *Talanta* **2018**, *190*, 382. [Crossref]
28. Carvalho, R. R. V.; Coelho, J. A. O.; Santos, J. M.; Aquino, F. W. B.; Carneiro, R. L.; Pereira-Filho, E. R.; *Talanta* **2015**, *134*, 278. [Crossref]
29. Costa, V. C.; Castro, J. P.; Andrade, D. F.; Babos, D. V.; Garcia, J. A.; Sperança, M. A.; Catelani, T. A.; Pereira-Filho, E. R.; *TrAC, Trends Anal. Chem.* **2018**, *108*, 65. [Crossref]
30. Andrade, D. F.; Castro, J. P.; Garcia, J. A.; Machado, R. C.; Pereira-Filho, E. R.; Amarasiriwardena, D.; *Chemosphere* **2022**, *286*, 131739. [Crossref]
31. Ning, J.; Sun, J.; Li, S.; Sheng, M.; Zhang, Z.; *Int. J. Food Prop.* **2017**, *20*, 1515. [Crossref]
32. Moncayo, S.; Duponchel, L.; Mousavipak, N.; Panczer, G.; Trichard, F.; Bousquet, B.; Pelascini, F.; Motto-Ros, V.; *J. Anal. At. Spectrom.* **2018**, *33*, 210. [Crossref]

MATERIAL SUPLEMENTAR

Principal component analysis (PCA) para a avaliação de dados químicos e geração de *heat maps*: um tutorial

Dennis da Silva Ferreira[a], Leticia da Silva Rodrigues[b], Fabiola Manhas Verbi Pereira[b] e Edenir Rodrigues Pereira-Filho[a,*]

[a]Departamento de Química, Universidade Federal de São Carlos, 13565-905 São Carlos − SP, Brasil

[b]Instituto de Química, Universidade Estadual Paulista, 14800-060 Araraquara − SP, Brasil

*e-mail: erpf@ufscar.br

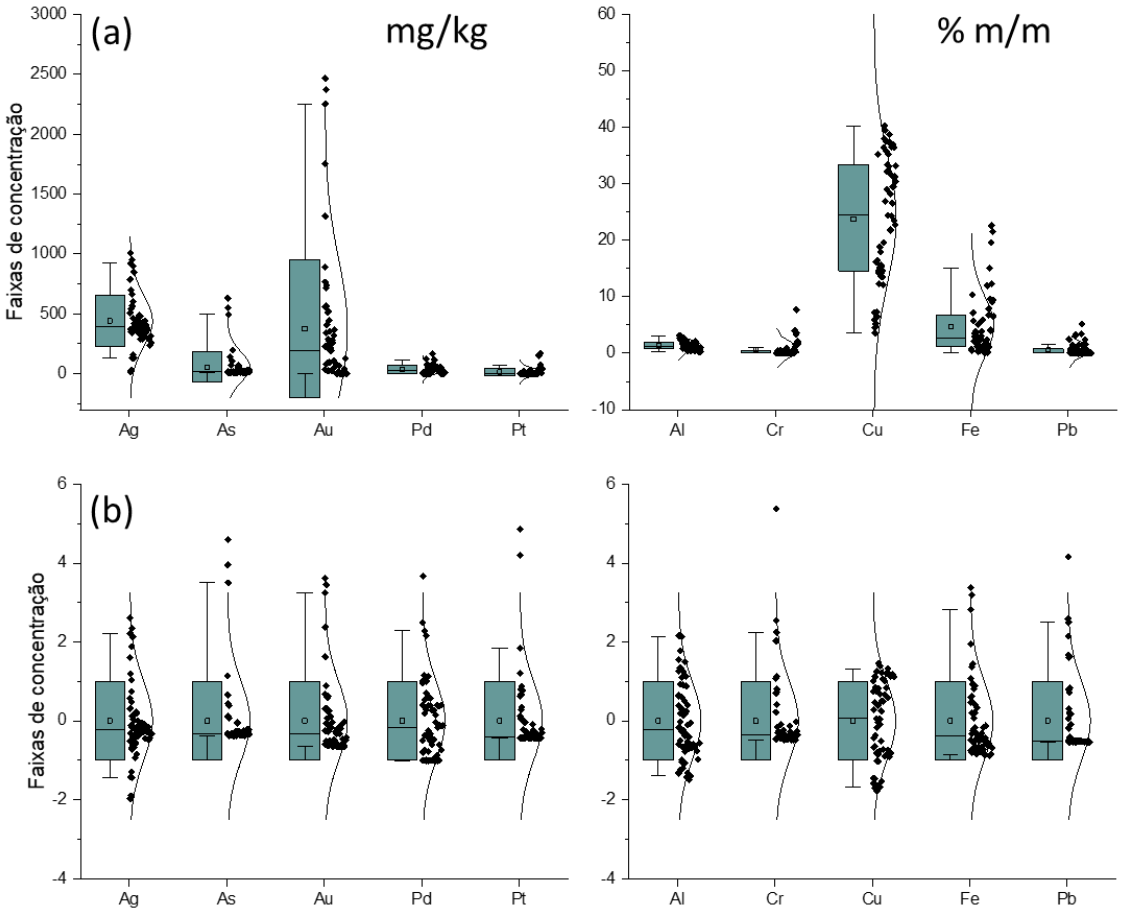

Figura 1S. *Box-plot das concentrações dos 10 analitos determinados: (a) dados originais e (b) autoescalados*

O elemento Cu, por exemplo, apresentou o menor valor de assimetria (-0,24). Com a Figura 1S(a) pode ser verificado, utilizando o *box-plot*, que a média dos dados para o Cu (quadrado no interior do *box-plot*) está próxima à linha horizontal no interior que representa a mediana.

O tamanho do box-plot da Figura 1S representa o desvio padrão dos dados e as barras de erros possuem 95% dos dados.

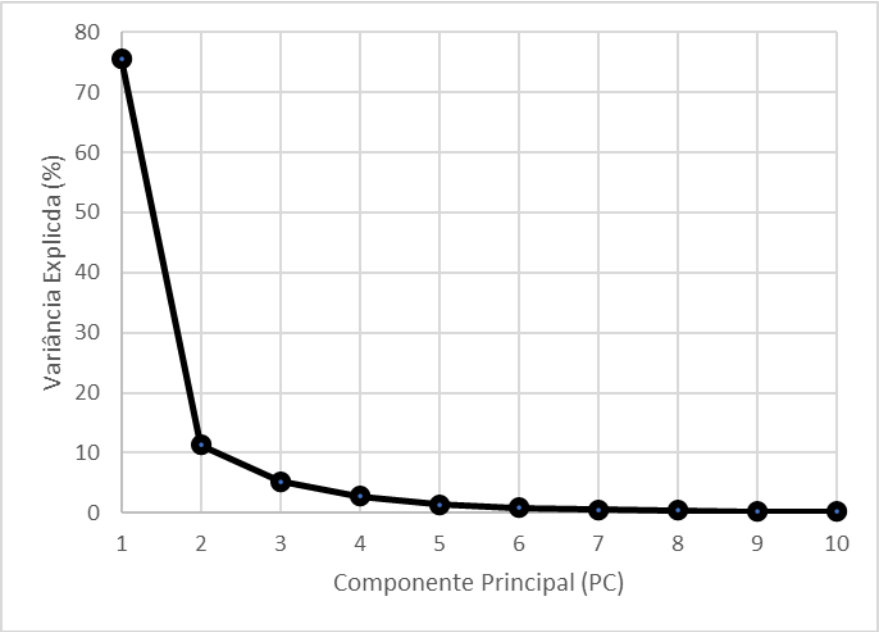

Figura 2S. *Porcentagem de variância explicada em função do número de componentes principais para o pulso 5 (ver mais detalhes na Figura 1)*

Descrição das rotinas computacionais utilizadas nos exemplos

LIBS_inverse:

```
function [MATRIZ] = LIBS_inverse(X,NP,NL,NC)
k=1;
s=0;
% criando matriz origem
M=ones(NL,NC*NP);
  for i=1:NL
      for j=1:NC*NP
          s=s+1;
          M(i,j)=s;
      end
  end
% mudança de ordem
for i=1:NL
    for j=1:NC*NP
        if mod(i,2)== 0
          Mc(i,j)=M(i,NC*NP+1-j);
        else
          Mc(i,j)= M(i,j);
        end
        Ml(k,1)=Mc(i,j);
        k=k+1;
    end
end
 % susbtituindo na matriz inicial
  MATRIZ= X(Ml,:);
```

data_pre:

```
function [Xauto,Xcm,xm,xstd] = data_pre(X);
    % [Xauto,Xcm,xm,xstd] = data_pre(X);
    % Esta função tem como objetivo centrar na média e
autoescalar uma matriz X.
    % Inputs: Matriz X (m linhas e n colunas)
    % Outputs:
    % Xauto: Matriz autoescalada
    % Xcm: Matriz centrada na média
    % xm: vetor contendo a média das variáveis
    % xstd: vetor contendo o desvio padrão das variáveis
    % Efetivação dos cálculos

    [m,n]=size(X);     % Este comando permite a
visualização do número de linhas e colunas da matriz X.
    xm=mean(X);        % Cálculo da média
    xstd=std(X);       % Cálculo do desvio padrão
    A=ones(m,1)*xm;    % Uso da função ones para
regularizar o tamanho das matrizes.
    B=ones(m,1)*xstd;
    Xauto = (X-A)./B;  % Geração da matriz autoescalada
    Xcm=X-A;           % Geração da matriz centrada na
médiar

    % Visualização dos dados antes e após o pré-
processamento

    plot(X','-');
    xlabel ('Variáveis')
    ylabel ('Sinais')
    title ('Dados originais')

    figure
    plot(Xauto','-')
    xlabel ('Variáveis')
    ylabel ('Sinais autoescalados')
    title ('Dados autoescalados')

    figure
    plot(Xcm','-')
    xlabel ('Variáveis')
    ylabel ('Sinais centrados na média')
    title ('Dados centrados na média')
```

pca_dis:

```
function [scores, loads, var_exp] = pca_dis (X)
    % [scores, loads, var_exp] = pca_dis (X)
    % Esta função tem como objetivo efetuar os cálculos de
uma Análise por Componentes Principais (PCA).
    % Neste caso está sendo utilizada a função svd já
disponível no Octave.
    % Efetivação dos cálculos
    [m,n]=size(X);
    [U,S,V]=svd(X,'econ');

    % Cálculos dos scores, loadings e variância explicada
    scores = U*S;
    loads = V;
    var_exp=(diag(S).^2)*100/(sum(diag(S).^2));

    % Gráficos para visualização dos dados

    plot (var_exp,'-b^')
    xlabel ('Componente Principal (PC)')
    ylabel ('Variância Explicada (%)')
    title ('Variância Explicada')

    figure
    plot (scores(:,1),scores(:,2),'ro')
    xlabel ('PC1')
    ylabel ('PC2')
    title ('Scores PC1xPC2')
    grid
    % Nesta parte foi inserido um loop para identificar as
amostras
    for i=1:m
        text(scores(i,1),scores(i,2),num2str(i))
    end

    figure
    plot (loads(:,1),loads(:,2),'gv')
    xlabel ('PC1')
    ylabel ('PC2')
    title ('Loadings PC1xPC2')
    grid
    % Nesta parte foi inserido um loop para identificar as
variáveis
    for i=1:n
        text(loads(i,1),loads(i,2),num2str(i))
    end
```

libs:

```
function [MAPS,T,P,Var_exp] = libs(MATRIZ,NT,NPH,NPV,PCS)

% Parâmetros de entrada
% MATRIZ, matriz com todos os tiros e todos os pontos na
forma:
% NT, Número de tiros;
% NPH, Número de pontos na horizontal;
% NPV, Número de pontos na vertical;
% PCS, Número de mapas de escores;
% Parâmetros de saída
% MAPS, mapas de escores em tensor 4D na forma NT x PCS x NPV
x NPH
% T, escores na forma NT x NP x componentes principais
% P, loadings na forma NT x comprimento de onda x componentes
principais
% Var_exp, porcentagem de variância explicada por cada PC na
forma NT x
% Matriz X na forma: X(tiros, pontos, espectro)
% TPT, Total de pontos;

TPT = NPH * NPV * NT;
for j=1:NT; ctr=0;
for i=j:NT:TPT
ctr=ctr+1;
X(j,ctr,:)=MATRIZ(i,:);
end
end
% Fazendo o PCA para cada matriz:
for i = 1:NT
    [u,s,v]=svd(squeeze(X(i,:,:)),0);
    T(i,:,:)=u(:,1:PCS)*s(1:PCS,1:PCS);
    P(i,:,:)=v(:,1:PCS);
    Var_exp(i,:)=(diag(s).^2)./sum(diag(s).^2)*100;
end
% Mapa de scores
for i = 1:NT
    for j = 1:PCS; ctr = 0;
        for k = 1:NPV
            for l = 1:NPH
                ctr = ctr + 1;
                MAPS(i,j,k,l) = T(i,ctr,j);
            end
        end
    end
end
```

libs_plot:

```
function libs_plot(MAPS,TIRO,PCS)

% Parâmetros de entrada
% MAPS, mapas de escores em tensor 4D na forma NT x PCS x NPV
x NPH
% TIRO, número do tiro para o qual quer ver os mapas de
escores
% PCS, mapas até qual componente principal? Tem que ser menor
que o valor
% de PCS do MAPS calculado.

for i = 1:PCS
figure(i);contourf(squeeze(squeeze(MAPS(TIRO,i,:,:))));view([
0,270]);
xlabel('Axis x'); ylabel('Axis y');
title (['Score maps of PC',num2str(i),' from pulse
',num2str(TIRO),'']);
colorbar
end
```

Tabela 1S. Tabela de caracterização em ICP OES dos *e-waste* escolhidos para este tutorial

Amostra	ID	Tamanho (µm)	Ag (mg kg^{-1})	Au (mg kg^{-1})	Pt (mg kg^{-1})	Pd (mg kg^{-1})	As (mg kg^{-1})	Al % (m/m)	Cu % (m/m)	Fe % (m/m)	Cr % (m/m)	Pb % (m/m)
1	MB1	< 106	508,88	560,37	0,04	7,46	16,78	3,12	5,93	0,74	0,03	2,46
2	MB2	< 106	372,77	229,19	0,42	9,60	11,24	3,11	7,25	0,46	0,03	2,38
3	N1	< 106	544,56	33,57	0,04	0,01	12,25	2,63	4,47	10,39	0,44	0,05
4	N2	< 106	564,95	77,53	0,04	0,01	9,54	3,09	3,60	7,14	0,06	0,02
5	N3	< 106	465,43	563,77	0,04	0,01	14,47	2,40	5,22	5,74	0,25	0,66
6	N4	< 106	417,44	340,85	0,04	0,01	12,05	2,46	4,75	7,21	0,30	0,40
7	T1	< 106	449,83	765,77	7,31	18,41	139,00	2,26	16,19	2,12	0,26	0,02
8	T2	< 106	406,47	231,56	0,04	0,01	11,08	2,39	7,22	2,96	0,10	0,02
9	T3	< 106	352,82	213,82	0,04	0,48	11,73	2,58	6,52	3,43	0,09	0,02
10	S1	< 106	342,55	2468,06	17,96	126,00	70,63	1,69	16,50	3,65	0,04	1,49
11	S2	< 106	364,72	891,68	12,97	72,93	110,34	0,92	35,20	3,86	0,52	0,11
12	S3	< 106	388,18	717,60	0,04	22,73	105,05	2,81	14,63	1,85	0,14	0,05
13	S4	< 106	394,72	2254,93	1,71	77,88	551,75	1,55	14,20	2,17	0,24	0,04
14	S5	< 106	415,15	2372,41	5,08	71,03	494,96	1,27	12,34	2,01	0,19	0,04
15	S6	< 106	359,60	737,94	1,13	55,45	631,36	2,29	15,14	1,25	0,17	0,03
16	S7	< 106	389,35	1755,36	4,21	22,26	199,27	0,99	18,85	3,04	0,34	0,01
17	MB1	106-212	443,71	86,44	0,62	27,43	15,91	1,90	17,95	0,43	0,01	2,99

Tabela 1S. Tabela de caracterização em ICP OES dos *e-waste* escolhidos para este tutorial (cont.)

Amostra	ID	Tamanho (µm)	Ag (mg kg^{-1})	Au (mg kg^{-1})	Pt (mg kg^{-1})	Pd (mg kg^{-1})	As (mg kg^{-1})	Al % (m/m)	Cu % (m/m)	Fe % (m/m)	Cr % (m/m)	Pb % (m/m)
18	MB2	106-212	476,85	289,68	1,28	24,45	11,19	2,13	15,62	0,24	0,01	3,38
19	N1	106-212	490,43	21,53	0,04	0,01	14,69	1,86	13,59	5,11	0,19	0,05
20	N2	106-212	481,74	24,03	0,04	8,45	9,36	2,12	14,17	2,64	0,02	0,04
21	N3	106-212	400,17	275,89	0,04	20,23	11,24	1,37	15,37	2,09	0,04	0,94
22	N4	106-212	377,95	409,31	0,04	18,15	12,25	1,18	13,54	2,13	0,03	0,83
23	T1	106-212	429,79	353,89	16,34	72,49	8,92	0,34	14,57	0,51	0,11	0,15
24	T2	106-212	380,75	95,47	0,04	19,31	18,15	0,60	12,13	1,24	0,05	0,02
25	T3	106-212	424,17	91,60	0,04	14,75	11,91	1,63	19,63	2,65	0,06	0,01
26	S1	106-212	331,58	511,18	34,55	168,48	24,02	0,86	36,49	3,04	0,03	1,48
27	S3	106-212	346,07	191,27	3,60	58,28	9,75	1,21	40,28	0,58	0,09	0,02
28	S4	106-212	401,14	519,92	4,44	77,10	51,54	1,10	39,56	0,62	0,14	0,04
29	S5	106-212	287,00	1316,78	11,32	118,48	65,80	0,40	26,99	5,84	0,48	0,04
30	S6	106-212	377,64	253,44	6,27	114,12	48,69	1,11	37,61	1,26	0,28	0,03
31	S7	106-212	305,50	442,43	4,97	50,45	22,00	0,55	35,79	0,90	0,18	0,02
32	MB1	212-600	443,05	280,26	0,04	43,34	18,97	1,50	29,03	0,43	0,00	3,48
33	MB2	212-600	407,71	192,23	0,81	46,47	13,19	1,53	32,25	0,17	0,02	5,22
34	N1	212-600	922,29	23,17	0,04	50,06	21,74	1,31	33,41	1,62	0,03	0,03

Tabela 1S. Tabela de caracterização em ICP OES dos *e-waste* escolhidos para este tutorial (cont.)

Amostra	ID	Tamanho (µm)	Ag (mg kg^{-1})	Au (mg kg^{-1})	Pt (mg kg^{-1})	Pd (mg kg^{-1})	As (mg kg^{-1})	Al % (m/m)	Cu % (m/m)	Fe % (m/m)	Cr % (m/m)	Pb % (m/m)
35	N2	212-600	912,76	43,53	0,04	34,85	10,69	1,79	24,45	1,62	0,05	0,02
36	N3	212-600	1006,99	259,81	0,04	57,10	17,56	0,89	35,25	2,13	0,03	1,40
37	N4	212-600	950,83	318,91	0,04	50,33	17,42	1,07	32,16	1,38	0,02	0,79
38	T2	212-600	789,02	108,86	2,73	46,09	12,86	0,98	33,10	1,71	0,11	0,02
39	T3	212-600	335,97	98,96	0,04	30,32	11,44	0,83	37,42	2,41	0,18	0,02
40	S1	212-600	346,90	365,47	0,04	45,88	20,27	0,44	38,73	11,94	0,03	0,81
41	S2	212-600	293,18	216,67	23,47	61,76	23,58	0,77	37,96	3,82	0,94	0,03
42	MB1	> 600	13,41	93,48	0,04	41,93	16,40	1,58	28,24	0,04	0,00	2,41
43	MB2	> 600	30,00	63,20	0,04	32,36	12,39	2,09	21,84	0,29	0,00	1,53
44	N1	> 600	901,74	0,01	0,04	50,61	23,74	1,34	37,11	7,86	0,61	0,02
45	N2	> 600	700,32	0,70	0,04	49,77	13,31	0,90	36,53	6,83	0,19	0,02
46	N3	> 600	666,15	15,27	0,04	31,72	8,16	1,71	24,37	7,97	0,30	0,02
47	N4	> 600	850,31	67,02	7,52	50,41	16,34	0,85	31,44	1,12	0,18	0,50
48	T1	> 600	602,11	0,01	149,84	1,89	17,72	0,54	26,61	15,06	3,99	0,01
49	T2	> 600	378,15	0,01	39,97	32,11	11,80	0,91	29,56	9,64	1,57	0,03
50	T3	> 600	368,94	0,01	25,32	3,62	13,49	0,87	37,03	4,08	1,18	0,02
51	S1	> 600	131,70	0,01	53,10	0,01	16,41	0,25	29,44	19,64	3,32	0,07

Tabela 1S. Tabela de caracterização em ICP OES dos *e-waste* escolhidos para este tutorial (cont.)

Amostra	ID	Tamanho (µm)	Ag (mg kg^{-1})	Au (mg kg^{-1})	Pt (mg kg^{-1})	Pd (mg kg^{-1})	As (mg kg^{-1})	Al % (m/m)	Cu % (m/m)	Fe % (m/m)	Cr % (m/m)	Pb % (m/m)
52	S2	> 600	159,71	0,01	171,50	0,01	31,17	0,34	23,47	22,61	7,74	0,00
53	S3	> 600	292,78	0,01	73,80	0,01	18,30	0,78	36,47	12,31	3,61	0,01
54	S4	> 600	237,60	38,55	35,68	4,90	27,01	0,61	31,27	9,04	1,60	0,04
55	S5	> 600	317,44	129,75	4,70	0,01	20,66	0,21	22,77	21,58	2,06	0,01
56	S6	> 600	257,62	0,01	42,43	14,51	28,99	0,94	33,23	9,39	2,13	0,02
57	S7	> 600	128,58	0,01	39,02	9,96	13,24	0,28	30,43	6,54	1,71	0,01

Chapter 3 - Development of a method for the direct and non-evasive determination in e-waste

3. Development of a method for the direct and non-evasive determination of e-waste

3.1. Regression analysis for e-waste

Regression models are fundamental tools for the quantitative analysis of data in various areas of science, including analytical spectroscopy. The methods traditionally employed include Ordinary Least Squares (OLS), Multiple Linear Regression (MLR), and Principal Component Regression (PCR), which enable the modeling of relationships between dependent variables and multiple independent variables, even in scenarios of multicollinearity or high data dimensionality [110]. Furthermore, Partial Least Squares (PLS) regression has established itself as one of the most widespread techniques, especially in spectroscopy, such as LIBS, as it effectively addresses issues like matrix effects and the redundancy of spectral variables [111,112].

3.1.1. Non-traditional models: MLPCR and ECPR

To address the challenges posed by complex sample matrices and the demand for more robust models, advanced techniques such as Maximum Likelihood Principal Component Regression (MLPCR) [113,114] and Error Covariance Penalized Regression (ECPR) [115] have emerged.

MLPCR evolves from traditional PCR by replacing the Ordinary Least Squares method with Maximum Likelihood Estimation (MLE). This approach, which explicitly models measurement noise, optimizes prediction in scenarios with high correlation and significant noise [116]. Its primary advantage is statistical robustness, but its performance relies on the assumption that errors follow a specific probability distribution, which is its main limitation.

On the other hand, ECPR focuses on correcting correlations among model errors, a common issue caused by instrumental drift. ECPR introduces a penalty term to the error covariance matrix, thereby mitigating the influence of correlated errors and enhancing model stability. While its ability to handle structured errors is a unique advantage, the technique requires the careful optimization of a penalty parameter [117].

Both strategies demonstrate superior analytical performance in their respective niches, achieving high sensitivity, low Limits of Detection (LOD) and Quantification (LOQ)[118] , and relative errors between 1–20%. These results, validated in various scientific applications, establish MLPCR and ECPR as powerful alternatives to conventional methods, making them essential tools for analyses that demand maximum precision, robustness, and reliability [119,120].

3.2. Data fusion

Data fusion is a consolidated approach in the analytical sciences, aimed at combining information from multiple sources to obtain more robust and accurate models. In the context of spectroscopy, especially in the use of techniques such as LIBS, Raman, infrared (IR) or XRF, among other techniques, data fusion has proved essential to overcome analytical limitations associated with matrix effects, spectral interferences and the low selectivity of certain methods [121].

The integration of different data sources can take place at different levels: (i) low-level fusion, where the raw or pre-processed data from each sensor is simply concatenated; (ii) medium-level fusion, where features extracted from the data are combined, such as principal component scores; and (iii) high-level fusion, which involves combining the decisions or predictions of models built separately for each sensor [122]. The data fusion is particularly relevant when different spectroscopic techniques provide complementary information - atomic, molecular or structural - about the sample [123,124].

Proper data pre-processing is essential in this context, since the different sensors can operate in different intensity ranges and units. Thus, normalization techniques, such as the use of the Euclidean norm, are often applied to homogenize the data before fusion [125]. Multivariate models are then applied for regression or classification, such as PLS, Support Vector Machines (SVM) or Artificial Neural Networks (ANN), maximizing the predictive potential of the combined analysis [126].

In recent years, various combinations involving LIBS and other analytical techniques have been proposed, particularly integration with vibrational spectroscopies such as Raman and IR. The combination of LIBS with Raman, for example, allows elemental and molecular information to be obtained simultaneously, providing more comprehensive analyses, as demonstrated by Gibbons et al. [127] and Manrique-Martinez et al. [128], who obtained significant improvements in the accuracy of mineral classification with the use of low-level data fusion.

In the field of infrared spectroscopy, the fusion of LIBS with techniques such as Fourier transform infrared (FTIR) and Near-infrared (NIR) has driven the development of hybrid models for the analysis of complex materials, including coal, fertilizers and agricultural products. Strategies that combine data fusion with advanced variable selection methods, such as particle swarm optimization (PSO), have shown a significant reduction in prediction errors compared to using each technique alone [129].

Furthermore, the fusion of LIBS with techniques such as XRF has made it possible to overcome the specific limitations of each method. XRF, with its high sensitivity for elements with a higher atomic number, and LIBS, which is efficient in detecting light elements, form a complementary combination that enables the complete elemental characterization of solid samples [130–132].

In this chapter, calibration strategies were developed using traditional methods such as PLS and PCR, as well as advanced techniques such as MLPCR and ECPR, which explicitly incorporate the errors of the covariance matrix. In addition, data fusion from LIBS and ED-XRF techniques was proposed for the analysis of e-waste samples. This study was carried out during my internship at the Universidad Nacional de Rosario (Argentina), under the supervision of Prof. Dr. Alejandro Olivieri.

3.3. Electronic waste analysis using laser-induced breakdown spectroscopy (LIBS) and X-ray fluorescence (XRF): Critical evaluation of data fusion for the determination of Al, Cu and Fe

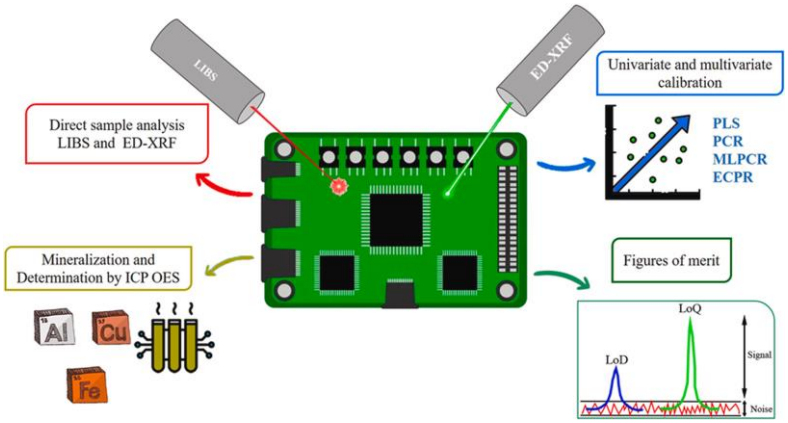

Analytica Chimica Acta 1303 (2024) 342522

Contents lists available at ScienceDirect

Analytica Chimica Acta

journal homepage: www.elsevier.com/locate/aca

Electronic waste analysis using laser-induced breakdown spectroscopy (LIBS) and X-ray fluorescence (XRF): Critical evaluation of data fusion for the determination of Al, Cu and Fe

Dennis S. Ferreira [a,c,d], Fabiola M.V. Pereira [b], Alejandro C. Olivieri [c,d], Edenir R. Pereira-Filho [a,*]

[a] Group of Applied Instrumental Analysis (GAIA), Department of Chemistry, Federal University of São Carlos (UFSCar), P.O. Box 676, São Carlos, São Paulo State, 13565-905, Brazil
[b] Group of Alternative Analytical Approaches (GAAA), Bioenergy Research Institute (IPBEN), Institute of Chemistry, São Paulo State University (UNESP), Araraquara, São Paulo, 14800-060, Brazil
[c] Departamento de Química Analítica, Facultad de Ciencias Bioquímicas y Farmacéuticas, Universidad Nacional de Rosario, Suipacha 531, 2000, Rosario, Argentina
[d] Instituto de Química Rosario (CONICET-UNR), 27 de Febrero 210 Bis, 2000, Rosario, Argentina

HIGHLIGHTS

- Data fusion is applied for enhanced e-waste analysis.
- Direct analytical methods are employed for e-waste characterization.
- E-waste is evaluated with accuracy and precision.
- Resource recovery and environmental stewardship are addressed.
- Global impact and environmental conservation are discussed.

GRAPHICAL ABSTRACT

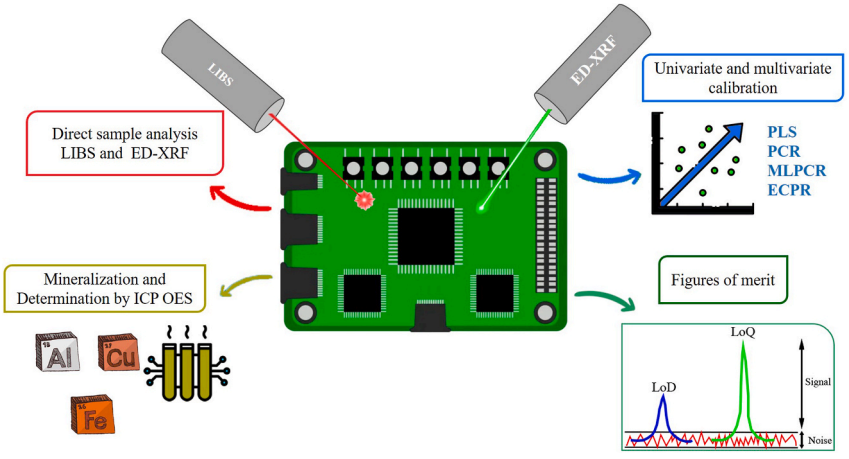

ARTICLE INFO

Handling Editor: Prof. L. Buydens

Keywords:
E-waste
LIBS
Multivariate calibration

ABSTRACT

Background: Electronic waste (e-waste) proliferation and its implications underscore the imperative for advanced analytical methods to mitigate its environmental impact. It is estimated that e-waste production stands at a staggering 20–50 million tons yearly, of which merely 20–25% undergo formal recycling. The e-waste samples evaluated contain computers, laptops, smartphones, and tablets.

* Corresponding author. Group of Applied Instrumental Analysis (GAIA), Department of Chemistry, Federal University of São Carlos (UFSCar), P.O. Box 676, São Carlos, São Paulo State, 13565-905, Brazil.
E-mail address: erpf@ufscar.br (E.R. Pereira-Filho).

https://doi.org/10.1016/j.aca.2024.342522
Received 27 November 2023; Received in revised form 20 March 2024; Accepted 22 March 2024
Available online 22 March 2024

Figure of merit
Data fusion

Results: Forty-one samples were processed, involving the disassembly and separation of components. Subsequently, two analytical techniques, laser-induced breakdown spectroscopy (LIBS) and energy dispersive X-ray fluorescence (ED-XRF), were applied to quantify aluminum (Al), copper (Cu), and iron (Fe) in the e-waste samples. The samples were then analyzed after acid mineralization with 50% v v^{-1} aqua regia in a digester block and finally by ICP OES. A solid residue composed of Si and Ti was observed after the digestion of the samples. Multivariate calibration strategies such as partial least-squares regression (PLS), principal component regression (PCR), maximum likelihood principal component regression (MLPCR), and error covariance penalized regression (ECPR) were used for calibration. Finally, the figures of merit were calculated to verify the most suitable models. The results revealed robust models with notable sensitivity, varying from 8.98 to 35.04 Signal (a.u.)(% w w^{-1}) $^{-1}$, low Limits of Detection (LoD) within the range of 0.001–0.2 % w w^{-1}, and remarkable relative errors ranging from 2% to 33%, particularly for Cu and Fe.
Significance: Notably, the models for Al faced inherent challenges, thus highlighting the complexities associated with its quantification in e-waste samples. In conclusion, this research represents an important step toward a more sustainable and efficient future for electronic waste recycling, signifying its relevance to global environmental welfare and resource conservation.

1. Introduction

Electronic device technology innovation and high consumer demand have revolutionized social investments in network infrastructure, leading to a fast expansion of international trade. However, the short life expectancy of these devices, driven by fast innovation, miniaturization, and affordability, has led to a massive increase in the waste of electric and electronic equipment (WEEE or e-waste) [1].

Electronic waste is one of the fastest-growing streams worldwide, increasing by 3%–5% annually. This type of residue is estimated to represent 8% of urban waste. According to the United Nations (UN), between 20 and 50 Mt of e-waste are generated worldwide yearly, and only 20–25% of this volume is formally recycled. According to data from the e-waste monitor, 53.6 Mt of residue was generated in 2019, an increase of around 8% compared to the previous year [2,3].

The e-waste has various constituents, accounting for around 70 chemical elements from the periodic table. Therefore, e-waste can be considered a barren mine of precious, technological, and base elements, mainly composed of value-added elements: Au, Ag, Cu, Pd, and Pt. Other dangerous constituents such as As, Cd, Pb, and polychlorinated biphenyls can negatively impact the environment when incorrectly discarded, leading to several adverse consequences for health [4,5].

Table 1 [6–15] shows the typical concentration of precious metals in printed circuit boards (PCB) from different types of e-waste, such as computers, cell phones, and tablets. As can be observed, there is a significant variability in the composition, which requires the development of analytical methods for characterization and recycling strategies to recover these important technological, economical, and profitable resources [2].

Table 1
Concentration levels (% w w^{-1}) of Au, Ag, Cu, Pd, and Pt in PCBs from computers and cell phones summarized according to different scientific literature studies.

Elements concentrations (% w w^{-1})					References
Au	Ag	Cu	Pd	Pt	
0.02	0.51	40.90	5.00	2.00	**DERVIŠEVIĆ et al., 2013** [6]
0.02	-	36.00	-	-	**SARVAR et al, 2015** [7]
0.04–0.06	0.18–0.2	14.30–14.80	0.02–0.03	-	**HUBAU et al., 2019** [8]
0.02	0.52–0.63	20.6–22.6	-	-	**PRIYA and HAIT, 2018** [9]
0.02–0.04	0.40–1.48	30.7–96.3	5.0	2.4	**KAMBEROVIĆ et al, 2018** [10]
0.01	0.09	12.20	-	-	**ANDRADE et al, 2019** [11]
0.02	0.09	14.08	-	-	**ANDRADE et al, 2019** [12]
0.02	-	14.8	-	-	**ANDRADE et al, 2021** [13]
0.15	0.07	30.00	0.31	0.11	**CASTRO et al, 2020** [14]
0.08	0.44	85.20	0.08	-	**LIU et al., 2019** [15]

Therefore, it is essential to have an overview of the e-waste stream and develop processing and recycling strategies. In this sense, chemical inspection using analytical techniques is critical in improving recycling methods to recover elements from this large e-waste stream [13].

For example, developing spectroscopic methods based on direct analysis of solid samples could lead to low-cost analytical methods with high analytical frequency of controlling and recovering these residues. Many analytical techniques have been applied in this area, such as wavelength dispersive X-ray fluorescence spectrometry (WD-XRF) [16], energy dispersive X-ray fluorescence (ED-XRF), laser-induced breakdown spectroscopy (LIBS) [13,17,18], near-infrared spectroscopy (NIR) [19] and Raman spectroscopy [20]. These instrumental techniques have been applied to polymer characterization, magnet analysis, and PCB evaluation, among other goals. The chemical information that can be recorded is related to emission spectra, fluorescence, scattering, and absorption in large data matrices. It is, therefore, a challenge to develop new data mining methods to extract and understand this. Chemometric methods have significantly facilitated the sustainable management of these wastes [11–13].

Another advantage of chemometrics is the fusion of data obtained from these techniques. This combination can be at different levels. The raw data are concatenated in low-level data fusion into a single matrix used for multivariate classification and regression. In mid-level fusion, the relevant data are previously extracted from each source and merged into a single matrix. In high-level data fusion, the results collected from each model are combined to provide an accurate prediction [21,22].

In this search for new methods, the present study aims to characterize and quantitatively analyze a set of electronic residues using two techniques, LIBS and ED-XRF, and evaluate the applicability of the fusion of these two datasets to improve the inspection of these residues.

2. Material and methods

2.1. Instrumentation

The determination of Al, Cu, and Fe in electronic waste (e-waste) samples was carried out using a LIBS instrument, J200 model from Applied Spectra (Fremont, USA) equipped with an Nd: YAG laser (1064 nm) used for the emission data acquisition step. The instrument contains a color camera imaging system with a metal oxide semiconductor (CMOS) and 1280 × 1024 resolution. The motion of the sample is made with the automated XYZ stage. An optical fiber bundle is coupled to a 6-channel charged-coupled device (CCD) spectrometer to convert the plasma emission radiation into spectra, with a range of emission signals

between 186 and 1042 nm, resulting in 12,288 variables. The operating parameters were 1000 J cm^{-2} laser pulse fluence, 100 μm spot size, 1 μs delay time, and laser pulse energy of 80 mJ. More details about the spectra acquisition will be provided in the following sections.

A commercial ED-XRF spectrometer obtained X-ray fluorescence signals: Rigaku NEX QC^{+} (Austin, USA), equipped with an Ag target X-ray tube and a Be detector window that can be operated at a maximum voltage of 50 kV.

The reference concentration values for Al, Cu, and Fe were obtained using an ICP OES, iCAP 7000 series (Thermo Fisher Scientific, Madison, USA). The plasma conditions and emission lines used in the analysis are described in Table 1S in the Supplementary Material (SM).

2.2. Reagents

Ultrapure water produced in a Milli-Q® Plus (Millipore Corp, Bedford, MA, USA) was used to prepare all solutions throughout the study. All glassware and polypropylene flasks were previously decontaminated with detergent and immersed in nitric acid solution (HNO_3 10% v v^{-1}) (Synth, Diadema, Brazil) for 24 h and previously rinsed with ultrapure water. The external calibration curves for Al, Cu, and Fe were prepared using appropriate and successive dilutions of 1000 mg L^{-1} stock solution (Specsol, São Paulo, Brazil) with HNO_3 solution. The concentrated acid was previously distilled using the Distillacid™ BSB-939-IR (Berghof, Eningen, Germany).

2.3. Sampling and sample preparation

The e-waste samples consist of computers, laptops, smartphones, and tablets. A total of two end-of-life (EoL) computers, four laptops, seven smartphones, and three tablets were obtained. These were previously manually disassembled and segregated into different parts: polymers, cables, and PCBs. The target sample employed in this study were the PCBs that were ground in a knife mill (Tecnal TE-650, Piracicaba, Brazil), sieved, and segregated into four different particle sizes: (i) < 106 μm; (ii) 106–212 μm; (iii) 212–600 μm and (iv) > 600 μm. As the material is hard to mill, these particle sizes were used in the study development. At the end of the sieving process, 41 samples were obtained (see SM Table 2S).

The ED-XRF analyses were conducted on the powders obtained from the previously described milling process. For the LIBS analyses, the milled samples were previously weighed (500 mg) and pressed in a hydraulic press (Shimadzu SSP-10, Brazil) with a force of 60 kN for 1 min to form pellets with diameters of 12 mm and 2 mm thickness, thus facilitating obtaining the data in the instrument.

From the set of 41 samples, 25 were randomly selected and subjected to reanalysis using the LIBS and ED-XRF techniques in quintuplicate ($n = 5$) for subsequent error covariance calculations, which will be applied to compute the experimental error in multivariate models. All the steps performed to prepare the samples are shown in Fig. 1.

2.4. Reference method: Al, Cu, and Fe determination by ICP OES

The method used as a reference was developed by Andrade et al. [23] and adapted for this study with the following characteristics. Mass samples of 100 mg were weighted directly into closed vials of tetrafluoroethylene-perfluoro (alkoxy vinyl ether) (Savillex, 50 mL PFA block digestion tube with closure, model 210-050-70), with aqua regia (3 parts of HCl and 1 part of HNO_3) diluted (1:1) with deionized water. Both concentrated HNO_3 and HCl (Synth) were previously distilled. The samples were mineralized in a digest block (Marconi MA4025, Piracicaba, Brazil) at a heating temperature of 95 °C for 2 h. The acid extracts were diluted to 50 mL with deionized water, and then Al, Cu, and Fe were determined using ICP OES. All procedures were carried out in triplicates ($n = 3$).

2.5. Spectra acquisition and LIBS data processing

For quantitative analysis of Al, Cu, and Fe using LIBS, a total of 130 spectra were acquired *per* sample using the raster mode of analysis [17]. Microsoft Excel® and MATLAB (R2019b, The Mathworks, USA) were used to process the data and calculate the models. MATLAB was used to apply laboratory codes developed by our research group for data processing [24,25], and Microsoft Excel software was essential to organize the data. The emission lines obtained by LIBS were identified using the Aurora software (Applied Spectra). This program has a database with thousands of emission lines, their concomitants (potential interferents), and relative intensity. The most intense, visually free of shoulders, and double peaks emission lines for each analyte were prioritized and selected.

The spectra obtained by LIBS are highly complex due to the sample microheterogeneity and the signal fluctuation during data acquisition on the solid surface. Thus, to minimize these effects, the data was evaluated using 12 different normalization modes (1-norm, 2-norm,

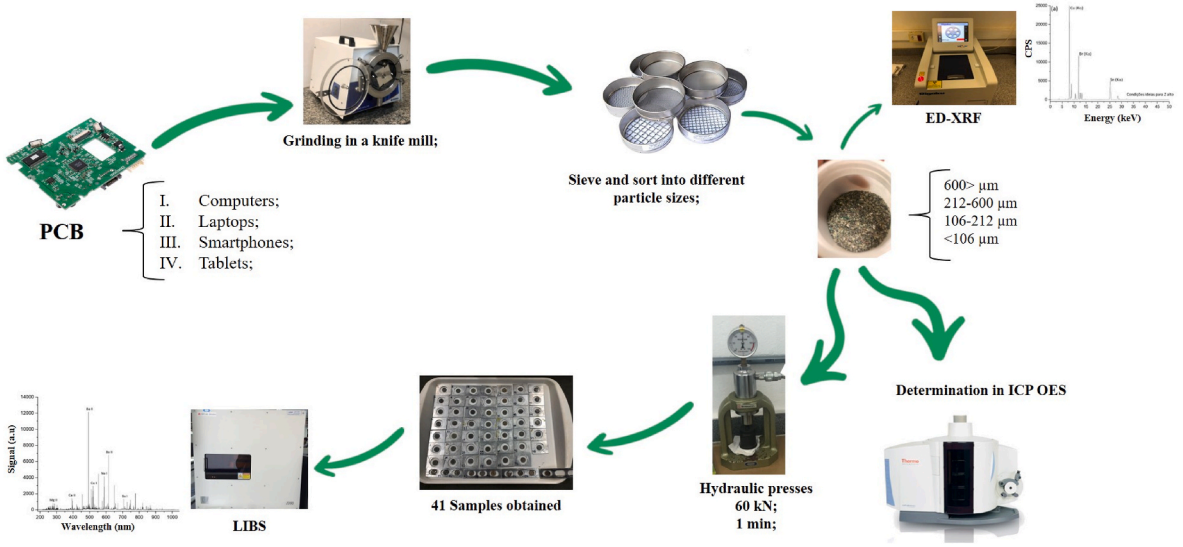

Fig. 1. Pictorial description of the experimental procedure used for sample preparation: LIBS and ED-XRF direct analysis and mineralization for ICP OES determination.

normalization by the highest signal, by the total peak profile, by carbon emission lines, among others), as described by Castro and Pereira-Filho [26].

2.6. Spectra acquisition and ED-XRF data processing

For quantitative analysis using ED-XRF, the samples were separately analyzed in air and He atmosphere under three different instrumental conditions: (i) High atomic number (Ru to Pr and K to Br), 50 kV voltage, 10 μA current and type B filter; (ii) intermediate atomic number (K to Mo and Sn to U), 30 kV voltage, 10 μA current and type A filter and (iii) low atomic number (Sn to U and Na to Cl), 6.5 kV voltage, 50 μA current and no filter. The spectra generated covered the range from 0 to 49.94 keV (0.024 keV resolution), obtaining 2048 energy channels (keV) for each previously described instrumental condition.

2.7. Calibration strategies

The theory behind partial least-squares regression (PLS) and principal component regression (PCR) calibration are well-known and documented in the literature [27–34], and more details are described in the SM. Maximum likelihood principal component regression (MLPCR) and error covariance penalized regression (ECPR) are not common in the literature and will be briefly discussed in the following sections.

In all cases, a calibration data matrix $\mathbf{X}$ ($I \times J$, I = number of samples, J = number of variables) and a calibration concentration vector for the analyte $\boldsymbol{y}$ ($I \times 1$) were subjected to calibration with the multivariate models. This produces a regression vector $\mathbf{b}$ ($J \times 1$), quantifying the analyte using the prediction expression:

$$\hat{y} = \mathbf{x}^{\mathrm{T}}\mathbf{b}$$

Where $\mathbf{x}$ is the spectrum of the validation sample, size $J \times 1$, and the hat () implies the predicted value.

2.7.1. Maximum likelihood principal component regression (MLPCR)

MLPCR is a multivariate calibration strategy based on ML principal component analysis (MLPCA), a decomposition method related to PCA, which considers measurement uncertainties and places less emphasis on measurements with considerable variation in the decomposition process [35]. MLPCR uses an ML projection and differs from PCA, which uses an orthogonal projection. Equation (1) is used for ML projection in the column space where the variables are usually located [36,37].

$$\hat{\mathbf{x}}_i = \widehat{\mathbf{W}}\left(\widehat{\mathbf{W}}^{\mathrm{T}}\Sigma_i^{-1}\widehat{\mathbf{W}}\right)^{-1}\widehat{\mathbf{W}}^{\mathrm{T}}\Sigma_i^{-1}\mathbf{x}_i \tag{1}$$

Where $\mathbf{x}_i$ is a column vector of the calibration data matrix $\mathbf{X}$, $\hat{\mathbf{x}}_i$ is the spectrum of the i-th. sample, $\widehat{\mathbf{W}}$ latent MLPCA projections in space, Σ_i^{-1} the error variance-covariance matrix. The latter matrix can be generated from replicates of the calibration samples.

2.7.2. Error covariance penalized regression (ECPR)

The first version of the ECPR technique was developed by Brown [38], based on inverse least-squares, and only applicable when all the sample constituents are known. The model used in the present study was adapted from the latter by Allegrini et al. [39], in which the authors consider that the measured spectra are from a mixture, but a single analyte is known. The mathematical expression of the model is described by equations (2) and (3):

$$\mathbf{y} = \mathbf{X}\mathbf{b} \tag{2}$$

$$\mathbf{b} = \left(\mathbf{X}^{\mathrm{T}}\mathbf{X} + I\Sigma_i^{-1} + \lambda I\right)^{-1}\mathbf{X}^{\mathrm{T}}\mathbf{y} \tag{3}$$

where $\mathbf{I}$ is an identity matrix of appropriate dimensions and λ is an adjustable parameter, which can be estimated by cross-validation.

The ECPR model has been used in several studies, such as retrieving neural networks from data [40], macroeconomic predictions [41] and also in a statistical context in a calibration model, using sample residuals as a penalty term [42,43], as discussed in the present study.

2.8. Figures of merit and analytical application

Multivariate calibration is an essential spectroanalytical tool for quantitative and semi-quantitative analysis of complex samples. In this study, a method published by Fragoso et al. [44] will be applied to estimate the prediction uncertainties of first-order multivariate models. Therefore, to estimate the model sensitivity, we assume that the error structure for noise is identically and independently distributed (iid), and thus, we can apply the following general Equation (4) for sensitivity:

$$\mathrm{SEN} = \frac{1}{\left(\mathbf{b}^{\mathrm{T}}\mathbf{b}\right)^{\frac{1}{2}}} \tag{4}$$

where $\mathbf{b}$ is the vector of regression coefficients obtained from the calibration phase. However, Equation (4) only applies to PLS and PCR models; for models in which the error covariance is embedded, the expression $(\mathbf{b}^{\mathrm{T}}\mathbf{b})$ is replaced by $(\mathbf{b}^{\mathrm{T}}\Sigma_i^{-1}\mathbf{b})$.

We can also estimate the prediction variance using the following mathematical expression on a theoretical basis (Equation (5)):

$$\sigma_y^2 = SEN^{-2}\sigma_x^2 + hSEN^{-2}\sigma_x^2 + h\sigma_{ycal}^2 \tag{5}$$

where σ_y^2 is the variance of the prediction, σ_x^2 is the variance of the error in the signal, σ_{ycal}^2 is the variance of the errors in the calibration concentrations, SEN is the sensitivity (see Equation (4)), and h is the leverage, a dimensionless parameter calculated using calibration and validation scores. The parameter h is expressed as follows:

$$h = \mathbf{t}^{\mathrm{T}}\left(\mathbf{T}^{\mathrm{T}}\mathbf{T}\right)^{-1}\mathbf{t} \tag{6}$$

where $\mathbf{t}$ is the score vector of the prediction sample, and $\mathbf{T}$ is the calibration score matrix.

The Limit of Detection (LoD) is a function of the analytical signal of the blank and its standard deviation. Therefore, to calculate the LoD for a multivariate model, it is necessary to extrapolate σ_y^2 to a concentration of zero for the analyte of interest. This can be achieved by calculating an orthogonal projection of the scores onto the hyperplane defined by the scores for analyte concentrations equal to zero. This mathematical demonstration was conducted by Allegrini and Olivieri [45], proving to be suitable for estimating LoD in multivariate models across a range of values encompassing both the minimum ($\mathrm{LoD_{min}}$) and maximum ($\mathrm{LoD_{max}}$) (Equation (7)) [46].

$$\begin{aligned} \mathrm{LoD_{min}} &= 3.3\sigma^2_{\mathrm{y\ min}} \quad \mathrm{LoQ_{min}} = 10\ \sigma^2_{\mathrm{y\ min}} \\ \mathrm{LoD_{max}} &= 3.3\sigma^2_{\mathrm{y\ max}} \quad \mathrm{LoQ_{max}} = 10\ \sigma^2_{\mathrm{y\ max}} \end{aligned} \tag{7}$$

More details on how the expressions were developed can be found in Refs. [45–47].

The following Relative error (RE) expression will be used to evaluate the best multivariate models obtained:

$$RE\ (\%) = \frac{|\,RC\ (ICP\ OES)\ -\ PC|}{RC\ (ICP\ OES)} \times 100 \tag{8}$$

Where RC (ICP OES) and PC are reference concentrations obtained using ICP OES determinations and predicted concentrations, respectively. Our main goal was to obtain a model with RE around 0.

3. Results and discussion

3.1. Reference method: ICP OES

The e-waste samples were mineralized by acid block digestion and

analyzed by ICP OES for Al, Cu, and Fe determination. The concentration values obtained were used as a reference to propose multivariate models based on LIBS and ED-XRF signals. The samples' concentrations (% w w^{-1} for Al, Cu, and Fe are shown in Table 2S of the SM. The concentration range for Al, Cu, and Fe varied from 0.21 to 2.81, 4.75–40.28, and 0.04–22.61 % w w^{-1}, respectively. As expected (see Table 1), Cu presented the highest concentration.

3.2. Univariate calibration models for LIBS and ED-XRF

After acquiring around 130 spectra for each sample using LIBS, 12 normalization modes were calculated, and using the code libs_par2 [25], the areas and heights of the signals were calculated for the region of the emission line of interest specified by the user. The monitored emission lines are shown in Table 2: 14 emission lines (λ1- λ14) were monitored for Al, 37 (λ15 – λ51) for Cu, and 30 (λ52- λ81) for Fe. The best results were identified for univariate calibration using LIBS, considering the lowest Root Mean Square Error of Calibration (RMSEC), normalization modes, and their relative errors (Equation (8)) values.

The univariate calibration and RMSEC were also calculated for ED-XRF, but the normalization process was unnecessary since the peak signals were well-defined for the studied elements. The condition chosen for Al was the low atomic number, in which the 1.366–1.610 keV (11 variables) region for Al Kα (1.487 keV) was selected. This condition was chosen because it has the best spectrum definition for this analyte. For Cu and Fe, the condition selected was the high atomic number. The region chosen for Cu was from 7.660 to 8.465 (35 variables) for Cu Kα (8.042 keV) and from 8.733 to 9.074 (15 variables) for Cu Kβ (8.906 keV); for Fe it was the region from 6.141 to 6.635 (22 variables) for Fe Kα (6.400 keV) and from 6.806 to 7.294 (20 variables) for Fe Kβ (7.058 keV). The areas and heights of these analytes from these regions were estimated using the code libs_par [25,48]. Fig. 2 shows the best RMSEC obtained by LIBS and ED-XRF using univariate calibration.

In general, the univariate calibration models resulting from LIBS and ED-XRF cannot correctly predict the concentration values in the samples. This is due to the complexity of the sample, spectral interferences, physical characteristics, and lack of homogeneity of the analytes, which can compromise the determination of metals, as shown by the RMSEC values of the models. For instance, in the case of Fe, the RMSEC values were around 50 % w w^{-1}, much larger than the reference concentrations (see Table 2S, SM) presented between square brackets at the bottom of Fig. 2. Therefore, alternative multivariate calibration strategies are needed to improve the prediction capacity of the models.

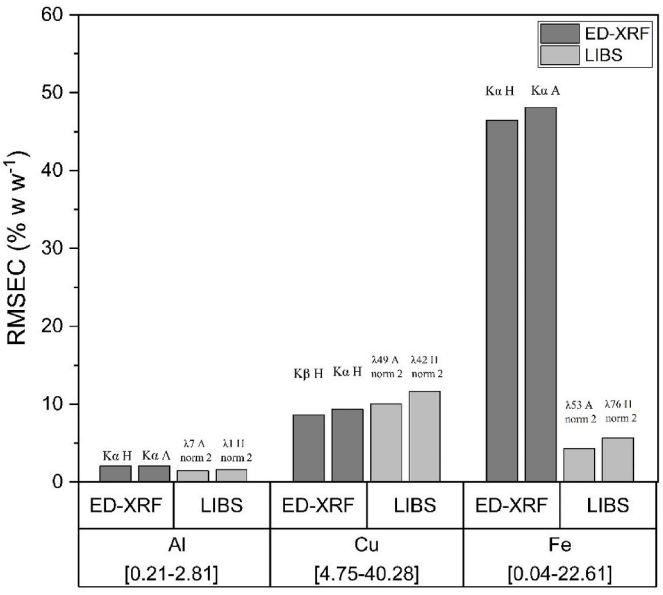

Fig. 2. Root mean squared error of calibration (RMSEC) in % w w^{-1} for univariate calibration strategy using LIBS and ED-XRF. The analytes concentration range is in square brackets for better comparison.

3.3. Multivariate calibration using LIBS data

The multivariate calibration tools were PLS, PCR, MLPCR, and ECPR. Some of these tools are widely used, especially PLS and PCR, due to their ability to deal with multicollinearities, dimensionality reduction, and noisy data. The same area and height data used in the univariate calibration were used for the multivariate calibration strategy, in which all the area and height values were merged into a single **X** matrix (Table 2). For example, for the Cu analyte, all the area data from the 37 wavelengths (see Table 2) were used, generating an **X** matrix (41 × 37): 41 samples with 37 variables (areas of the 37 signals). The same was replicated for the height data and the other analytes using normalization mode 2 (2-norm), which was considered the best because it had the lowest RMSEC in the univariate models (See Fig. 2).

The error covariance was estimated using data obtained in quintuplicate from 25 random samples. With the data obtained, the covariance error of each quintuplicate sample was calculated and then summed to obtain an overall covariance error. This overall covariance error matrix was applied to the multivariate MLPCR and ECPR methods.

Table 2
Emission lines selected and evaluated in the calibration strategies for the elements Al (λ1- λ14), Cu (λ15- λ51), and Fe (λ52- λ81).

Emission lines (nm) for Al		Emission lines (nm) for Cu				Emission lines (nm) for Fe			
λ1	236.930	λ15	203.586	λ34	271.351	λ52	238.204	λ67	274.320
λ2	237.200	λ16	210.479	λ35	272.167	λ53	240.488	λ68	274.407
λ3	237.313	λ17	211.731	λ36	276.637	λ54	241.052	λ69	274.648
λ4	257.509	λ18	212.605	λ37	303.607	λ55	249.326	λ70	274.948
λ5	265.248	λ19	213.598	λ38	306.341	λ56	252.629	λ71	275.403
λ6	274.893	λ20	218.963	λ39	309.993	λ57	252.913	λ72	275.573
λ7	305.007	λ21	219.568	λ40	324.316	λ58	252.955	λ73	276.752
λ8	305.468	λ22	219.975	λ41	324.754	λ59	254.961	λ74	298.357
λ9	305.714	λ23	221.027	λ42	327.396	λ60	256.253	λ75	357.025
λ10	308.215	λ24	221.811	λ43	330.795	λ61	258.588	λ76	358.119
λ11	309.271	λ25	224.261	λ44	427.511	λ62	259.940	λ77	373.486
λ12	309.284	λ26	224.700	λ45	458.701	λ63	260.709	λ78	373.713
λ13	394.400	λ27	227.626	λ46	465.112	λ64	261.187	λ79	374.948
λ14	396.152	λ28	244.164	λ47	510.554	λ65	263.132	λ80	375.823
		λ29	248.579	λ48	515.324	λ66	273.955	λ81	438.354
		λ30	260.027	λ49	521.820				
		λ31	268.930	λ50	578.213				
		λ32	270.096	λ51	809.263				
		λ33	270.319						

Among the 41 studied samples, 30 (73%) were selected for model calibration, and 11 (27%) were used for validation. The well-known Kennard and Stone [49,50] uniform subset selection algorithm was employed to select the calibration samples.

Fig. 3 shows the RMSEC (a) and RMSEV (b) values for Al, Cu, and Fe calculated from the peak heights and areas using only LIBS data. In order to assess which were the best regression models, the main parameter is the RMSEV, as it indicates how close the reference values for the validation samples are to those predicted by the model, which was built with the calibration data.

Evaluating the models for Al presented an RMSEC of 0.68 % w w^{-1} (for the PCR model based on the peak area), with 5 principal components and an RMSEV of 0.69 % w w^{-1}. These values are very close to those rendered by the PLS and EPCR models: RMSEC of 0.74 and 0.59 % w w^{-1}, respectively and RMSEV of 0.71 % w w^{-1} for both. The best model for calibration and prediction was MLPCR with peak area, with an RMSEC value of 0.57 % w w^{-1} and an RMSEV of 0.75 % w w^{-1}. Inspecting Fig. 1S (SM), which shows reference vs. predicted values for all the models, we conclude that the MLPCR model has the best linearity and the lowest RMSEV and is the one that best quantifies Al in the electronic residues using only the LIBS data.

Evaluating the models obtained for the Cu in Fig. 3, those with the best calibration fit were ECPR with peak height, with an RMSEC of 0.002 % w w^{-1}, and PCR and PLS with peak area, both with an RMSEC value of 0.10 % w w^{-1}. The prediction plots (Fig. 2S, SM) showed excellent linearity. The models with the lowest RMSEV values were PLS with peak height, with RMSEV 0.51 % w w^{-1} and ECPR with peak area with RMSEV 0.52 % w w^{-1}. Although the previous models presented a perfect fit, they had larger RMSEV values. Hence, the models best suited to estimating Cu concentration were PLS with peak height and ECPR with peak area. Inspecting Fig. 3 and 2S (SM), the ECPR model presented the best calibration model with an RMSEC of 0.17 % w w^{-1}, which is theoretically considered the most suitable model for estimating Cu under these conditions. From a practical point of view, however, PLS is the most suitable one because it does not require replicates to calculate the error covariance matrix, making this strategy more accessible and cheaper from an industrial perspective.

Among the models proposed to quantify Fe, those with the best calibration performance, according to Fig. 3, were ECPR with peak area, with RMSEC = 0.12 % w w^{-1} and MLPCR with peak height with RMSEC = 0.17 % w w^{-1}. Analyzing Fig. 3S (SM), both models show excellent linearity. Considering the RMSEV values, the best models were PCR and ECPR, with peak height and RMSEV = 0.31 and 0.53 % w w^{-1}, respectively. Regarding the linearity of the models in Fig. 3S (SM), we conclude that both models are suitable for quantifying Fe in e-waste. However, PCR is the most industrially viable model because it does not require replicates, as discussed for the determination of Cu.

3.4. Multivariate calibration using LIBS + ED-XRF data fusion

Interest was focused on the combination of LIBS and ED-XRF data to obtain better models, taking advantage of the selectivity contributed by each technique to a model built with fused data. With this aim, LIBS and ED-XRF data were merged using 2-norm, where each signal is divided by the Euclidean norm of the respective spectra to ensure that the amplitude of the signals is of the same magnitude (same norm). In the same way, as in the previous section, all four multivariate strategies were applied to verify if the results improved when compared to the models only based on LIBS data.

As regards the results obtained for Al (see Fig. 4), the best model is PCR with peak area fusion with 5 PCs, RMSEV = 0.69 % w w^{-1} and RMSEC = 0.68 % w w^{-1}. However, when Fig. 4S (SM) is analyzed, the predicted vs. reference plots are highly dispersed. The same situation occurs for the remaining fusion models, and thus, it is concluded that data fusion for this element makes the obtained models unsuitable for estimating Al.

For Cu (Fig. 4), the best calibration models were PLS and PCR, both with peak area fusion data with RMSEC = 0.12 % w w^{-1} and ECPR for peak height fusion data with RMSEC = 0.13 % w w^{-1}, while the models with the best validation parameters were PCR with peak height fusion with RMSEV = 0.44 % w w^{-1}, and ECPR with peak area data fusion, presenting RMSEV = 0.47 % w w^{-1}. We conclude that both fit well and can be used to predict Cu by evaluating the multivariate regression profile in Fig. 5S (SM) for the models with the best validation performance. The improvement obtained with the fusion models is ca. 16 %, a slight improvement which may not be significant because of the difficulties associated with data collection on two different instruments.

Regarding the models from data fusion for the Fe element, the values in Fig. 4 show that the best calibration models were ECPR and PLS with peak area fusion with RMSEC = 0.09 and 0.29 % w w^{-1}, respectively. Fig. 6S (SM) shows that both models have excellent linearity. The best validation values were for MLPCR and ECPR with peak height fusion, with RMSEV = 0.30 and 0.31 % w w^{-1}, respectively. Both have good linearity and are suitable models for estimating Fe. However, when comparing the RMSEV values obtained from the fusion with the LIBS-only data, the improvement is only 3%.

In sum, comparing the results obtained with and without data fusion, it can be concluded that the model was degraded to completely losing linearity for the Al. On the other hand, the improvement is minimal for the Cu and Fe elements, making the data fusion strategy unfeasible from an industrial point of view.

3.5. Figures of merit and Analytical application

The best multivariate models obtained in the previous sections were selected, and the figures of merit were estimated: SEN, LoD (minimum

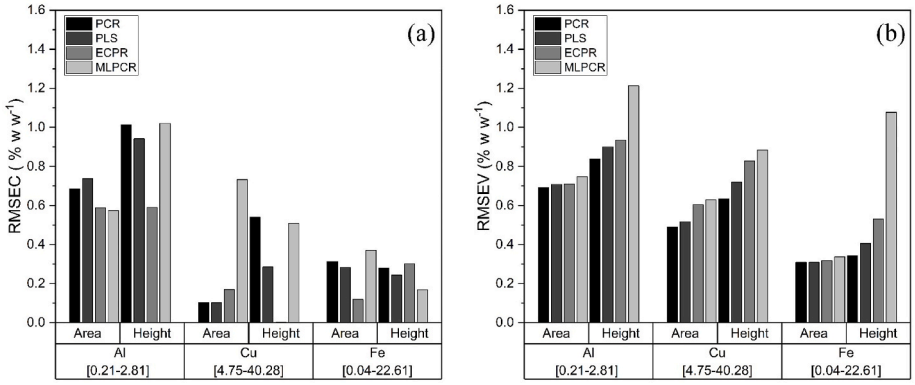

Fig. 3. RMSEC (a) and RMSEV (b) values estimated in % w w^{-1} for each calibration model using LIBS data only. The analytes concentration range is in square brackets for better comparison.

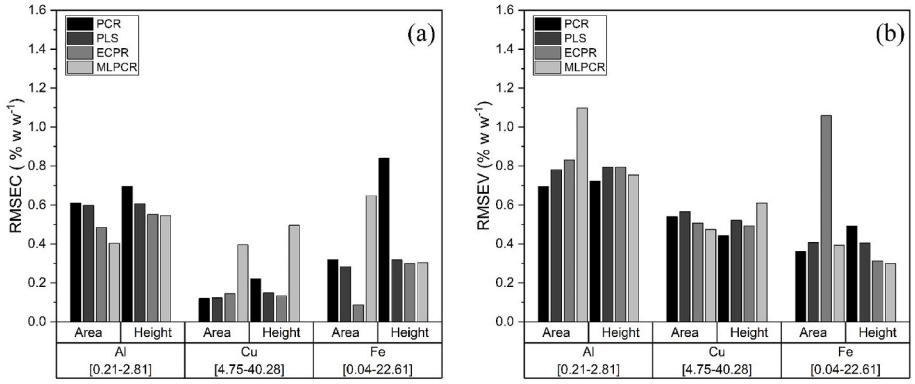

Fig. 4. RMSEC (a) and RMSEV (b) values estimated in % w w^{-1} for each calibration model using LIBS and ED-XRF data fusion. The analytes concentration range is in square brackets for better comparison.

and maximum), LoQ (minimum and maximum), and accuracy values, available in Table 3. For Al, the results were not satisfactory (Table 3), and the conclusion is that the models are unsuitable for this element due to the abovementioned factors that interfere with obtaining the LIBS signal. The relative error values varied from 78 to 444%. The LoD and LoQ values for Al were not reported because they were unreasonably small. Fig. 7S shows the integrated area for the 14 emission lines selected for Al (λ1 up to λ14; see more details in Table 2), considering Sample 33. This sample was one of the selected samples to calculate the covariance matrix used in the regression models. Five replicates were obtained for each emission line, and as can be noted, the integrated areas are very stable. The relative standard error (RSD) for this case varied from 0.5 (emission line λ1) up to 7.2 % (emission line λ13). These low RSD values led to very optimistic results for limits.

For Cu, the figures of merit values were estimated for the four best models mentioned in the previous section (Table 3). All the models showed SEN values between 8.98 and 17.38 Signal (a.u.)(% w w^{-1})$^{-1}$, LoDs between 0.004 and 0.2 % w w^{-1}, and LoQs between 0.01 and 0.6 % w w^{-1}. These values are well below the lowest copper concentration of 4.75 % w w^{-1} (see Table 2S, SM, and Figs. 2–4) and have relative errors between 9 and 30%. Therefore, all the estimated models are satisfactory and can be chosen for Cu determination in e-waste. However, from a theoretical point of view, the best model is PCR, showing the largest SEN, the lowest LoD and LoQ values, and the best relative errors (2–30%). In the case of Cu, 33 emission lines (λ15 up to λ51, see Table 2) were selected, and Fig. 8S shows a considerable variability in the integrated areas. The RSD values for Cu varied from 9.4 (emission line λ44) up to 87.2% (emission line λ31). This high variability is reflected in more realistic values of limits.

Finally, the figures of merit for Fe considering the four best models were estimated (Table 3). SEN values ranged from 7.9 to 35.04 Signal (a.u.)(% w w^{-1})$^{-1}$, LoDs from 0.001 to 0.03 % w w^{-1}, LoQs from 0.001 to 0.10 % w w^{-1}, and relative errors from 8 to 33 %. For this element, the models were satisfactory, with high sensitivity, low LoD and LoQ values, and optimum relative errors for this type of direct calibration.

4. Conclusions

This study addressed an alternative way of solving e-waste management issues, focusing on the determination of at least two critical elements (Cu and Fe). E-waste is a growing problem worldwide due to the rapid generation of electronic devices that contain valuable elements and hazardous components, making developing efficient recycling and analysis methods essential. In the present study, e-waste was characterized by the acid block method and the direct analysis of samples by two analytical techniques, LIBS and ED-XRF, which were employed to characterize, calibrate, and quantify the elements Al, Cu, and Fe in different materials.

The results indicate that univariate calibration models for LIBS and ED-XRF had limitations due to the complexity and heterogeneity of e-waste samples. The study, therefore, explored multivariate calibration strategies, including PLS, PCR, MLPCR, and ECPR as calibration models.

Table 3
Estimated figures of merit for the best multivariate models calculated for LIBS data and LIBS + ED-XRF fusion data.

Analytes and concentration range in square brackets (% w w^{-1})	Model	Remark	Parameter method	SEN (Signal (a.u.) (% w w^{-1}) $^{-1}$)	Limits of detection and quantification (% w w^{-1})				RE (%)
					LoD_{min}	LoD_{max}	LoQ_{min}	LoQ_{max}	
Al [0.21–2.81]	MLPCR**	Area	11	21.63	N.R.[a]	N.R.[a]	N.R.[a]	N.R.[a]	69–339
	PCR**	Fusion Area	6	21.85	N.R.[a]	N.R.[a]	N.R.[a]	N.R.[a]	78–444
Cu [4.75–40.28]	EPCR***	Area	0.27	12.89	0.02	0.04	0.06	0.1	9–26
	EPCR	Fusion Area	11	11.97	0.07	0.2	0.2	0.6	6–27
	PLS*	Height	7	8.98	0.03	0.04	0.09	0.1	7–25
	PCR	Fusion Height	18	17.38	0.004	0.010	0.01	0.02	2–30
Fe [0.04–22.61]	PCR	Height	17	22.92	0.001	0.001	0.002	0.003	14–33
	EPCR	Height	0.10	35.04	0.001	0.003	0.002	0.008	18–24
	MLPCR	Fusion Height	13	7.90	0.02	0.03	0.07	0.1	8–26
	EPCR	Fusion Height	0.10	30.72	0.001	0.004	0.003	0.01	10–29

Latent variable*. Principal Component**. λ***.
[a] N.R. = not reported. The estimated values using the standard equations are unreasonably low in view of the poor analyte recoveries for this element.

For Al, MLPCR using peak area provided the most accurate results. Quantification of Cu was best achieved using PLS with peak height or ECPR with peak area, both showing excellent linearity. The most suitable model for Fe quantification was PCR with peak area or ECPR with peak height. In addition, the study attempted to improve the models by merging LIBS and ED-XRF data. However, the fusion only marginally improved the results for Cu and Fe, being unnecessary in an industrial application.

The numerical figures of merit showed that the best models obtained satisfactory results for Cu and Fe, with good sensitivity, LoD, LoQ, and low relative error. These models can be used effectively to quantitatively determine Cu and Fe in electronic waste. However, the quantification of Al proved to be challenging due to the factors affecting the acquisition of the LIBS signal.

In summary, this research is of high relevance for efficient e-waste management. It highlights the potential of multivariate calibration strategies to improve the quantification accuracy of valuable elements in e-waste without destroying the sample to quantify elements with potential added value. The study results can improve industrial practices and promote more sustainable e-waste recycling processes. On the other hand, there is enough room for improvements targeting noble elements such as Ag and Au, but the sensitivity of the commercial LIBS system is still a challenging limitation.

CRediT authorship contribution statement

Dennis S. Ferreira: Visualization, Software, Methodology, Investigation, Formal analysis, Data curation. **Fabiola M.V. Pereira:** Resources, Project administration, Methodology, Investigation, Funding acquisition, Formal analysis. **Alejandro C. Olivieri:** Supervision, Methodology, Investigation, Funding acquisition, Formal analysis, Conceptualization. **Edenir R. Pereira-Filho:** Supervision, Resources, Project administration, Methodology, Investigation, Funding acquisition, Formal analysis, Conceptualization.

Declaration of competing interest

The authors declare that they have no known competing financial interests or personal relationships that could have appeared to influence the work reported in this paper.

Data availability

Data will be made available on request.

Acknowledgments

The authors are grateful for grants from the São Paulo State Research Foundation (FAPESP) [processes 2016/17221–8, 2019/24223–5, 2019/01102–8, 2021/10882–7 and 2022/02232–5]; National Council for Scientific and Technological Development, CNPq [grants no. 302085/2022–0,140867/2021–0, 302719/2020–2 and 307328/2019–8]. This study was partly funded by the Coordination for the Improvement of Higher Education Personnel - Brazil (CAPES) - Funding Code 001. A.C.O. thanks Universidad Nacional de Rosario, CONICET, and ANPCyT (Project PICT 2020–00179) for financial support.

Appendix A. Supplementary data

Supplementary data to this article can be found online at https://doi.org/10.1016/j.aca.2024.342522.

References

[1] J. Li, X. Zeng, M. Chen, O.A. Ogunseitan, A. Stevels, "control-Alt-Delete": rebooting solutions for the E-waste problem, Environ. Sci. Technol. 49 (2015) 7095–7108, https://doi.org/10.1021/acs.est.5b00449.
[2] V. Forti, C. Peter Baldé, The Global E-waste Monitor 2020. Quantities, flows, and the circular economy potential. https://www.researchgate.net/publication/342783104, 2020.
[3] R. Widmer, H. Oswald-Krapf, D. Sinha-Khetriwal, M. Schnellmann, H. Böni, Global perspectives on e-waste, Environ. Impact Assess. Rev. 25 (2005) 436–458, https://doi.org/10.1016/J.EIAR.2005.04.001.
[4] S. Zhang, Y. Ding, B. Liu, C. chi Chang, Supply and demand of some critical metals and present status of their recycling in WEEE, Waste Manag. 65 (2017) 113–127, https://doi.org/10.1016/J.WASMAN.2017.04.003.
[5] M. Ottoni, P. Dias, L.H. Xavier, A circular approach to the e-waste valorization through urban mining in Rio de Janeiro, Brazil, J. Clean. Prod. 261 (2020) 120990, https://doi.org/10.1016/J.JCLEPRO.2020.120990.
[6] I. Dervišević, D. Minić, Ž. Kamberović, V. Ćosović, M. Ristić, Characterization of PCBs from computers and mobile phones, and the proposal of newly developed materials for substitution of gold, lead and arsenic, Environ. Sci. Pollut. Res. Int. 20 (2013) 4278–4292, https://doi.org/10.1007/S11356-012-1448-1.
[7] M. Sarvar, M.M. Salarirad, M.A. Shabani, Characterization and mechanical separation of metals from computer Printed Circuit Boards (PCBs) based on mineral processing methods, Waste Manag. 45 (2015) 246–257, https://doi.org/10.1016/J.WASMAN.2015.06.020.
[8] A. Hubau, A. Chagnes, M. Minier, S. Touzé, S. Chapron, A.G. Guezennec, Recycling-oriented methodology to sample and characterize the metal composition of waste Printed Circuit Boards, Waste Manag. 91 (2019) 62–71, https://doi.org/10.1016/J.WASMAN.2019.04.041.
[9] A. Priya, S. Hait, Comprehensive characterization of printed circuit boards of various end-of-life electrical and electronic equipment for beneficiation investigation, Waste Manag. 75 (2018) 103–123, https://doi.org/10.1016/J.WASMAN.2018.02.014.
[10] Ž. Kamberović, M. Korać, D. Ivšić, V. Nikolić, M. Ranitović, Hydrometallurgical process for extraction of metals from electronic waste-part I: material characterization and process option selection, J. Inst. Eng. 15 (2018) 231–243, https://doi.org/10.30544/382.
[11] D.F. Andrade, R.C. Machado, M.A. Bacchi, E.R. Pereira-Filho, Proposition of electronic waste as a reference material – part 1: sample preparation, characterization and chemometric evaluation, J Anal At Spectrom 34 (2019) 2394–2401, https://doi.org/10.1039/C9JA00283A.
[12] D.F. Andrade, R.C. Machado, E.R. Pereira-Filho, Proposition of electronic waste as a reference material – part 2: homogeneity, stability, characterization, and uncertainties, J Anal At Spectrom 34 (2019) 2402–2410, https://doi.org/10.1039/C9JA00284G.
[13] D.F. Andrade, E. de Almeida, H.W.P. de Carvalho, E.R. Pereira-Filho, D. Amarasiriwardena, Chemical inspection and elemental analysis of electronic waste using data fusion - application of complementary spectroanalytical techniques, Talanta 225 (2021) 122025, https://doi.org/10.1016/J.TALANTA.2020.122025.
[14] J.P. Castro, E.R. Pereira-Filho, Chemical exploratory analysis of printed circuit board (PCB) using inductively coupled plasma optical emission spectrometry (ICP OES): data treatment and elements correlation, Detritus 13 (2020) 131, https://doi.org/10.31025/2611-4135/2020.14039.
[15] W. Liu, P. Ford, H. Uvegi, F. Margarido, E. Santos, P. Ferrão, E. Olivetti, Economics of materials in mobile phone preprocessing, focus on non-printed circuit board materials, Waste Manag. 87 (2019) 78–85, https://doi.org/10.1016/J.WASMAN.2019.01.044.
[16] J.P. Castro, M.A. Sperança, D.V. Babos, D.F. Andrade, E.R. Pereira-Filho, Neodymium determination in hard drive disks magnets using different calibration approaches for wavelength dispersive X-ray fluorescence, Spectrochim. Acta Part B At. Spectrosc. 164 (2020) 105763, https://doi.org/10.1016/J.SAB.2019.105763.
[17] J.A. Garcia, J.R.A. da Silva, E.R. Pereira-Filho, LIBS as an alternative method to control an industrial hydrometallurgical process for the recovery of Cu in waste from electro-electronic equipment (WEEE), Microchem. J. 164 (2021) 106007, https://doi.org/10.1016/J.MICROC.2021.106007.
[18] D.F. Andrade, F.M. Fortunato, E.R. Pereira-Filho, Calibration strategies for determination of the in content in discarded liquid crystal displays (LCD) from mobile phones using laser-induced breakdown spectroscopy (LIBS), Anal. Chim. Acta 1061 (2019) 42–49, https://doi.org/10.1016/J.ACA.2019.02.038.
[19] S. Mukherjee, A. Gowen, A review of recent trends in polymer characterization using non-destructive vibrational spectroscopic modalities and chemical imaging, Anal. Chim. Acta 895 (2015) 12–34, https://doi.org/10.1016/J.ACA.2015.09.006.
[20] K.M.M. Shameem, K.S. Choudhari, A. Bankapur, S.D. Kulkarni, V.K. Unnikrishnan, S.D. George, V.B. Kartha, C. Santhosh, A hybrid LIBS–Raman system combined with chemometrics: an efficient tool for plastic identification and sorting, Anal. Bioanal. Chem. 409 (2017) 3299–3308, https://doi.org/10.1007/s00216-017-0268-z.
[21] E. Szymańska, Modern data science for analytical chemical data - a comprehensive review, Anal. Chim. Acta 1028 (2018) 1–10, https://doi.org/10.1016/J.ACA.2018.05.038.
[22] D. Lahat, T. Adali, C. Jutten, Multimodal data fusion: an overview of methods, challenges, and prospects, Proc. IEEE 103 (2015) 1449–1477, https://doi.org/10.1109/JPROC.2015.2460697.
[23] D.F. Andrade, R.C. Machado, M.A. Bacchi, E.R. Pereira-Filho, Proposition of electronic waste as a reference material – part 1: sample preparation,

characterization and chemometric evaluation, J Anal At Spectrom 34 (2019) 2394–2401, https://doi.org/10.1039/C9JA00283A.
[24] G. Galbács, Laser-Induced Breakdown Spectroscopy in Biological, Forensic and Materials Sciences, Springer International Publishing, 2022, https://doi.org/10.1007/978-3-031-14502-5.
[25] E.R. Pereira-Filho, Laser-induced breakdown spectroscopy (LIBS): applications and calibration strategies, Editora Ibero-Americana de Educação (2021), https://doi.org/10.47519/EIE.978-65-86839-05-0.
[26] J.P. Castro, E.R. Pereira-Filho, Twelve different types of data normalization for the proposition of classification, univariate and multivariate regression models for the direct analyses of alloys by laser-induced breakdown spectroscopy (LIBS), J Anal At Spectrom 31 (2016) 2005–2014, https://doi.org/10.1039/C6JA00224B.
[27] A.C. Olivieri, Introduction to Multivariate Calibration, Springer International Publishing, 2018, https://doi.org/10.1007/978-3-319-97097-4.
[28] H.C. Goicoechea, A.C. Olivieri, La calibración en química analítica, first ed., Universidad Nacional Del Litoral, 2007.
[29] R. De Maesschalck, F. Estienne, J. Verdú-Andrés, A. Candolfi, V. Centner, F. Despagne, D. Jouan-Rimbaud, B. Walczak, D.L. Massart, S. De Jong, O.E. De Noord, C. Puel, B.M.G. Vandeginste, The development of calibration models for spectroscopic data using principal component regression, Internet J. Chem. 2 (1999).
[30] P. Geladi, B.R. Kowalski, Partial least-squares regression: a tutorial, Anal. Chim. Acta 185 (1986) 1–17, https://doi.org/10.1016/0003-2670(86)80028-9.
[31] T. Rajalahti, O.M. Kvalheim, Multivariate data analysis in pharmaceutics: a tutorial review, Int. J. Pharm. 417 (2011) 280–290, https://doi.org/10.1016/J.IJPHARM.2011.02.019.
[32] M.S. Collado, V.E. Mantovani, H.C. Goicoechea, A.C. Olivieri, Simultaneous determination of nicotinamide and inosine in ophthalmic solutions by uv spectrophotometry and pls-1 multivariate calibration, Anal. Lett. 34 (2001) 363–376, https://doi.org/10.1081/AL-100102579.
[33] H.C. Goicoechea, A.C. Olivieri, Wavelength selection by net analyte signals calculated with multivariate factor-based hybrid linear analysis (HLA). A theoretical and experimental comparison with partial least-squares (PLS), Analyst 124 (1999) 725–731, https://doi.org/10.1039/A900325H.
[34] M.É. Ribone, A.P. Pagani, A.C. Olivieri, Determination of the minor component bromhexine in cotrimoxazole-containing tablets by absorption spectrophotometry and partial least-squares (PLS-1) multivariate calibration, J. Pharm. Biomed. Anal. 23 (2000) 591–595, https://doi.org/10.1016/S0731-7085(00)00344-7.
[35] L. Vega-Montoto, P.D. Wentzell, Maximum likelihood parallel factor analysis (MLPARAFAC), J. Chemom. 17 (2003) 237–253, https://doi.org/10.1002/CEM.789.
[36] S.K. Schreyer, M. Bidinosti, P.D. Wentzell, Application of maximum likelihood principal components regression to fluorescence emission spectra, Appl. Spectrosc. 56 (2002) 789–796, https://doi.org/10.1366/000370202760076857.
[37] D.T. Andrews, P.D. Wentzell, Applications of maximum likelihood principal component analysis: incomplete data sets and calibration transfer, Anal. Chim. Acta 350 (1997) 341–352, https://doi.org/10.1016/S0003-2670(97)00270-5.
[38] C.D. Brown, Discordance between net analyte signal theory and practical multivariate calibration, Anal. Chem. 76 (2004) 4364–4373, https://doi.org/10.1021/AC049953W.
[39] F. Allegrini, J.W.B. Braga, A.C.O. Moreira, A.C. Olivieri, Error Covariance Penalized Regression: a novel multivariate model combining penalized regression with multivariate error structure, Anal. Chim. Acta 1011 (2018) 20–27, https://doi.org/10.1016/J.ACA.2018.02.002.
[40] H. Alidaee, E. Auerbach, M.P. Leung, Recovering network structure from aggregated relational data using penalized regression, ArXiv Preprint 1 (2020) 1–17, https://doi.org/10.48550/arXiv.2001.06052.
[41] S. Smeekes, E. Wijler, Macroeconomic forecasting using penalized regression methods, Int. J. Forecast. 34 (2018) 408–430, https://doi.org/10.1016/J.IJFORECAST.2018.01.001.
[42] Y.J. Yoon, C. Park, T. Lee, Penalized regression models with autoregressive error terms, J. Stat. Comput. Simulat. 83 (2013) 1756–1772, https://doi.org/10.1080/00949655.2012.669383.
[43] J.H. Kalivas, B. Brownfield, B.J. Karki, Sample-wise spectral multivariate calibration desensitized to new artifacts relative to the calibration data using a residual penalty, J. Chemom. 31 (2017) e2873, https://doi.org/10.1002/CEM.2873.
[44] W. Fragoso, F. Allegrini, A.C. Olivieri, A new and consistent parameter for measuring the quality of multivariate analytical methods: generalized analytical sensitivity, Anal. Chim. Acta 933 (2016) 43–49, https://doi.org/10.1016/J.ACA.2016.06.022.
[45] F. Allegrini, A.C. Olivieri, IUPAC-consistent approach to the limit of detection in partial least-squares calibration, Anal. Chem. 86 (2014) 7858–7866, https://doi.org/10.1021/ac501786u.
[46] F. Allegrini, A.C. Olivieri, Recent advances in analytical figures of merit: heteroscedasticity strikes back, Anal. Methods 9 (2017) 739–743, https://doi.org/10.1039/C6AY02916G.
[47] A.C. Olivieri, N.M. Faber, J. Ferré, R. Boqué, J.H. Kalivas, H. Mark, Uncertainty estimation and figures of merit for multivariate calibration: (IUPAC technical report), Pure Appl. Chem. 78 (2006) 633–661, https://doi.org/10.1351/pac200678030633.
[48] M.A. Sperança, P.A.M. Nascimento, F.M.V. Pereira, Impurity in sugarcane juice as mineral content: a prospect for analysis using energy-dispersive X-ray fluorescence (EDXRF) and chemometrics, Microchem. J. 164 (2021) 105951, https://doi.org/10.1016/J.MICROC.2021.105951.
[49] G.K. Krug, Computer aided design of experiments, Period. Polytech. - Electr. Eng. 19 (1975) 181–189, https://doi.org/10.2307/1266770.
[50] M. Daszykowski, B. Walczak, D.L. Massart, Representative subset selection, Anal. Chim. Acta 468 (2002) 91–103, https://doi.org/10.1016/S0003-2670(02)00651-7.

ELECTRONIC WASTE ANALYSIS USING LASER-INDUCED BREAKDOWN SPECTROSCOPY (LIBS) AND X-RAY FLUORESCENCE (XRF): CRITICAL EVALUATION OF DATA FUSION FOR THE DETERMINATION OF Al, Cu AND Fe

Dennis S. Ferreira,[a,c] Fabiola M. V. Pereira,[b] Alejandro C. Olivieri[c] and Edenir R. Pereira-Filho[a*]

[a]Group of Applied Instrumental Analysis (GAIA), Department of Chemistry, Federal University of São Carlos (UFSCar), P.O. Box 676, São Carlos, São Paulo State, 13565-905, Brazil

[b]Group of Alternative Analytical Approaches (GAAA), Bioenergy Research Institute (IPBEN), Institute of Chemistry, São Paulo State University (UNESP), Araraquara, São Paulo, 14800-060, Brazil

[c]Departamento de Química Analítica, Facultad de Ciencias Bioquímicas y Farmacéuticas, Universidad Nacional de Rosario, Suipacha 531 (2000) Rosario, Argentina, and Instituto de Química Rosario (CONICET-UNR), 27 de Febrero 210 Bis (2000) Rosario, Argentina

[*]Corresponding author: Edenir R. Pereira-Filho

Phone number: +55 16 3351-8092

E-mail: erpf@ufscar.br

1. Principal component regression (PCR)

For the principal component regression model, the calibration data matrix **X** (size $I \times J$, I = number of calibration samples, J = number of predictor variables) is decomposed into the product of two smaller matrices, capturing the variance in **X**. The decomposition renders the score matrix **T** (size $I \times A$) and the loading matrix **P** (size $J \times A$), where A is the optimum number of latent variables, usually estimated by leave-one-out cross-validation [1].

In the prediction phase, the analyte content in a test sample whose spectrum is **x** is estimated according to:

$$\hat{y} = \mathbf{x}^{\mathrm{T}}\,\mathbf{b} \qquad (1)$$

In the latter equation, **b** is the vector of model regression coefficients obtained during the calibration step from:

$$\mathbf{b} = \mathbf{P}\,\mathbf{T}^{+}\mathbf{y} \qquad (2)$$

the superscript '+' indicates the pseudoinverse operation, and **y** is the vector of reference calibration values for the analyte of interest.

2. Partial least squares regression (PLS)

In the partial least-squares regression model [2], the calibration data matrix **X** is decomposed into the product of two smaller matrices, capturing at the same time the variance in **X** and the covariance between **X** and the vector of target analyte concentrations **y**. The decomposition renders the score matrix **T** (size $I \times A$), the loading matrix **P** (size $J \times A$), and the weight loading matrix **W** (size $J \times A$), where A is the optimum number of latent variables, also estimated by leave-one-out cross-validation.

The prediction expression is analogous to PCR, i.e., equation (2) above, where **b** is the vector of PLS regression coefficients obtained during the calibration step from:

$$\mathbf{b} = \mathbf{W}(\mathbf{P}^{\mathrm{T}}\mathbf{W})^{-1}\mathbf{T}^{+}\mathbf{y} \qquad (3)$$

Table 1S

Parameters of instrumental operation for determinations using ICP OES.

Instrumental parameter	**Operational condition**
Integration time (s)	15 to 5
RF applied power (kW)	1.15
Coolant Ar gas flow rate (L min^{-1})	12.00
Auxiliary Ar gas flow rate (L min^{-1})	0.50
Nebulizer Ar gas flow rate (L min^{-1})	0.70
Sample introduction flow rate (L min^{-1})	2.10
Nebulizer	Mira Mist
Spray chamber	Cyclonic
Analyte and wavelength (nm)*	Al I 308.215, Cu I 327.396, Fe II 259.940
LoD (mg kg^{-1})	Al – 0.02 Fe – 0.004 Cu – 0.006

*Axial viewing mode.

Table 2S

Concentration levels were obtained for Al, Cu, and Fe in % w w^{-1} from ICP OES determination in the 41 samples and their particle size (μm).

Samples	Size	Al	Cu	Fe	Samples	Size	Al	Cu	Fe
1	<106	2.40 ± 0.14	5.22 ± 0.23	5.74 ± 0.26	22	212-600	1.79 ± 0.17	24.45 ± 1.65	1.62 ± 0.41
2	<106	2.46 ± 0.13	4.75 ± 0.23	7.21 ± 0.51	23	212-600	0.89 ± 0.09	35.25 ± 0.57	2.13 ± 0.22
3	<106	2.39 ± 0.05	7.22 ± 0.26	2.96 ± 0.09	24	212-600	1.07 ± 0.15	32.16 ± 2.79	1.38 ± 0.12
4	<106	2.81 ± 0.10	14.63 ± 0.67	1.85 ± 0.08	25	212-600	0.98 ± 0.05	33.10 ± 0.91	1.71 ± 0.16
5	<106	1.55 ± 0.64	14.20 ± 3.88	2.17 ± 0.96	26	212-600	0.83 ± 0.05	37.42 ± 1.23	2.41 ± 0.34
6	<106	1.27 ± 0.99	12.34 ± 7.72	2.01 ± 0.46	27	212-600	0.44 ± 0.15	38.73 ± 2.07	11.94 ± 1.71
7	<106	2.29 ± 0.12	15.14 ± 0.89	1.25 ± 0.08	28	>600	1.58 ± 0.84	28.24 ± 3.30	0.04 ± 0.01
8	<106	0.99 ± 0.10	18.85 ± 1.76	3.04 ± 0.29	29	>600	2.09 ± 1.27	21.84 ± 4.71	0.29 ± 0.43
9	106-212	1.90 ± 0.11	17.95 ± 0.11	0.43 ± 0.02	30	>600	0.90 ± 0.05	36.53 ± 2.27	6.83 ± 0.97
10	106-212	1.86 ± 0.03	13.59 ± 0.44	5.11 ± 0.19	31	>600	1.71 ± 0.70	24.37 ± 0.99	7.97 ± 3.37
11	106-212	2.12 ± 0.03	14.17 ± 0.02	2.64 ± 0.03	32	>600	0.85 ± 0.06	31.44 ± 1.69	1.12 ± 1.04
12	106-212	1.18 ± 0.24	13.54 ± 3.91	2.13 ± 0.53	33	>600	0.54 ± 0.15	26.61 ± 6.05	15.06 ± 3.18
13	106-212	1.63 ± 0.05	19.63 ± 1.25	2.65 ± 0.27	34	>600	0.91 ± 0.10	29.56 ± 5.35	9.64 ± 4.48
14	106-212	1.21 ± 0.14	40.28 ± 3.07	0.58 ± 1.11	35	>600	0.87 ± 0.18	37.03 ± 1.82	4.08 ± 1.25
15	106-212	1.10 ± 0.07	39.56 ± 1.01	0.62 ± 0.17	36	>600	0.34 ± 0.03	23.47 ± 1.74	22.61 ± 1.6
16	106-212	0.40 ± 0.05	26.99 ± 1.38	5.84 ± 0.23	37	>600	0.78 ± 0.17	36.47 ± 2.90	12.31 ± 1.55
17	106-212	1.11 ± 0.05	37.61 ± 2.72	1.26 ± 0.83	38	>600	0.61 ± 0.05	31.27 ± 2.90	9.04 ± 1.69
18	106-212	0.55 ± 0.12	35.79 ± 2.54	0.90 ± 0.51	39	>600	0.21 ± 0.00	22.77 ± 3.10	21.58 ± 4.79
19	212-600	1.50 ± 0.08	29.03 ± 3.87	0.43 ± 0.28	40	>600	0.94 ± 0.17	33.23 ± 1.00	9.39 ± 4.04
20	212-600	1.53 ± 0.46	32.25 ± 2.56	0.17 ± 0.39	41	>600	0.28 ± 0.04	30.43 ± 3.99	6.54 ± 3.15
21	212-600	1.31 ± 0.16	33.41 ± 1.44	1.62 ± 0.17					

Fig. 1S. Reference vs. predicted concentration levels in % w w^{-1} for the Al with LIBS data only. Comparing the different calibration strategies. a) models for area and b) height models.

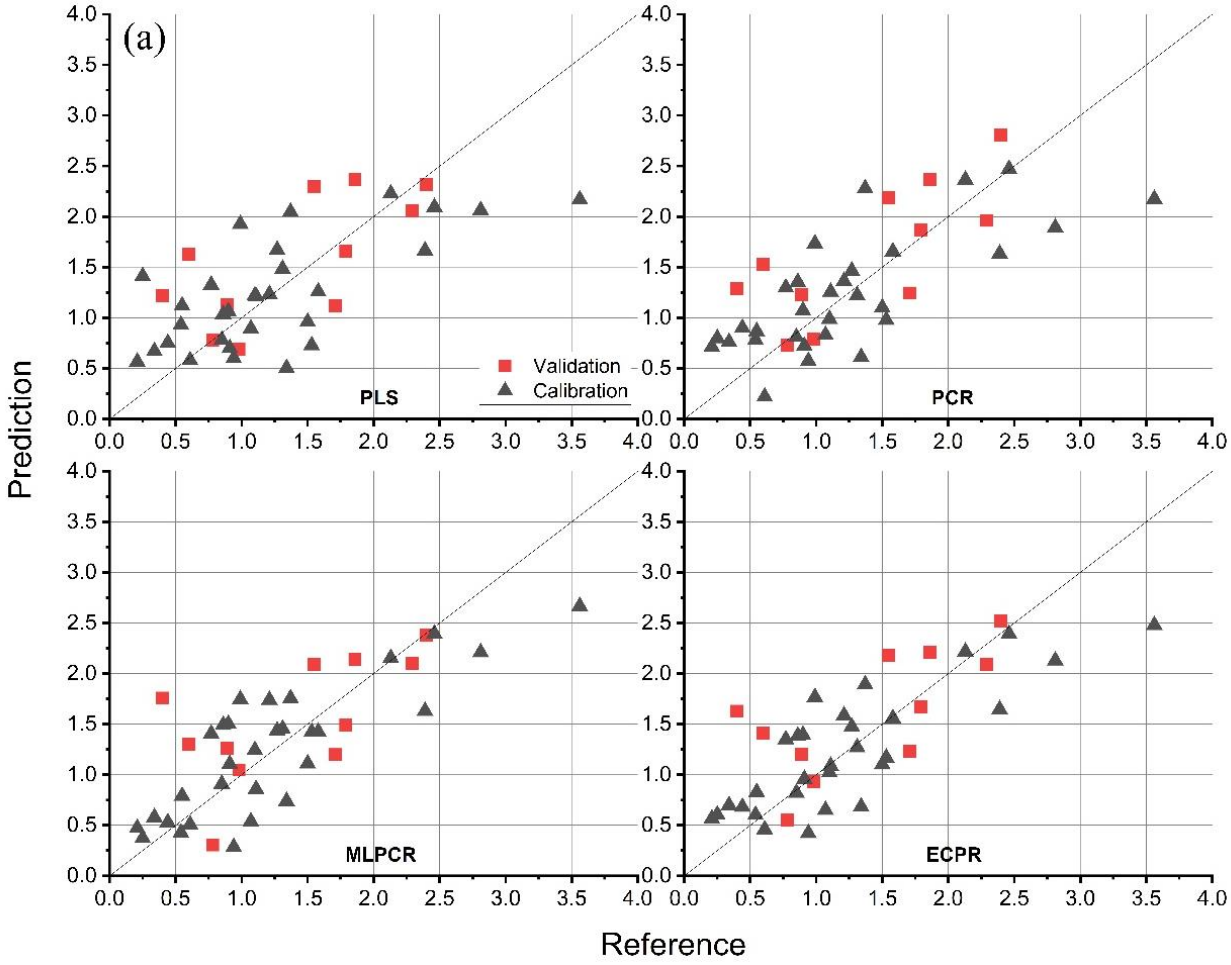

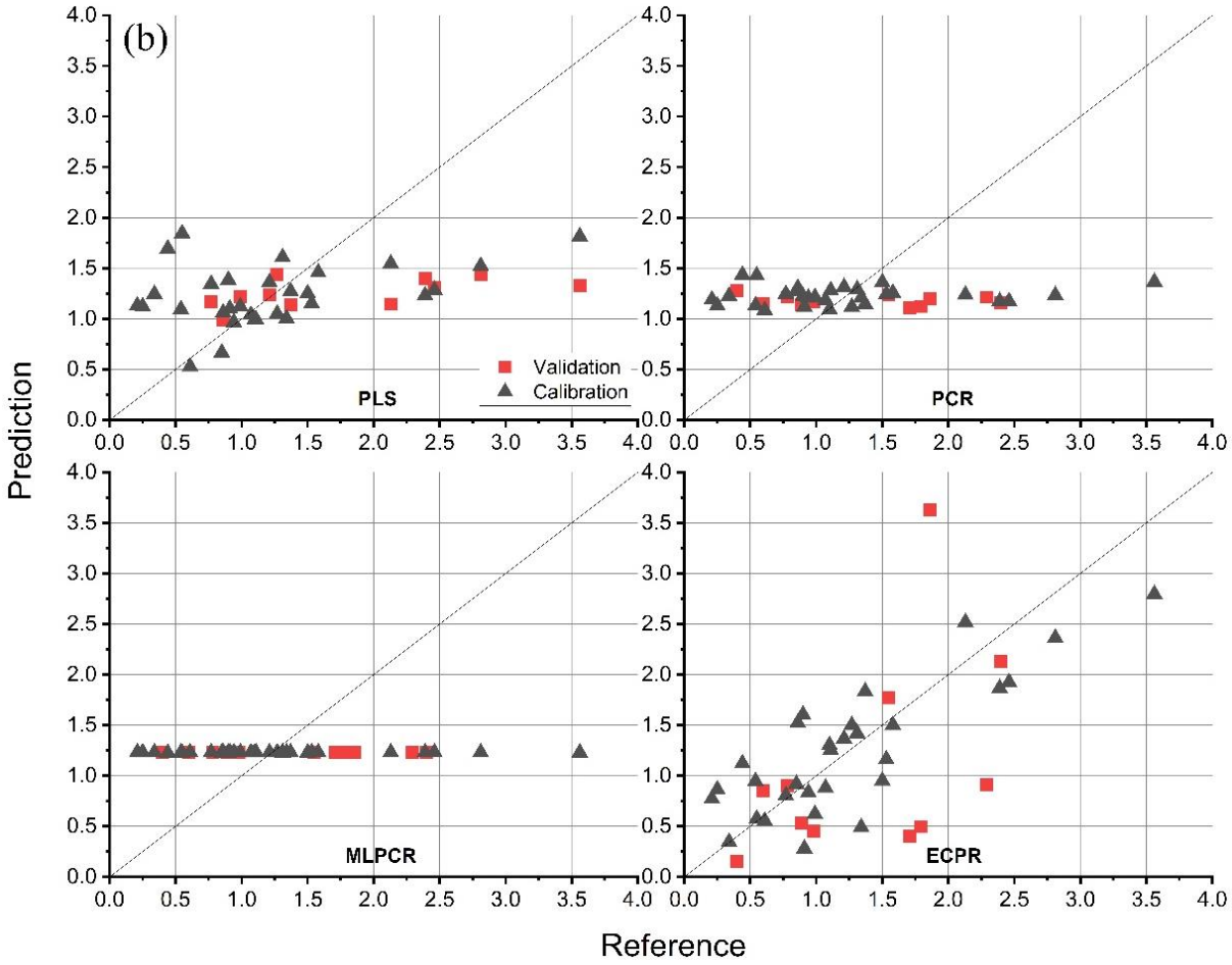
(b)
PLS
PCR
MLPCR
ECPR
Validation
Calibration
Prediction
Reference

Fig. 2S. Reference vs. predicted concentration levels in % w w^{-1} for the Cu with LIBS data only. Comparing the different calibration strategies. a) models for area and b) height models.

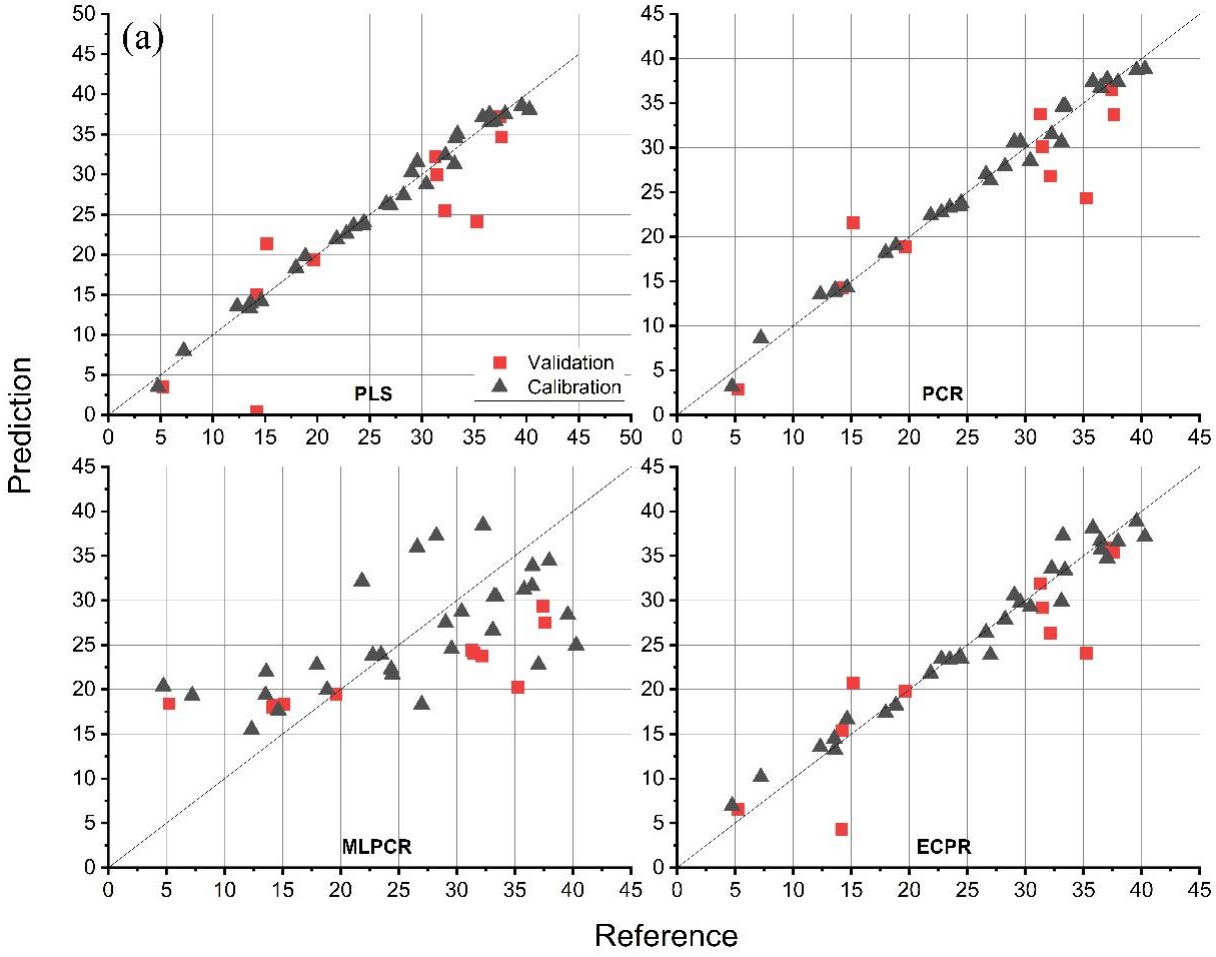

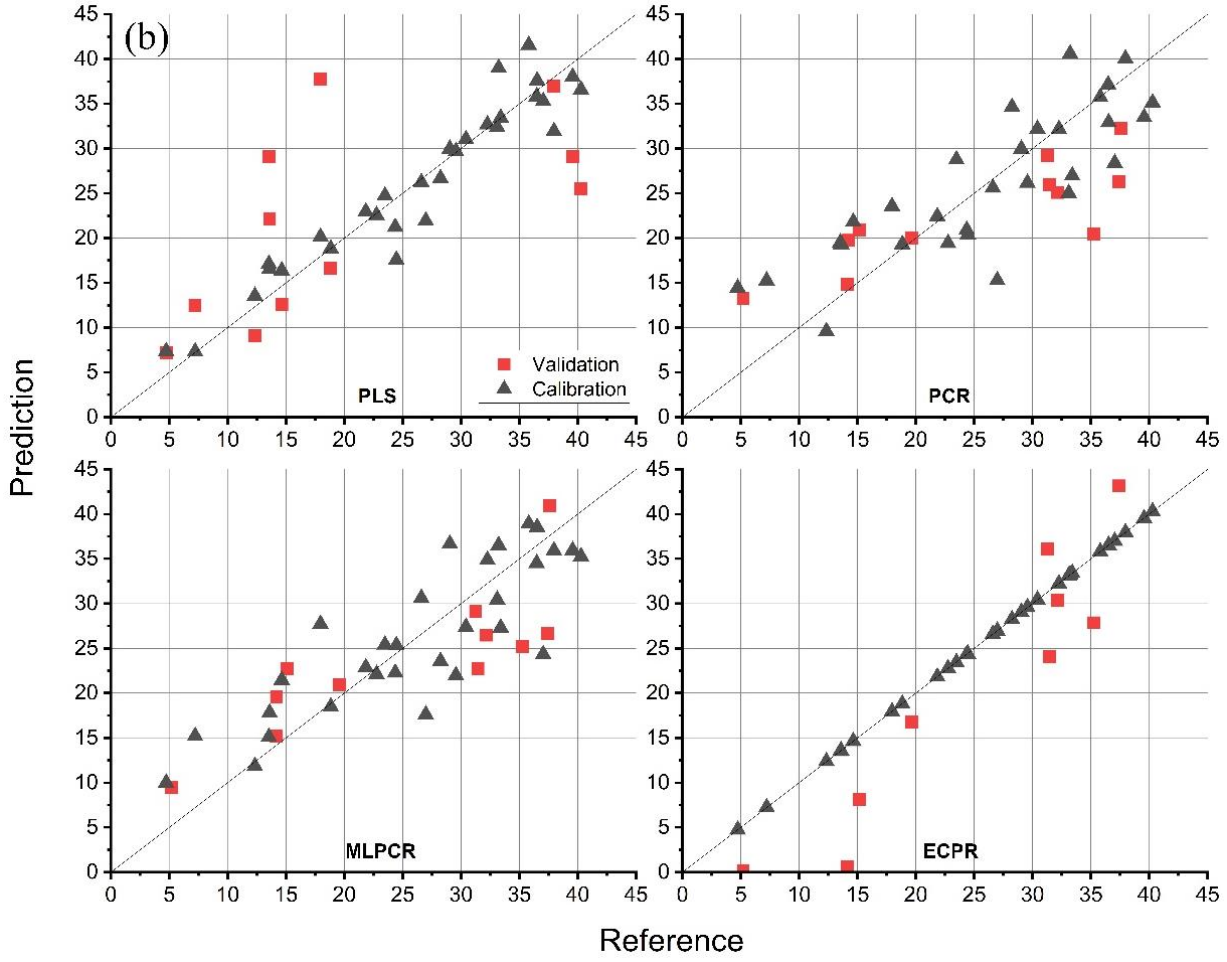
(b)
PLS
PCR
MLPCR
ECPR
Validation
Calibration
Prediction
Reference

Fig. 3S. Reference vs. predicted concentration levels in % w w^{-1} for the Fe with LIBS. Comparing the different calibration strategies. a) models for area and b) height models.

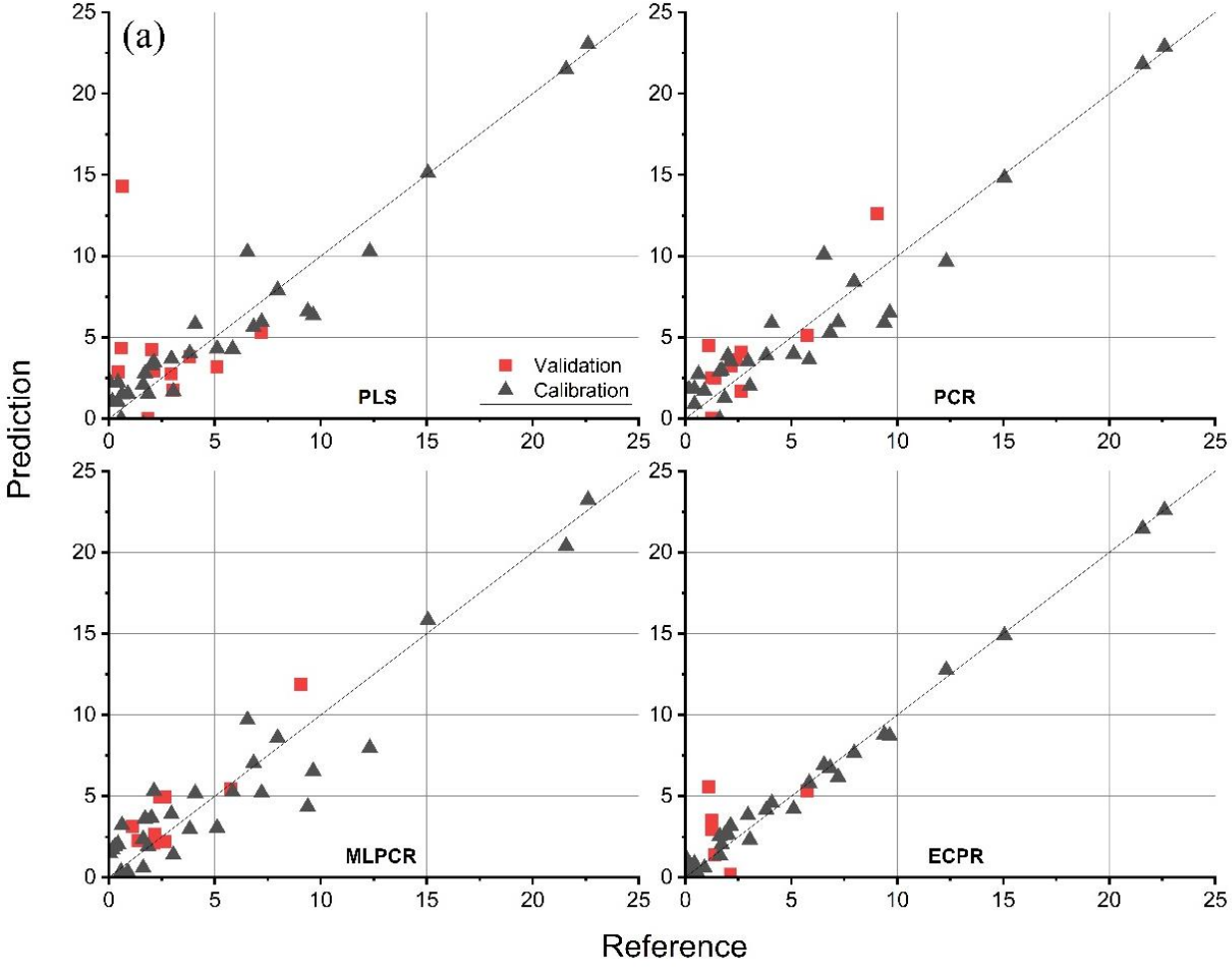

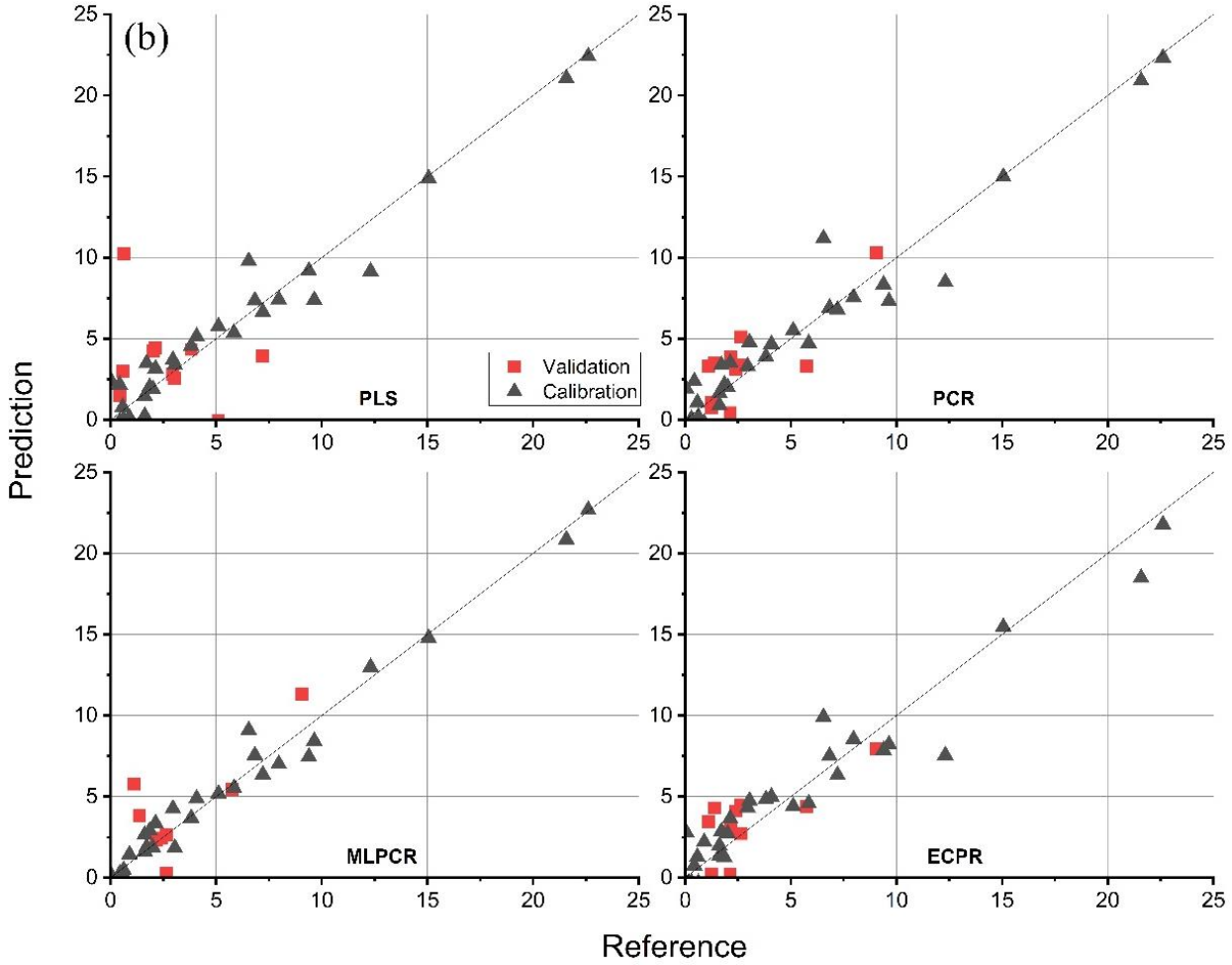
(b)
PLS
PCR
MLPCR
ECPR
Validation
Calibration
Prediction
Reference
0
5
10
15
20
25

Fig. 4S. Reference vs. predicted concentration levels in % w w^{-1} for the Al with LIBS + ED-XRF fusion data. Comparing the different calibration strategies. a) models for area and b) height models.

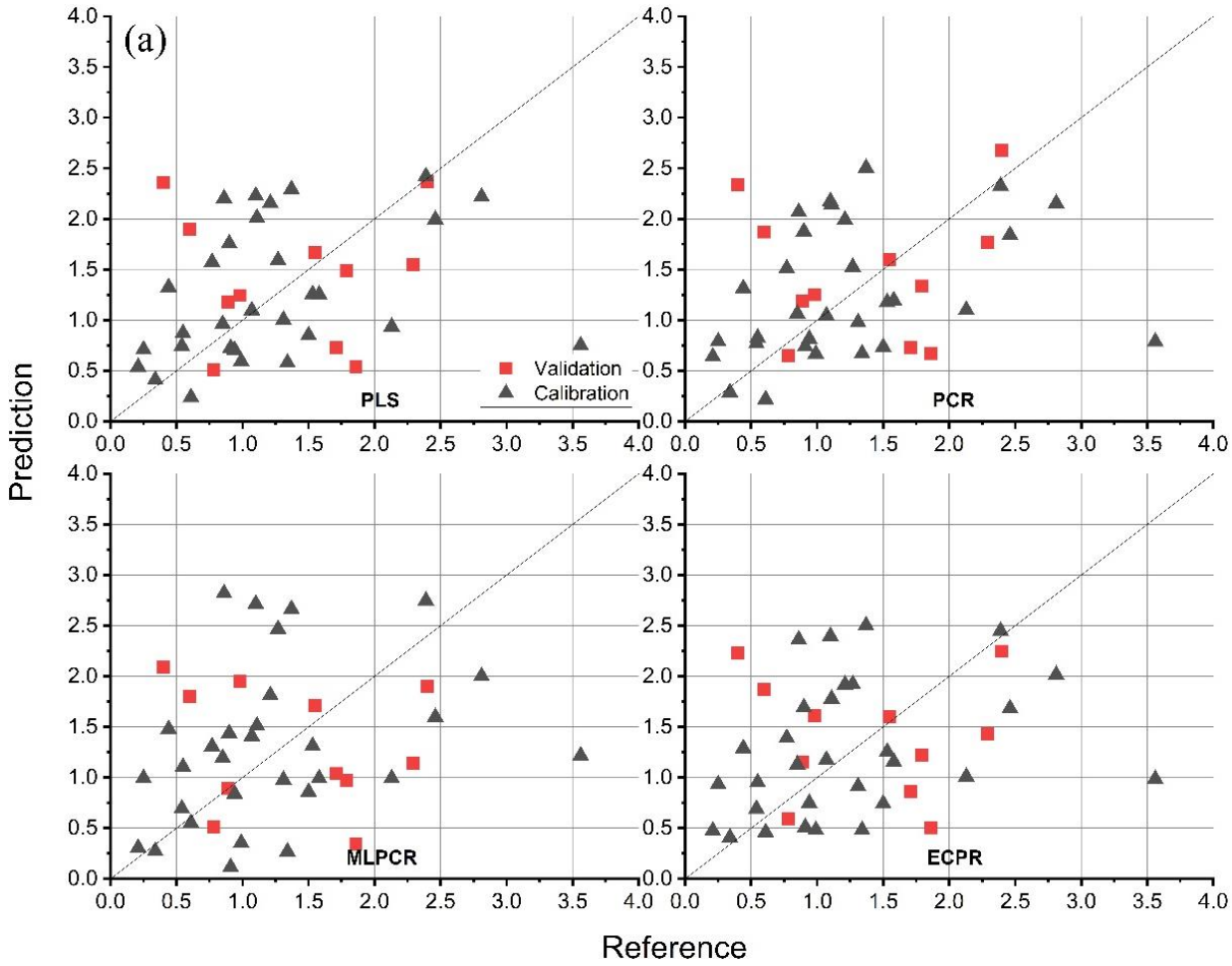

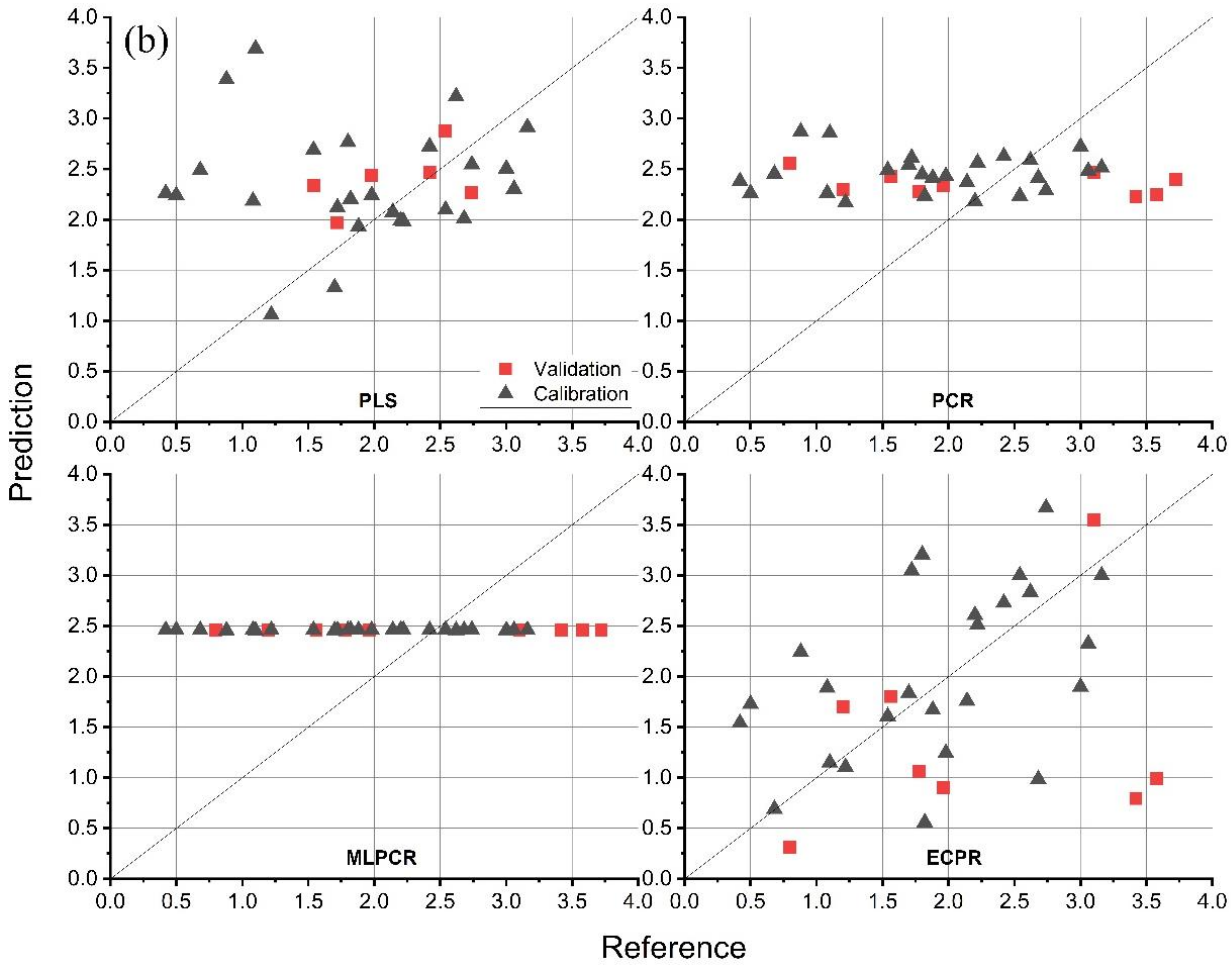
(b)
PLS
PCR
MLPCR
ECPR
Validation
Calibration
Prediction
Reference
0.0
0.5
1.0
1.5
2.0
2.5
3.0
3.5
4.0

Fig. 5S. Reference vs. predicted concentration levels in % w w^{-1} for the Cu with LIBS + ED-XRF fusion data. Comparing the different calibration strategies. a) models for area and b) height models.

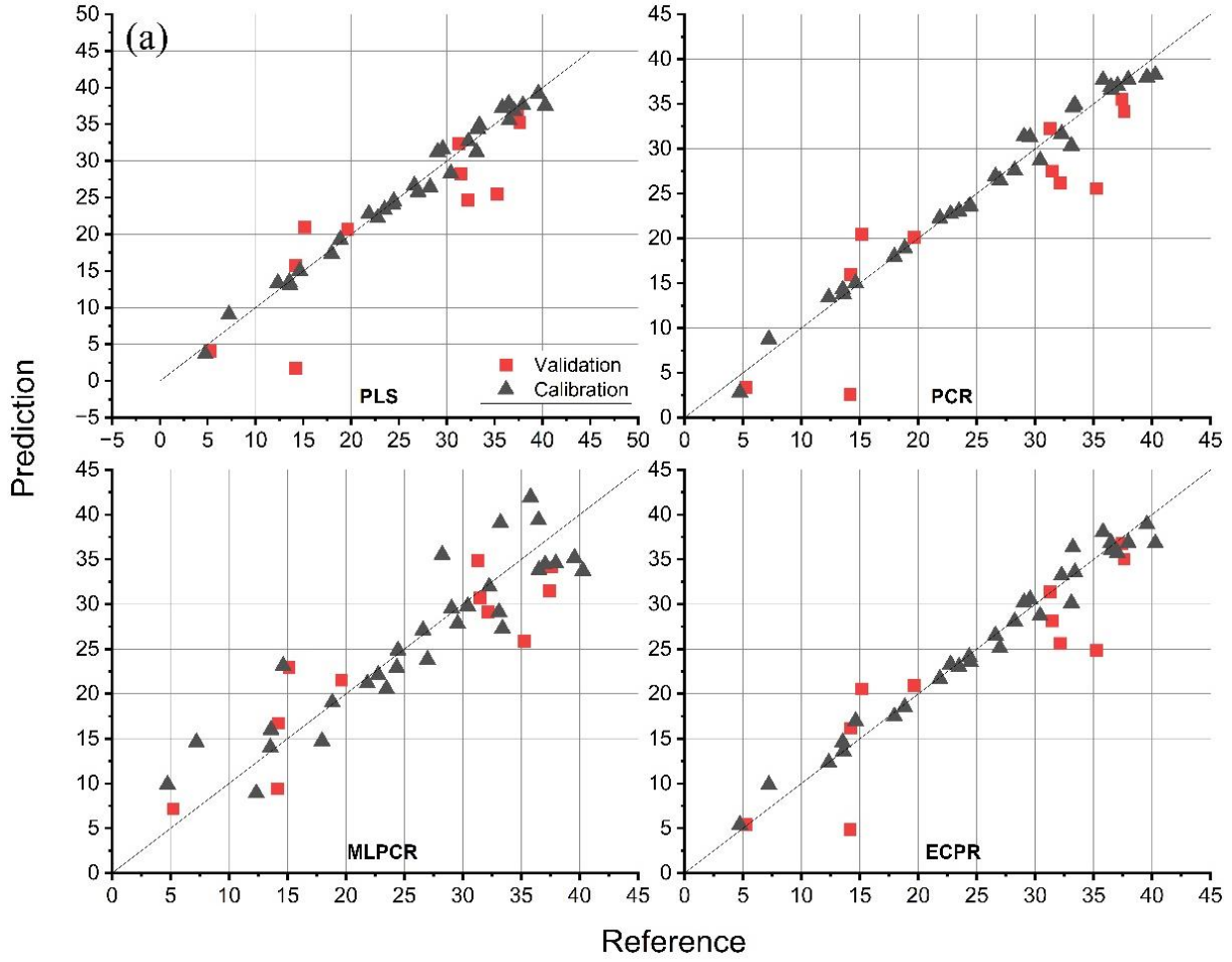

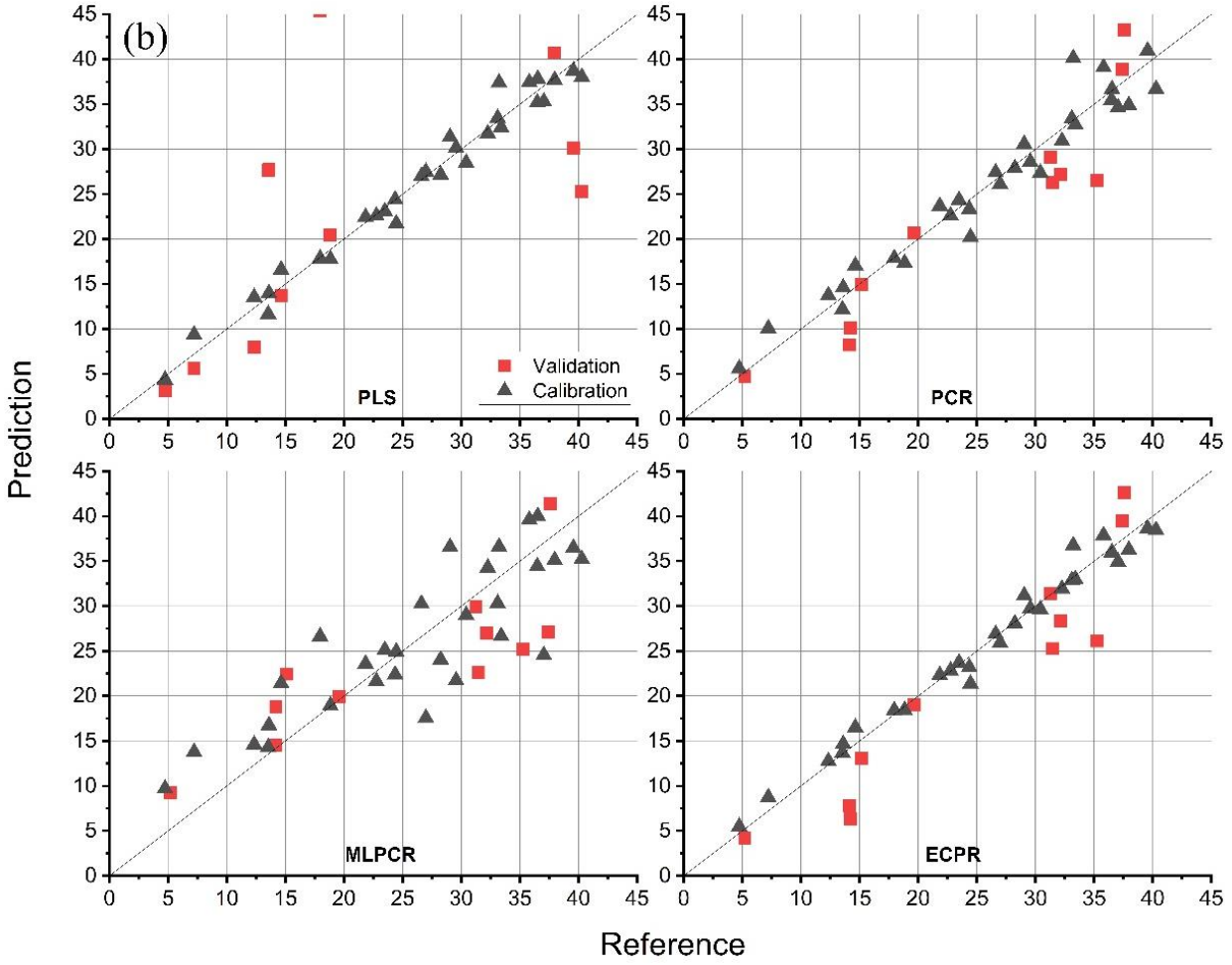
(b)
PLS
PCR
MLPCR
ECPR
Validation
Calibration
Prediction
Reference
0
5
10
15
20
25
30
35
40
45

Fig. 6S. Reference vs. predicted concentration levels in % w w^{-1} for the Fe with LIBS + ED-XRF fusion data. Comparing the different calibration strategies. a) models for area and b) height models.

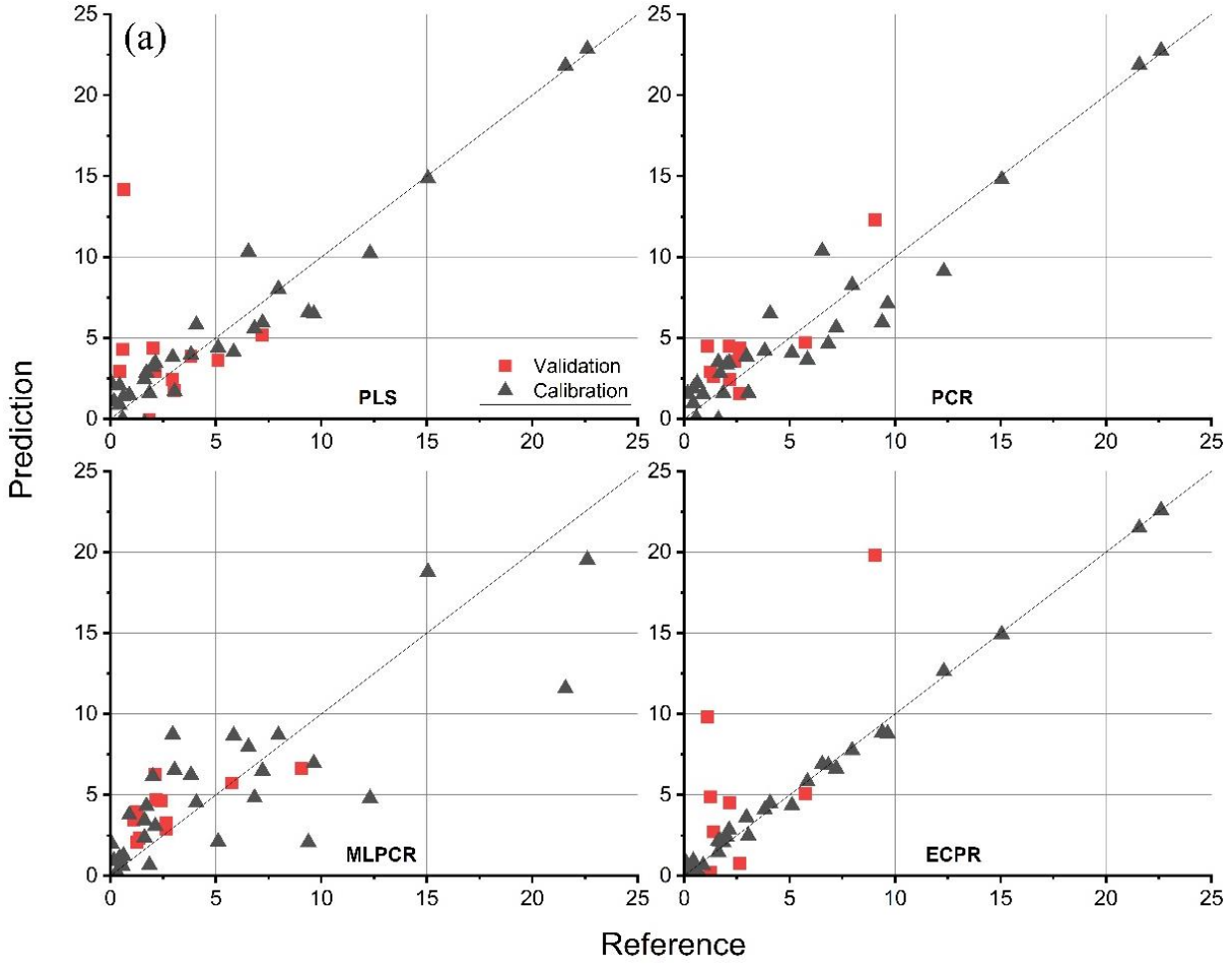

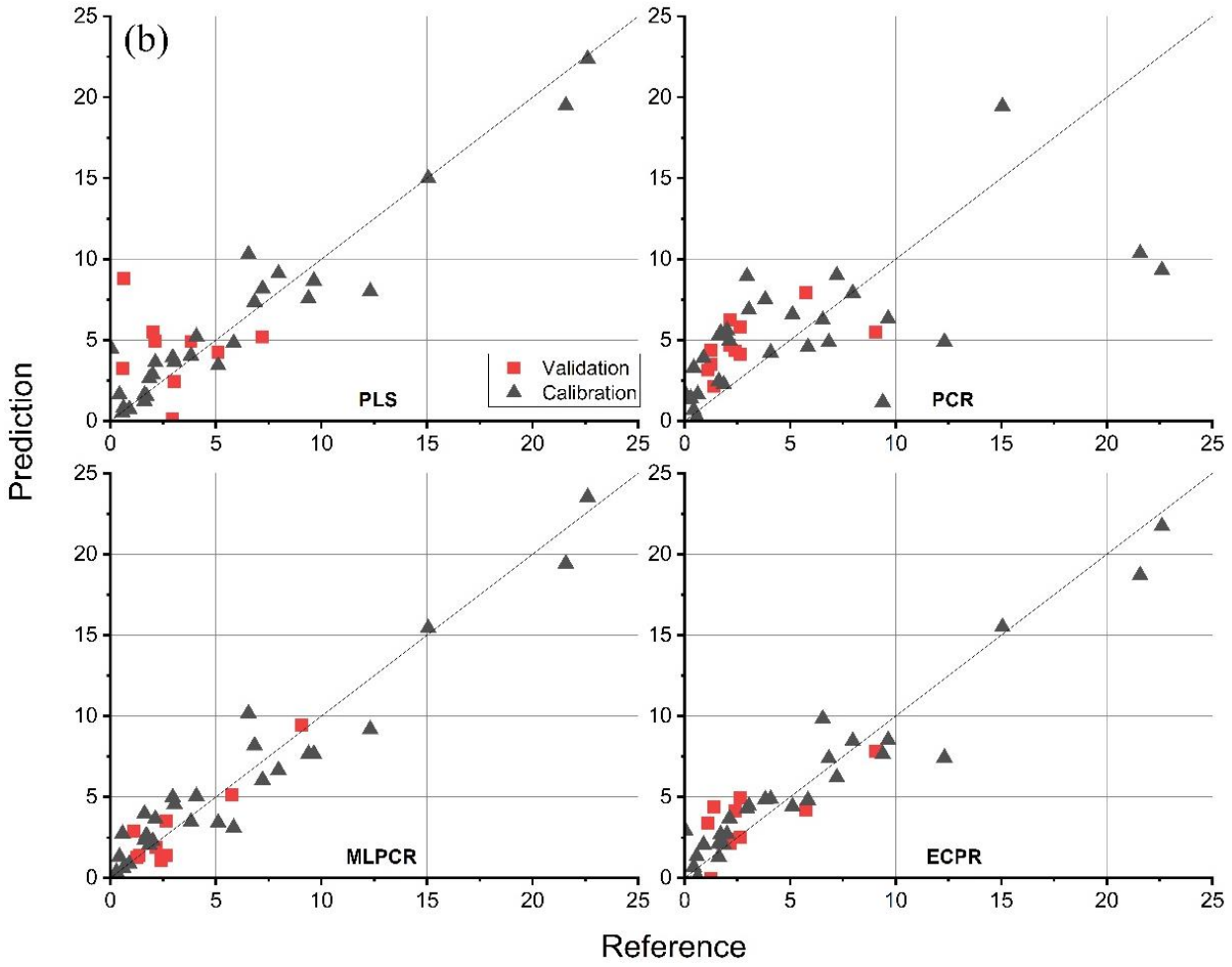
(b)
PLS
PCR
MLPCR
ECPR
Validation
Calibration
Prediction
Reference
0
5
10
15
20
25

Fig. 7S. Comparison of the Al areas from the 14 emission lines (λ1 up to λ14) for sample 33.

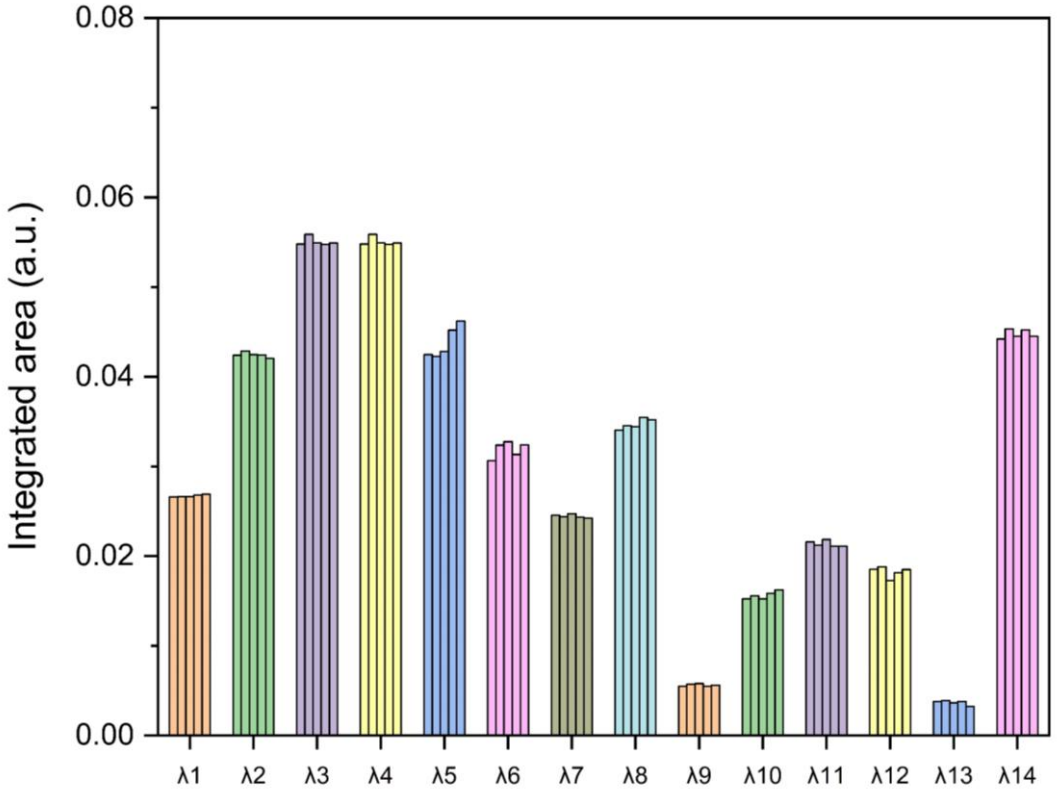

Fig. 8S. Comparison between replicates of the Cu from the 33 emission lines (λ15 up to λ51)areas for sample 33.

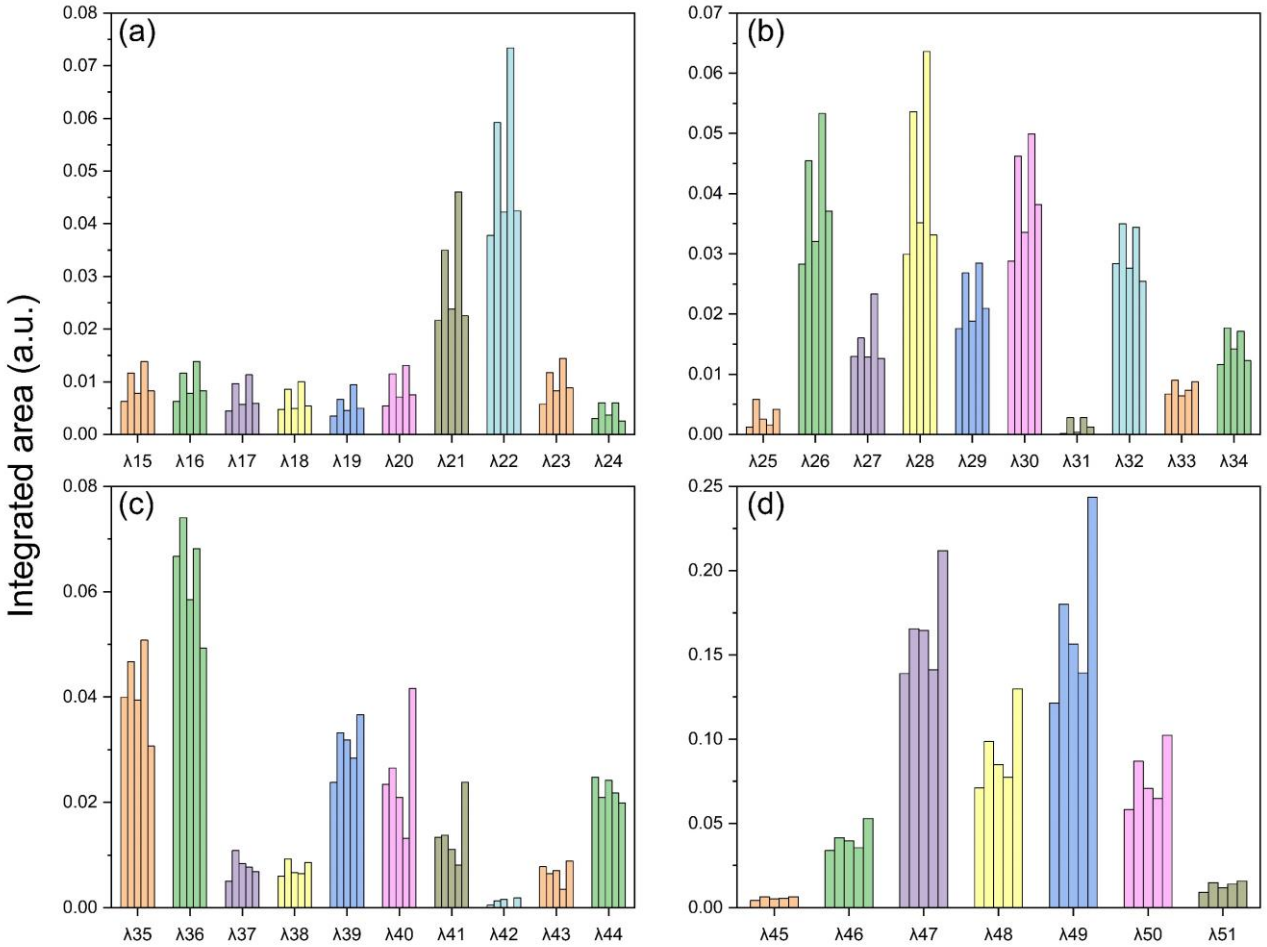
Integrated area (a.u.)
(a)
(b)
(c)
(d)
λ15 λ16 λ17 λ18 λ19 λ20 λ21 λ22 λ23 λ24
λ25 λ26 λ27 λ28 λ29 λ30 λ31 λ32 λ33 λ34
λ35 λ36 λ37 λ38 λ39 λ40 λ41 λ42 λ43 λ44
λ45 λ46 λ47 λ48 λ49 λ50 λ51

References

[1] S. Wold, M. Sjöström, L. Eriksson, PLS-regression: a basic tool of chemometrics Chemom. Intell. Lab. Syst. 58 (2001) 109-130.

[2] E.V. Thomas, D.M. Haaland, Partial least-squares methods for spectral analyses. 1. Relation to other quantitative calibration methods and the extraction of qualitative information, Anal. Chem. 60 (1988) 1193-1202.

Chapter 4 - Proposal for the sustainable recycling of electronic waste

4. Proposal for the sustainable recycling of electronic waste

4.1. An overview of e-waste recycling

The generation of e-waste is growing at an alarming rate, consolidating its position as one of the fastest growing groups of solid waste globally. As previously mentioned, approximately 62 Mt of e-waste was generated in 2022, with an annual growth of around 2 Mt. Despite the significant value of the materials present in e-waste estimated at around US$ 60 billion annually only 22.3% of this volume was formally collected and recycled in 2022, with the rest being treated informally or disposed inappropriately [7]. This scenario results in the release of toxic substances such as Pb, Hg and brominated flame retardants into the environment, especially affecting communities in low- and middle-income countries [133].

The complex composition of e-waste, which includes precious metals such as Au, Ag and Pd, as well as plastics and other materials, makes recycling challenging. However, recent technological advances, such as the integration of cyber-physical systems (CPS) and mechatronics-based automation, are being exploited to improve the efficiency and sustainability of recycling processes [134]. E-waste recycling mainly involves pyrometallurgical and hydrometallurgical processes. Pyrometallurgy uses high temperatures to melt the waste and recover metals such as Cu, Au and Ag [135]. Hydrometallurgy, on the other hand, uses chemical solutions to leach valuable metals, offering greater selectivity and efficiency in recovery [136].

The adoption of sustainable technologies for the recycling and recovery of precious metals from e-waste is essential to mitigate the environmental and economic impacts associated with this type of waste. In addition, effective public policies and raising society's awareness are key to promoting responsible consumption practices and encouraging the circular economy in the electronics sector [137].

4.2. Recovery Methods: Hydrometallurgical Processes

The recovery of metals from e-waste through hydrometallurgical processes has emerged as an alternative way of conserving resources and environmental sustainability. As electronic devices become ubiquitous, their eventual disposal results in a significant accumulation of e-waste, containing valuable metals such as Cu, Au and rare earth elements. Conventional methods of recovering these metals, mainly pyrometallurgy, are generally energy-intensive and harmful to the environment due to the release of emissions and hazardous waste. In contrast, hydrometallurgy offers a more sustainable approach by using aqueous solutions for metal

extraction, thus minimizing the ecological impact and optimizing recovery efficiency [138,139].

Hydrometallurgical processes involve several stages, including leaching, separation and purification. The leaching stage is crucial, in which suitable solvents, such as acids or organic compounds, dissolve the desired metals from the e-waste matrix [140,141]. For example, citric acid has been shown to leach Cu with high efficiency, making it a promising solvent for extracting metals from e-waste [141]. After leaching, metals can be selectively precipitated from solution, allowing the recovery of specific elements based on their chemical properties [142]. This selectivity is particularly advantageous in the context of e-waste, which contains a complex mixture of metals and materials [143].

Another important aspect of hydrometallurgical recovery is its operational flexibility. Advances in coordination chemistry have made it possible to optimize these methods, favoring environmentally sustainable practices [138]. These advances reflect the transition from metallurgy to more environmentally friendly processes, with an emphasis on reducing waste and recycling reagents [144]. This chapter presents a sequential and sustainable method for recovering Ag, Au, Cu and Sn from e-waste.

4.3. A preliminary study of a sequential leaching process to recover Ag, Au, Cu, and Sn from E-waste

Hydrometallurgy 235 (2025) 106476

Contents lists available at ScienceDirect

Hydrometallurgy

journal homepage: www.elsevier.com/locate/hydromet

A preliminary study of a sequential leaching process to recover Ag, Au, Cu, and Sn from E-waste

Dennis Silva Ferreira, Edenir Rodrigues Pereira-Filho *

Group of Applied Instrumental Analysis, Chemistry Department, Federal University of São Carlos, São Carlos 13565-905, São Paulo, Brazil

ARTICLE INFO

Keywords:
Sequential leaching
Noble metals
Copper
Electronic waste
Acid leaching
Green chemistry

ABSTRACT

The rapid growth of electronic waste (e-waste) presents both environmental challenges and economic opportunities. This study investigates efficient methods for recovering valuable metals from printed circuit boards (PCBs) using hydrometallurgical processes. The PCB samples from various end-of-life electronic devices were subjected to a series of five leaching stages targeting the leaching of Ag, Au, Cu, and Sn. The first stage using 3 mol/L nitric acid achieved 97 % Cu leaching, reducing Cu content from an average of 20 % (*w*/w) to 0.74 % (w/w). This stage also affected other metals, leaching 53 % of Ag and 78 % of Sn. Subsequent leaching with thiourea in acidic media containing $Fe(NO_3)_3$ leached 75 % of Au. An iodine/iodide leach with H_2O_2 as an oxidizer proved highly effective for Ag, with 99 % leaching. This stage also leached an additional 62 % of Au. Two methods for Sn leaching were compared: HCl leaching achieved 98 % efficiency; H_2SO_4 with $CuSO_4$ also achieved 98 % leaching efficiency. Inductively Coupled Plasma Optical Emission Spectrometry (ICP OES) was used to analyze metal concentrations throughout the process. This sequential leaching approach demonstrates the potential for high-efficiency recovery of valuable metals from e-waste, contributing to both economic benefits and environmental sustainability in electronic waste management. The study highlights the complexity of metal interactions with leaching reagents and the importance of optimizing each stage for selective and efficient recovery of metals from e-waste.

1. Introduction

Electrical and electronic equipment (EEE) are characterized by relatively short obsolescence cycles, usually between 2 and 3 years, and its production is encouraged by continuous technological innovation. This short life cycle contributes significantly to the global increase of electronic waste (e-waste or WEEE). This type of waste flow is one that globally presents the fastest growing, with an estimated annual increase of between 3 % and 5 % (Huang et al., 2009). The United Nations Institute for Training and Research (UNITAR) estimates that 62.0 million tons (Mt) of e-waste was generated in 2022, with only 22.3 % of this amount being properly recycled (Baldé et al., 2024). It is estimated that WEEE will exceed 74 Mt. in 2030, and 110 Mt. are expected in 2050 (Forti et al., 2020; Parajuly et al., 2019).

The environmental impact of this growing volume of WEEE is alarming, as improper disposal can result in the release of toxic chemical elements and substances, affecting ecosystems and human health. Most of the WEEE in several countries, including Brazil, are mainly handled following informal collection system, and, because of this inadequate management, around 58 tons of Hg and 45,000 tons of plastic containing brominated flame retardants (BFR) are released into the environment. This has a direct and severe impact on the environment and people's health (Alabi et al., 2021; Lin et al., 2022). However, the recovery of precious and strategic metals as Ag, Au, Cu, Fe, Sn, among others, from WEEE offers a promising economic and environmental solution. By 2022, the economic value of the metals contained in WEEE is estimated at US$91 billion. Metals such as Au, Cu and Fe values can be estimated from US$15 billion (for Au) up to US$19 billion (for Cu). These metals can be recovered efficiently with high recycling rates using simple waste management technologies (Baldé et al., 2024; Diallo et al., 2024; Van Yken et al., 2023).

Hydrometallurgical methods have stood out for their precision, predictability and lower environmental impact when compared to traditional pyrometallurgical processes (Gulliani et al., 2023; Yang et al., 2011). These methods require less financial investment and operating costs, as well as being more easily adaptable, resulting in significant economic benefits and meeting the growing demands for ecological considerations (Syed, 2006). For example, the recovery of Au

* Corresponding author.
E-mail address: erpf@ufscar.br (E.R. Pereira-Filho).

https://doi.org/10.1016/j.hydromet.2025.106476
Received 22 October 2024; Received in revised form 31 March 2025; Accepted 4 April 2025
Available online 5 April 2025

can offer an economic incentive from US$1400 up to US$15,200 per ton of printed circuit boards (PCB), and these values show how profitable the development of recovery methods for this waste can be (Wang and Gaustad, 2012).

Leaching, a key component of hydrometallurgical processes, is particularly advantageous due to its ability to selectively recover metals with high purity and efficiency. Studies indicate that the development of small-scale, low-cost hydrometallurgical processes for the treatment of PCBs is the ideal approach for recovering metals of interest from WEEE (Golev and Corder, 2017; Tamboli and Sengupta, 2025). In addition, these processes are more environmentally friendly as they avoid initial incineration which releases toxic gases and presents high cost (Birloaga et al., 2013; Huang et al., 2009).

The growing production and accumulation of WEEE represents a significant global challenge, with increasingly worrying environmental and public health impacts. In this context, the UN's Sustainable Development Goals (SDGs) have emerged as an important guide for tackling these challenges. WEEE management and recycling are directly linked to several SDGs, including Health and Well-being (SDG-3), Decent Work (SDG-8) and Responsible Consumption and Production (SDG-12). In Brazil (Seixas et al., 2020) and other countries (Anuardo et al., 2023; Castro and Pereira-Filho, 2020; Kumar et al., 2022), the implementation of sustainable WEEE management practices is essential to protect the environment, promote public health and foster a circular economy. This study proposes to develop environmentally friendly leaching methods to recover valuable metals such as Ag, Au, Cu, and Sn, helping to reduce mineral leaching and mitigate pollution, thus aligning with global demands for innovative and sustainable solutions in electronic waste management (Botelho Junior et al., 2023; Emmons-Burzyńska et al., 2025; Fatimah et al., 2024).

2. Experimental methods

2.1. Reagents

Ultrapure water produced in a Milli-Q® Plus (Millipore Corp, Bedford, MA, USA) was used to prepare all the solutions during the study. All glassware and polypropylene vials were previously decontaminated with detergent and immersed in nitric acid solution (HNO_3 10 % (*v*/v), analytical grade (AR), Synth, Diadema, Brazil) for 24 h and rinsed with ultrapure water. The external calibration curves for Ag, Au, Cu, and Sn were prepared using appropriate and successive dilutions of the 1000 mg/L stock solution (Specsol, São Paulo, Brazil) with HNO_3 solution. The reagents used in the leaching process were: HNO_3, H_2SO_4 (AR, Synth), HCl (AR, Química Moderna, Barueri, Brazil), I_2 (AR, Grupo Química, Penha, Brazil), KI (AR, Synth), Thiourea (AR, Neon, Suzano, Brazil), $Fe(NO_3)_3$ (AR, Synth) and $CuSO_4$ (AR, Synth). The concentrated HNO_3 and HCl acids were previously distilled using Distillacid™ BSB-939-IR (Berghof, Eningen, Germany).

2.2. Preparation and chemical characterization of PCB samples

Some end-of-life (EoL) WEEE samples from computers, laptops, smartphones, and tablets with a total weight of 12 kg and an average age between 5 and 20 years were obtained from different suppliers. Previously, this material was manually disassembled and separated into different parts: polymers (4.5 kg), PCBs (2.8 kg), screens, and frames, among others (4.7 kg). The PCBs obtained were ground in a knife mill (Tecnal TE-650, Piracicaba, Brazil), and sieved until particle sizes <106 μm and 106–212 μm were obtained. Because the material is difficult to grind, both particle sizes were combined, homogenized, and used in the development of the study. At the end of the process, 1.2 kg of powder PCB was obtained and used for the leaching experiments (See Fig. S1a in the Supplementary Material (SM)).

The method used to obtain reference concentration information for the target elements was developed by Andrade et al. (2019) and adapted by Ferreira et al. (2024). Samples with a mass of 100 mg were added to closed vials of tetrafluoroethylene-perfluoro (alkoxy vinyl ether, Savillex, 50 mL PFA block digestion tube with cap, model 210–050-70) with a mixture of aqua regia (3 parts HCl and 1part HNO_3) diluted (1,1) with deionized water. The system was heated up to 100 °C for 2 h. Then the cooled digestion solution was filtered with filter paper and diluted to the appropriate concentration range using deionized water. Inductively Coupled Plasma Optical Emission Spectrometer (ICP OES), model iCAP 7000 (Thermo Fisher Scientific, Madison, USA) was used to determine the concentrations of Ag, Au, Cu, and Sn present in the digestion solution. The gas used to generate the plasma, nebulization, and auxiliary was 99.996 % argon (White Martins-Praxair, Sertãozinho, SP, Brazil). The plasma conditions and emission lines used in the determination are described in Table 1S (SM).

The characterization steps of the PCB samples are shown in Fig. S1b (SM). In this study, all the ICP OES determinations were carried out in triplicate ($n = 3$) and later the results were averaged.

2.3. Leaching procedures

All the experimental leaching conditions described in the next sections are illustrated in Fig. 1. The first goal was to selectively extract Cu and obtain a solid residue with only Ag, Au, and Sn. Another point that needs to be emphasized is related to analytical quality control. After each leaching condition, the four target elements were determined in both liquid and solid residue. The solid residue was submitted to sample preparation following the procedure proposed by Andrade et al. (2019). In this case, seven different calibration curves were prepared following the composition of the extractor solutions. This approach was made to avoid matrix interference (Castro et al., 2024). During all the leaching procedures, the blanks were carried out simultaneously and in triplicate (n = 3). The selection of leaching agents was based on a literature review conducted in the Web of Science (WoS) database, using the following main criteria: i) high leaching efficiency, ii) low operating cost, iii) selectivity of the leaching process, iv) environmental friendliness, and v) studies published within the last 10 years (2014–2024). The general search used the keyword "e-waste recovery," yielding over 1500 articles. These articles were analyzed and selected based on the aforementioned criteria, resulting in 100 relevant studies. The leaching agents selected, along with their respective experimental conditions, are those used in this study.

2.3.1. Leaching of Cu using HNO_3

To leach the Cu content in the analyzed samples, 200 mL of 3 mol/L HNO_3 solution and 10 g of PCB powder were transferred to a 500 mL beaker and mixed in a heated magnetic stirrer model 752 A (Fisatom, São Paulo, Brazil). The rotation speed was fixed at 300 rpm for 2 h at a temperature of 70 °C (343 K). This procedure was carried out on 15 parallel samples. The experimental conditions adopted were based on those optimized by Dutta et al. (2018). After leaching, the solid/liquid separation was carried out using a quantitative filter paper (Unifil, black tape 125 mm ∅, Germany) for all 15 sub-samples. Then, the sub-samples were combined and homogenized into a single sample with a mass of approximately 120 g. The leachate was then analyzed for Ag, Au, Cu, and Sn determination using ICP OES (see instrumental conditions in Table 1S (SM)). The solid residue (unleached PCB powder) after washing

Table 1
Concentrations of metals in WEEE determined for Ag, Au, Cu and Sn using the ICP OES reference method ($n = 3$).

Elements	Concentrations
Ag (mg/kg)	1225 ± 144
Au (mg/kg)	196 ± 21
Cu (% (*w*/w))	19 ± 3
Sn (% (w/w))	4.5 ± 0.6

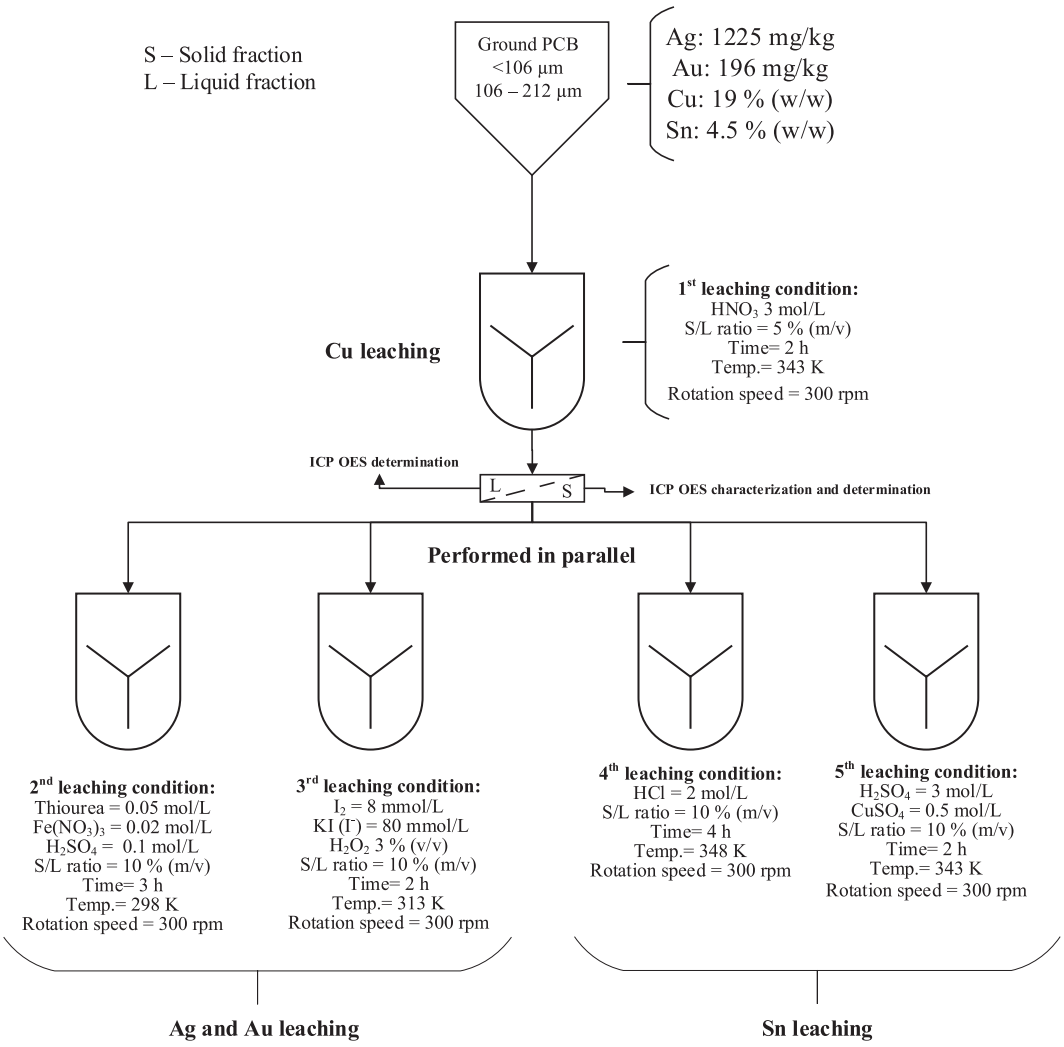

Fig. 1. The proposed process flowchart for the recovery of Ag, Au, Cu, and Sn from PCB waste.

with deionized water, was used for the second leaching condition (see Fig. 1).

2.3.2. Leaching of Ag and Au using thiourea in the presence of H_2SO_4/Fe $(NO_3)_3$

For the second leaching process with the aim of leaching Ag and Au, 5 g of the solid residue from the first leaching was weighed and mixed with 50 mL of a solution containing 0.05 mol/L of thiourea, 0.02 mol/L of $Fe(NO_3)_3$ as an oxidizer and 0.1 mol/L of H_2SO_4. This mixture was prepared in a 150 mL beaker. The beaker was placed on a magnetic stirrer and stirred for 3 h at a constant rotation speed of 300 rpm and at room temperature (298 K). These experimental conditions were adopted based on the conditions optimized by Behnamfard et al. (2013). The mixture was then filtered and both liquid and solid extracts were prepared and analyzed focusing the target elements determination using ICP OES.

2.3.3. Leaching of Ag and Au with iodine/iodide

For the third leach with the aim of also leaching Ag and Au, 5 g of the solid residue from the first leach was weighed and mixed with 50 mL of a solution containing 8 mmol/L of iodine, 80 mmol/L of potassium iodide and H_2O_2 (3 %) as an oxidizer. The mixture was prepared in a 150 mL beaker. The beaker was placed on a magnetic stirrer and mixed for 2 h at a constant rotation speed of 300 rpm and a temperature of 40 °C (313*K*). These experimental conditions were adapted based on the conditions previously optimized by Xiu et al. (2015). The mixture was then filtered and both liquid and solid extracts were prepared and analyzed focusing the target elements determination using ICP OES.

2.3.4. Leaching of Sn with HCl

To leach Sn in acidic media with HCl, the solid residue from the 1st leach, together with 50 mL of leach solution containing 2 mol/L HCl, were placed in a 150 mL beaker and magnetically stirred for 4 h at a temperature of 75 °C (348 K). These experimental conditions were adapted based on the conditions previously optimized by Moosakazemi et al. (2019). The mixture was then filtered and both liquid and solid extracts were prepared and analyzed focusing the target elements determination using ICP OES.

2.3.5. Leaching of Sn with H_2SO_4 in the presence of $CuSO_4$

For the fifth leaching with the aim of leaching only Sn, 5 g of the solid residue from the first leach was weighed and mixed with 50 mL of a solution containing 3 mol/L H_2SO_4 and 0.5 mol/L $CuSO_4$, being prepared in a 150 mL beaker. The beaker was placed on a magnetic stirrer and stirred for 2 h at a constant rotation speed of 300 rpm and at a temperature of 70 °C (343 K). These experimental conditions were adapted based on the conditions previously optimized by Guo et al. (2020). The mixture was then filtered and both liquid and solid extracts were prepared and analyzed focusing the target elements determination using ICP OES.

3. Result and discussion

3.1. Chemical analysis of PCB

Table 1 shows the initial concentrations of Ag (1225 mg/kg), Au (196 mg/kg), Cu (19 % (w/w)), and Sn (4.5 % (w/w)) in the feed sample prepared according to Fig. S1 (SM).These concentrations, for example for Cu, are on average 19-fold higher than the levels found in copper ores by mining companies, which vary from 0.5 % to 1 % (w/w) (Lagos et al., 2018). In the case of Au, concentrations can be up to 33-fold higher than those found in gold ores, which have levels of around 6 mg/kg (Martinez et al., 2021). This pattern also applies to Ag (6-fold higher) and Sn (4.5-fold higher) (Reichl and Schartz, 2024; U.S. Geological Survey, 2024), indicating a growing trend of increasing concentrations of these elements in the urban environment, while primary sources, such as mines, show a reduction in available concentrations. This panorama highlights the importance of recycling and recovering metals from WEEE as a viable and sustainable alternative.

3.2. Leaching cu with HNO_3

The copper leaching was carried out on 15 sub-samples of 10 g each, taken from the original PCB sample after grinding. The sub-samples were leached in HNO_3 (as shown in Fig. 1). After filtering, both the liquid (L) and solid (S) extracts were prepared and analyzed with a focus on determining the target elements using ICP OES.

Based on the initial concentrations of the elements determined by ICP OES, as shown in Table 2, and the masses obtained through the mass balance in the initial and final stages of each leaching process, the masses of each analyte were calculated. These values were then normalized to 100 % for each analyte, allowing the preparation of Fig. 2, to facilitate the interpretation and visualization of the data. Fig. 2 shows that the first leaching stage not only leached almost all Cu but also affected the leaching of other elements. The leaching of Cu was significant, with 97 % of the total being removed from the solid.

In addition, leaching affected Ag, with approximately 47 % remaining in the solid fraction. A similar pattern was observed for Sn, where 22 % remained in the solid fraction and 78 % was leached into the liquid fraction. These results highlight the effectiveness of the leaching process, showing the conversion of the metals in the sample to appropriate salts. Eq. (1) shows the reaction of Cu with HNO_3 (Dutta et al., 2018):

$$Cu(s) + 4HNO_3(aq) \leftrightarrows 2NO_2(g) + Cu(NO_3)_2(aq) + 2H_2O(l) \quad (1)$$

The results indicate that although the method is used to selectively extract Cu, it can still react with other metals present in the PCB samples due to its strong oxidizing potential, allowing the oxidation of Ag and Sn metals and the formation of their respective nitrates, according to reaction (2).

Thermodynamically, the leaching reaction is favored, due to the negative free energy of reaction (2):

Table 2
Standard Reduction Potentials (E^0) of metals leached from electronic waste.

Reduction reaction	E^0 (V)
$Cu^{2+}+2e^- = Cu$	+0.34
$Ag^{+}+e^- = Ag$	+0.80
$Sn^{2+}+2e^- = Sn$	−0.14
$Au^{+}+e^- = Au$	+1.69
$NO_3^- + 3H^+ + 3e^- = NO + 2H_2O$	+0.94
$Fe^{3+}+e^- = Fe^{2+}$	+0.76
$I_2 + 2e^- = 2I^-$	+0.53
$I_3^- + 2e^- = 3I^-$	+0.54

References: (Bard et al., 2017; CRC Handbook of Chemistry and Physics, 2016).

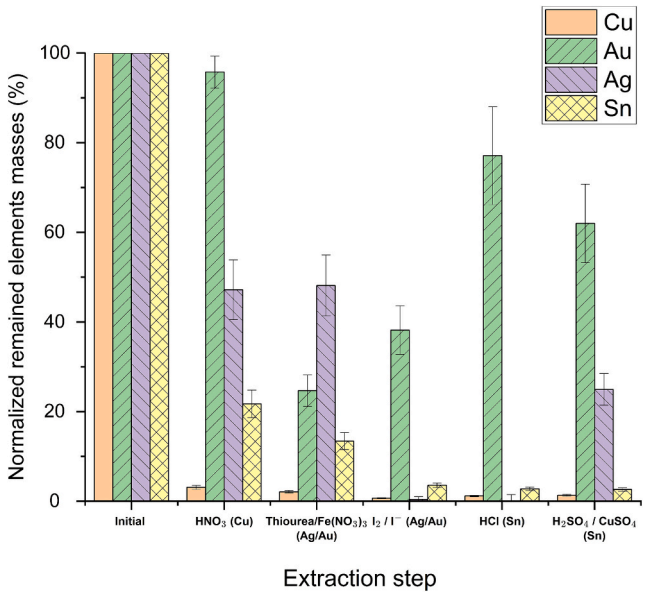

Fig. 2. Normalized remained masses of Ag, Au, Cu and Sn in % in the solid residues in all leaching conditions applied to the PCB samples.

$$M^0(s) + 2nHNO_3(aq) \leftrightarrows nNO_2\ (g) + M^{n+}(NO_3)_n\ (aq) + nH_2O\ (l)\ (M: Cu, Ag\ and\ Sn) \quad (2)$$

For example, the leaching of Ag, Cu and Sn is favored by a negative free energy: $\Delta G_{343}^{\circ} = -13.55$ kJ/mol (Ag), $\Delta G_{343}^{\circ} = -115.41$ kJ/mol (Cu), and $\Delta G_{343}^{\circ} = -206.48$ kJ/mol (Sn), based on the electrode potentials reported in Table 2 (also see Eq. 8). Despite the lower potential of Sn (−0.14 V), compared to Cu (+0.34 V), copper had a higher extent of leaching (or leaching efficiency %), while Sn had the second highest leaching efficiency (Lee and Mishra, 2018; Mecucci and Scott, 2002) in HNO_3, due to the greater quantity and greater surface area of Cu in the sample compared to Sn.

In addition, the reduction potential of Ag (0.80 V) is higher than that for Cu (0.34 V), which suggests that even higher concentrations of HNO_3 or the maintenance of a high redox potential are necessary for the complete leaching of Ag (Bas et al., 2014; Mecucci and Scott, 2002).

In the case of Au, the concentration remained unchanged (Fig. 2) due to its chemical properties as a noble element, which makes it resistant to corrosion and oxidation by HNO_3. The reaction of Au with HNO_3 does not occur due to its high reduction potential (+1.69 V), compared to that of HNO_3 (+0.94 V). This results in a positive $\Delta G_{343}^{\circ} = +161.57$ kJ/mol, which makes Au less reactive and more resistant to oxidation by HNO_3 (Hojo et al., 2017; Sulcius, 2015). It is also important to note that Au^+ ions are not stable in water. Therefore, the oxidation and dissolution of gold requires the presence of a complexing agent capable of stabilizing these ions, which influences the effective potential required for the reaction to proceed (Saha et al., 2023; Schmidt et al., 1991).

As for HNO_3, although it is not considered an environmentally friendly acid, it can be considered as a recyclable reagent. Nitric acid can be regenerated through the nitric oxides (NO and NO_2) that are formed as reaction products, which can contribute to a more sustainable approach when compared to other methods that do not allow the reagent to be regenerated (Bizzi et al., 2021; Chung et al., 2009).

3.3. Acid leaching of ag and au using thiourea in the presence of Fe $(NO_3)_3$

After completing the Cu leaching stage, the resulting solid residue, weighing 120 g, was carefully homogenized, and four aliquots of 5 g each were collected for use in subsequent leaching procedures. The

subsequent procedures were conducted in parallel with this division (Fig. 1), and the results obtained from these steps are discussed below. The first portion was leached using thiourea in an acidic medium in the presence of Fe^{3+} (2nd leaching described in Fig. 1). The leachate and the residual solid were analyzed by ICP OES for Ag, Au, Cu and Sn and the normalized masses are shown in Fig. 2. It can be seen that 25 % of the Au content remained in the residue after this second leaching. In the case of Ag, Fig. 2 shows that the normalized remained mass has not changed. The general equation for the dissolution reaction of both analytes can be explained using eqs. 3 and 4 (Jing-ying et al., 2012; Zheng and Wang, 2006):

$$Au(s) + 2CS(NH_2)_2(aq) + Fe^{3+}(aq) \leftrightarrows Au\left[CS(NH_2)_2\right]_2^{+}(aq) + Fe^{2+}(aq) \quad (3)$$

$$Ag(s) + 3CS(NH_2)_2(aq) + Fe^{3+}(aq) \leftrightarrows Ag\left[CS(NH_2)_2\right]_3^{+}(aq) + Fe^{2+}(aq) \quad (4)$$

Gold showed a higher extent of leaching compared to Ag due to several factors. For example, the reduction potential (Table 2) indicates that Au^{+} is more easily reduced than Ag^{+}, allowing thiourea to donate electrons more spontaneously to Au. The complexation reactions result in more stable thiourea complexes with Au, with formation constant (pK_f) of 21.75 for $Au\left[CS(NH_2)_2\right]_2^{+}$ (Gönen et al., 2007; Jing-ying et al., 2012), while for Ag with $pK_f = 13.1$ for $Ag\left[CS(NH_2)_2\right]_3^{+}$ (Li and Miller, 2007; Murthy et al., 2003). Here pK_f = -LogK_f, and K_f represents the equilibrium constant for formation of these complex species from Au^{+} or Ag^{+} ions. In addition, the kinetics of reaction 3 with Au are faster ($3.58 \times 10^{\hat{}-7}$ mol $L^{\hat{}-1}$ $min^{\hat{}-1}$), compared to that of Ag (8.98×10^{-9} mol $L^{\hat{}-1}$ $min^{\hat{}-1}$) (Li and Miller, 2007), resulting in higher metal recovery efficiency. These reasons may justify the higher recovery efficiency of Au compared to Ag in the leaching with thiourea and ferric sulfate.

Thiourea used in this study is a less toxic and more sustainable alternative when compared with cyanide (CN^{-}) for the recovery of Au and Ag. Some studies have shown that while cyanide has high toxicity and environmental persistence, thiourea requires higher concentrations to cause adverse effects and is considered less toxic to aquatic organisms and humans (Cui and Zhang, 2008; Syed, 2012). In addition, the degradation products of thiourea tend to be less persistent in the environment (Ubaldini et al., 1998). However, its toxicity at high concentrations and the possibility of soil and water contamination requires proper monitoring (Hilson and Monhemius, 2006; Li et al., 2012).

3.4. Leaching of ag and au with iodine/iodide

The second aliquot (5 g) of remnant solid sample after Cu leaching, as described in Section 3.2, was leached with an iodine/iodide solution for Au and Ag leaching in a neutral pH solution with H_2O_2 as an oxidizing agent to speed up the leaching process (see Fig. 1). The liquid and solid extracts were separated and analyzed for the determination of the target elements using ICP OES. The results are shown in Fig. 2. The normalized remained mass of Au decreased to 38 %, with the majority of Au still present in the leachate, indicating that only a small fraction was not leached. The normalized remaining mass of Ag fell to 0.4 %, indicating that 99.6 % of the Ag is in the leachate. The remnant Sn of 3.6 % in the remaining solid phase indicates that 96.4 % of Sn dissolved after two consecutive leaching stages (1 and 3). The dissolution reaction of Au and Ag can be represented using eqs. 5–7 (Liang and Li, 2019; Xiu et al., 2015):

$$I_2^{-}(aq) + I^{-}(aq) \leftrightarrows I_3^{-}(aq) \quad (5)$$

$$2Au(s) + I_3^{-}(aq) + I^{-}(aq) \leftrightarrows 2AuI_2^{-}(aq) \quad (6)$$

$$2Ag(s) + I_3^{-}(aq) + I^{-}(aq) \leftrightarrows 2AgI_2^{-}(aq) \quad (7)$$

The high leaching efficiency of Ag compared to Au and Sn using iodine and iodide can be attributed to thermodynamic and kinetic factors (Konyratbekova et al., 2015; Qi and Hiskey, 1991). One of the main factors is the standard reduction potential of Ag, which is intermediate (See Table 2, making it easier to oxidize than Au, but more stable in solution than Sn (Bard et al., 2017). This factor contributes significantly to the higher leaching efficiency.

As noted in Section 3.2, thermodynamics of the reaction also play a crucial role. The change in free energy for the reaction can be expressed by Eq. 8 as noted by Xiu et al. (2015):

$$\Delta G_{298}^{\circ} = -\left[E_1^{\circ} - \left(E_2^{\circ} - \frac{0.0592}{n}\log(K)\right)\right]nF \quad (8)$$

E_1° being the standard electrode potential for I_3^{-}/I^{-}, E_2° the standard electrode potential for M^{n+}/M (M = Au or Ag), n is the number of moles of electrons transferred in the reaction, F the Faraday constant and K the stability constant for AuI_2^{-} or AgI_2^{-} (Davis et al., 1993; Xiu et al., 2015). This equation shows how the concentrations of iodine and iodide, as well as the stability constants of the complexes formed, influence the spontaneity of the leaching process.

The formation of complexes is another important factor. Silver forms stable and soluble complexes with iodides (AgI_2^{-} and AgI_3^{2-}), which are more soluble than Au complexes (AuI_2^{-}) and much more soluble than Sn iodides (SnI_2, $K_{sp} = 8.50 \times 10^{-9}$) (Baghalha, 2012; Davis et al., 1993). This makes it easier to dissolve and keep Ag in solution during the leaching process. The reaction kinetics and activation energy also favor the leaching of Ag. The reaction kinetics of Ag with iodine/iodide is generally faster due to its electronic structure and atomic size. In addition, the activation energy for Ag leaching is lower than that for Au (Angelidis et al., 1993; Qi and Hiskey, 1991), which results in a faster and more efficient reaction.

The stability of Ag-iodide complexes over a wide pH range and the lower sensitivity of Ag leaching to pH variations compared to Sn (Chung et al., 2021) also contribute to its higher leaching efficiency. This allows the process to be carried out under less controlled pH conditions. The concentration of the reagents also plays a crucial role. The leaching of Au and Ag in the iodine-iodide system is highly dependent on the concentration of iodide, which controls the oxidation half-reaction, and the concentration of iodine (which controls the reduction half-reaction). By adjusting these concentrations, it is possible to optimize the leaching process.

All these characteristics combined result in more efficient leaching of Ag in the iodine-iodide system compared to the other metals evaluated (Chung et al., 2021; Konyratbekova et al., 2015; Qi and Hiskey, 1991). Silver has a higher extraction efficiency than gold due to its more favorable oxidation potential (Table 2). This results in a higher leaching rate for Ag compared to Au under the same experimental conditions. This characteristic in WEEE makes Ag recovery more efficient, contributing to more effective extraction in this leaching process, compared to Au (Fig. 2).

One of the advantages of using iodine/iodide in leaching is that it offers a more sustainable alternative, due to its lower toxicity compared to conventional leaching agents such as cyanide or aqua regia (Konyratbekova et al., 2015). This process offers advantages such as reagent recyclability, energy efficiency and greater selectivity for precious metals (Chung et al., 2021; Davis et al., 1993). Operating under milder conditions, the method reduces energy consumption and emission of toxic gases (Batnasan et al., 2019). The possibility of developing a closed-loop process and the biodegradability of iodine compounds contribute to minimizing environmental impact (Serpe et al., 2015). Its versatility allows it to process different types of WEEE to recover and recycle metals, potentially reducing the need for primary mining. However, challenges such as the cost of reagents and the need to optimize the process for different types of WEEE must still be addressed before large-scale implementation can be achieved (Akcil et al., 2015).

3.5. Leaching Sn with HCl

For the Sn leaching, the third aliquot (5 g) of remnant solid sample after Cu leaching, as described in Section 3.2, was leached in a 2 mol/L HCl solution at a temperature of 348 K for 4 h. Fig. 2 show the results based on the analysis of liquid and solid. It is apparent that 97 % of the Sn was leached, with only 3 % remaining in the solid fraction. Silver, on the other hand, was completely leached out, with no residue remaining in the solid phase, while Au released about 77 % in its solid fraction with 23 % leaching efficiency. The general equation for the dissolution reaction of Sn in HCl can be explained as follows (Moosakazemi et al., 2019), see Eq. 9:

$$Sn(s) + 2HCl(aq) \leftrightarrows SnCl_2(aq) + H_2(g) \quad (9)$$

$$SnCl_2(aq) + 2Cl^-(aq) \leftrightarrows [SnCl_4]^{2-}(aq) \quad (10)$$

In Eq. 9, metallic Sn reacts with HCl being oxidized forming $SnCl_2$, and releasing H_2. With the excess of Cl^-, $SnCl_2$ tends to form a more stable complex in solution ($[SnCl_4]^{2-}$), shown in Eq. 10. This occurs due to the favorable Gibbs energy: $\Delta G_{348}^{\circ} = -22.696$ kJ/mol at 348 K. These thermodynamic factors make this leaching process efficient for extracting Sn from PCB samples.

The selective leaching of Ag and Sn to the detriment of Au in this leaching with HCl can be explained by electrochemical and thermodynamic principles. Electrochemically, the standard reduction potentials of these metals (See in Table 2) indicate that Au is the most noble and therefore the most difficult to oxidize (Kim et al., 2011; Lee et al., 2015). Moreover, HCl does not have sufficient potential to oxidize Au. In contrast, Ag and Sn are more easily oxidized, forming soluble chloride complexes. Thermodynamically, the free energies for the leaching reactions of Ag and Sn with HCl are negative, indicating spontaneity, while for Au, the reaction is not spontaneous without an additional strong oxidizer.

The kinetics of the reactions also have a major impact. Studies show that the activation energy for the dissolution of Au in chloride solutions, even with strong oxidizers, can reach 55 kJ/mol (Senanayake, 2004). This explains the slow dissolution kinetics of Au compared to other metals. In addition, the formation of a passivating layer of AgCl on the surface of Ag can initially slow down its dissolution, but excess chloride ions lead to the formation of soluble complexes such as $[AgCl_2]^-$ (Lee et al., 2015). The combination of electrochemical, thermodynamic, and kinetic factors results in the selective leaching of Ag and Sn, while Au remains inert under typical HCl leaching conditions (Fig. 2).

The reason for using HCl as a Sn extractant is that the acid is considered environmentally friendly for several reasons: (i) HCl is a relatively less aggressive acid when compared to other strong acids, such as HNO_3 or H_2SO_4, thus reducing the risks of environmental contamination (Ghosh et al., 2015); (ii) the leaching process does not require high temperatures or pressures, which reduces energy consumption and, consequently, the associated carbon footprint (Habib Al Razi, 2016); (iii) HCl can also be easily regenerated and reused in the process, minimizing waste generation (Jha et al., 2012); (iv) the selectivity of HCl in Sn leaching allows for the efficient recovery of this strategic metal in WEEE, contributing to the reduction of primary mining and its associated environmental impacts (Nekouei et al., 2018).

3.6. Leaching of Sn with H_2SO_4 in the presence of $CuSO_4$

For the Sn leaching, in sulfate medium, the fourth aliquot (5 g) of remnant solid sample after Cu leaching, as described in Section 3.2, was leached using a solution of H_2SO_4 and $CuSO_4$. The results for leaching in sulfate medium (Fig. 2) are similar to the leaching results with HCl, where 97 % of the Sn was leached out, leaving only 3 % in the solid fraction. Silver showed approximately 25 % in the solid fraction, while 62 % of the Au remained in the solid phase. The dissolution reaction is given by Eq. 11(Mishra et al., 2021):

$$Sn(s) + 2H_2SO_4(aq) \leftrightarrows SnSO_4(s) + SO_2(g) + 2H_2O\ (l) \quad (11)$$

The leaching of Ag, Au and Sn using H_2SO_4 is a complex process involving electrochemical, thermodynamic and kinetic principles. The standard reduction potentials of these metals (Table 2) indicate their different susceptibility to oxidation (Hirato, 2014; Murphy, 1966). Concentrated H_2SO_4 acts as a strong acid and a moderate oxidizing agent, capable of oxidizing these metals to varying degrees. For example, the oxidation of some metals in concentrated H_2SO_4 occurs according to the reactions described in Eqs. (12) and (13) (Habashi, 1999; Hirato, 2014):

$$2Ag(s) + 2H_2SO_4(aq) \leftrightarrows Ag_2SO_4(s) + SO_2(g) + 2H_2O\ (l) \quad (12)$$

$$2Au(s) + 6H_2SO_4(aq) \leftrightarrows Au_2(SO_4)_3(aq) + 3SO_2\ (g) + 6H_2O\ (l) \quad (13)$$

The formation of soluble sulphate complexes (e.g., $AgSO_4^-$) also contributes to the effectiveness of the process (Senanayake, 2004) High temperatures are often employed to increase the reaction rate and overcome thermodynamic barriers, especially for more noble metals such as Au. Marsden and House (2006) reported that the leaching of Au in concentrated, hot H_2SO_4 follows the same reaction as Eq. (13). The leaching efficiency and selectivity vary significantly with the process conditions, such as acid concentration and temperature. Studies by Ghosh et al. (2015) have shown that while lower concentrations of H_2SO_4 are sufficient to leach Ag, Cu and Sn, the efficient leaching of Au requires more aggressive conditions, including concentrated H_2SO_4 and high temperatures.

The overall reaction that describes the role of $CuSO_4$ in facilitating the oxidation of Sn in an acidic medium can be expressed as Eq. 14 (Zhang et al., 2015):

$$Sn(s) + Cu^{2+}(aq) \leftrightarrows Sn^{2+}(aq) + Cu(s) \quad (14)$$

The reaction takes place in an acidic medium, typically using H_2SO_4, which provides an environment conducive to the solubilization of Sn (Guo et al., 2020).

In the thermodynamic context, the viability of this reaction can be assessed using potential-pH diagrams, which illustrate the conditions under which the ionic species are in equilibrium. Based on this principle, $CuSO_4$ is used to displace Sn from the H_2SO_4 leaching residue. As the displacement reaction must take place under a certain acid concentration, H_2SO_4 was introduced to control the pH below 2.0 (Kaye and Thompson, 2011).

This method of Sn leaching using H_2SO_4 is not considered environmentally friendly in its conventional form due to several factors: (i) the use of concentrated H_2SO_4 poses significant environmental risks due to the production of SO_2 as a by-product which contributes to atmospheric pollution and acid rain, (ii) the high temperatures required increase energy consumption and the carbon footprint. Moreover, the lack of selectivity of the process, i.e., the simultaneous leaching of several metals, complicates the recovery and purification of individual elements, even when used as a final process step to extract only waste metals (Cui and Zhang, 2008; Huang et al., 2009).

Nevertheless, there are several strategies to make the process more sustainable which include: (i) the addition of weaker organic acids or alternative leaching solutions (Li et al., 2015), (ii) the implementation of SO_2 capture and treatment systems (Sethurajan et al., 2018), (iii) the development of low-temperature processes or the use of renewable energy sources, and (iv) the incorporation of H_2SO_4 recycling and reuse techniques (Tuncuk et al., 2012). In addition, the exploration of pretreatment methods to increase selectivity and the investigation of the use of bioleaching as a more environmentally friendly alternative (Ilyas et al., 2007) are promising approaches to improve the sustainability of the recovery process of Sn and other metals from WEEE.

3.7. Evaluating the best strategy for sequential leaching

Based on the leaching results described so far, combinations were made between the different leaching strategies to recover the metals Ag, Au and Sn, with the aim of determining the leaching sequence that would maximize the recovery of all the target analytes. The leaching of Cu using HNO_3 was established as initial, with experimental conditions previously optimized by Dutta et al. (2018), showing reproducible results and efficiency of approximately 100 % for the samples described in this study. The leaching combinations are illustrated in Fig. 3. The first test was for the leaching of Ag and Au using the solid residue obtained from the leaching of Cu. The reagents evaluated were (a) thiourea (Fig. 3a) and (b) iodine/iodide (Fig. 3b) and the appropriate leachate obtained from these tests was used to extract Sn with HCl. The second test was carried out by alternating the order of leaching, i.e., Sn with (c) HCl (Fig. 3c) and (d) with H_2SO_4 (Fig. 3d), and then Ag and Au. The evaluation was also carried out with the solids obtained after leaching Cu with HNO_3. The solid and liquid phases resulting from the leaching were analyzed using ICP OES. The concentration data obtained from the last leaching is shown in Fig. 4(a-d), following the leaching sequence shown in Fig. 3 (a-d).

According to Fig. 4, the Ag leaching efficiency was close to 100 % for all the sequences in the WEEE. For Au, the thiourea (Fig. 4a) and iodine/iodide (Fig. 4b) sequences showed moderate leaching efficiencies,

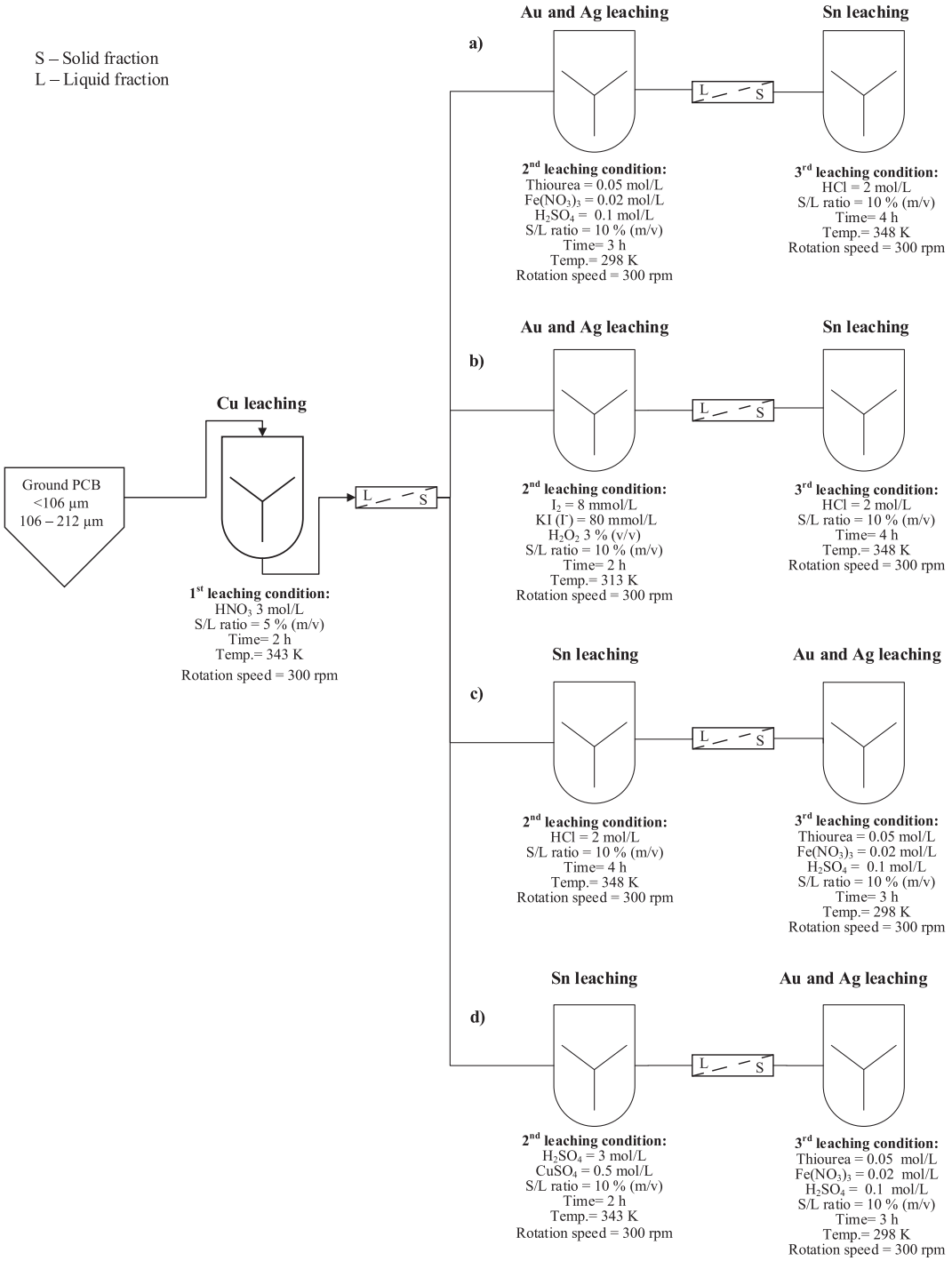

Fig. 3. Evaluation of the best sequencing for leaching Ag, Au, Cu and Sn from e-waste.

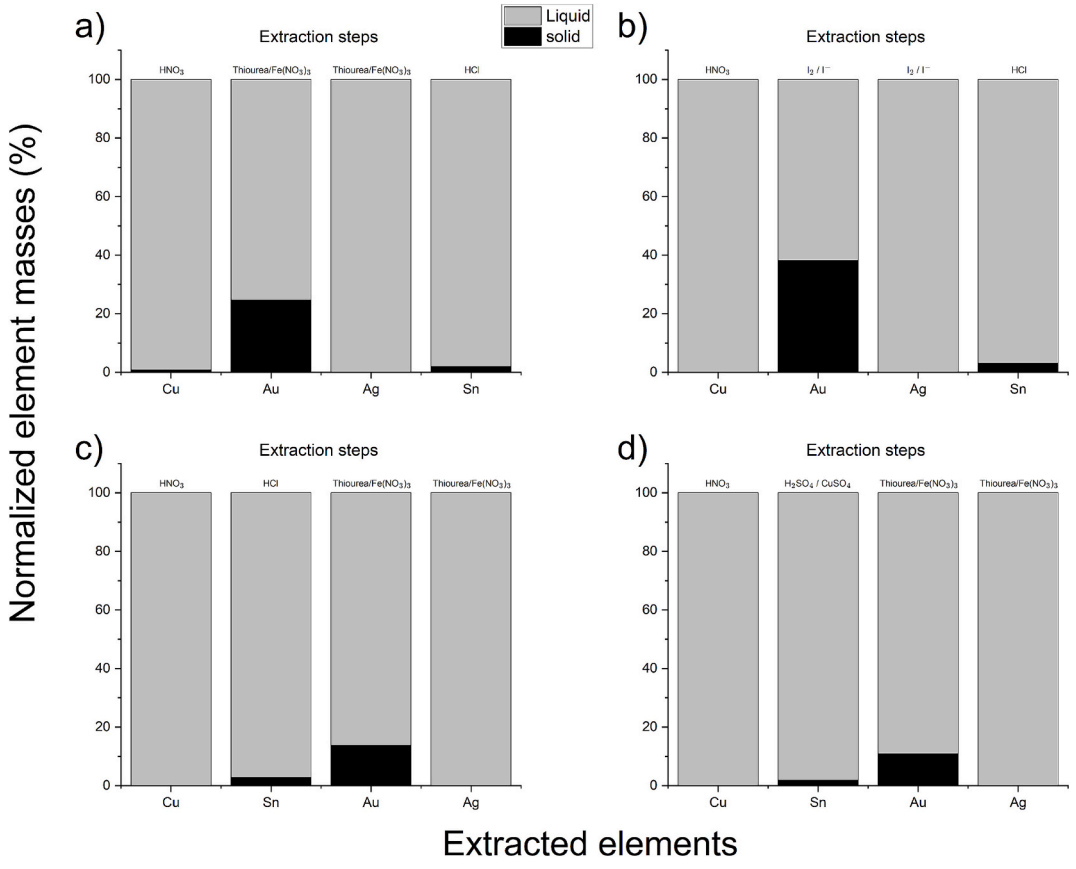

Fig. 4. Normalized remained masses of Ag, Au, Cu and Sn analytes in % in the solid residues obtained for each leaching sequence evaluated.

ranging from 25 % to 38 % in the solid phase, resulting in an average Au normalized mass of 69 % in the liquid phase. Other sequences, in which Sn was leached before Au, achieved an average Au leaching efficiency of approximately 88 % in the liquid phase. For Sn, the leaching sequence using both HCl (Fig. 4c) and H_2SO_4 (Fig. 4d) showed an average efficiency of 98 %. As the aim here is to maximize leaching using environmentally friendly reagents/methods, the leaching sequence shown in Fig. 4c is the most suitable, with a leaching efficiency of 100 % for Ag and Cu, 98 % Sn and 86 % Au. The reason for this leaching sequence having such a high leaching rate is due to the complementary synergy between each leaching condition which focuses on selectively leaching each of the target elements.

4. Conclusions

This study systematically investigated a leaching process for the recovery of valuable and strategic metals from PCBs originating from electronic waste. The process developed consisted of multiple leaching conditions, each aimed at leaching a specific metal. Leaching with HNO_3 proved to be highly effective for the leaching of Cu, achieving an efficiency of 97 % in the first leaching. For the recovery of precious metals, the solids resulting from the leaching of Cu were used for the leaching of Au and Ag with thiourea and $Fe(NO_3)_3$, resulting in an efficiency of 75 % for the leaching of Au, while leaching with iodine/iodide showed excellent performance for the leaching of Ag, with 100 % efficiency, Sn leaching was carried out with H_2SO_4 and HCl, with an average efficiency of 97 % for both.

When evaluating which leaching sequence would maximize the leaching of all elements, the leaching route that showed the best efficiency rates was the sequence of HNO_3-H_2SO_4-I_2/KI described in Fig. 4d: (i) HNO_3 leaching 100 % of Cu, (ii) H_2SO_4 leaching 98 % of Sn, and (iii) iodine/iodide leaching 100 % of Ag and 90 % of Au (these elements were co-leached). The proposed leaching sequencing process has several advantages, including high selectivity in leaching the target metals.

However, the leaching route described in Fig. 4c presents the HNO_3-HCl-I_2/KI sequence of low environmental impact compared to traditional methods: (i) HNO_3 leaching 100 % of Cu, (ii) HCl leaching 98 % of Sn, and (iii) iodine/iodide co-leaching 100 % of Ag and 86 % of Au. These characteristics make the route promising for application on an industrial scale, contributing to more sustainable WEEE management to recycle metals.

Despite the promising results, additional studies are needed to further optimize the leaching and metal precipitation conditions. This could lead to an increase in leaching efficiencies, especially for Au, whose current recovery rate still leaves room for improvement. Furthermore, future investigations could focus on the applicability of the method to a wider range of electronic waste materials, on assessing its economic viability on a large scale, and recovery of the acids used, proposing a close loop system for leaching-purification-recovery.

CRediT authorship contribution statement

Dennis Silva Ferreira: Writing – original draft, Visualization, Validation, Methodology, Investigation. **Edenir Rodrigues Pereira-Filho:** Supervision, Resources, Project administration, Funding acquisition, Formal analysis, Data curation.

Declaration of competing interest

The authors declare that they have no known competing financial interests or personal relationships that could have appeared to influence the work reported in this paper.

Acknowledgements

The authors are grateful for grants from the São Paulo State Research Foundation (FAPESP) [processes 2016/01513–0, 2019/24223–5]; National Council for Scientific and Technological Development, CNPq [grants no.140867/2021–0, 302719/2020–2]. This study was partly funded by the Coordination for the Improvement of Higher Education Personnel - Brazil (CAPES) - Funding Code 001.

Appendix A. Supplementary data

Supplementary data to this article can be found online at https://doi.org/10.1016/j.hydromet.2025.106476.

References

Akcil, A., Erust, C., Gahan, C.S., Ekhar Ozgun, M., Sahin, M., Tuncuk, A., 2015. Precious metal recovery from waste printed circuit boards using cyanide and non-cyanide lixiviants – a review. Waste Manag. 45, 258–271. https://doi.org/10.1016/J.WASMAN.2015.01.017.

Habib Al Razi, K.M., 2016. Resourceful recycling process of waste desktop computers: a review study. Resour. Conserv. Recycl. 110, 30–47. https://doi.org/10.1016/J.RESCONREC.2016.03.017.

Alabi, O.A., Adeoluwa, Y.M., Huo, X., Xu, X., Bakare, A.A., 2021. Environmental contamination and public health effects of electronic waste: an overview. J. Environ. Health Sci. Eng. 19, 1209. https://doi.org/10.1007/S40201-021-00654-5.

Andrade, D.F., Machado, R.C., Bacchi, M.A., Pereira-Filho, E.R., 2019. Proposition of electronic waste as a reference material – part 1: sample preparation, characterization and chemometric evaluation. J. Anal. At. Spectrom 34, 2394–2401. https://doi.org/10.1039/C9JA00283A.

Angelidis, T.N., Kydros, K.A., Matis, K.A., 1993. A fundamental rotating disk study of gold dissolution in iodine-iodide solutions. Hydrometallurgy 34, 49–64. https://doi.org/10.1016/0304-386X(93)90080-W.

Anuardo, R.G., Espuny, M., Costa, A.C.F., Espuny, A.L.G., Kazançoğlu, Y., Kandsamy, J., de Oliveira, O.J., 2023. Transforming E-waste into opportunities: driving organizational actions to achieve sustainable development goals. Sustainability 15, 14150. https://doi.org/10.3390/SU151914150.

Baghalha, M., 2012. The leaching kinetics of an oxide gold ore with iodide/iodine solutions. Hydrometallurgy 113–114, 42–50. https://doi.org/10.1016/J.HYDROMET.2011.11.013.

Baldé, C.P., Kuehr, R., Yamamoto, T., McDonald, R., Althaf, S., Bel, G., Deubzer, O., Fernandez-Cubillo, E., Forti, V., Gray, V., Herat, S., Honda, S., Iattoni, G., Khetriwal, D.S., Luda di Cortemiglia, V., 2024. The Global E-Waste Monitor, p. 2024.

Bard, A.J., Jordan, Joseph, Parsons, Roger, 2017. Standard Potentials in Aqueous Solution. Routledge.

Bas, A.D., Deveci, H., Yazici, E.Y., 2014. Treatment of manufacturing scrap TV boards by nitric acid leaching. Sep. Purif. Technol. 130, 151–159. https://doi.org/10.1016/J.SEPPUR.2014.04.008.

Batnasan, A., Haga, K., Huang, H.H., 2019. High-pressure oxidative leaching and iodide leaching followed by selective precipitation for recovery of base and precious metals from waste printed circuit boards ash. Metals (Basel) 9, 363. https://doi.org/10.3390/MET9030363.

Behnamfard, A., Salarirad, M.M., Veglio, F., 2013. Process development for recovery of copper and precious metals from waste printed circuit boards with emphasize on palladium and gold leaching and precipitation. Waste Manag. 33, 2354–2363. https://doi.org/10.1016/J.WASMAN.2013.07.017.

Birloaga, I., De Michelis, I., Ferella, F., Buzatu, M., Vegliò, F., 2013. Study on the influence of various factors in the hydrometallurgical processing of waste printed circuit boards for copper and gold recovery. Waste Manag. 33, 935–941. https://doi.org/10.1016/J.WASMAN.2013.01.003.

Bizzi, C.A., Pedrotti, M.F., Betiolo, D.M., Nascimento, M.S., Muller, E.I., Cravotto, G., Flores, E.M.M., 2021. Development of an eco-friendly sample preparation protocol for metal determination in food samples: an oxygen pressurized single reaction chamber using diluted nitric acid. Anal. Methods 13, 5555–5563. https://doi.org/10.1039/D1AY01510A.

Botelho Junior, A.B., Martins, F.P., Cezarino, L.O., Liboni, L.B., Tenório, J.A.S., Espinosa, D.C.R., 2023. The sustainable development goals, urban mining, and the circular economy. Extr Ind Soc 16, 101367. https://doi.org/10.1016/J.EXIS.2023.101367.

Castro, J.P., Pereira-Filho, E.R., 2020. Chemical exploratory analysis of printed circuit board (PCB) using inductively coupled plasma optical emission spectrometry (ICP OES): data treatment and elements correlation. Detritus 13, 131. https://doi.org/10.31025/2611-4135/2020.14039.

Castro, J.P., Garcia, J.A., Souza, R.G., Pereira-Filho, E.R., 2024. Indium recovery from end-of-life E-waste: important details related to spectroanalytical determination and recycling viability. J. Braz. Chem. Soc. 35, 20230201–20230202. https://doi.org/10.21577/0103-5053.20230201.

Chung, S.J., Pillai, K.C., Moon, I.S., 2009. A sustainable environmentally friendly NOx removal process using ag(II)/ag(I)-mediated electrochemical oxidation. Sep. Purif. Technol. 65, 156–163. https://doi.org/10.1016/J.SEPPUR.2008.10.030.

Chung, J., Seo, B., Lee, J., Kim, J.Y., 2021. Comparative analysis of I2-KI and HNO3 leaching in a life cycle perspective: towards sustainable recycling of end-of-life c-Si PV panel. J. Hazard. Mater. 404, 123989. https://doi.org/10.1016/J.JHAZMAT.2020.123989.

CRC Handbook of Chemistry and Physics, 2016. CRC Handbook of Chemistry and Physics. https://doi.org/10.1201/9781315380476.

Cui, J., Zhang, L., 2008. Metallurgical recovery of metals from electronic waste: a review. J. Hazard. Mater. 158, 228–256. https://doi.org/10.1016/J.JHAZMAT.2008.02.001.

Davis, A., Tran, T., Young, D.R., 1993. Solution chemistry of iodide leaching of gold. Hydrometallurgy 32, 143–159. https://doi.org/10.1016/0304-386X(93)90020-E.

Diallo, S., Tran, L.H., Larivière, D., Blais, J.F., 2024. Mass balance and economic study of a treatment chain for rare earths, base metals and precious metals recovery from used smartphones. Miner. Eng. 215, 108824. https://doi.org/10.1016/J.MINENG.2024.108824.

Dutta, D., Panda, R., Kumari, A., Goel, S., Jha, M.K., 2018. Sustainable recycling process for metals recovery from used printed circuit boards (PCBs). Sustain. Mater. Technol. 17, e00066. https://doi.org/10.1016/J.SUSMAT.2018.E00066.

Emmons-Burzyńska, M., Jędrzejczak, E., Piasecki, A., Ławniczak, Ł., Regel-Rosocka, M., Wysokowski, M., 2025. Leaching of metals from electronic waste using carboxylic acid-based deep eutectic solvents: preliminary laboratory studies and molecular modelling. Hydrometallurgy 234, 106465. https://doi.org/10.1016/J.HYDROMET.2025.106465.

Fatimah, Y.A., Govindan, K., Sasongko, N.A., Hasibuan, Z.A., 2024. The critical success factors for sustainable resource management in circular economy: assessment of urban mining maturity level. J. Clean. Prod. 469, 143084. https://doi.org/10.1016/J.JCLEPRO.2024.143084.

Ferreira, D.S., Pereira, F.M.V., Olivieri, A.C., Pereira-Filho, E.R., 2024. Electronic waste analysis using laser-induced breakdown spectroscopy (LIBS) and X-ray fluorescence (XRF): critical evaluation of data fusion for the determination of Al, Cu and Fe. Anal Chim Acta 1303, 342522. https://doi.org/10.1016/J.ACA.2024.342522.

Forti, V., Baldé, C.P., Kuehr, R., Bel, G., 2020. The Global E-Waste Monitor 2020: Quantities, Flows, and the Circular Economy Potential.

Ghosh, B., Ghosh, M.K., Parhi, P., Mukherjee, P.S., Mishra, B.K., 2015. Waste printed circuit boards recycling: an extensive assessment of current status. J. Clean. Prod. 94, 5–19. https://doi.org/10.1016/J.JCLEPRO.2015.02.024.

Golev, A., Corder, G.D., 2017. Quantifying metal values in e-waste in Australia: the value chain perspective. Miner. Eng. 107, 81–87. https://doi.org/10.1016/J.MINENG.2016.10.021.

Gönen, N., Körpe, E., Yildirim, M.E., Selengil, U., 2007. Leaching and CIL processes in gold recovery from refractory ore with thiourea solutions. Miner. Eng. 20, 559–565. https://doi.org/10.1016/J.MINENG.2006.11.003.

Gulliani, S., Volpe, M., Messineo, A., Volpe, R., 2023. Recovery of metals and valuable chemicals from waste electric and electronic materials: a critical review of existing technologies. RSC Sustainability 1, 1085–1108. https://doi.org/10.1039/D3SU00034F.

Guo, X., Qin, H., Tian, Q., Li, D., 2020. Recovery of metals from waste printed circuit boards by selective leaching combined with cyclone electrowinning process. J. Hazard. Mater. 384, 121355. https://doi.org/10.1016/J.JHAZMAT.2019.121355.

Habashi, F., 1999. A Textbook of Hydrometallurgy. Métallurgie Extractive Quebec.

Hilson, G., Monhemius, A.J., 2006. Alternatives to cyanide in the gold mining industry: what prospects for the future? J. Clean. Prod. 14, 1158–1167. https://doi.org/10.1016/J.JCLEPRO.2004.09.005.

Hirato, T., 2014. Thermodynamics of aqueous phases. In: Treatise on Process Metallurgy. Elsevier, pp. 641–652. https://doi.org/10.1016/B978-0-08-096986-2.00036-9.

Hojo, M., Iwasaki, S., Okamura, K., 2017. Pure gold dissolution with hydrogen peroxide as the oxidizer in HBr or HI solution. J. Mol. Liq. 246, 372–378. https://doi.org/10.1016/J.MOLLIQ.2017.09.080.

Huang, K., Guo, J., Xu, Z., 2009. Recycling of waste printed circuit boards: a review of current technologies and treatment status in China. J. Hazard. Mater. 164, 399–408. https://doi.org/10.1016/J.JHAZMAT.2008.08.051.

Ilyas, S., Anwar, M.A., Niazi, S.B., Afzal Ghauri, M., 2007. Bioleaching of metals from electronic scrap by moderately thermophilic acidophilic bacteria. Hydrometallurgy 88, 180–188. https://doi.org/10.1016/J.HYDROMET.2007.04.007.

Jha, M.K., Choubey, P.K., Jha, A.K., Kumari, A., Lee, J., Chun Kumar, V., Jeong, J., 2012. Leaching studies for tin recovery from waste e-scrap. Waste Manag. 32, 1919–1925. https://doi.org/10.1016/J.WASMAN.2012.05.006.

Jing-ying, L., Xiu-li, X., Wen-quan, L., 2012. Thiourea leaching gold and silver from the printed circuit boards of waste mobile phones. Waste Manag. 32, 1209–1212. https://doi.org/10.1016/J.WASMAN.2012.01.026.

Kaye, M.H., Thompson, W.T., 2011. Computation of Pourbaix diagrams at elevated temperature. In: Uhlig's Corrosion Handbook: Third Edition, 111–122. https://doi.org/10.1002/9780470872864.CH9.

Kim, E.Y., Kim, M.S., Lee, J.C., Pandey, B.D., 2011. Selective recovery of gold from waste mobile phone PCBs by hydrometallurgical process. J. Hazard. Mater. 198, 206–215. https://doi.org/10.1016/J.JHAZMAT.2011.10.034.

Konyratbekova, S.S., Baikonurova, A., Ussoltseva, G.A., Erust, C., Akcil, A., 2015. Thermodynamic and kinetic of iodine–iodide leaching in gold hydrometallurgy. Trans. Nonferrous Met. Soc. Chin. 25, 3774–3783. https://doi.org/10.1016/S1003-6326(15)63980-2.

Kumar, S., Agarwal, N., Anand, S.K., Rajak, B.K., 2022. E-waste management in India: a strategy for the attainment of SDGs 2030. Mater Today Proc 60, 811–814. https://doi.org/10.1016/J.MATPR.2021.09.296.

Lagos, G., Peters, D., Videla, A., Jara, J.J., 2018. The effect of mine aging on the evolution of environmental footprint indicators in the Chilean copper mining

industry 2001–2015. J. Clean. Prod. 174, 389–400. https://doi.org/10.1016/J.JCLEPRO.2017.10.290.
Lee, H., Mishra, B., 2018. Selective recovery and separation of copper and iron from fine materials of electronic waste processing. Miner. Eng. 123, 1–7. https://doi.org/10.1016/J.MINENG.2018.04.021.
Lee, S.H., Yoo, K., Jha, M.K., Lee, J.C., 2015. Separation of Sn from waste Pb-free Sn–ag–cu solder in hydrochloric acid solution with ferric chloride. Hydrometallurgy 157, 184–187. https://doi.org/10.1016/J.HYDROMET.2015.08.016.
Li, J., Miller, J.D., 2007. Reaction kinetics of gold dissolution in acid thiourea solution using ferric sulfate as oxidant. Hydrometallurgy 89, 279–288. https://doi.org/10.1016/J.HYDROMET.2007.07.015.
Li, J., Safarzadeh, M.S., Moats, M.S., Miller, J.D., Levier, K.M., Dietrich, M., Wan, R.Y., 2012. Thiocyanate hydrometallurgy for the recovery of gold.: part II: the leaching kinetics. Hydrometallurgy 113–114, 10–18. https://doi.org/10.1016/J.HYDROMET.2011.11.007.
Li, J., Zeng, X., Chen, M., Ogunseitan, O.A., Stevels, A., 2015. "Control-alt-delete": rebooting solutions for the E-waste problem. Environ. Sci. Technol. 49, 7095–7108. https://doi.org/10.1021/ACS.EST.5B00449/SUPPL_FILE/ES5B00449_SI_001.PDF.
Liang, C.J., Li, J.Y., 2019. Recovery of gold in iodine-iodide system – a review. Sep. Sci. Technol. 54, 1055–1066. https://doi.org/10.1080/01496395.2018.1523931.
Lin, S., Ali, M.U., Zheng, C., Cai, Z., Wong, M.H., 2022. Toxic chemicals from uncontrolled e-waste recycling: exposure, body burden, health impact. J. Hazard. Mater. 426, 127792. https://doi.org/10.1016/J.JHAZMAT.2021.127792.
Marsden, J., House, I., 2006. The chemistry of gold extraction, 2nd ed. Gold Bulletin. https://doi.org/10.1007/BF03215543.
Martinez, G., Restrepo-Baena, O.J., Veiga, M.M., 2021. The myth of gravity concentration to eliminate mercury use in artisanal gold mining. Extr Ind Soc 8, 477–485. https://doi.org/10.1016/J.EXIS.2021.01.002.
Mecucci, A., Scott, K., 2002. Leaching and electrochemical recovery of copper, lead and tin from scrap printed circuit boards. J. Chem. Technol. Biotechnol. 77, 449–457. https://doi.org/10.1002/JCTB.575.
Mishra, S., Panda, S., Akcil, A., Dembele, S., Agcasulu, I., 2021. A review on chemical versus microbial leaching of electronic wastes with emphasis on base metals dissolution. Minerals 11, 1255. https://doi.org/10.3390/MIN11111255.
Moosakazemi, F., Ghassa, S., Mohammadi, M.R.T., 2019. Environmentally friendly hydrometallurgical recovery of tin and lead from waste printed circuit boards: thermodynamic and kinetics studies. J. Clean. Prod. 228, 185–196. https://doi.org/10.1016/J.JCLEPRO.2019.04.024.
Murphy, G.W., 1966. Potential-pH Diagrams: Atlas of Electrochemical Equilibria in Aqueous Solutions. By Marcel Pourbaix. James A. Franklin, Transl. Centre Belge d' Etude de la Corrosion (CEBELCOR), Brussels; Pergamon, New York, 1966. 644 illus. $36,. Science (1979) 154, 1537–1537. doi:https://doi.org/10.1126/SCIENCE.154.3756.1537.A.
Murthy, D.S.R., Kumar, V., Rao, K.V., 2003. Extraction of gold from an Indian low-grade refractory gold ore through physical beneficiation and thiourea leaching. Hydrometallurgy 68, 125–130. https://doi.org/10.1016/S0304-386X(02)00197-4.
Nekouei, R.K., Pahlevani, F., Rajarao, R., Golmohammadzadeh, R., Sahajwalla, V., 2018. Two-step pre-processing enrichment of waste printed circuit boards: mechanical milling and physical separation. J. Clean. Prod. 184, 1113–1124. https://doi.org/10.1016/J.JCLEPRO.2018.02.250.
Parajuly, K., Kuehr, R., Awasthi, A., Fitzpatrick, C., Lepawsky, J., Smith, E., Widmer, R., Zeng, X., 2019. Future E-Waste Scenarios.
Qi, P.H., Hiskey, J.B., 1991. Dissolution kinetics of gold in iodide solutions. Hydrometallurgy 27, 47–62. https://doi.org/10.1016/0304-386X(91)90077-Y.
Reichl, C., Schartz, M., 2024. World Mining Data 2024, Vienna.
Saha, S., Bhadyopadhyay, D., Choudhury, N., 2023. Solvation structure and dynamics of aqueous solutions of au+ ions: a molecular dynamics simulation study. J. Solution Chem. 52, 326–342. https://doi.org/10.1007/S10953-022-01234-3/FIGURES/10.
Schmidt, S., Dietze, F., Hoyer, E., 1991. Zur Stabilität von PdII-, AuIII- und HgII-Komplexen mit N-Acyl-thioharnstoffen in Lösung. Z. Anorg. Allg. Chem. 603, 33–39. https://doi.org/10.1002/ZAAC.19916030106.
Seixas, C.S., Prado, D.S., Joly, C.A., May, P.H., Neves, E.M.S.C., Teixeira, L.R., 2020. Governança ambiental no Brasil: rumo aos objetivos do desenvolvimento sustentável (ODS)? Cadernos Gestão Pública e Cidadania 25. https://doi.org/10.12660/cgpc.v25n81.81404.
Senanayake, G., 2004. Gold leaching in non-cyanide lixiviant systems: critical issues on fundamentals and applications. Miner. Eng. 17, 785–801. https://doi.org/10.1016/J.MINENG.2004.01.008.
Serpe, A., Rigoldi, A., Marras, C., Artizzu, F., Mercuri, M.L., Deplano, P., 2015. Chameleon behaviour of iodine in recovering noble-metals from WEEE: towards sustainability and "zero" waste. Green Chem. 17, 2208–2216. https://doi.org/10.1039/C4GC02237H.
Sethurajan, M., van Hullebusch, E.D., Nancharaiah, Y.V., 2018. Biotechnology in the management and resource recovery from metal bearing solid wastes: recent advances. J. Environ. Manage. 211, 138–153. https://doi.org/10.1016/J.JENVMAN.2018.01.035.
Sulcius, A., 2015. Reactions of metals in nitric acid: writing equations and calculating electromotive force of redox reaction. J. Chem. Educ. 92, 1971–1972. https://doi.org/10.1021/ACS.JCHEMED.5B00328/SUPPL_FILE/ED5B00328_SI_002.DOCX.
Syed, S., 2006. A green technology for recovery of gold from non-metallic secondary sources. Hydrometallurgy 82, 48–53. https://doi.org/10.1016/J.HYDROMET.2006.01.004.
Syed, S., 2012. Recovery of gold from secondary sources—a review. Hydrometallurgy 115–116, 30–51. https://doi.org/10.1016/J.HYDROMET.2011.12.012.
Tamboli, C., Sengupta, B., 2025. Recovery of copper oxide from e-waste using ashing, size reduction, nitric acid leaching, solvent extraction and stripping-precipitation: parametric and scaling up studies and fate of scarce metals. Hydrometallurgy 233, 106451. https://doi.org/10.1016/J.HYDROMET.2025.106451.
Tuncuk, A., Stazi, V., Akcil, A., Yazici, E.Y., Deveci, H., 2012. Aqueous metal recovery techniques from e-scrap: hydrometallurgy in recycling. Miner. Eng. 25, 28–37. https://doi.org/10.1016/J.MINENG.2011.09.019.
U.S. Geological Survey, 2024. Mineral commodity summaries 2024. Reston. https://doi.org/10.3133/mcs2024.
Ubaldini, S., Fornari, P., Massidda, R., Abbruzzese, C., 1998. An innovative thiourea gold leaching process. Hydrometallurgy 48, 113–124. https://doi.org/10.1016/S0304-386X(97)00076-5.
Van Yken, J., Boxall, N.J., Cheng, K.Y., Nikoloski, A.N., Moheimani, N., Kaksonen, A.H., 2023. Techno-economic analysis of an integrated bio- and hydrometallurgical process for base and precious metal recovery from waste printed circuit boards. Hydrometallurgy 222, 106193. https://doi.org/10.1016/J.HYDROMET.2023.106193.
Wang, X., Gaustad, G., 2012. Prioritizing material recovery for end-of-life printed circuit boards. Waste Manag. 32, 1903–1913. https://doi.org/10.1016/J.WASMAN.2012.05.005.
Xiu, F.R., Qi, Y., Zhang, F.S., 2015. Leaching of au, ag, and Pd from waste printed circuit boards of mobile phone by iodide lixiviant after supercritical water pre-treatment. Waste Manag. 41, 134–141. https://doi.org/10.1016/J.WASMAN.2015.02.020.
Yang, H., Liu, J., Yang, J., 2011. Leaching copper from shredded particles of waste printed circuit boards. J. Hazard. Mater. 187, 393–400. https://doi.org/10.1016/J.JHAZMAT.2011.01.051.
Zhang, X., Guan, J., Guo, Y., Yan, X., Yuan, H., Xu, J., Guo, J., Zhou, Y., Su, R., Guo, Z., 2015. Selective Desoldering separation of tin-Lead alloy for dismantling of electronic components from printed circuit boards. Sustainable Chemistry and Engineering 3, 1696–1700. https://doi.org/10.1021/ACSSUSCHEMENG.5B00136/ASSET/IMAGES/LARGE/SC-2015-00136D_0006.JPEG.
Zheng, S., Wang, Y., Yan, Chai, L.Y., 2006. Research status and prospect of gold leaching in alkaline thiourea solution. Miner. Eng. 19, 1301–1306. https://doi.org/10.1016/j.mineng.2005.12.009.

A preliminary study of a sequential leaching process to recover Ag, Au, Cu, and Sn from e-waste

Dennis Silva Ferreira, Edenir Rodrigues Pereira-Filho

Group of Applied Instrumental Analysis, Chemistry Department, Federal University of São Carlos, São Carlos 13565-905, São Paulo State, Brazil

*Corresponding author: erpf@ufscar.br

Table 1S

Instrumental operation parameters for Ag, Au, Cu, and Sn determinations using ICP OES.

Instrumental parameter	**Operational condition**
Integration time (s)	5 to 15
Radio frequency applied power (kW)	1.15
Coolant Ar gas flow rate (L/min)	12.00
Auxiliary Ar gas flow rate (L/min)	0.50
Nebulizer Ar gas flow rate (L/min)	0.70
Sample introduction flow rate (L/min)	2.10
Nebulizer type	Mira Mist
Spray chamber type	Cyclonic
Analytes and monitored wavelength (nm)	Ag I 328.068[b], Au I 267.595[a], Cu I 327.396[b], Sn I 283.999[b]
Limit of Detection (LoD, mg/kg)	Ag = 0.001 Au = 0.004 Cu = 0.006 Sn = 0.04

[a] Axial viewing mode. [b] Radial viewing mode.
I - Atomic and II – Ionic emission lines

Fig. 1S. Pictorial description of the experimental procedure used to a) prepare and b) characterize the samples.

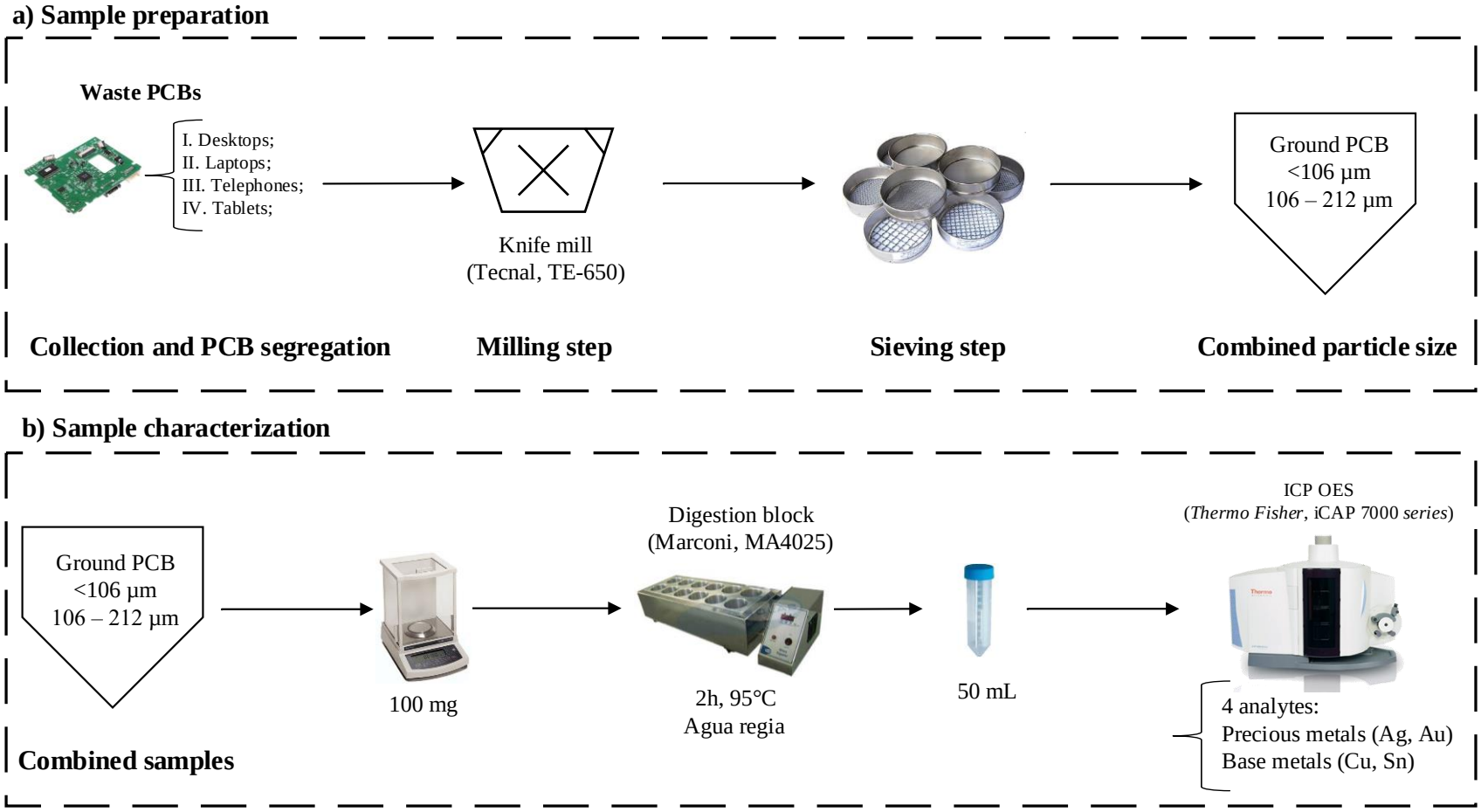

4.4. LIBS and hyperspectral imaging as a real-time process control tool for metal recovery from e-waste

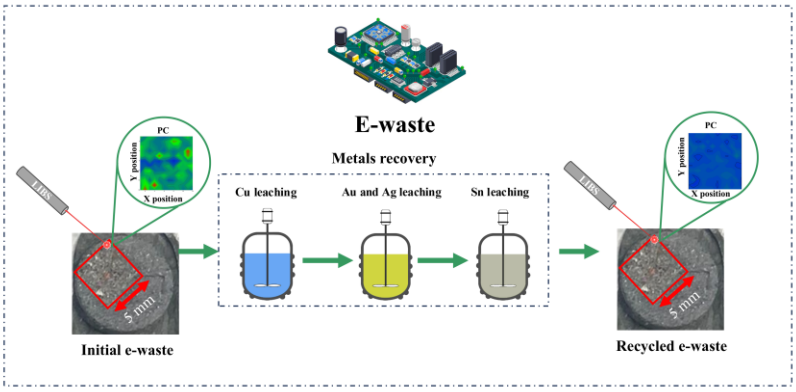

Full Paper

Journal of the Brazilian Chemical Society

https://dx.doi.org/10.21577/0103-5053.20250130

J. Braz. Chem. Soc. **2025**, *36*, 12, e-20250130, 1-13

LIBS and Hyperspectral Imaging as a Real-Time Process Control Tool for Metal Recovery from E-Waste

Dennis S. Ferreira[a] *and Edenir R. Pereira-Filho*[*,a]

[a]*Departamento de Química, Universidade Federal de São Carlos, 13565-905 São Carlos-SP, Brazil*

The rapid increase in e-waste creates challenges, requiring more efficient recycling methods. This study explores the application of laser-induced breakdown spectroscopy (LIBS) combined with hyperspectral imaging to monitor leaching processes of Ag, Au, Cu and Sn in e-waste recycling. The method involved the use of sequential leaching strategies of printed circuit boards (PCBs), the best strategy was applied using HNO_3 for Cu, HCl for Sn and thiourea/$Fe(NO_3)_3$ for Ag and Au. Inductively coupled plasma optical emission spectrometry (ICP OES) was used to validate the metal extraction efficiency, achieving recoveries of 100% for Cu and Ag, 97% for Sn and 86% for Au. LIBS spectra showed a strong correlation with the ICP OES data, revealing reductions in the emission signals corresponding to the extracted elements. Hyperspectral imaging provided an analysis of the spatial distribution of trace elements, confirming the progressive extraction of metals. The results indicate that LIBS, associated with multivariate analysis, offers a fast and economical alternative.

Keywords: e-waste recycling, LIBS, hyperspectral imaging, sustainable recovery, ICP OES, circular economy

Introduction

The rapid technological advancement and increasing demand for electronic equipment have led to an exponential growth in electronic waste (e-waste) generation. This issue is exacerbated by planned obsolescence, particularly in small electronic devices such as smartphones and tablets, which often have lifespans of only 2-3 years.[1,2] In 2022, an estimated 62 million metric tons (Mt) of e-waste were generated globally, and projections indicate this could surpass 110 Mt by 2050.[3] Alarmingly, only 22.3% of this waste is formally recycled, while a large portion is either processed informally or improperly discarded in landfills, leading to environmental and health risks.[4,5]

Informal recycling is frequently carried out under unsafe conditions, releasing hazardous substances such as polychlorinated dibenzofurans (PCDFs) and dioxins. These persistent organic pollutants (POPs), mainly associated with the non-metallic fraction of e-waste, represent significant risks to human health and ecosystems.[6] In this context, the implementation of safe, scalable, and sustainable recycling practices is urgently needed to support environmental regulations such as the Stockholm Convention.[7,8]

Hydrometallurgical methods have emerged as an environmentally friendly alternative to pyrometallurgy for metal recovery from printed circuit boards (PCBs). These processes are cost-effective, adaptable, and operate under milder conditions than pyrometallurgical routes.[9] Pyrometallurgy requires energy-intensive furnaces operating at temperatures typically exceeding 1200 °C, a condition known to promote the formation of hazardous byproducts such as polychlorinated and polybrominated dibenzofurans (PCDFs/PBDFs) and dioxins from the combustion of the plastic and flame-retardant fraction of the e-waste.[10,11]

In contrast, hydrometallurgical leaching operates at or near atmospheric pressure and at significantly lower temperatures, generally below 100 °C and often at room temperature, as employed in this study.[12,13] This fundamental difference not only reduces energy consumption but, critically, prevents the formation of the previously mentioned thermogenic persistent organic pollutants (POPs), shifting the environmental challenge from air emissions to the management of aqueous effluents.[14]

Among the stages involved leaching, separation, and purification leaching plays a critical role, as it directly determines the efficiency of metal recovery.[15,16] However, challenges remain regarding extraction selectivity, operational control, and scalability, particularly in

*e-mail: erpf@ufscar.br
Editor handled this article: Josué Carinhanha Caldas Santos (Associate)

multi-element systems containing both base and precious metals such as Cu, Ag, Au, and Sn.[17,18]

Process monitoring is essential for optimizing leaching efficiency, minimizing chemical consumption, and reducing environmental impact. Conventional techniques such as inductively coupled plasma optical emission spectrometry (ICP OES) and X-ray fluorescence (XRF) are reliable but limited by high costs, complex sample preparation, and the need for laboratory infrastructure.[19,20] In contrast, optical spectroscopic techniques especially laser-induced breakdown spectroscopy (LIBS) offer a promising alternative for real-time, *in situ* analysis. LIBS is fast, versatile, requires minimal sample preparation, and can be combined with chemometric tools such as Principal Component Analysis (PCA) or Partial Least Squares (PLS) to extract meaningful insights from complex data sets.[21-23]

However, the feasibility and optimization of these processes on an industrial scale are fundamentally limited by an analytical difficulty: the absence of process technology capable of monitoring the solid phase in real-time. The reliance on *ex situ* laboratory analyses, such as ICP OES, hinders dynamic and fast control of the process, resulting in non-optimized residence times and excessive reagent consumption.[24,25]

This research is therefore justified by the critical need to overcome this limitation. The aim is to validate a method that integrates the speed of LIBS analysis with the spatial resolution of hyperspectral imaging, establishing a robust tool for directly monitoring the concentration reduction of metals in the solid matrix. We thus aim to provide the missing analytical link to enable intelligent control and real-time optimization of hydrometallurgical processes applied to complex wastes.

Experimental

Instrumentation

Laser-induced breakdown spectroscopy (LIBS)

The LIBS spectra were obtained using the LIBS J200 instrument (Applied Spectra, Fremont, CA, USA), controlled by the Axiom 2.5 software (Applied Spectra), which is responsible for configuring the operating parameters. The equipment consists of an Nd:YAG laser (Quantel Ultra, Bozeman, MT, USA) with a wavelength of 1064 nm, a laser pulse duration of 5 ns and a maximum energy of 100 mJ *per* pulse, as well as a 6-channel charge-coupled device (CCD) spectrometer that records spectral information in the 186 to 1042 nm range. The spectral ranges and resolutions of each spectrometer channel are as follows: 186-311 nm (0.059 nm), 311-465 nm (0.073 nm), 465-591 nm (0.062 nm), 591-693 nm (0.050 nm), 693-884 nm (0.094 nm) and 884-1042 nm (0.079 nm).

The adjustable operating parameters include the laser pulse energy, which varies from 0 to 100 mJ, the delay time, which corresponds to the interval between the emission of the laser pulse and the start of recording by the spectrometer, and can vary from 0 to 2 μs, and the spot size, which represents the diameter of the laser beam, adjustable between 50 and 250 μm. The sample is moved with the aid of a programmable XYZ stage, integrated with an image capture system consisting of a CMOS (complementary metal-oxide-semiconductor) color camera with a resolution of 1280 × 1024 pixels, allowing precise visualization and alignment. In addition, Aurora software version Rev 2.0 (Applied Spectra, Fremont, CA, USA) was used to identify the characteristic emission lines of each chemical element present in the spectra obtained.

Inductively coupled plasma optical emission spectrometry (ICP OES)

Reference or confirmatory values for the elements Ag, Au, Cu and Sn were obtained using the iCAP 7000 Series ICP OES instrument (Thermo Fisher Scientific, Waltham, MA, USA), operated under robust conditions, with axial and radial observations mode. All measurements were carried out using high purity argon gas (Ar) (99.999%, White Martins-Praxair). The instrumental conditions followed the recommendations of the manufacturer, with the radio frequency (RF) power set at 1.15 kW, the plasma flow rate at 12.0 L min^{-1}, the auxiliary flow rate at 0.50 L min^{-1}, and the nebulizer flow rate at 0.70 L min^{-1}. The integration time varied between 5 and 15 s, and a Mira Mist nebulizer and a cyclonic spray chamber were used. The emission lines monitored for the elements were: Ag (I 328.068 nm), Au (I 267.595 nm), Cu (I 327.296 nm) and Sn (I 283.999 nm). The limits of detection (LOD) were estimated according to the methods recommended by International Union of Pure and Applied Chemistry (IUPAC),[26] giving the following values: Ag (0.001 mg kg^{-1}), Au (0.004 mg kg^{-1}), Cu (0.006 mg kg^{-1}) and Sn (0.04 mg kg^{-1}).

Reagents and standard solutions

All the solutions used in this study were prepared with ultrapure water produced in a Milli-Q® Plus system (Millipore Corp., Bedford, MA, USA). Before use, all the glassware and polypropylene bottles were decontaminated with detergent, immersed for 24 h in a solution of nitric acid (HNO_3 10% v v^{-1}) (Synth, Diadema, Brazil) and then rinsed with ultrapure water. The external calibration curves for the elements Au, Ag, Cu and Sn were drawn up by

successive and appropriate dilutions of a standard stock solution of 1000 mg L^{-1} (Specsol, São Paulo, Brazil) using HNO_3 solution. The reagents used in the leaching processes included: HNO_3, H_2SO_4 (Synth, Diadema, Brazil), HCl (Química Moderna, Barueri, Brazil), I_2 (Grupo Química, Penha, Brazil), KI (Synth, Diadema, Brazil), thiourea (Neon, Suzano, Brazil), $Fe(NO_3)_3$ (Synth, Diadema, Brazil) and $CuSO_4$ (Synth, Diadema, Brazil). The concentrated acids HNO_3 and HCl were previously purified by distillation using the Distillacid™ BSB-939-IR system (Berghof, Eningen, Germany).

Sampling, preparation and characterization of samples

The material utilized in this study was a 1.2 kg composite powder of PCBs. This composite was prepared from PCBs recovered from various end-of-life (EoL) electronic equipment, with the following mass distribution: computers (56.7%), laptops (34.4%), tablets (4.8%), and cellphones (4.1%). To obtain the final analytical sample, these collected PCBs were first processed in a knife mill (Tecnal TE-650, Piracicaba, Brazil). The resulting powder was then thoroughly homogenized and subsequently sieved to isolate a standardized particle sizes fraction of less than 212 µm. This final, homogeneous powder served as the starting material for all characterization, leaching, and LIBS experiments.

The method adapted from Ferreira *et al.*[27] was used to characterize the samples. In this procedure, 100 mg of ground PCB sample was weighed and transferred to closed tetrafluoroethylene-perfluoro (alkoxy vinyl ether) vials (Savillex, 50 mL PFA block digestion tube, model 210-050-70). A mixture of 50% v v^{-1} aqua regia was then added, the tubes were closed and the system was heated to 100 °C in a model MA4025 digestion block (Marconi, Piracicaba, SP, Brazil) for 2 h. After cooling, the resulting solution from the digestion was filtered through filter paper and diluted to the appropriate concentration range using deionized water. The concentrations of Au, Ag, Cu and Sn present in the digested solution were determined by ICP OES, with all analyses carried out in triplicate and the results expressed as averages. All the steps mentioned are depicted in Figure S1 (see the Supplementary Information (SI) section).

E-waste leaching procedure

Sequential leaching was designed to maximize the selective extraction of Cu, Sn, Ag, and Au from PCB samples. The conditions for each step including the choice of leaching agent, temperature, and acid concentration were adapted from optimized literature methods, with each set of parameters tailored to maximize the dissolution of a specific metal while minimizing the co-extraction of others. The underlying principle is to use different chemical environments (oxidizing acids, complexing agents) to sequentially target base metals (Cu for instance) and, subsequently, the more inert precious metals (Ag and Au).

After each leaching step, both the solid and liquid fractions were separated, quantified, and stored for subsequent analysis (Figure 1). The solid residue was prepared for analysis according to the method adapted by Ferreira *et al.*[27] During all the leaching procedures, blank samples were processed simultaneously, in triplicate (n = 3).

Leaching Cu with HNO_3

For the leaching of Cu from the samples, 150 g of PCB were weighed and divided into 15 parallel sub-samples of

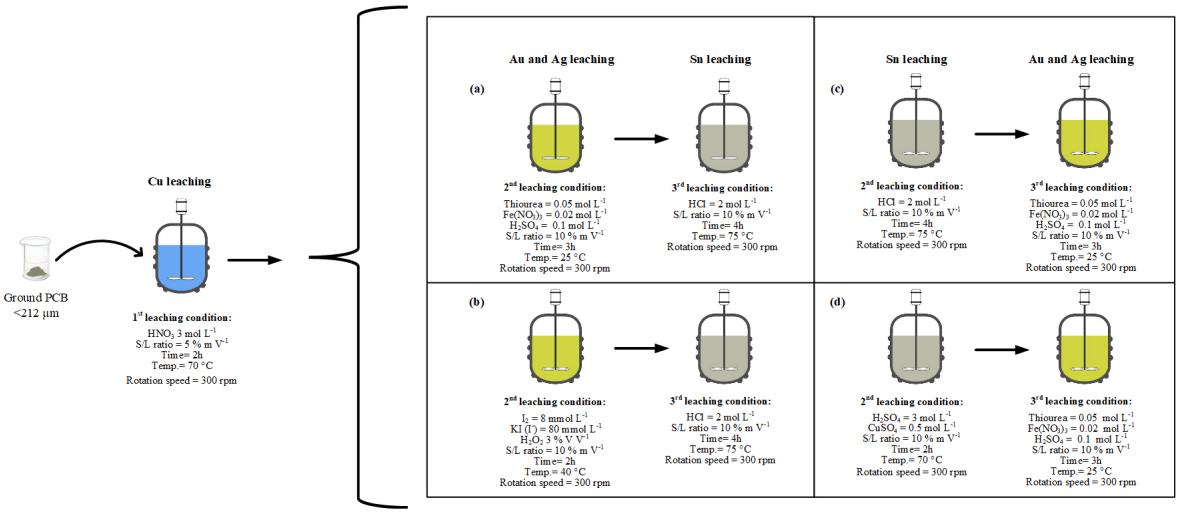

Figure 1. Sequential leaching tests for the extraction of Ag, Au, Cu and Sn from e-waste. (a) Acid leaching using thiourea with $Fe(NO_3)_3$; (b) leaching with iodine/iodide; (c) leaching with HCl; (d) leaching with H_2SO_4 and $CuSO_4$.

10 g each. The sub-samples were transferred to a 500 mL beaker and 200 mL of a 3 mol L^{-1} HNO_3 solution was added.

The HNO_3 was selected as a strong oxidizing agent capable of efficiently dissolving Cu, the primary metallic component, thereby simplifying the matrix for subsequent precious metal recovery. The mixture was stirred in a heated magnetic stirrer (model 752A, Fisatom, São Paulo, Brazil) at 300 rpm for 2 h at a temperature of 70 °C. This procedure adopted experimental conditions based on the parameters optimized by Dutta *et al*.[28] After the leaching stage, the solid and liquid phases were separated using quantitative filter paper (Unifil, black tape, 125 mm diameter, Germany).

The filtered sub-samples were combined and homogenized. The leached liquid was analyzed by ICP OES to determine the concentrations of Ag, Au, Cu, and Sn. The remaining solid residue was washed with deionized water and characterized according to the method described in the previous section, to evaluate the residual concentrations of the elements in the solid. A fraction of this solid residue was stored for subsequent leaching steps and LIBS analysis.

Leaching of Ag and Au

Acid leaching using thiourea with $Fe(NO_3)_3$

The leaching process was carried out to extract Ag and Au. Five g of the solid residue that was already submitted to Cu extraction, was weighed and mixed with 50 mL of a solution containing 0.05 mol L^{-1} of thiourea, 0.02 mol L^{-1} of $Fe(NO_3)_3$ as an oxidizing agent and 0.1 mol L^{-1} of H_2SO_4 (Figure 1a).

This step utilizes thiourea, a well-established complexing agent, which in the presence of an oxidant (Fe^{3+}) forms stable aqueous complexes with Au and Ag, enabling their extraction under mild acidic conditions. The solution was prepared in a 150 mL beaker, which was then placed on a magnetic stirrer. The mixture was stirred for 3 h at a constant speed of 300 rpm at room temperature. The experimental conditions adopted followed the parameters optimized by Behnamfard *et al*.[29] After leaching, the mixture was filtered to separate the solid and liquid phases. The extracts obtained were properly prepared and the concentrations of the target elements (Ag and Au) were determined using ICP OES. A fraction of this solid residue was stored for the next leaching and LIBS analysis.

Leaching with iodine/iodide

For this leaching process, 5 g of the solid residue was weighed and mixed with 50 mL of a solution consisting of 8 mmol L^{-1} of iodine, 80 mmol L^{-1} of iodide, and H_2O_2 (3%) as an oxidizing agent. The mixture was prepared in a 150 mL beaker and stirred on a magnetic stirrer at a constant speed of 300 rpm for 2 h at 40 °C (Figure 1b). The experimental conditions were adapted based on the parameters previously optimized by Xiu *et al*.[30] After the leaching stage, the mixture was filtered to separate the solid and liquid phases. The liquid and solid extracts were properly prepared, and the target elements were determined using ICP OES. A fraction of this solid residue was stored for the next leaching and LIBS analysis.

Leaching of Sn

Leaching with HCl

The leaching process was carried out to extract Sn in an acidic medium containing HCl. Specifically, 5 g of the solid residue was weighed and combined with 50 mL of a 2 mol L^{-1} HCl leaching solution (Figure 1c). The HCl was employed because the Cl^- effectively form stable aqueous complexes with Sn, promoting its dissolution at elevated temperatures.

The mixture was transferred to a 150 mL beaker and subjected to magnetic stirring for 4 h at a controlled temperature of 75 °C. The experimental conditions were adapted from the optimized parameters established by Moosakazemi *et al*.[31] Following the leaching procedure, the mixture was filtered to separate the solid and liquid phases. The resulting filtrates were subsequently prepared and analyzed to determine the concentrations of the target elements using ICP OES. A fraction of this solid residue was stored for the next leaching and LIBS analysis.

Leaching with H_2SO_4 and $CuSO_4$

For the acid leaching process with H_2SO_4, 5 g of the solid residue was weighed and mixed with 50 mL of a solution containing 3 mol L^{-1} of H_2SO_4 and 0.5 mol L^{-1} of $CuSO_4$. The mixture was prepared in a 150 mL beaker and stirred on a magnetic stirrer at a constant speed of 300 rpm for 2 h at a temperature of 70 °C (Figure 1d). The experimental conditions were adapted based on the parameters previously optimized by Guo *et al*.[32] After leaching, the mixture was filtered to separate the solid and liquid phases. The resulting extracts were prepared and analyzed, with a focus on determining the target elements by ICP OES. A fraction of this solid residue was stored for the next leaching and LIBS analysis.

LIBS data as an alternative process control in e-waste recycling

To prepare the samples for LIBS analysis, the solid residues were previously homogenized manually after each leaching process. Approximately 500 mg of each sample were weighed and pressed in a hydraulic press

model SSP-10 (Shimadzu, São Paulo, SP, Brazil) with a force of 60 kN, for 1 min, to form pellets with a diameter of 12 mm and a thickness of 2 mm, to optimize data acquisition by the instrument. All pellets were prepared in triplicate (n = 3).

The operating parameters used to acquire the spectra included laser pulse fluence of 1000 J cm^{-2}, spot size of 100 μm, a delay time of 1 μs, and laser pulse energy of 80 mJ. These parameters were selected based on previously established optimized conditions. After adjusting the parameters, the samples were placed in the ablation chamber in triplicate, and the laser focus was adjusted. The spectra acquisition pattern followed a 12 × 12 points arrangement, with 5 pulses applied to each point. The spectral data obtained generated a matrix with a dimension of 720 × 12,288, where 720 represents the total number of pulses (spectral signals = 12 × 12 × 5 = 720) recorded in the sample and 12,288 corresponds to the number of emission lines detected in the spectral range from 186 to 1,042 nm. All the steps of the LIBS analysis are illustrated in Figure S2 (see SI section).

Data processing and chemometric analysis

Raw spectral data from the LIBS analysis were initially organized using Microsoft Excel (Microsoft Corp., Redmond, WA, USA) and subsequently processed in MATLAB (R2019b, The MathWorks, USA). Due to the zigzag acquisition pattern intrinsic to the J200 LIBS system, a custom routine named LIBS_inverse developed by Ferreira *et al*.[33] was used to standardize the spatial order of the spectra into a linear format from left to right, enabling proper matrix manipulation and image generation.

The libs_par2 routine, developed by the GAIA research group,[23] was used to extract relevant spectral parameters from each spectrum, including (*i*) signal-to-background ratio, (*ii*) total signal area (sum of all peaks in a given interval), and (*iii*) maximum peak intensity. Specific emission lines for each element (Ag, Au, Cu, Sn) were selected based on their relative intensity and absence of spectral interference, as confirmed by Aurora software and summarized in Table 1.

Each set of 720 spectra (12 × 12 grid × 5 pulses *per* point) was compiled into a matrix **M** (720 × E), where E is the number of selected emission lines *per* element. These matrices were normalized by the relative intensity of each emission line to improve the correlation between signal magnitude and concentration. Next, matrices from each leaching step were combined into a single $\mathbf{M}_{\text{combined}}$ matrix (2880 × E), encompassing the original sample size (12 × 12), 5 pulse *per* point and the four sequentially leached residues (12 × 12 × 5 × 4 = 2880).

Data were auto-scaled and submitted to PCA to reduce dimensionality and highlight variance patterns (correlations) related to metal concentrations. PCA scores were then reshaped into 12 × 12 matrices to reconstruct score maps for each element. These images were used to visually assess the spatial distribution and depletion of elements throughout the leaching process. In addition, this type of visualization related to computer vision improves the identification of patterns among the different extractors, and correlation among target metals.

Results and Discussion

Reference concentration obtained by ICP OES

After sequential leaching and sample preparation, as shown in Figure 1, the initial concentrations of the target elements were determined by ICP OES as: Ag at 1,225 mg kg^{-1}, Au at 196 mg kg^{-1}, Cu at 19% m m^{-1} and Sn at 4.5% m m^{-1}. These values can vary significantly depending on the type of e-waste. For example, the average concentration of Cu is 16% in computers and 22% m m^{-1}

Table 1. Emission lines selected for the calculations of maps of scores for the elements Ag, Au, Cu and Sn

Emission line (relative intensity) / nm							
Ag		Au		Cu		Sn	
λ1	224.643 (123)	λ1	204.454 (703)	λ1	213.598 (6104)	λ1	224.605 (2545)
λ2	228.003 (281)	λ2	211.068 (2384)	λ2	224.261 (7634)	λ2	231.723 (1218)
λ3	546.550 (643)	λ3	212.529 (1078)	λ3	224.700 (8046)	λ3	249.570 (1197)
		λ4	443.511 (231)	λ4	324.754 (16256)	λ4	257.158 (1385)
		λ5	460.751 (341)	λ5	327.396 (15301)	λ5	266.124 (1110)
		λ6	481.160 (390)	λ6	515.324 (8297)	λ6	277.981 (1224)
				λ7	521.820 (12349)	λ7	285.062 (2110)
						λ8	452.474 (2741)
						λ9	579.918 (1008)

in cell phones, while that of Au is 430 mg kg^{-1} in cell phones and 390 mg kg^{-1} in computers.[34-37] This variation in concentrations, which depends on both the type of e-waste and the date of manufacture, is a crucial factor in optimizing recovery processes. Knowing these differences allows extraction methods to be adjusted to improve efficiency in the recovery of precious and industrial metals present in e-waste.

Figure 1 shows the leaching sequence applied to the e-waste after the first leach with HNO_3. The remaining leaching tests were designed with the aim of achieving the best conditions for extracting Ag, Au and Sn, maximizing the efficiency of the process. The subsequent leaches tested were carefully planned to improve the synergy between the different leaches used, taking advantage of their complementary characteristics. In addition, the process was structured to minimize possible adverse effects, such as the dissolution of unwanted elements or matrix interference. This approach allows for more precise control of the process and contributes to selective and efficient extraction of the elements of interest.

The results of the leaching tests are shown in Figure 2, where is possible to see the performance obtained in each sequential step.

In Figure 2a, for instance, the HNO_3 lixiviant showed an extraction efficiency of approximately 97% for Cu, 53% for Ag and 79% for Sn, while it was not effective for Au, as this element is not efficiently leached in an acidic medium containing only HNO_3. The leaching sequence in Figures 2b and 2c shows that the simultaneous extractions of Ag and Au were satisfactory, demonstrating significant efficiency for these elements. However, when compared to the stages illustrated in Figures 2d and 2e, it can be seen that the latter were more efficient. This is probably because, in the initial stages, the majority metals, such as Cu and Sn, were extracted first, which influenced the efficiency of the subsequent stages for the minority metals, such as Ag and Au.

Based on the results presented, we can conclude that the most efficient and environmentally friendly sequence was the one illustrated in Figure 2d. In this step, an extraction efficiency of 100% was achieved for Cu and Ag, 97% for Sn

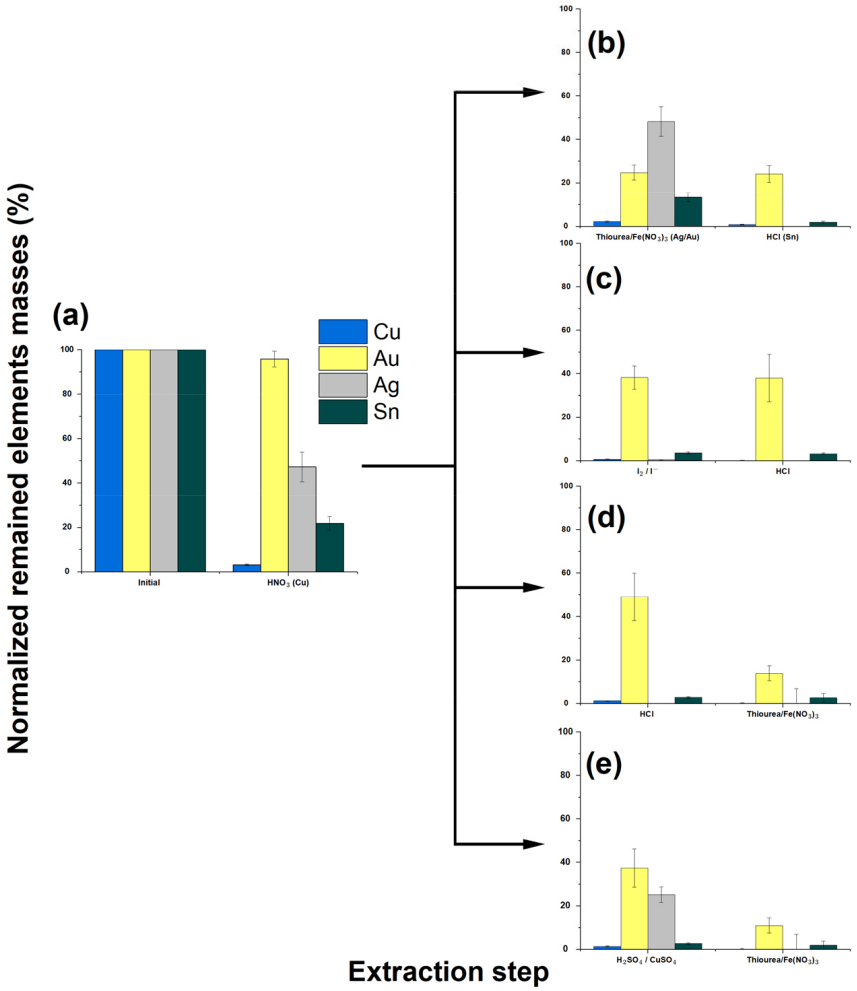

Figure 2. Comparison of the normalized concentrations of sequential leaching obtained by ICP OES: (a) Cu extraction, (b up to e) Ag, Au and Sn extraction with thiourea and $Fe(NO_3)_3$ (for Ag and Au), HCl (for Sn), iodine (I_2)/iodide (I^-) (for Ag and Au), and H_2SO_4 and $CuSO_4$ (for Sn).

and 86% for Au. These results highlight the importance of proper sequence planning to maximize extraction efficiency and minimize the environmental impacts associated with the process.

LIBS as an alternative process control in e-waste recycling

The goal was to evaluate whether the LIBS technique, combined with hyperspectral imaging, could serve as a less expensive alternative to the ICP OES technique for monitoring the consecutive leaching processes of waste-waste. Comparative studies were carried out, as ICP OES is often used in this type of analysis. For this evaluation, the solid waste obtained from the leaching stages shown in Figure 1 was used. The solid material remaining from each experiment was analyzed using the LIBS technique, making it possible to identify the target elements directly on the surface of the samples. This approach sought to verify the effectiveness of LIBS as a fast and cost-effective analysis tool for monitoring selective leaching processes.

Evaluating the LIBS spectra

To carry out the analysis, all the procedures required for pellet formation were followed, without the use of binders, as shown in Figure S2 (SI section). The aim was to assess whether the LIBS technique is robust enough to detect variations in the concentrations of the target elements. To do this, the average emission spectra of the first leaching sequence was analyzed (Figure 1a). Figure 3 shows the spectral regions corresponding to each target element.

In Figure 3a, it can be seen that the Ag emission line signal at 224.64 nm decreases progressively with each leaching step, with the intensity dropping from approximately 3000 a.u. to 10 a.u. This same behavior was identified for Au (Figure 3b), Cu (Figure 3c), and Sn (Figure 3d). They all showed high initial intensities, which progressively decreased to almost zero values at the end of the leaching processes. For example, the Cu emission line at 521.82 nm (Figure 3c), the majority element in the sample, showed a reduction in intensity from 10,000 a.u. to values close to zero. Gold, whose emission line at 443.51 nm (Figure 3b) was monitored, had its intensity reduced from 670 to 21 a.u.

These results show that the LIBS technique has sufficient sensitivity to detect significant changes in the concentration of elements, both for those present in high concentrations, such as Cu and for minority elements, such as Ag and Au. This highlights the potential of LIBS as an effective tool for monitoring concentration variations in electronic waste-leaching processes.

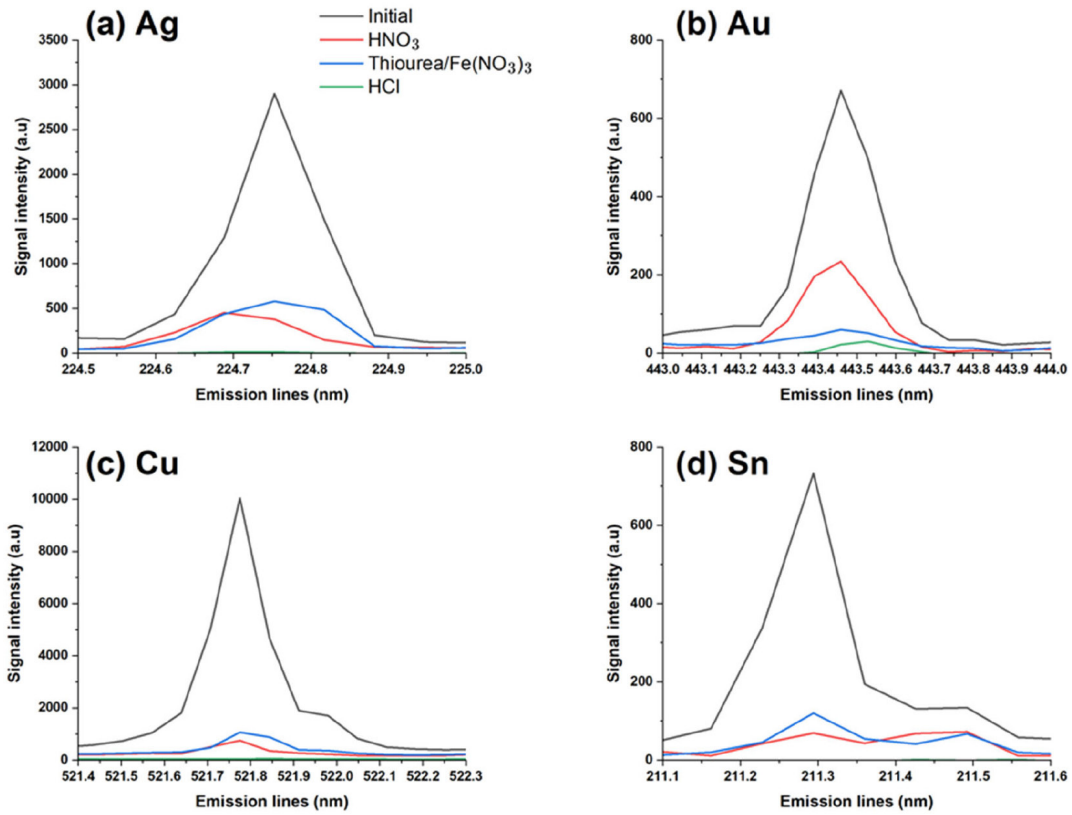

Figure 3. Average emission spectra (arbitrary units) for a sample leached in 3 stages (HNO_3, thiourea, and HCl), considering the emission range of the target elements.

Hyperspectral image interpretation and analysis

After evaluating the average LIBS spectra in the previous section, the most suitable emission lines were selected, avoiding spectral interferences and self-absorption effects, using the Aurora software (Applied Spectra) and the LIBS_par2 routine. The selected lines are shown in Table 1. Based on these lines, the areas of the emission peaks were calculated using the LIBS_par2 routine, generating an **M** matrix of dimension 720 × **E** for each sample in the different leaching stages, where **E** represents the area of each emission line of the target elements. To minimize matrix effects and enable a visual inspection of the quantitative element profiles after each leaching step, the matrix was normalized using relative intensity of each selected emission line (see also Table 1).

With the matrix normalized, the areas corresponding to each leaching step were combined, resulting in the $\mathbf{M}_{\text{combined}}$ matrix, with a dimension of 2880 × **E**. The combination was structured so that each set of 720 spectra represented a leaching stage, in other words, the first 720 × **E** corresponds to the original sample, the spectra from 721 to 1440 × **E** to the sample leached with HNO_3, and so on (see sequence in Figure 1). These combined matrices were generated for each target element and leaching strategy evaluated in this study (Figure 1).

After auto-scaling the data, a PCA was performed for each set of 5 pulses to map the pellet surfaces, and the score values obtained were organized to build a map of scores representing the distribution of elements on the pellet surface after each leaching step.

Figure 4 shows the results obtained for each leaching stage (y-axis) and the respective elements determined. The aim of the hyperspectral images is to visually illustrate the progressive reduction in the signals of the elements at each stage of the process, since, as the elements are extracted, they migrate to the liquid phase, resulting in a lower signal in the solid phase, as observed in the images.

Analysis of the map of scores of the first leaching strategy (Figure 4a) shows that, in the initial phase, all the elements are 100% in the solid fraction, with score values ranging from 4 to 15 (colors from dark green to red). After leaching with HNO_3, aimed at extracting Cu, there is a drop in the Ag, Cu, and Sn signals, while Au remains partially unchanged, since the reaction does not favor its extraction.

A comparison between the maps of scores and the extraction percentages obtained by ICP OES confirms the consistency of the results. For example, Cu, which had an initial average score of 4.29, fell to –0.52 after the last HCl leaching stage. In the case of Ag, during the stages with HNO_3 and thiourea/$Fe(NO_3)_3$, its concentration in the solid phase remained almost constant (47 to 48%), which was reflected in the LIBS spectra, with average scores of 2.0 and 1.8, respectively. This behavior was also observed for the other elements, reinforcing the ability of LIBS associated with hyperspectral images to monitor the extraction of metals throughout the process.

The reliability of this approach is reinforced by the explained variance of calculated PC1 in Figure 4a, which was 99.44% for Ag, 76.78% for Au, 92.43% for Cu, and 83.48% for Sn.

Further evidence of the effectiveness of LIBS can be seen in Figure 4b, where the Au signals in the leaching steps with I_2/I^- and HCl show very similar concentrations. This similarity is also reflected in the map of scores, with average values of 0.26 and 0.24, respectively. The same behavior is visible for Sn (Figure 4c), whose initial concentration of 100% in the solid fraction progressively decreased to 21.7% after leaching with HNO_3, 2.7% after HCl and 2.6% after thiourea/$Fe(NO_3)_3$. This decrease is evident in the hyperspectral image and in the reduction in average scores values, which went from 6.3 in the initial sample to –0.07, –1.19 and –0.98 at the end of the process.

For Ag (Figure 4d), a progressive decrease in the signal is also observed, with average scores reducing from 2.55 (100% in the solid) to 2.06 (47.2% in the solid) after leaching with HNO_3, 0.74 (25.1% in the solid) after $H_2SO_4/CuSO_4$ and –0.65 (0% in the solid) after leaching with HCl. These results show that LIBS is sensitive enough to detect variations in concentration, even at very low levels, such as the reduction in Sn from 21.7 to 2.6% after leaching with thiourea/$Fe(NO_3)_3$.

The central question is: would it be possible to use only LIBS to assess the efficiency of each leaching stage, without ICP OES concentration data? Analysis of the hyperspectral images and average scores indicates that it is, as there are clear differences between each stage.

Considering the average scores in the last leaching stage, the most efficient strategy was the one shown in Figure 4d, with values of –0.59 for Ag, –0.68 for Au, –1.02 for Cu and –1.68 for Sn, resulting in an overall average score of –0.99 (average of the scores for the four elements). The sequence shown in Figure 4c was the second most efficient (overall average score of –0.74), followed by the strategies in Figure 4a (–0.69) and 6b (–0.38).

This result confirms the analysis carried out using ICP OES, which also indicated that the best strategy is the sequential leaching of Cu with HNO_3, Sn with HCl and Ag/Au with thiourea/$Fe(NO_3)_3$, both from the point of view of efficiency and environmental impact. Therefore, despite its limitations, LIBS showed good results in this

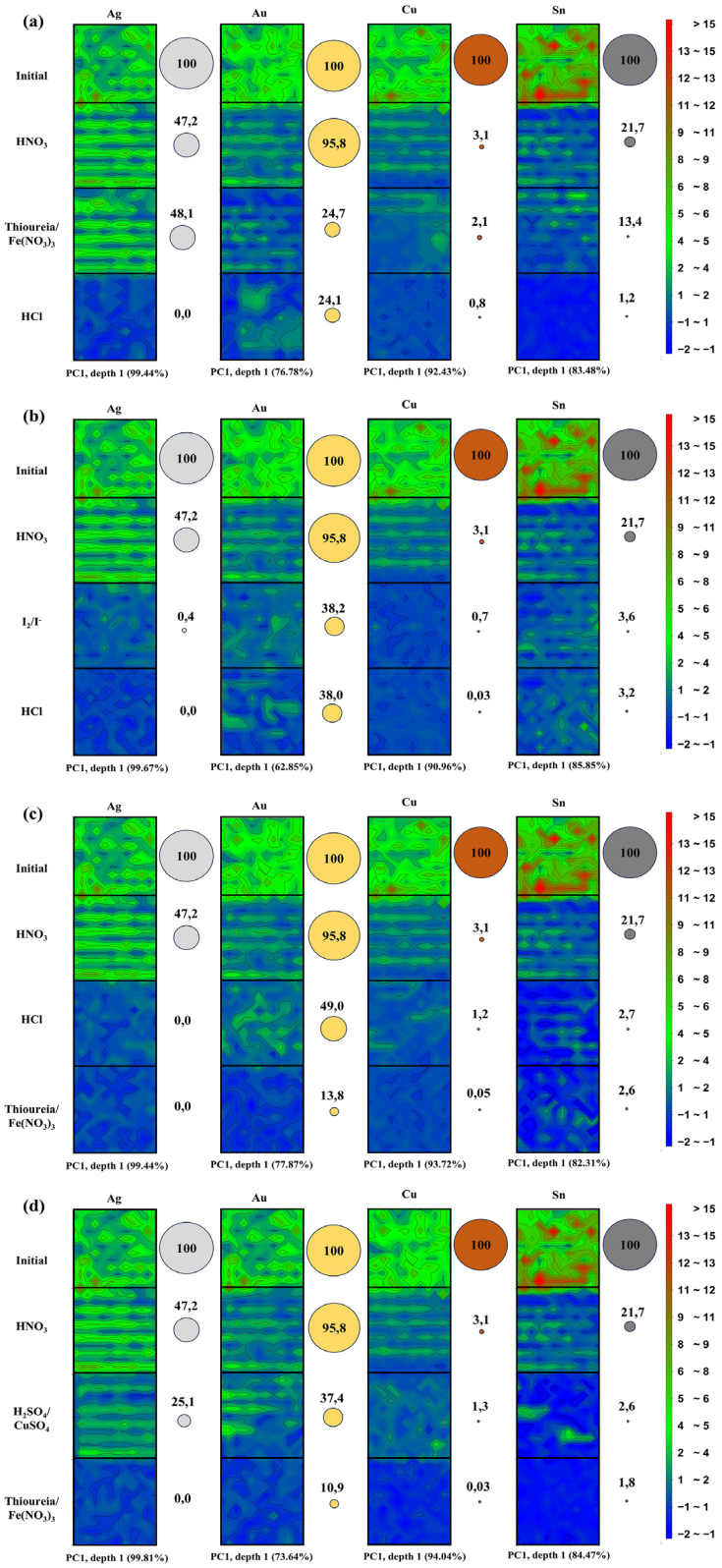

Figure 4. Hyperspectral images generated from PCA scores for the target elements (Ag, Au, Cu, and Sn) after each step of different sequential leaching strategies. Each panel (a-d) represents a unique leaching sequence: (a) leaching with HNO_3, followed by thiourea/$Fe(NO_3)_3$, and finally HCl; (b) leaching with HNO_3, followed by I_2/I^-, and finally HCl; (c) leaching with HNO_3, followed by HCl, and finally thiourea/$Fe(NO_3)_3$; and (d) leaching with HNO_3, followed by $H_2SO_4/CuSO_4$, and finally thiourea/$Fe(NO_3)_3$. The color scale on the right represents the normalized score values, where red tones indicate higher elemental concentration in the solid phase and blue tones indicate lower concentration. The circles next to each score show the percentage of each element remaining in the solid waste after this stage, as determined by ICP OES.

application, demonstrating its potential as an alternative for monitoring e-waste leaching processes.

To correctly interpret these results, it is crucial to clarify the relationship between the static image of the pellet and the dynamic leaching process. As described in the method, the metal extraction is performed with the e-waste powder in suspension. For each monitoring step, a representative aliquot of this powder (inert material) is collected, dried, and pressed into a new pellet for LIBS analysis. The pellet itself, therefore, is not leached, serving as a sampling device that presents a flat, representative surface of the system's solid state for the analysis.

An important consideration is whether the hyperspectral imaging component is fundamental to the monitoring process, or if the average signal from all 720 pulses would be sufficient. While the average LIBS spectra (as shown in Figure 3) are indeed capable of indicating the overall depletion trend of the target elements, relying solely on this integrated signal can be misleading and masks crucial information regarding process efficiency. The primary justification for the imaging approach lies in the inherent heterogeneity of the solid sample, which was quantitatively confirmed by the high initial relative standard deviations (RSD) values (up to 26.8%) reported in Table 2. An average signal could decrease to an acceptable level even if the leaching is occurring non-uniformly, for instance, being highly efficient in some areas of the pellet while completely stalled in others due to poor mixing or surface passivation.

The hyperspectral maps, however, provide essential spatial and diagnostic information, working together with computational vision. They allow for a visual assessment of the uniformity of the reaction, confirming that the metal decrease is occurring across the entire surface and not just in isolated hotspots. This approach can be also implemented in a conveyor belt for real time monitoring of the solid residue after leaching. Therefore, while the average signal can answer if the overall concentration is decreasing, the hyperspectral image is fundamental to understanding how this decrease is happening, providing a much deeper and more reliable level of process control.

Comparative analysis of error and analytical performance of the alternative method

To evaluate the proposed alternative method, a comparative analysis was conducted to assess the analytical errors associated with the LIBS monitoring technique and the ICP OES reference method. The ICP OES served as a reference for quantitative validation, providing accurate reference values for the mass concentration of the elements after sample digestion. This technique is characterized by high precision, with RSD typically between 1 and 5% for homogeneous liquid samples, and very low limits of detection, which were determined in the mg kg^{-1} range for the target elements.

For the LIBS method, precision was assessed to validate the data acquisition strategy, which involved averaging 5 sequential pulses at each of the 144 analytical points. To investigate the characteristics of the sample in detail, a pulse-by-pulse analysis of the precision was conducted by calculating the RSD for each individual pulse across the 144-point grid of the initial, non-leached sample. The results are presented in Table 2.

The data in Table 2 reveal an aspect of this complex material. Unlike homogeneous samples where the RSD typically decreases significantly after the first pulse due to surface cleaning, the RSD for the e-waste sample remains consistently high across all five pulses. For instance, the RSD for Cu, the major element, fluctuates in the high range of 46-53% without a clear downward trend. A similar behavior is observed for the other elements. This sustained high variance is attributed to the extreme micro-heterogeneity of the sample. The pressed pellet is a composite of distinct metallic and polymeric particles. Within a single 100 μm analysis spot, the five sequential laser pulses are not ablating a uniform surface, but are likely drilling through different materials (for example, a

Table 2. Pulse-to-pulse analysis of the RSD calculated from the 144-point grid for the initial (non-leached) sample

Laser pulse	RSD / %			
	Ag (224.64 nm)	Au (211.06 nm)	Cu (521.82 nm)	Sn (303.41 nm)
1st pulse	45.65	28.37	50.50	29.08
2nd pulse	45.75	27.84	53.06	27.86
3rd pulse	48.73	28.78	51.89	28.56
4th pulse	42.24	28.70	50.95	30.99
5th pulse	46.56	29.80	46.54	30.23
5-pulse average	45.79	28.70	50.59	29.34

RSD: relative standard deviation.

Table 3. Pulse-to-pulse analysis of the RSD for the sample after the final leaching step of sequence Figure 4c

Laser pulse	RSD / %			
	Ag (224.64 nm)	Au (211.06 nm)	Cu (521.82 nm)	Sn (303.41 nm)
1st pulse	83.37	71.86	78.67	60.48
2nd pulse	88.91	62.17	87.03	55.48
3rd pulse	69.34	66.28	78.97	58.28
4th pulse	86.44	70.10	82.16	53.52
5th pulse	86.55	71.51	72.82	62.35
5-pulse average	82.92	67.51	79.93	58.02

RSD: relative standard deviation.

Cu fragment, then a polymer particle), causing significant pulse-to-pulse signal fluctuation.

To further investigate how the leaching process affects this heterogeneity, the same pulse-by-pulse analysis was performed on the solid residue after the final leaching step of sequence Figure 4c. The results are presented in Table 3.

A direct comparison between the data from the initial sample (Table 2) and the final leached sample (Table 3) reveals a significant increase in RSD. This trend is characteristic of measurements approaching the limit of detection in heterogeneous materials and confirms efficient extraction. After leaching, only sparse and isolated metal fragments remain. The analysis results in a signal distribution with many low values and a few high-intensity peaks, which mathematically leads to a very high RSD. Therefore, this increase in RSD serves as a quantitative indicator of the effectiveness of leaching.

With the 5-pulse average method validated as essential for this type of sample, Table 4 summarizes the resulting average RSD for each complete leaching step across all strategies. This table allows for an evaluation of the overall spatial heterogeneity at each stage of the process.

The RSD values for the initial non-leached sample were significantly high (e.g., 23.1% for Ag and 22.9% for Cu), as shown in Table 4. This quantitatively confirms the considerable spatial heterogeneity of the metal distribution on the pellet surface, a key finding that validates the use of a spatially resolved technique such as hyperspectral imaging rather than simple point-and-shoot analysis. Interestingly, the RSD for certain elements increased during the intermediate leaching stages (Cu to 40.3% after leaching with HNO_3), indicating that the leaching process itself occurs unevenly, temporarily increasing the relative heterogeneity of the remaining metal. In addition, the extremely high RSD values in the final leaching stage (> 100% for Ag) are characteristic of signals approaching the limit of detection of the method. This does not indicate low precision, but confirms a highly efficient extraction, where the residual signal is comparable to instrumental noise.

Table 4. RSD calculated from the LIBS signal intensity for each leaching step of the sequences described in Figure 4

Leaching step	RSD / %			
	Ag	Au	Cu	Sn
Sequence (Figure 4a)				
Initial	23.1	22.2	22.9	11.8
HNO_3	12.3	40.3	31.2	11.7
Thiourea/$Fe(NO_3)_3$	66.7	64.4	56.6	59.3
HCl	146.2	12.2	18.3	13.1
Sequence (Figure 4b)				
Initial	23.1	22.2	21.3	26.8
HNO_3	12.3	40.3	21.8	6.3
I_2/I^-	78.8	17.7	19.2	14.3
HCl	47.6	10.9	8.7	8.3
Sequence (Figure 4c)				
Initial	23.1	22.2	21.3	26.8
HNO_3	12.3	40.3	21.8	6.3
HCl	63.3	12.3	13.8	51.7
Thiourea/$Fe(NO_3)_3$	164.9	11.7	10.8	13.4
Sequence (Figure 4d)				
Initial	23.1	22.2	21.3	11.8
HNO_3	12.3	40.3	21.8	11.7
$H_2SO_4/CuSO_4$	129.3	11.8	11.1	15.6
Thiourea/$Fe(NO_3)_3$	19.0	10.9	9.5	12.6

Data obtained from analysis of emission lines: Ag (224.643 nm), Au (211.068 nm), Cu (521.82 nm), Sn (303.412 nm).

Conclusions

This study demonstrated the application of the LIBS technique associated with hyperspectral images as an alternative for controlling metal leaching processes in e-waste. The optimized leaching strategy, validated by ICP OES, proved highly efficient, achieving extraction rates of 100% for Cu and Ag, 97% for Sn, and 86% for Au. The LIBS data showed excellent correlation with these findings; the progressive reduction in spectral signals was compatible with the extraction efficiencies, with the signal

from the majority element, Cu, being reduced to near-zero values by the end of the process.

These results show that the LIBS technique is promising for monitoring e-waste recycling processes, providing a faster and more economical alternative to ICP OES. The claim that this approach is more economical than conventional monitoring via ICP OES is based on two fronts. Firstly, on direct analytical costs: the LIBS method eliminates the need for expensive consumables, such as the high-purity argon gas required by ICP OES, and dispenses with the time-consuming acid digestion step, which requires reagents and specialized labor. Secondly, and more importantly, the economic advantage lies in implementing LIBS as a process analytical technology. The ability to obtain real-time data on leaching efficiency allows for dynamic process control, making it possible to stop the reaction at the optimal moment. This translates into a significant reduction in the consumption of leaching reagents and energy, in addition to increasing plant throughput economic benefits on an industrial scale that far outweigh the cost of the analysis itself.

However, future studies could focus on improving chemometric models to optimize the element quantification process and minimize matrix interference. In addition, the application of LIBS on an industrial scale can contribute significantly to optimizing metal recovery, strengthening the circular economy and reducing the environmental impacts associated with the inappropriate disposal of e-waste.

Supplementary Information

Supplementary information is available free of charge at http://jbcs.sbq.org.br as PDF file.

Data Availability Statement

We declare that all the experimental data in this paper are obtained through experimental tests and have absolute authenticity. All relevant data are within the paper.

Acknowledgments

This study was financed, in part, by the São Paulo Research Foundation (FAPESP), Brazil, Process No. 2019/24223-5. The authors are also grateful to National Council for Scientific and Technological Development, CNPq (grants No. 140867/2021-0, 302719/2020-2, and 304684/2024-4). This study was partly funded by the Coordination for the Improvement of Higher Education Personnel - Brazil (CAPES) - Funding Code 001.

Author Contributions

Dennis S. Ferreira was responsible for writing original draft, visualization, validation, methodology, investigation and Edenir R. Pereira-Filho for supervision, resources, project administration, funding acquisition, formal analysis, data curation.

References

1. Patil, R. A.; Ramakrishna, S.; *Environ. Sci. Pollut. Res.* **2020**, *27*, 14412. [Crossref]
2. Zhang, L.; Qu, J.; Sheng, H.; Yang, J.; Wu, H.; Yuan, Z.; *Resour. Conserv. Recycl.* **2019**, *143*, 210. [Crossref]
3. Baldé, C. P.; Kuehr, R.; Yamamoto, T.; McDonald, R.; Althaf, S.; Bel, G.; Deubzer, O.; Fernandez-Cubillo, E.; Forti, V.; Gray, V.; Herat, S.; Honda, S.; Iattoni, G.; Khetriwal, D. S.; Luda, V. C.; *The Global E-waste Monitor 2024*; ITU and UNITAR: Geneva, Bonn, 2024.
4. Parajuly, K.; Kuehr, R.; Awasthi, A.; Fitzpatrick, C.; Lepawsky, J.; Smith, E.; Widmer, R.; Zeng, X.; *Future E-waste Scenarios*; UNU/UNEP: Bonn, Osaka, 2019.
5. Forti, V.; Baldé, C. P.; Kuehr, R.; Bel, G.; *The Global E-waste Monitor 2020: Quantities, Flows and the Circular Economy Potential*; UNU/UNITAR, ITU and ISWA: Bonn, Geneva, Rotterdam, 2020.
6. Sengupta, D.; Ilankoon, I. M. S. K.; Kang, K. D.; Chong, M. N.; *Miner. Eng.* **2023**, *200*, 108154. [Crossref]
7. Stockholm Convention on Persistent Organic Pollutants (POPs); *The Convention - Overview*; http://www.pops.int/TheConvention/Overview/tabid/3351/Default.aspx, accessed in August 2025.
8. United Nations Industrial Development Organization (UNIDO); https://www.unido.org/our-focus/safeguarding-environment/implementation-multilateral-environmental-agreements/stockholm-convention, accessed in August 2025.
9. Dutta, D.; Rautela, R.; Gujjala, L. K. S.; Kundu, D.; Sharma, P.; Tembhare, M.; Kumar, S.; *Sci. Total Environ.* **2023**, *859*, 160391. [Crossref]
10. Xavier, L. H.; Ottoni, M.; Abreu, L. P. P.; *Resour. Conserv. Recycl.* **2023**, *190*, 106840. [Crossref]
11. Dobó, Z.; Dinh, T.; Kulcsár, T.; *Energy Rep.* **2023**, *9*, 6362. [Crossref]
12. Li, X. G.; Gao, Q.; Jiang, S. Q.; Nie, C. C.; Zhu, X. N.; Jiao, T. T.; *J. Environ. Manage.* **2023**, *348*, 119288. [Crossref]
13. Ferreira, D. S.; Pereira-Filho, E. R.; *Hydrometallurgy* **2025**, *235*, 106476. [Crossref]
14. Tembhare, S. P.; Bhanvase, B. A.; Barai, D. P.; Dhoble, S. J.; *Environ. Develop. Sustainable* **2022**, *24*, 8965. [Crossref]
15. Mishra, K.; Siwal, S. S.; Thakur, V. K.; *Curr. Opin. Green Sustainable Chem.* **2024**, *47*, 100900. [Crossref]
16. Debnath, B.; Chowdhury, R.; Ghosh, S. K.; *Front. Environ. Sci. Eng.* **2018**, *12*, 2. [Crossref]

17. Muscetta, M.; *Chem. Eng. Process.* **2024**, *204*, 109937. [Crossref]
18. Binnemans, K.; Jones, P. T.; *J. Sustainable Metall.* **2022**, *9*, 1. [Crossref]
19. Limbeck, A.; Bonta, M.; Nischkauer, W.; *J. Anal. At. Spectrom.* **2017**, *32*, 212. [Crossref]
20. Desroches, D.; Bédard, L. P.; Lemieux, S.; Esbensen, K. H.; *Miner. Eng.* **2018**, *126*, 36. [Crossref]
21. Castro, J. P.; Machado, R. C.; Andrade, D. F.; de Babos, D. V.; Pereira-Filho, E. R.; Garcia, J. A.; Sperança, M. A.; Gamela, R. R.; Costa, V. C.; *Quantitative Analysis*, 1st ed.; Springer International Publishing: Cham, 2017.
22. Brunnbauer, L.; Gajarska, Z.; Lohninger, H.; Limbeck, A.; *TrAC, Trends Anal. Chem.* **2023**, *159*, 116859. [Crossref]
23. Pereira-Filho, E. R.; *Laser-Induced Breakdown Spectroscopy (LIBS): Applications and Calibration Strategies*; Editora Ibero-Americana de Educação: São Carlos, 2021.
24. Noll, R.; Sturm, V.; Aydin, Ü.; Eilers, D.; Gehlen, C.; Höhne, M.; Lamott, A.; Makowe, J.; Vrenegor, J.; *Spectrochim. Acta, Part B* **2008**, *63*, 1159. [Crossref]
25. Myakalwar, A. K.; Sandoval, C.; Velásquez, M.; Sbarbaro, D.; Sepúlveda, B.; Yáñez, J.; *Minerals* **2021**, *11*, 1073. [Crossref]
26. International Union of Pure and Applied Chemistry (IUPAC); *Spectrochim. Acta, Part B* **1978**, *33*, 241. [Crossref]
27. Ferreira, D. S.; Pereira, F. M. V.; Olivieri, A. C.; Pereira-Filho, E. R.; *Anal. Chim. Acta* **2024**, *1303*, 342522. [Crossref]
28. Dutta, D.; Panda, R.; Kumari, A.; Goel, S.; Jha, M. K.; *Sustainable Mater. Technol.* **2018**, *17*, e00066. [Crossref]
29. Behnamfard, A.; Salarirad, M. M.; Veglio, F.; *Waste Manage.* **2013**, *33*, 2354. [Crossref]
30. Xiu, F. R.; Qi, Y.; Zhang, F. S.; *Waste Manage.* **2015**, *41*, 134. [Crossref]
31. Moosakazemi, F.; Ghassa, S.; Mohammadi, M. R. T.; *J. Cleaner Prod.* **2019**, *228*, 185. [Crossref]
32. Guo, X.; Qin, H.; Tian, Q.; Li, D.; *J. Hazard. Mater.* **2020**, *384*, 121355. [Crossref]
33. Ferreira, D. S.; Rodrigues, L. S.; Pereira, F. M. V.; Pereira-Filho, E. R.; *Quim. Nova* **2023**, *46*, 747. [Crossref]
34. Lu, Y.; Xu, Z.; *Resour., Conserv. Recycl.* **2016**, *113*, 28. [Crossref]
35. Chen, M.; Wang, J.; Chen, H.; Ogunseitan, O. A.; Zhang, M.; Zang, H.; Hu, J.; *Environ. Sci. Technol.* **2013**, *47*, 12409. [Crossref]
36. Jing-ying, L.; Xiu-li, X.; Wen-quan, L.; *Waste Manage.* **2012**, *32*, 1209. [Crossref]
37. Sheng, P. P.; Etsell, T. H.; *Waste Manage. Res.* **2007**, *25*, 380. [Crossref]

Submitted: June 16, 2025
Final version online: August 20, 2025

Supplementary Information

LIBS and Hyperspectral Imaging as a Real-Time Process Control Tool for Metal Recovery from E-Waste

Dennis S. Ferreira[a] and Edenir R. Pereira-Filho *,[a]

[a]*Departamento de Química, Universidade Federal de São Carlos, 13565-905 São Carlos-SP, Brazil*

*e-mail: erpf@ufscar.br

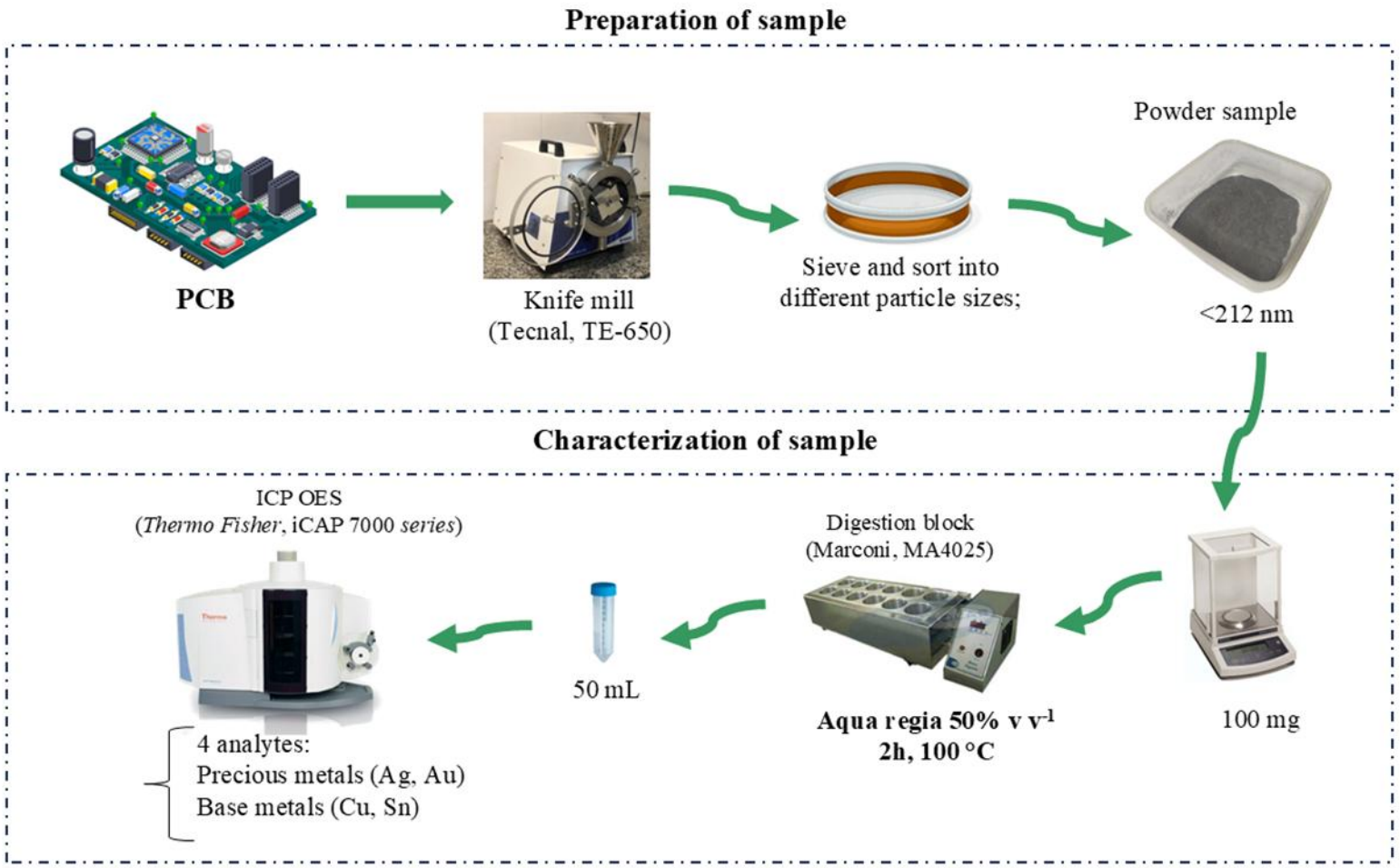

Figure S1. Description of the experimental procedure for sample preparation and characterization.

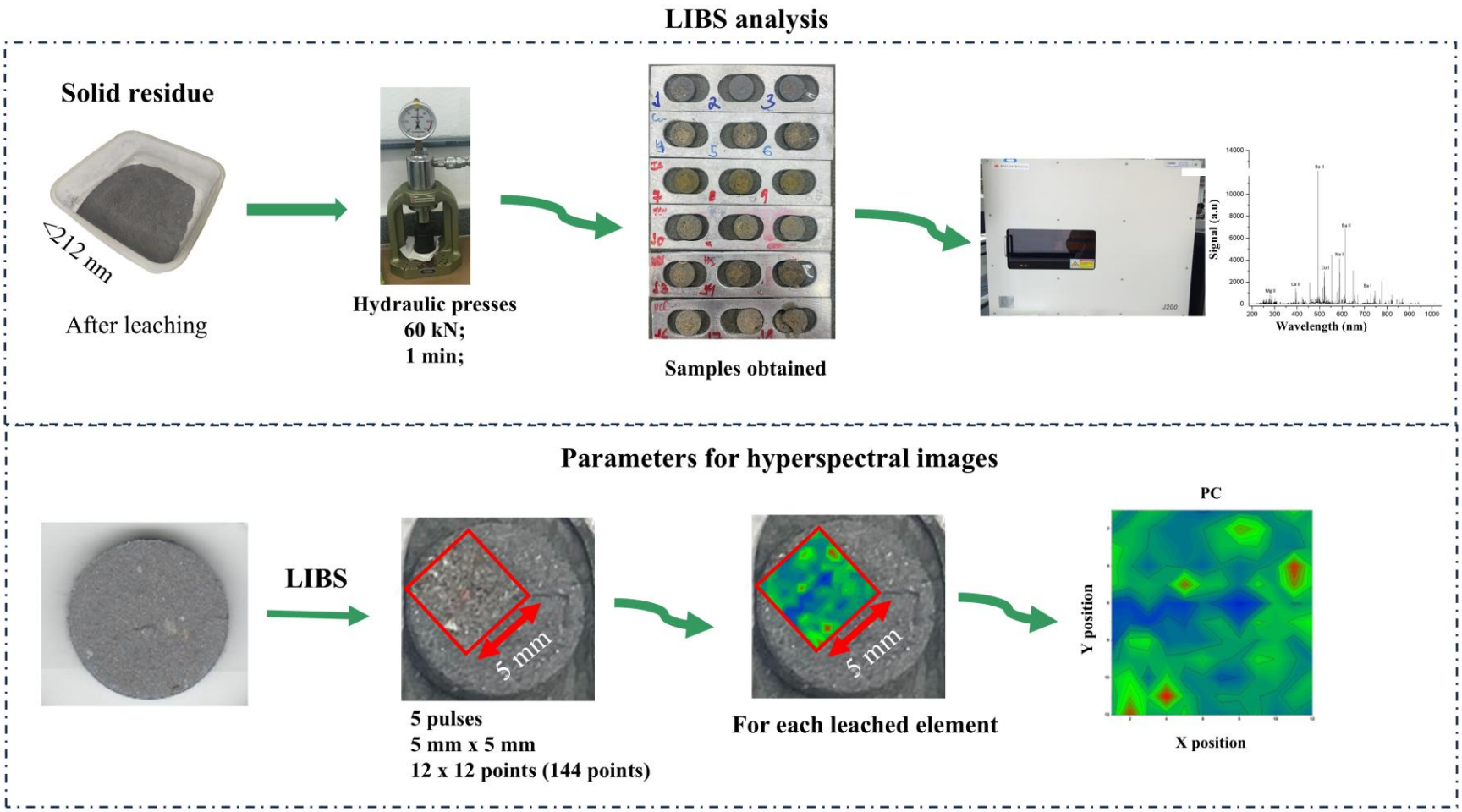

Figure S2. Experimental description of pellet preparation and LIBS analysis for hyperspectral imaging.

Chapter 5 - Conclusion

5. Conclusion

The growing generation of e-waste and the lack of proper management represent an environmental, social and technological challenge for society. As discussed in Chapters 1, in addition to causing significant impacts on the environment and human health, a large number of valuable materials, such as Au, Ag, Cu and Sn, is still wasted due to the low efficiency of conventional recycling processes, especially in developing countries.

Given this scenario, this thesis proposed a comprehensive analytical approach for the characterization and sustainable recovery of noble metals present in e-waste, with a focus on PCBs. The study started with an extensive review of the generation, composition and processing routes of this waste, also considering the legal and operational aspects of e-waste management in Brazil and worldwide.

Chapters 2 and 3 demonstrated that direct analysis techniques for solid samples, LIBS and ED-XRF, are promising for both qualitative and quantitative purposes. The application of these techniques has made it possible to obtain fast and reliable information, without the need for destructive or time-consuming sample preparation steps, making them strategic tools for monitoring the chemical composition of e-waste.

Also in Chapter 3, some methods were proposed to overcome the challenges inherent in the direct quantitative analysis of solids. Data fusion strategies between LIBS and XRF were employed, using traditional regression strategies (PLS and PCR) and alternative regressions such as MLPCR and ECPR with incorporation of error into the models, for the determination of Al, Cu and Fe in PCBs, with superior performance to non-traditional calibration approaches, MLPCR and ECPR, proving effective in dealing with the spectral complexity of the data.

In Chapter 4, a preliminary sequential leaching protocol was developed for the selective recovery of metals of interest (Ag, Au, Cu and Sn), which proved to be technically feasible and in line with the principles of Green Chemistry. This hydrometallurgical route, combined with the application of analytical techniques, represents an important step towards the automation and sustainability of industrial recycling processes.

Moreover, chapter 4 presented results from the joint use of LIBS and hyperspectral imaging as real-time process control tools. This integration enabled the construction of chemical maps of the PCB surface, highlighting patterns of element distribution and opening up new possibilities for the optimization and continuous monitoring of industrial processes.

This collection of study makes a significant contribution to science by proposing sustainable, robust and low environmental impact methodologies with direct application potential in the recycling industry. The integration of spectroanalytical techniques with

advanced chemometric tools expands the possibilities for characterizing and recovering valuable metals in complex waste such as e-waste. In addition, the results obtained point to the development of more intelligent, efficient and environmentally responsible technological solutions, promoting a bridge between academic research and industrial innovation.

For future work, some key points relevant to the area can be studied:

- **Expansion and economic analysis:** Transition of the developed leaching protocol from a laboratory scale to a pilot scale in order to evaluate its performance under pre-industrial conditions, accompanied by a technical-economic analysis to determine its market viability.
- **Expansion of the analytical scope:** Apply LIBS, XRF, and hyperspectral imaging methodologies to characterize and quantify other high-value or hazardous elements (For example., rare earth elements, Pd, Pb, Cd) and extend the study to other complex e-waste streams, such as batteries, solar panels, and LCD/OLED screens.
- **Advances in data processing:** Explore the use of deep learning and other advanced artificial intelligence algorithms to improve the accuracy of quantitative models and real-time classification and mapping of materials, paving the way for intelligent automated recycling systems.
- **Life cycle assessment (LCA):** Conduct a comprehensive LCA to quantitatively compare the environmental footprint of the proposed hydrometallurgical route with traditional pyrometallurgical methods and less sophisticated recycling methods, thereby validating its alignment with Green Chemistry principles.

6. References

[1] H.Y. Kang, J.M. Schoenung, Electronic waste recycling: A review of U.S. infrastructure and technology options, Resour Conserv Recycl 45 (2005) 368–400. https://doi.org/10.1016/J.RESCONREC.2005.06.001.

[2] K. Liu, Q. Tan, J. Yu, M. Wang, A global perspective on e-waste recycling, Circular Economy 2 (2023) 100028. https://doi.org/10.1016/J.CEC.2023.100028.

[3] J. Li, X. Zeng, M. Chen, O.A. Ogunseitan, A. Stevels, "control-Alt-Delete": Rebooting Solutions for the E-Waste Problem, Environ Sci Technol 49 (2015) 7095–7108. https://doi.org/10.1021/ACS.EST.5B00449/SUPPL_FILE/ES5B00449_SI_001.PDF.

[4] M. Chen, J. Huang, O.A. Ogunseitan, N. Zhu, Y. min Wang, Comparative study on copper leaching from waste printed circuit boards by typical ionic liquid acids, Waste Management 41 (2015) 142–147. https://doi.org/10.1016/J.WASMAN.2015.03.037.

[5] V. Forti, C.P. Baldé, R. Kuehr, G. Bel, L. Jinhui, D.S. Khetriwal, J. Linnell, F. Magalini, I.C. Nnororm, P. Onianwa, D. Ott, A. Ramola, U. Silva, R. Stillhart, D. Tillekeratne, V. Van Straalen, M. Wagner, Yamamoto, The Global E-waste Monitor 2020: Quantities, Flows, and Resources, Ensure Healthy Lives and Promote Well-Being for All. Experiences of Community Health, Hygiene, Sanitation and Nutrition (2020) 121–135. https://www.researchgate.net/publication/342783104_The_Global_E-waste_Monitor_2020_Quantities_flows_and_the_circular_economy_potential (accessed October 30, 2023).

[6] D. Dutta, S. Arya, S. Kumar, E. Lichtfouse, Electronic waste pollution and the COVID-19 pandemic, Environ Chem Lett 20 (2022) 971. https://doi.org/10.1007/S10311-021-01286-9.

[7] C.P. Baldé, R. Kuehr, T. Yamamoto, R. McDonald, S. Althaf, G. Bel, O. Deubzer, E. Fernandez-Cubillo, V. Forti, V. Gray, S. Herat, S. Honda, G. Iattoni, D.S. Khetriwal, V. Luda di Cortemiglia, The global E-waste monitor 2024, 2024. https://www.itu.int/itu-d/sites/environment.

[8] K. Parajuly, R. Kuehr, A. Awasthi, C. Fitzpatrick, J. Lepawsky, E. Smith, R. Widmer, X. Zeng, Future E-waste Scenarios, 2019.

[9] M. Kaya, Recovery of metals and nonmetals from electronic waste by physical and chemical recycling processes, Waste Management 57 (2016) 64–90. https://doi.org/10.1016/J.WASMAN.2016.08.004.

[10] K. Makenji, M. Salvage, Waste electrical and electronic equipment (WEEE) handbook / edited by Vannessa Goodship and Ab Stevels., Woodhead Publishing Limited, 2012. http://www.sciencedirect.com:5070/book/9780857090898/waste-electrical-and-electronic-equipment-weee-handbook (accessed October 30, 2023).

[11] W. Li, V. Achal, Environmental and health impacts due to e-waste disposal in China – A review, Science of The Total Environment 737 (2020) 139745. https://doi.org/10.1016/J.SCITOTENV.2020.139745.

[12] S. Ahsan, M. Ali, R. Islam, E-Waste Trading Impact on Public Health and Ecosystem Services in Developing Countries International Journal of Waste Resources, Int J Waste Resources 5 (2015) 4. https://doi.org/10.4172/2252-5211.1000188.

[13] D.N. Perkins, M.N. Brune Drisse, T. Nxele, P.D. Sly, E-Waste: A Global Hazard, Ann Glob Health 80 (2014) 286–295. https://doi.org/10.1016/J.AOGH.2014.10.001.

[14] I.M.S.K. Ilankoon, Y. Ghorbani, M.N. Chong, G. Herath, T. Moyo, J. Petersen, E-waste in the international context – A review of trade flows, regulations, hazards, waste management strategies and technologies for value recovery, Waste Management 82 (2018) 258–275. https://doi.org/10.1016/J.WASMAN.2018.10.018.

[15] R. Widmer, H. Oswald-Krapf, D. Sinha-Khetriwal, M. Schnellmann, H. Böni, Global perspectives on e-waste, Environ Impact Assess Rev 25 (2005) 436–458. https://doi.org/10.1016/J.EIAR.2005.04.001.

[16] J.M. Yoo, J. Jeong, K. Yoo, J. chun Lee, W. Kim, Enrichment of the metallic components from waste printed circuit boards by a mechanical separation process using a stamp mill, Waste Management 29 (2009) 1132–1137. https://doi.org/10.1016/J.WASMAN.2008.06.035.

[17] D.F. Andrade, R.C. Machado, M.A. Bacchi, E.R. Pereira-Filho, Proposition of electronic waste as a reference material – part 1: sample preparation, characterization and chemometric evaluation, J Anal At Spectrom 34 (2019) 2394–2401. https://doi.org/10.1039/C9JA00283A.

[18] D.F. Andrade, R.C. Machado, E.R. Pereira-Filho, Proposition of electronic waste as a reference material – part 2: homogeneity, stability, characterization, and uncertainties, J Anal At Spectrom 34 (2019) 2402–2410. https://doi.org/10.1039/C9JA00284G.

[19] A. Hubau, A. Chagnes, M. Minier, S. Touzé, S. Chapron, A.G. Guezennec, Recycling-oriented methodology to sample and characterize the metal composition of waste Printed Circuit Boards, Waste Management 91 (2019) 62–71. https://doi.org/10.1016/J.WASMAN.2019.04.041.

[20] M. Sahan, M.A. Kucuker, B. Demirel, K. Kuchta, A. Hursthouse, Determination of Metal Content of Waste Mobile Phones and Estimation of Their Recovery Potential in Turkey, International Journal of Environmental Research and Public Health 2019, Vol. 16, Page 887 16 (2019) 887. https://doi.org/10.3390/IJERPH16050887.

[21] W. Liu, P. Ford, H. Uvegi, F. Margarido, E. Santos, P. Ferrão, E. Olivetti, Economics of materials in mobile phone preprocessing, focus on non-printed circuit board materials, Waste Management 87 (2019) 78–85. https://doi.org/10.1016/J.WASMAN.2019.01.044.

[22] D.T. Buechler, N.N. Zyaykina, C.A. Spencer, E. Lawson, N.M. Ploss, I. Hua, Comprehensive elemental analysis of consumer electronic devices: Rare earth, precious, and critical elements, Waste Management 103 (2020) 67–75. https://doi.org/10.1016/J.WASMAN.2019.12.014.

[23] M. Tunali, M.M. Tunali, O. Yenigun, Characterization of different types of electronic waste: heavy metal, precious metal and rare earth element content by comparing different digestıon methods, J Mater Cycles Waste Manag 23 (2021) 149–157. https://doi.org/10.1007/S10163-020-01108-0/TABLES/3.

[24] D.F. Andrade, E. de Almeida, H.W.P. de Carvalho, E.R. Pereira-Filho, D. Amarasiriwardena, Chemical inspection and elemental analysis of electronic waste using data fusion - Application of complementary spectroanalytical techniques, Talanta 225 (2021) 122025. https://doi.org/10.1016/J.TALANTA.2020.122025.

[25] J. Huang, M. Chen, H. Chen, S. Chen, Q. Sun, Leaching behavior of copper from waste printed circuit boards with Brønsted acidic ionic liquid, Waste Management 34 (2014) 483–488. https://doi.org/10.1016/J.WASMAN.2013.10.027.

[26] C. Ma, J. Yu, B. Wang, Z. Song, J. Xiang, S. Hu, S. Su, L. Sun, Chemical recycling of brominated flame retarded plastics from e-waste for clean fuels production: A review, Renewable and Sustainable Energy Reviews 61 (2016) 433–450. https://doi.org/10.1016/J.RSER.2016.04.020.

[27] M.T. Lecler, F. Zimmermann, E. Silvente, A. Masson, Y. Morèle, A. Remy, A. Chollot, Improving the work environment in the fluorescent lamp recycling sector by optimizing mercury elimination, Waste Management 76 (2018) 250–260. https://doi.org/10.1016/J.WASMAN.2018.02.037.

[28] M. Bigum, A. Damgaard, C. Scheutz, T.H. Christensen, Environmental impacts and resource losses of incinerating misplaced household special wastes (WEEE, batteries, ink cartridges and cables), Resour Conserv Recycl 122 (2017) 251–260. https://doi.org/10.1016/J.RESCONREC.2017.02.013.

[29] Q. Song, J. Li, Environmental effects of heavy metals derived from the e-waste recycling activities in China: A systematic review, Waste Management 34 (2014) 2587–2594. https://doi.org/10.1016/J.WASMAN.2014.08.012.

[30] S.M. Parvez, F. Jahan, M.N. Brune, J.F. Gorman, M.J. Rahman, D. Carpenter, Z. Islam, M. Rahman, N. Aich, L.D. Knibbs, P.D. Sly, Health consequences of exposure to e-waste: an updated systematic review, Lancet Planet Health 5 (2021) e905–e920. https://doi.org/10.1016/S2542-5196(21)00263-1/ASSET/9D294B19-9AE6-43CD-9A1C-B4DE2DAA89C0/MAIN.ASSETS/GR1.JPG.

[31] D. Beula, M. Sureshkumar, A review on the toxic E-waste killing health and environment – Today's global scenario, Mater Today Proc 47 (2021) 2168–2174. https://doi.org/10.1016/J.MATPR.2021.05.516.

[32] S. Lin, M.U. Ali, C. Zheng, Z. Cai, M.H. Wong, Toxic chemicals from uncontrolled e-waste recycling: Exposure, body burden, health impact, J Hazard Mater 426 (2022) 127792. https://doi.org/10.1016/J.JHAZMAT.2021.127792.

[33] A. Sepúlveda, M. Schluep, F.G. Renaud, M. Streicher, R. Kuehr, C. Hagelüken, A.C. Gerecke, A review of the environmental fate and effects of hazardous substances released from electrical and electronic equipments during recycling: Examples from China and India, Environ Impact Assess Rev 30 (2010) 28–41. https://doi.org/10.1016/J.EIAR.2009.04.001.

[34] C.S.C. Wong, N.S. Duzgoren-Aydin, A. Aydin, M.H. Wong, Evidence of excessive releases of metals from primitive e-waste processing in Guiyu, China, Environmental Pollution 148 (2007) 62–72. https://doi.org/10.1016/J.ENVPOL.2006.11.006.

[35] C. Frazzoli, O.E. Orisakwe, R. Dragone, A. Mantovani, Diagnostic health risk assessment of electronic waste on the general population in developing countries' scenarios, Environ Impact Assess Rev 30 (2010) 388–399. https://doi.org/10.1016/J.EIAR.2009.12.004.

[36] S. Wen, F.X. Yang, Y. Gong, X.L. Zhang, Y. Hui, J.G. Li, A.I.L. Liu, Y.N. Wu, W.Q. Lu, Y. Xu, Elevated levels of urinary 8-hydroxy-2′-deoxyguanosine in male electrical and electronic equipment dismantling workers exposed to high concentrations of polychlorinated dibenzo-p-dioxins and dibenzofurans, polybrominated diphenyl ethers, and polychlorinated biphenyls, Environ Sci Technol 42 (2008) 4202–4207. https://doi.org/10.1021/ES800044M/SUPPL_FILE/ES800044M-FILE005.PDF.

[37] X. Zeng, S.H. Ali, J. Tian, J. Li, Mapping anthropogenic mineral generation in China and its implications for a circular economy, Nature Communications 2020 11:1 11 (2020) 1–9. https://doi.org/10.1038/s41467-020-15246-4.

[38] K. Grant, F.C. Goldizen, P.D. Sly, M.N. Brune, M. Neira, M. van den Berg, R.E. Norman, Health consequences of exposure to e-waste: A systematic review, Lancet Glob Health 1 (2013) e350–e361. https://doi.org/10.1016/S2214-109X(13)70101-3/ATTACHMENT/6A0D7741-9DC9-4EEC-AC7B-000950400E6B/MMC1.PDF.

[39] J.K.Y. Chan, M.H. Wong, A review of environmental fate, body burdens, and human health risk assessment of PCDD/Fs at two typical electronic waste recycling sites in China, Science of The Total Environment 463–464 (2013) 1111–1123. https://doi.org/10.1016/J.SCITOTENV.2012.07.098.

[40] V. Forti, C. Peter Baldé, The Global E-waste Monitor 2020. Quantities, flows, and the circular economy potential, 2020. https://www.researchgate.net/publication/342783104.

[41] X. Zeng, H. Duan, F. Wang, J. Li, Examining environmental management of e-waste: China's experience and lessons, Renewable and Sustainable Energy Reviews 72 (2017) 1076–1082. https://doi.org/10.1016/J.RSER.2016.10.015.

[42] W. Li, V. Achal, Environmental and health impacts due to e-waste disposal in China – A review, Science of The Total Environment 737 (2020) 139745. https://doi.org/10.1016/J.SCITOTENV.2020.139745.

[43] K. Bhaskar, R.M.R. Turaga, India's E-Waste Rules and Their Impact on E-Waste Management Practices: A Case Study, J Ind Ecol 22 (2018) 930–942. https://doi.org/10.1111/JIEC.12619.

[44] J.K. Pradhan, S. Kumar, Informal e-waste recycling: Environmental risk assessment of heavy metal contamination in Mandoli industrial area, Delhi, India, Environmental Science and Pollution Research 21 (2014) 7913–7928. https://doi.org/10.1007/S11356-014-2713-2,.

[45] C.W. Babbitt, H. Madaka, S. Althaf, B. Kasulaitis, E.G. Ryen, Disassembly-based bill of materials data for consumer electronic products, Sci Data 7 (2020) 1–8. https://doi.org/10.1038/S41597-020-0573-9;SUBJMETA=172,4081,559,685,703,704,706,844;KWRD=ENVIRONMENTAL+IMPACT,SUSTAINABILITY,TECHNOLOGY.

[46] S. Althaf, C.W. Babbitt, R. Chen, The evolution of consumer electronic waste in the United States, J Ind Ecol 25 (2021) 693–706. https://doi.org/10.1111/JIEC.13074.

[47] U.N. UN, Brasil produziu 1,4 milhão de toneladas de resíduos eletrônicos em 2014, afirma novo relatório da ONU, (2015). https://brasil.un.org/pt-br/69560-brasil-produziu-14-milh%C3%A3o-de-toneladas-de-res%C3%ADduos-eletr%C3%B4nicos-em-2014-afirma-novo-relat%C3%B3rio (accessed December 16, 2024).

[48] M.G. Araújo, A. Magrini, C.F. Mahler, B. Bilitewski, A model for estimation of potential generation of waste electrical and electronic equipment in Brazil, Waste Management 32 (2012) 335–342. https://doi.org/10.1016/J.WASMAN.2011.09.020.

[49] C.H. Da Paixão, A.L. Oliveira, PROCESSAMENTO DE RESÍDUOS ELÉTRICOS NO BRASIL, Revista Interface Tecnológica 20 (2023) 554–565. https://doi.org/10.31510/infa.v20i1.1593.

[50] L.H. Xavier, R. Sierpe, M. Ottoni, J. dos S. Cugula, Método para a categorização e a estimativa da geração de resíduos eletroeletrônicos no Brasil, Revista Brasileira de Gestão Ambiental e Sustentabilidade 8 (2021) 1533–1551. https://doi.org/10.21438/rbgas(2021)082017.

[51] A.C. Rodrigues, W.M.R. Gunther, M.E.G. Boscov, Estimativa da geração de resíduos de equipamentos elétricos e eletrônicos de origem domiciliar: proposição de método e aplicação ao município de São Paulo, São Paulo, Brasil, Engenharia Sanitaria e Ambiental 20 (2015) 437–447. https://doi.org/10.1590/S1413-41522015020000133701.

[52] M.I. Prado, Eletrônicos: do lixo ao lucro: a escassez de matéria prima para a contínua produção de equipamentos eletrônicos e o peso para a reciclagem pós-consumo - doi: 10.5102/un.gti.v2i1.1576, Universitas: Gestão e TI 2 (2012). https://doi.org/10.5102/un.gti.v2i1.1576.

[53] G.L. de P. Franca, L. de J.R. Barros, Situação atual de resíduos eletrônicos no Brasil., Revista Interface Tecnológica 14 (2017) 96–104.

[54] Brazil, LEI Nº 12.305, DE 2 DE AGOSTO DE 2010, Brasilia, 2010. https://www.planalto.gov.br/ccivil_03/_ato2007-2010/2010/lei/l12305.htm (accessed December 16, 2024).

[55] F.J. KRUG, F.R.P. ROCHA, MÉTODOS DE PREPARO DE AMOSTRAS PARA ANÁLISE ELEMENTAR, 2nd ed., EditSBQ, Sao Paulo, 2019.

[56] R.C. Richter, J.A. Nobrega, C. Pirola, Think blank clean chemistry for Atomic Spectroscopy, 1st ed., Milestone Press, Sorisole, 2016.

[57] J.A. Nóbrega, C. Pirola, Think green. Modern approaches to microwave-assisted digestion, 1st ed., Ikonos, 2018.

[58] R.C. Machado, D.F. Andrade, D. V. Babos, J.P. Castro, V.C. Costa, M.A. Sperança, J.A. Garcia, R.R. Gamela, E.R. Pereira-Filho, Solid sampling: advantages and challenges for chemical element determination—a critical review, J Anal At Spectrom 35 (2020) 54–77. https://doi.org/10.1039/C9JA00306A.

[59] U. Kurfürst, Solid Sample Analysis, Springer Berlin Heidelberg, 1998. https://doi.org/10.1007/978-3-662-03716-4.

[60] U. Kurfürst, ed., Solid Sample Analysis, Springer Berlin Heidelberg, Berlin, Heidelberg, 1998. https://doi.org/10.1007/978-3-662-03716-4.

[61] A.L. Vieira, D.A. Gonçalves, A. Virgilio, E.C. Ferreira, B.T. Jones, G.L. Donati, J.A. Gomes Neto, Multi-energy calibration for the determination of non-metals by high-

resolution continuum source molecular absorption spectrometry, J Anal At Spectrom 34 (2019) 972–978. https://doi.org/10.1039/C9JA00006B.

[62] M. Resano, L. Rello, M. Flórez, M.A. Belarra, On the possibilities of high-resolution continuum source graphite furnace atomic absorption spectrometry for the simultaneous or sequential monitoring of multiple atomic lines, Spectrochim Acta Part B At Spectrosc 66 (2011) 321–328. https://doi.org/10.1016/J.SAB.2011.03.008.

[63] G. Galbács, Laser-Induced Breakdown Spectroscopy in Biological, Forensic and Materials Sciences, Springer International Publishing, 2022. https://doi.org/10.1007/978-3-031-14502-5/COVER.

[64] R. Noll, Laser-induced breakdown spectroscopy: Fundamentals and applications, Springer Berlin Heidelberg, 2012. https://doi.org/10.1007/978-3-642-20668-9/COVER.

[65] D.A. Cremers, L.J. Radziemski, Handbook of Laser-Induced Breakdown Spectroscopy: Second Edition, John Wiley and Sons, 2013. https://doi.org/10.1002/9781118567371.

[66] C. Pasquini, J. Cortez, L.M.C. Silva, F.B. Gonzaga, Laser Induced Breakdown Spectroscopy, J Braz Chem Soc 18 (2007) 463–512. https://doi.org/10.1590/S0103-50532007000300002.

[67] V.C. Costa, A.S. Augusto, J.P. Castro, R.C. Machado, D.F. Andrade, D. V. Babos, M. Speranca, R.R. Gamela, E.R. Pereira-Filho, LASER INDUCED-BREAKDOWN SPECTROSCOPY (LIBS): HISTÓRICO, FUNDAMENTOS, APLICAÇÕES E POTENCIALIDADES, Quim Nova 42 (2019) 527–545. https://doi.org/10.21577/0100-4042.20170325.

[68] D. Fernandes Andrade, E.R. Pereira-Filho, D. Amarasiriwardena, Current trends in laser-induced breakdown spectroscopy: a tutorial review, Appl Spectrosc Rev 56 (2021) 98–114. https://doi.org/10.1080/05704928.2020.1739063.

[69] E.R.P. Filho, Laser-Induced Breakdown Spectroscopy (LIBS), Editora Ibero-Americana de Educação, 2023. https://doi.org/10.47519/EIE.978-65-86839-05-0.

[70] D.A. Cremers, R.C. Chinni, Laser-induced breakdown spectroscopy-capabilities and limitations, Appl Spectrosc Rev 44 (2009) 457–506. https://doi.org/10.1080/05704920903058755;SUBPAGE:STRING:FULL.

[71] L. Brunnbauer, Z. Gajarska, H. Lohninger, A. Limbeck, A critical review of recent trends in sample classification using Laser-Induced Breakdown Spectroscopy (LIBS), TrAC Trends in Analytical Chemistry 159 (2023) 116859. https://doi.org/10.1016/J.TRAC.2022.116859.

[72] S.K. Hussain Shah, J. Iqbal, P. Ahmad, M.U. Khandaker, S. Haq, M. Naeem, Laser induced breakdown spectroscopy methods and applications: A comprehensive review, Radiation Physics and Chemistry 170 (2020) 108666. https://doi.org/10.1016/J.RADPHYSCHEM.2019.108666.

[73] E. Marguí, I. Queralt, E. de Almeida, X-ray fluorescence spectrometry for environmental analysis: Basic principles, instrumentation, applications and recent trends, Chemosphere 303 (2022) 135006. https://doi.org/10.1016/J.CHEMOSPHERE.2022.135006.

[74] R. Cesareo, X-Ray Fluorescence Spectrometry, John Wiley & Sons, Ltd, Weinheim, Germany, 2010. https://doi.org/10.1002/14356007.B05_675.PUB2.

[75] M. West, A.T. Ellis, P.J. Potts, C. Streli, C. Vanhoof, D. Wegrzynek, P. Wobrauschek, Atomic spectrometry update–X-ray fluorescence spectrometry, J Anal At Spectrom 25 (2010) 1503–1545. https://doi.org/10.1039/C005501H.

[76] C. Vanhoof, J.R. Bacon, U.E.A. Fittschen, L. Vincze, Atomic spectrometry update – a review of advances in X-ray fluorescence spectrometry and its special applications, J Anal At Spectrom 36 (2021) 1797–1812. https://doi.org/10.1039/D1JA90033A.

[77] X. Feng, H. Zhang, P. Yu, X-ray fluorescence application in food, feed, and agricultural science: a critical review, Crit Rev Food Sci Nutr 61 (2021) 2340–2350. https://doi.org/10.1080/10408398.2020.1776677.

[78] P.J. Potts, M. Sargent, In situ measurements using hand-held XRF spectrometers: a tutorial review, J Anal At Spectrom 37 (2022) 1928–1947. https://doi.org/10.1039/D2JA00171C.

[79] F. Li, L. Ge, Z. Tang, Y. Chen, J. Wang, Recent developments on XRF spectra evaluation, Appl Spectrosc Rev 55 (2020) 263–287. https://doi.org/10.1080/05704928.2019.1580715.

[80] A. Harth, X-ray fluorescence (XRF) on painted heritage objects: a review using topic modeling, Heritage Science 2024 12:1 12 (2024) 1–20. https://doi.org/10.1186/s40494-024-01135-2.

[81] I. Liritzis, N. Zacharias, Portable XRF of Archaeological Artifacts: Current Research, Potentials and Limitations, in: X-Ray Fluorescence Spectrometry (XRF) in Geoarchaeology, Springer, New York, NY, 2011: pp. 109–142. https://doi.org/10.1007/978-1-4419-6886-9_6.

[82] S. Serranti, G. Capobianco, S. Malinconico, G. Bonifazi, MICRO X-RAY FLUORESCENCE IMAGING COUPLED WITH CHEMOMETRICS TO DETECT AND CLASSIFY ASBESTOS FIBERS IN DEMOLITION WASTE, Detritus 2019 - Volume 12 (2020) 150. https://doi.org/10.31025/2611-4135/2020.14007.

[83] V.M. Neves, G.M. Heidrich, E.S. Rodrigues, M.S.P. Enders, E.I. Muller, F.T. Nicoloso, H.W.P. De Carvalho, V.L. Dressler, La2O3 Nanoparticles: Study of Uptake and Distribution in Pfaffia glomerata (Spreng.) Pedersen by LA-ICP-MS and μ-XRF, Environ Sci Technol 53 (2019) 10827–10834. https://doi.org/10.1021/ACS.EST.9B02868/ASSET/IMAGES/LARGE/ES9B02868_0002.JPEG.

[84] M. Haschke, Laboratory Micro-X-Ray Fluorescence Spectroscopy, Springer International Publishing, Cham, 2014. https://doi.org/10.1007/978-3-319-04864-2.

[85] R.C. Machado, D.F. Andrade, D. V. Babos, J.P. Castro, V.C. Costa, M.A. Sperancą, J.A. Garcia, R.R. Gamela, E.R. Pereira-Filho, Solid sampling: advantages and challenges for chemical element determination—a critical review, J Anal At Spectrom 35 (2020) 54–77. https://doi.org/10.1039/C9JA00306A.

[86] H.P. Wang, P. Chen, J.W. Dai, D. Liu, J.Y. Li, Y.P. Xu, X.L. Chu, Recent advances of chemometric calibration methods in modern spectroscopy: Algorithms, strategy, and related issues, TrAC Trends in Analytical Chemistry 153 (2022) 116648. https://doi.org/10.1016/J.TRAC.2022.116648.

[87] B. Lavine, J. Workman, Chemometrics, Anal Chem 80 (2008) 4519–4531. https://doi.org/10.1021/AC800728T.

[88] M. Greenacre, P.J.F. Groenen, T. Hastie, A.I. D'Enza, A. Markos, E. Tuzhilina, Principal component analysis, Nature Reviews Methods Primers 2022 2:1 2 (2022) 1–21. https://doi.org/10.1038/s43586-022-00184-w.

[89] N. Kumar, A. Bansal, G.S. Sarma, R.K. Rawal, Chemometrics tools used in analytical chemistry: An overview, Talanta 123 (2014) 186–199. https://doi.org/10.1016/J.TALANTA.2014.02.003.

[90] D.F. Andrade, E. de Almeida, H.W.P. de Carvalho, E.R. Pereira-Filho, D. Amarasiriwardena, Chemical inspection and elemental analysis of electronic waste using data fusion - Application of complementary spectroanalytical techniques, Talanta 225 (2021) 122025. https://doi.org/10.1016/J.TALANTA.2020.122025.

[91] J.P. Castro, E.R. Pereira-Filho, Spectroanalytical method for evaluating the technological elements composition of magnets from computer hard disks, Talanta 189 (2018) 205–210. https://doi.org/10.1016/J.TALANTA.2018.06.062.

[92] E. Marguí, I. Queralt, M. Hidalgo, Application of X-ray fluorescence spectrometry to determination and quantitation of metals in vegetal material, TrAC Trends in Analytical Chemistry 28 (2009) 362–372. https://doi.org/10.1016/J.TRAC.2008.11.011.

[93] T.D.T. Oyedotun, X-ray fluorescence (XRF) in the investigation of the composition of earth materials: a review and an overview, Geology, Ecology, and Landscapes 2 (2018) 148–154. https://doi.org/10.1080/24749508.2018.1452459.

[94] A. Agbim, K.A. Schumacher, N. Sharp, R. Paul, R. Corzo, Elemental characterization of electronic waste: a review of research methodologies and applicability to the practice of e-waste recycling, Waste Management 187 (2024) 91–100. https://doi.org/10.1016/J.WASMAN.2024.07.009.

[95] W. Hao, X. Hao, Y. Yang, X. Liu, Y. Liu, P. Sun, R. Sun, Rapid classification of soils from different mining areas by laser-induced breakdown spectroscopy (LIBS) coupled with a PCA-based convolutional neural network, J Anal At Spectrom 36 (2021) 2509–2518. https://doi.org/10.1039/D1JA00078K.

[96] A.S. Maltsev, G. V. Pashkova, R. Fernández-Ruiz, E.I. Demonterova, A.N. Shuliumova, N.N. Umarova, D.L. Shergin, M.M. Mukhamedova, V.M. Chubarov, E.A. Mikheeva, Characterization of archaeological ceramics from eastern Siberia by total-reflection X-ray fluorescence spectrometry and principal component analysis, Spectrochim Acta Part B At Spectrosc 175 (2021) 106012. https://doi.org/10.1016/J.SAB.2020.106012.

[97] Z. Tian, J. Li, S. Wang, Y. Bai, Y. Zhao, L. Zhang, P. Zhang, Z. Ye, Z. Zhu, W. Yin, S. Jia, Development and industrial application of LIBS-XRF coal quality analyzer by

combining PCA and PLS regression methods, J Anal At Spectrom 38 (2023) 1421–1430. https://doi.org/10.1039/D3JA00015J.

[98] L. Li, Y. Chen, L. Yang, Z. Wang, H. Liu, Recent advances in applications of metal–organic frameworks for sample preparation in pharmaceutical analysis, Coord Chem Rev 411 (2020) 213235. https://doi.org/10.1016/J.CCR.2020.213235.

[99] S.R. Khan, B. Sharma, P.A. Chawla, R. Bhatia, Inductively Coupled Plasma Optical Emission Spectrometry (ICP-OES): a Powerful Analytical Technique for Elemental Analysis, Food Anal Methods 15 (2022) 666–688. https://doi.org/10.1007/S12161-021-02148-4/TABLES/6.

[100] C. Douvris, T. Vaughan, D. Bussan, G. Bartzas, R. Thomas, How ICP-OES changed the face of trace element analysis: Review of the global application landscape, Science of The Total Environment 905 (2023) 167242. https://doi.org/10.1016/J.SCITOTENV.2023.167242.

[101] R.D. Beaty, J.D. Kerber, Concepts, Instrumentation and Techniques in Atomic Absorption Spectrophotometry, 2nd ed., THE PERKIN-ELMER CORPORATION, 1993.

[102] C.B. Boss, K.J. Fredeen, Concepts, Instrumentation and Techniques in Inductively Coupled Plasma Optical Emission Spectrometry, 3rd ed., PerkinElmer, 2004. www.perkinelmer.com.

[103] M.S. Rocha, M.F. Mesko, F.F. Silva, R.C. Sena, M.C.B. Quaresma, T.O. Araújo, L.A. Reis, Determination of Cu and Fe in fuel ethanol by ICP OES using direct sample introduction by an ultrasonic nebulizer and membrane desolvator, J Anal At Spectrom 26 (2011) 456–461. https://doi.org/10.1039/C0JA00096E.

[104] F.R.S. Bentlin, D. Pozebon, Direct determination of lanthanides in environmental samples using ultrasonic nebulization and ICP OES, J Braz Chem Soc 21 (2010) 627–634. https://doi.org/10.1590/S0103-50532010000400007.

[105] V. Yilmaz, Z. Arslan, O. Hazer, H. Yilmaz, Selective solid phase extraction of copper using a new Cu(II)-imprinted polymer and determination by inductively coupled plasma optical emission spectroscopy (ICP-OES), Microchemical Journal 114 (2014) 65–72. https://doi.org/10.1016/J.MICROC.2013.12.002.

[106] A. Leclercq, A. Nonell, J.L. Todolí Torró, C. Bresson, L. Vio, T. Vercouter, F. Chartier, Introduction of organic/hydro-organic matrices in inductively coupled plasma optical emission spectrometry and mass spectrometry: A tutorial review. Part II. Practical considerations, Anal Chim Acta 885 (2015) 57–91. https://doi.org/10.1016/J.ACA.2015.04.039.

[107] Y. Liu, D. Xue, W. Li, C. Li, B. Wan, A simple method for the precise determination of multi-elements in pyrite and magnetite by ICP-MS and ICP-OES with matrix removal, Microchemical Journal 158 (2020) 105221. https://doi.org/10.1016/J.MICROC.2020.105221.

[108] A.F. Lagalante, Atomic absorption spectroscopy: A tutorial review, Appl Spectrosc Rev 34 (2004) 173–189. https://doi.org/10.1081/ASR-100100844;WGROUP:STRING:PUBLICATION.

[109] B. Meermann, V. Nischwitz, ICP-MS for the analysis at the nanoscale – a tutorial review, J Anal At Spectrom 33 (2018) 1432–1468. https://doi.org/10.1039/C8JA00037A.

[110] V. Costa, D. Babos, J. Castro, D. Andrade, R. Gamela, R. Machado, M. Sperança, A. Araújo, J. Garcia, E. Pereira-Filho, Calibration Strategies Applied to Laser-Induced Breakdown Spectroscopy: A Critical Review of Advances and Challenges, J Braz Chem Soc 31 (2021) 2439–2451. https://doi.org/10.21577/0103-5053.20200175.

[111] A.S. Araújo, J.P. Castro, M.A. Sperança, D.F. Andrade, M.L. De Mello, E.R. Pereira-Filho, Multiway Calibration Strategies in Laser-Induced Breakdown Spectroscopy: A Proposal, Anal Chem 93 (2021) 6291–6300. https://doi.org/10.1021/ACS.ANALCHEM.0C04722/ASSET/IMAGES/LARGE/AC0C04722_0009.JPEG.

[112] R.R. Gamela, B.M. Fontoura, V.C. Costa, D. V. Babos, E.R. Pereira-Filho, Matrix-Matching Calibration Using Solid Standards: A Comparison between Univariate and Multivariate Strategies for the Determination of Calcium and Magnesium in Bean Seed Samples Employing Laser-Induced Breakdown Spectroscopy (LIBS), Anal Lett 56 (2023) 944–957. https://doi.org/10.1080/00032719.2022.2111573;CTYPE:STRING:JOURNAL.

[113] S.K. Schreyer, M. Bidinosti, P.D. Wentzell, Application of Maximum Likelihood Principal Components Regression to Fluorescence Emission Spectra, Appl Spectrosc 56 (2002) 789–796. https://doi.org/10.1366/000370202760076857.

[114] D.T. Andrews, P.D. Wentzell, Applications of maximum likelihood principal component analysis: incomplete data sets and calibration transfer, Anal Chim Acta 350 (1997) 341–352. https://doi.org/10.1016/S0003-2670(97)00270-5.

[115] C.D. Brown, Discordance between net analyte signal theory and practical multivariate calibration, Anal Chem 76 (2004) 4364–4373. https://doi.org/10.1021/AC049953W/SUPPL_FILE/AC049953WSI20040430_020552.PDF.

[116] F. Allegrini, J.W.B. Braga, A.C.O. Moreira, A.C. Olivieri, Error Covariance Penalized Regression: A novel multivariate model combining penalized regression with multivariate error structure, Anal Chim Acta 1011 (2018) 20–27. https://doi.org/10.1016/J.ACA.2018.02.002.

[117] F. Allegrini, J.W.B. Braga, A.C.O. Moreira, A.C. Olivieri, Error Covariance Penalized Regression: A novel multivariate model combining penalized regression with multivariate error structure, Anal Chim Acta 1011 (2018) 20–27. https://doi.org/10.1016/J.ACA.2018.02.002.

[118] F. Allegrini, A.C. Olivieri, IUPAC-consistent approach to the limit of detection in partial least-squares calibration, Anal Chem 86 (2014) 7858–7866. https://doi.org/10.1021/AC501786U/ASSET/IMAGES/LARGE/AC-2014-01786U_0006.JPEG.

[119] D.S. Ferreira, F.M.V. Pereira, A.C. Olivieri, E.R. Pereira-Filho, Electronic waste analysis using laser-induced breakdown spectroscopy (LIBS) and X-ray fluorescence (XRF): Critical evaluation of data fusion for the determination of Al, Cu and Fe, Anal Chim Acta 1303 (2024) 342522. https://doi.org/10.1016/J.ACA.2024.342522.

[120] W. Fragoso, F. Allegrini, A.C. Olivieri, A new and consistent parameter for measuring the quality of multivariate analytical methods: Generalized analytical sensitivity, Anal Chim Acta 933 (2016) 43–49. https://doi.org/10.1016/J.ACA.2016.06.022.

[121] M. Dirks, D. Turner, D. Poole, Spectral sensor fusion for prediction of Li and Zr in rocks: Neural network and PLS methods, Chemometrics and Intelligent Laboratory Systems 240 (2023) 104915. https://doi.org/10.1016/J.CHEMOLAB.2023.104915.

[122] C. Yan, Y. Su, Y. Liu, T. Zhang, H. Li, Performing parameter optimization and variable selection simultaneously in Fourier transform infrared and laser-induced breakdown spectroscopy data fusion, J Anal At Spectrom 38 (2023) 2424–2432. https://doi.org/10.1039/D3JA00214D.

[123] D. Lahat, T. Adali, C. Jutten, Multimodal Data Fusion: An Overview of Methods, Challenges, and Prospects, Proceedings of the IEEE 103 (2015) 1449–1477. https://doi.org/10.1109/JPROC.2015.2460697.

[124] S.M. Azcarate, R. Ríos-Reina, J.M. Amigo, H.C. Goicoechea, Data handling in data fusion: Methodologies and applications, TrAC Trends in Analytical Chemistry 143 (2021) 116355. https://doi.org/10.1016/J.TRAC.2021.116355.

[125] M. Hoehse, A. Paul, I. Gornushkin, U. Panne, Multivariate classification of pigments and inks using combined Raman spectroscopy and LIBS, Anal Bioanal Chem 402 (2012) 1443–1450. https://doi.org/10.1007/S00216-011-5287-6/FIGURES/4.

[126] H.P. Wang, P. Chen, J.W. Dai, D. Liu, J.Y. Li, Y.P. Xu, X.L. Chu, Recent advances of chemometric calibration methods in modern spectroscopy: Algorithms, strategy, and related issues, TrAC Trends in Analytical Chemistry 153 (2022) 116648. https://doi.org/10.1016/J.TRAC.2022.116648.

[127] E. Gibbons, R. Léveillé, K. Berlo, Data fusion of laser-induced breakdown and Raman spectroscopies: Enhancing clay mineral identification, Spectrochim Acta Part B At Spectrosc 170 (2020) 105905. https://doi.org/10.1016/J.SAB.2020.105905.

[128] J.A. Manrique-Martinez, G. Lopez-Reyes, A. Alvarez-Perez, T. Bozic, M. Veneranda, A. Sanz-Arranz, J. Saiz, J. Medina-Garcia, F. Rull-Perez, Evaluation of multivariate analyses and data fusion between Raman and laser-induced breakdown spectroscopy in binary mixtures and its potential for solar system exploration, Journal of Raman Spectroscopy 51 (2020) 1702–1717. https://doi.org/10.1002/JRS.5819.

[129] T. He, J. Liang, H. Tang, T. Zhang, C. Yan, H. Li, Quantitative analysis of coal quality by mutual information-particle swarm optimization (MI-PSO) hybrid variable selection method coupled with spectral fusion strategy of laser-induced breakdown spectroscopy

(LIBS) and fourier transform infrared spectroscopy (FTIR), Spectrochim Acta Part B At Spectrosc 178 (2021) 106112. https://doi.org/10.1016/J.SAB.2021.106112.

[130] R.R. Gamela, E.R. Pereira-Filho, F.M.V. Pereira, Minimal-Invasive Analytical Method and Data Fusion: an Alternative for Determination of Cu, K, Sr, and Zn in Cocoa Beans, Food Anal Methods 14 (2021) 545–551. https://doi.org/10.1007/S12161-020-01904-2/FIGURES/5.

[131] M.C. Santos, F.M.V. Pereira, Direct Analysis of Human Hair Before and After Cosmetic Modification Using a Recent Data Fusion Method, J Braz Chem Soc 31 (2020) 33–39. https://doi.org/10.21577/0103-5053.20190121.

[132] D.F. Andrade, E. de Almeida, H.W.P. de Carvalho, E.R. Pereira-Filho, D. Amarasiriwardena, Chemical inspection and elemental analysis of electronic waste using data fusion - Application of complementary spectroanalytical techniques, Talanta 225 (2021) 122025. https://doi.org/10.1016/J.TALANTA.2020.122025.

[133] M. Abdullah, S. Adhikary, S. Bhattacharya, S. Hazra, A. Ganguly, S. Nanda, P. Rajak, E-waste in the environment: Unveiling the sources, carcinogenic links, and sustainable management strategies, Toxicology 509 (2024) 153981. https://doi.org/10.1016/J.TOX.2024.153981.

[134] N.K. Bhoi, Advancements in E-waste recycling technologies: A comprehensive overview of strategies and mechatronics integration for future development, Sustainable Materials and Technologies 42 (2024) e01182. https://doi.org/10.1016/J.SUSMAT.2024.E01182.

[135] A. Khaliq, M.A. Rhamdhani, G. Brooks, S. Masood, Metal Extraction Processes for Electronic Waste and Existing Industrial Routes: A Review and Australian Perspective, Resources 2014, Vol. 3, Pages 152-179 3 (2014) 152–179. https://doi.org/10.3390/RESOURCES3010152.

[136] S. Gulliani, M. Volpe, A. Messineo, R. Volpe, Recovery of metals and valuable chemicals from waste electric and electronic materials: a critical review of existing technologies, RSC Sustainability 1 (2023) 1085–1108. https://doi.org/10.1039/D3SU00034F.

[137] J. Xia, A. Ghahreman, Sustainable technologies for the recycling and upcycling of precious metals from e-waste, Science of The Total Environment 916 (2024) 170154. https://doi.org/10.1016/J.SCITOTENV.2024.170154.

[138] P. Ostellari, S. Gross, A Mature Tool to Address New Challenges: Harnessing Coordination Chemistry for The Sustainable Copper Recovery from Industrial and E-Waste in The Age of Energy Transition, Eur J Inorg Chem 28 (2024) e202400704. https://doi.org/10.1002/EJIC.202400704;WGROUP:STRING:PUBLICATION.

[139] S.K. Bhargava, M.I. Pownceby, R. Ram, Hydrometallurgy, Metals 2016, Vol. 6, Page 122 6 (2016) 122. https://doi.org/10.3390/MET6050122.

[140] A.I. Adetunji, P.J. Oberholster, M. Erasmus, Bioleaching of Metals from E-Waste Using Microorganisms: A Review, Minerals 2023, Vol. 13, Page 828 13 (2023) 828. https://doi.org/10.3390/MIN13060828.

[141] Y.M. Abdel-Fatah, T.A. Elbarbary, I.A. Ibrahim, Kinetic Studies of Copper Leaching From E-Waste Using Organic Acids, Int J Chem Kinet 57 (2025) 446–451. https://doi.org/10.1002/KIN.21788.

[142] A. Nag, M.K. Singh, C.A. Morrison, J.B. Love, [A Nag, M.K. Singh, C.A. Morrison, J.B. Love, Efficient Recycling of Gold and Copper from Electronic Waste by Selective Precipitation, Angewandte Chemie International Edition 62 (2023) e202308356. https://doi.org/10.1002/ANIE.202308356.

[143] A. Khaliq, M.A. Rhamdhani, G. Brooks, S. Masood, Metal Extraction Processes for Electronic Waste and Existing Industrial Routes: A Review and Australian Perspective, Resources 2014, Vol. 3, Pages 152-179 3 (2014) 152–179. https://doi.org/10.3390/RESOURCES3010152.

[144] K. Binnemans, P.T. Jones, The Twelve Principles of Circular Hydrometallurgy, Journal of Sustainable Metallurgy 2022 9:1 9 (2022) 1–25. https://doi.org/10.1007/S40831-022-00636-3.